HAL
open science

Non-equilibrium Casimir interactions : from dynamical to thermal effects

Antonio Noto

To cite this version:

Antonio Noto. Non-equilibrium Casimir interactions : from dynamical to thermal effects. Physics [physics]. Université Montpellier; Università degli studi (Palerme, Italie), 2016. English. NNT : 2016MONTT279 . tel-01808979

HAL Id: tel-01808979

https://theses.hal.science/tel-01808979v1

Submitted on 6 Jun 2018

HAL is a multi-disciplinary open access archive for the deposit and dissemination of scientific research documents, whether they are published or not. The documents may come from teaching and research institutions in France or abroad, or from public or private research centers.

L'archive ouverte pluridisciplinaire **HAL**, est destinée au dépôt et à la diffusion de documents scientifiques de niveau recherche, publiés ou non, émanant des établissements d'enseignement et de recherche français ou étrangers, des laboratoires publics ou privés.

Collège Doctoral du Languedoc-Roussillon

THÈSE

Pour obtenir le grade de

Docteur

Délivré en *cotutelle* par

UNIVERSITÀ DI PALERMO

UNIVERSITÉ DE MONTPELLIER

Dottorato di Ricerca in **Fisica** – XXVI ciclo

Presso **Dipartimento di Fisica e Chimica**

Préparée au sein de l'école doctorale **I2S**

Et de l'unité de recherche **Lab. C. Coulomb – UMR 5221**

Spécialité : **Physique**

Présentée par **Antonio NOTO**

Non equilibrium Casimir interactions: from dynamical to thermal effects

Les interactiones de Casimir hors d'équilibre: effets dynamiques et thermiques

Soutenue le 21/03/2016 devant le Jury composé de

M. Mauro ANTEZZA, Mcf. Univesité de Montpellier	Directeur de Thèse
M. Roberto PASSANTE, Ass. Prof. Università di Palermo	Directeur de Thèse
M. Brahim GUIZAL, Pr. Université de Montpellier	Co-Directeur de Thèse
M. Franco GELARDI, Full Prof. Università di Palermo	Examinateur
M. Marco PETTINI, Pr. Université Aix-Marseille	Rapporteur
M. Stefan BUHMANN, J. Prof. University of Freiburg	Rapporteur

UNIVERSITÀ DEGLI STUDI DI PALERMO

and

UNIVERSITÉ DE MONTPELLIER

Non-equilibrium Casimir interactions: from dynamical to thermal effects

PhD Thesis of

Antonio Noto

Dipartimento di Fisica e Chimica

and

Laboratoire Charles Coulomb

Supervisor:

Prof. Roberto Passante

Supervisor:

Prof. Mauro Antezza

Co-Supervisor:

Prof. Brahim Guizal

Abstract

In this thesis, after an introduction where we briefly present the general context of Casimir physics, we present the results obtained during the PhD. At first, we show our work about the van der Waals/Casimir-Polder interactions between two atoms in an out-of-equilibrium condition due to their uniformly accelerated motion. We study the system of two uniformly accelerated atoms in vacuum space, when they are in their ground-state and when they are in a correlated state (one excited and one ground-state atom). We analyze this system both with an heuristic semiclassical model and with a more rigorous method, based on a separation of radiation reaction and vacuum fluctuations contributions, that we extend starting from a general procedure known in literature. We find a change of the distance-dependence of the interaction due to the acceleration. We show that Casimir-Polder forces between two relativistic uniformly accelerated atoms, interacting with the scalar field, exhibit a transition from the short-distance thermal-like behavior predicted by the Unruh effect to a long-distance nonthermal behavior, associated with the breakdown of a local inertial description of the system. In addition, we obtain new features of the resonance interaction in the case of atoms interacting with the quantum electromagnetic field.

Next, we present our work about a new optomechanical coupling of an effectively oscillating mirror with a Rydberg atoms gas, mediated by the dynamical atom-mirror Casimir-Polder force. We find that this coupling may produce a near-field resonant atomic excitation not related to the excitation of atoms by the few real photons expected by dynamical Casimir effect. In accessible experimental conditions, this excitation probability is significant (about 20%) making the observation of this new dynamical Casimir-Polder effect possible. For this reason, we propose a realistic experimental configuration to realize this system made of a cold atom gas trapped in front of a semiconductor substrate, whose dielectric properties are periodically modulated in time.

Finally, we focus on our results obtained for the Casimir-Lifshitz pressure between two different dielectric lamellar gratings. This system is assumed to be in an out-of-thermal-equilibrium configuration, i.e. the two gratings have two different temperatures and they are immersed in a thermal bath having a third temperature. The computation of the pressure is based on a method exploiting the scattering operators of the bodies, deduced using the Fourier modal method. In our numerical results we characterize in detail the behavior of the pressure, both by varying the three temperatures and by changing the geometrical parameters of the gratings. In this way we show that it is possible to tune the force from attractive to repulsive or to strongly reduce the pressure for large ranges of temperatures. Moreover, we stress that the interplay between nonequilibrium effects and geometrical periodicity make this system particularly interesting for the observation of the repulsive Casimir force.

Résumé

Dans cette thèse, après une introduction où nous présentons brièvement la physique des forces de Casimir, nous montrons nos résultats obtenus pendant le doctorat. D'abord, nous montrons notre travail sur les interactions de van der Waals / Casimir-Polder lorsque le système est dans une configuration hors équilibre à cause du mouvement uniformément accéléré des atomes. Nous étudions le système de deux atomes uniformément accélérés dans le vide quantique quand ils sont dans leur état fondamental ou dans un état corrélé (un atome excité et un atome dans son état fondamental). Nous analysons ce système avec un modèle heuristique semi-classique et une méthode plus rigoureuse qui nous avons étendu à partir d'une procédure générale développée dans la littérature. Nous trouvons un changement de la dépendance de l'interaction de la distance en raison de l'accélération. Nous montrons que les forces de Casimir-Polder entre deux atomes uniformément accélérés en mouvement relativiste, qui interagissent avec le champ scalaire, présentent une transition à partir d'un comportement thermique à courtes distances, comme prédit par l'effet Unruh, à un comportement non thermique à longues distances, associé à la rupture de la description inertielle et locale du système. En plus, lorsque le cas d'atomes qui interagissent avec le champ électromagnétique quantique est considéré, on constate que de nouvelles caractéristiques apparaissent dans l'interaction.

Ensuite, nous présentons notre travail sur un nouveau couplage opto-mécanique d'un miroir oscillant de façon efficace avec un gaz d'atomes de Rydberg, médié par la force atome-miroir dynamique de Casimir-Polder. Nous constatons que ce couplage peut produire une excitation de résonance atomique de champ proche, qui n'est pas liée à l'excitation des atomes par les quelques photons réels attendus de l'effet Casimir dynamique. Dans des conditions expérimentales accessibles, cette probabilité d'excitation est importante (environ 20 %) et rend possible l'observation de ce nouvel effet Casimir-Polder dynamique. Don cnous proposons une configuration expérimentale réaliste pour réaliser ce système fait d'un gaz d'atomes froids piégés mis en face d'un substrat semi-conducteur, dont les propriétés diélectriques sont modulées dans le temps.

Enfin, nous nous concentrons sur nos résultats obtenus pour le calcul de la pression Casimir-Lifshitz entre deux réseaux lamellaires diélectriques différents. Ce système est supposé dans une configuration hors équilibre thermique. En fait, les deux réseaux présentent deux températures différentes et ils sont immergés dans un bain thermique ayant une troisième température. Le calcul de la pression est basé sur une méthode qui exploite les opérateurs de diffusion des réseaux, déduits en utilisant la méthode modale de Fourier. Nous présentons nos résultats numériques caractérisant en détail le comportement de la pression, en faisant varier les trois températures et en modifiant les paramètres géométriques des réseaux. Cette variation des paramètres du système permet de régler la force de répulsive à attractive ou de réduire fortement la pression pour des intervalles de températures. En outre, on montre que la combinaison des effets de non-équilibre et géométriques rend ce système particulièrement intéressant pour l'observation de la force de Casimir répulsive.

Contents

Introduction **I**

1 Casimir forces **1**
1.1 van der Waals force between neutral molecules 2
1.1.1 Resonance interaction between molecules 3
1.1.2 Dispersion interaction between molecules 6
1.1.3 Casimir-Polder interaction between atoms at nonzero temperature 12
1.2 Macroscopic manifestation of the vacuum fluctuations 15
1.2.1 The atom-wall Casimir-Polder interaction 15
1.2.2 The Casimir effect 17
1.2.3 A physical insight about the Casimir effect 20
1.3 Casimir forces and Experiments 22
References 25

2 Effects of uniform acceleration on atom-field interactions **30**
2.1 The Unruh effect 32
2.2 Some known effects of uniform acceleration in quantum electrodynamics . 35
2.3 van der Waals interaction energy between two accelerated atoms 39
2.3.1 The model for the van der Waals interaction in the accelerated frame 40
2.3.2 Concluding remarks on the results 48
2.4 A fourth order method for the calculation of the Casimir-Polder force . . . 50
2.4.1 Perturbative calculation of the variation rates 52
2.4.2 The vacuum fluctuations contribution 54
2.4.3 The radiation reaction contribution 58
2.4.4 The van der Waals force between two atoms at rest 60
2.5 Thermal and non-thermal signatures of the Unruh effect in Casimir-Polder forces 65
2.5.1 Thermal Casimir-Polder interactions 66
2.5.2 Unruh corrections to Casimir-Polder interactions 67
2.6 The resonance interaction between two uniformly accelerated identical atoms 70
2.6.1 The scalar field case 72
2.6.2 The electromagnetic field case 75
2.6.3 Conclusions and Future Perspectives 78
References 79

3 Dynamical Casimir-Polder effect **84**
3.1 The dynamical Casimir effect and the quantum friction 85
3.2 Experimental setups for DCE 90
3.3 Optomechanical Rydberg atoms excitation via dynamic Casimir-Polder coupling 92
3.3.1 Experimental proposal 96
References 99

4 Casimir-Lifshitz force out of thermal equilibrium between dielectric gratings **104**
4.1 A scattering-matrix approach to Casimir-Lifshitz force out of thermal equilibrium 106
4.1.1 Correlation functions of the total field 110
4.1.2 The force between two slabs 114
4.2 Methods for the diffraction by gratings 119
4.2.1 The Fourier Modal Method 119
4.2.2 Some other methods for the diffraction by gratings 128
4.3 OTE Casimir-Lifshitz force between two dielectric gratings 132
4.3.1 Numerical results 139
4.3.2 Dependence on geometrical parameters 143
4.3.3 Modulation of the attractive-repulsive transition 146
4.3.4 Concluding remarks 147
References 148

Conclusions **153**

Appendix A Linear susceptibility **157**

Introduction

In this thesis we discuss the work and the results obtained during the PhD in a joint supervision program between Università degli Studi di Palermo, Italy, and Université de Montpellier, France. The topic of the thesis concerns with the Casimir forces in conditions where the system is out of the equilibrium, dynamical or thermal, in the framework of Quantum Electrodynamics. Casimir forces are interactions among neutral arbitrary objects (atoms/molecules or macroscopic bodies) due to the fact that the quantum "vacuum is not empty". The latter statement could seem an oxymoron or a joke of a comedian but it is instead a direct consequence of the quantum nature of the fields. In fact, an important implication of field quantization is that, also when no external fields are present and the system is at zero temperature, fluctuations of the fields exist. In other words, while the quantum average of the fields is zero in the vacuum state, the expectation value of the squared fields is not null and virtual quanta of the field are always present. The interaction among these virtual quanta (photons in the case of the electromagnetic field) and the objects in the system generates the Casimir force.

Casimir interactions are usually very weak but, nonetheless, they are observable and, recently, they have been measured with remarkable precision in many different systems. In the last 60 years many scientists have studied the Casimir forces and there have been many efforts to better understand these interactions and making them detectable in increasingly realistic conditions. Several geometrical configurations have been studied and the peculiar feature of a strong geometry dependence of these interactions has been revealed as well as a dependence from the magnetodielectric properties of the objects. An important system that we want to mention is when diffraction gratings are present. The importance of the geometry on the Casimir force has been showed and experimentally observed in recent years. In particular, in 2013, using a configuration made of a metallic sphere in front of a metallic lamellar grating, a new unexpected regime in the Casimir force has been observed.

In the last 10 years new behaviors of these interactions have been found, specifically when the systems under scrutiny are in an out of equilibrium, because of dynamic boundary conditions or different temperatures among the objects composing the physical system. For example, it has been predicted and observed that when the system is in an out of thermal equilibrium, there is the possibility to observe a repulsive Casimir force, contrarily to typical Casimir interactions at equilibrium. Similarly, when the dynamical atom-wall Casimir-Polder interaction is studied under non-adiabatic conditions, it has been found that the atom-wall force shows an oscillating attractive to repulsive character.

In the work discussed in this thesis, inspired by the results mentioned above, we have in-

vestigated Casimir and Casimir-Polder forces in these out of equilibrium scenarios (thermal and dynamical). The main reasons behind our studies are two: fundamental theoretical research and possible experimental and/or technological applications.

The fundamental aim of our work is to increase the knowledge in one of the most important theory in physics, Quantum Electrodynamics, and related effects. This goal can be well described from the following words of the Nobel Laureate in Physics Claude Cohen-Tannoudji in an interview at the conference "La scienza della materia in Italia: idee e progetti di nuova organizzazione", September 17th 2007, Rome:

> "... I think that is important the applied research, the research that leads to the development of new things, but the core of the research is in basic research. All modern applications that have changed our lives, from the laser to the transistors, are the result of fundamental research. The problem is that we cannot establish of something before we deal with it. The researchers who worked on the laser did not know that the latter would have been applicable in several important fields, they did not know exactly what have been the appropriate usability, and only later they realized it would have been useful. The important thing, in my opinion, is to do quality research, if applied or fundamental research is only a secondary problem..."

Possible experimental and technological applications also inspired our work presented here. In fact, in relatively recent years, it has been shown that Casimir forces are particularly important in micro and nano-technology. They are relevant for the functioning of technological systems such as micro-electromechanical and nano-electromechanical devices. Moreover, Casimir forces may also have a fundamental role in a problematic phenomenon present in some micro and nano-devices, the so-called "stiction", an effect appearing when two surfaces, at a very small distance from each other, come into close proximity and are eventually led to permanently adhere determining the breakdown of the device. Then, studying new out of equilibrium conditions and new possible geometries could permit to control such effects and tune the force by appropriately changing some parameters of the physical system.

This thesis is structured as follows. In Chapter 1 we discuss the background for our original work, that is main aspects of Casimir forces. After a brief introduction on Casimir Physics we analyze the microscopic manifestations of these forces, i.e. the van der Waals and the retarded Casimir-Polder interaction between two atoms. After the derivation of their general expressions, and an analysis of the two regimes of near and far zone, we move on discussing these interactions when macroscopic objects are present. We describe the Casimir-Polder atom-wall interaction, and then derive a general formula for the Casimir effect between two dielectric half-spaces. We also discuss a physical intuitive picture to explain and derive the Casimir force between two perfectly conducting slabs based on vacuum radiation pressure. Finally, we shortly outline the current status of the experimental observations of the Casimir-effect, mentioning some of the experiments historically important in the literature on Casimir physics.

In Chapter 2 we present our work on the Casimir-Polder interaction between atoms, in an out of dynamical equilibrium condition due to their uniformly accelerated motion. Since the effect of the acceleration of the atoms is closely related to the Unruh effect, we start this chapter with a short introduction on this effect. Next we describe some effects of acceleration on Casimir forces already known in the literature. We then present our original work on the Casimir-Polder interaction between two uniformly accelerated atoms. In this work, we have first studied this interaction by means of a semiclassical model, based on vacuum-field spatial correlations, already applied to describe the static Casimir-Polder forces. We show and discuss qualitative modifications of the interaction energy between the two atoms, the connection with the Unruh effect and its possible observability through Casimir-Polder interactions. Succesively, we investigate the same problem with a more rigorous statistical approach, that we develop in detail, finding important qualitative modifications of the Casimir-Polder force in the case of a relativistic scalar field. Moreover, we show how a novel transition in its distance dependence occurs at a new length scale related to the acceleration. We discuss and propose new possible ways to detect the Unruh effect that, to this day, has not yet been observed. Finally, using the same statistical approach, we study the resonance interaction between two uniformly accelerated atoms, when the two atoms (one excited and the other in its ground state) are prepared in a correlated state. Again, we show and discuss the modification of their radiation-mediated interaction for the scalar and electromagnetic field cases and the connection with the Unruh effect.

In Chapter 3 we present our work on a new near-zone effect due to the Casimir-Polder interaction between an atom and an oscillating mirror. In this scenario we first introduce the dynamical Casimir effect, an effect closely related to oscillating mirrors. We consider a system of a dilute gas of Rydberg atoms trapped in front of an oscillating dynamical mirror in a near-field (non retarded) regime. We show that, because of the Casimir-Polder optomechanical coupling between the atom and the oscillating mirror, the atoms can be excited. We find that, using physical parameters currently achievable in the laboratory, the excitation probability of the atoms is significant (about 20%) making possible the observation of this new dynamical Casimir-Polder effect. We stress that the dynamical excitation process that we propose yields an excitation probability of the atoms much larger than that due to the absorption of the real photons emitted by dynamical Casimir effect. This suggests a good possibility to detect such a new effect with current experimental techniques. For this reason, we also present a detailed experimental proposal.

In Chapter 4 we study and obtain original results on another Casimir system in an out of equilibrium condition. This system is composed of two lamellar dielectric gratings in an out of thermal equilibrium configuration. This means that the gratings have a temperature different from each other. Moreover, they are immersed in a thermal bath at a third temperature which in general is not the same of the two gratings temperatures. To study this problem, we use a formal approach already developed in literature that we present at the beginning of the chapter. This formalism makes use of the scattering operators of the bodies under scrutiny. To deduce these operators we use and develop a well-known method, the Fourier Modal Method (FMM). Finally, we present our numerical results on the Casimir force between two dielectric gratings in the out of thermal equilibrium configuration above

described. We investigate the possibility to observe a repulsive Casimir force (effect due to the out-of-thermal-equilibrium condition) and we show how such a system allows us to control and tune the force by varying the temperature and the geometry parameters.

Chapter 1

Casimir forces

Contents

1.1 van der Waals force between neutral molecules **2**

1.1.1 Resonance interaction between molecules 3

1.1.2 Dispersion interaction between molecules 6

1.1.3 Casimir-Polder interaction between atoms at nonzero temperature 12

1.2 Macroscopic manifestation of the vacuum fluctuations **15**

1.2.1 The atom-wall Casimir-Polder interaction 15

1.2.2 The Casimir effect 17

1.2.3 A physical insight about the Casimir effect 20

1.3 Casimir forces and Experiments **22**

References **25**

From Quantum Electrodynamics it is known that the electromagnetic vacuum is equivalent to an infinite ensemble of ground-state harmonic oscillators [1, 2]. The so-called zero-point energy, i.e. the energy of the electromagnetic field when there are not real photons in the system is $E_0 = 1/2 \sum_{\mathbf{k}\lambda} \hbar\omega_k$ where ω_k and $\mathbf{k}$ are, respectively, the frequency and the wavevector of the photon while λ is its polarization. Since the sum is over an infinite set of possible wavevectors, it is evident that this zero-point energy is infinite. Nevertheless the zero-point energy and its fluctuations (which are related to the commutation rules of the electric and the magnetic fields predicted from Quantum Electrodynamics) are responsible for several observable effects, as example the Casimir forces and the Lamb shift.

Since the late nineteenth century, thanks to the work of van der Waals, it is well known that an attractive force between two neutral and non-polar molecules exists [3]. This force is not an electrostatic force because the molecules does not have neither a net charge nor a permanent multipolar moment. Later, works by Keesom, Debye and London confirmed the results of van der Waals obtaining the same characteristic dependence of the interaction from the intermolecule distance [4]. In 1948, with a fully quantum approach and including also retarded effects, Casimir and Polder studied the interactions between two neutral atoms giving a more fundamental explanation of the existence of these forces [5]. The conclusion

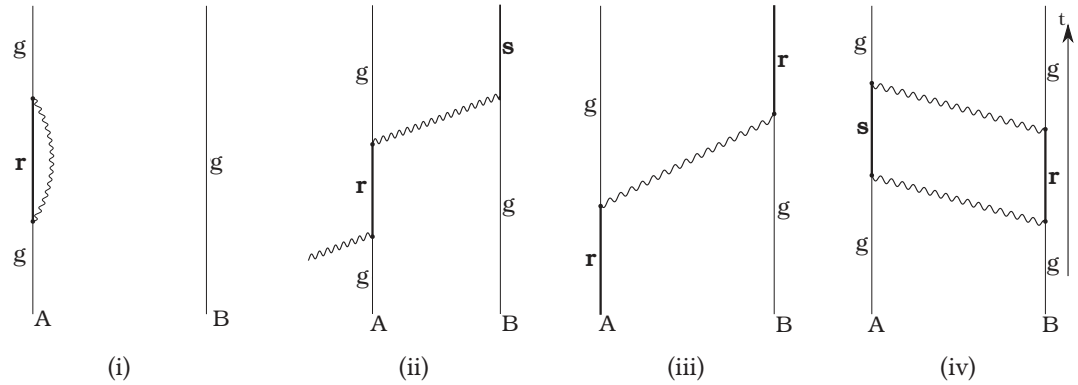

Figure 1.1 – Typical Feynman diagrams that must be considered when we treat the electrodynamic interaction between molecules. The arrow indicates that time flows upwards.

that follows is that vacuum fluctuations are responsible of the force since it is generated from the common interaction of the atoms/molecules with the zero-point electromagnetic field. In the same year, Casimir [6] found a related effect, which can be interpreted as a direct consequence of the vacuum fluctuations, describing an attractive force between two conducting neutral perfectly mirrors at zero temperature in the vacuum space. Successively, in 1956, the Casimir effect was generalized by Lifshitz to bodies having arbitrary optical properties and at finite temperature [7].

In this Chapter we present these effects, that we encase in the expression *Casimir forces* [8, 9]. In Section 1.1, we describe the expressions for the Casimir-Polder (retarded van der Waals) force between two atoms starting from the resonance interaction between two neutral atoms where one of the two atoms is in an excited state. Next we deal with the case of two atoms in the ground state at zero temperature and we distinguish the two limiting cases of near and far zone. We also consider the case of the thermal force. In Section 1.2, we present the Casimir forces when macroscopic bodies are considered. After a simple derivation of the atom-wall force, we introduce the Lifshitz formula and analyze the force between two perfectly conducting plate, giving an intuitive physical interpretation for this force. We conclude the Chapter giving in Section 1.3 an outline of the current situation of the experiments for measuring Casimir forces.

1.1 van der Waals force between neutral molecules

In this Section we focus on the van der Waals forces for atoms/molecules which do not have a permanent dipole moment (possible interactions due to quadrupole or higher multipole moments will be neglected) and we consider retardation effects (i.e. effects related to the finite speed of the light). We use the multipolar coupling formalism, which means that the interactions between the molecules are due to the exchange of transverse virtual photons. In Figure 1.1 typical Feynman diagrams relative to this case are shown. The diagram (i) of

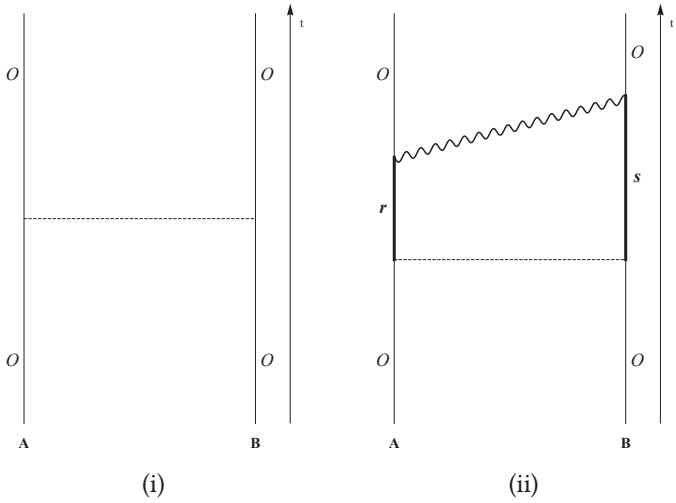

Figure 1.2 – Typical Feynman diagrams describing the electrostatic interaction between molecules. The horizontal line denotes instantaneous photon exchange.

Figure 1.1 is not considered in our calculations because there is not any photon exchange between the molecules, it does not describe an interaction between them. Also the diagram (ii) of Figure 1.1 is neglected because no external electromagnetic field is supposed. As a consequence, we will focus on the diagrams like those in Figure 1.1(iii) and 1.1(iv). When also the electrostatic interactions are considered there are two more kinds of diagrams that describe the interaction between the two molecules (see Figure 1.2). These, in the electric dipole approximation, give the following interaction energy [10]

$$V_{AB} = \frac{\mu_i^A \mu_j^B}{R^3} \left(\delta_{ij} - 3\hat{R}_i\hat{R}_j\right) \tag{1.1}$$

where $\boldsymbol{\mu}_i$ $(i = A, B)$ are the electric dipole moments and $\mathbf{R}$ the intermolecular distance vector. A CGS system of units (where not otherwise specified) is used from now on. Equation (1.1) will be used in Chapter 3 to describe the interaction between a dipole and its image dipole.

1.1.1 Resonance interaction between molecules

We now consider the resonance interaction between atoms/molecules. As we already said, this is the electromagnetic interaction between two neutral polarizable atoms/molecules where one of the two atoms is not in the ground state. We label with A and B the two identical molecules having an energy E_g in the ground state $\left|E_g\right\rangle$ and an energy E_e in the generic excited state $|E_e\rangle$. As a consequence, the generic states of the system $|E_g^A, E_e^B\rangle$ and $|E_e^A, E_g^B\rangle$ are degenerate with energy $E_g + E_e$. Let us suppose that in the initial condition the molecule A is in the excited state while the molecule B is in the ground state. In this system the excitation will oscillate from A to B and vice versa (see for example [11], [10] where a

two level system is analyzed). We can consider the following symmetric and antisymmetric states, where the excitation is delocalized between the two atoms,

$$|\Psi_{\pm}\rangle = \frac{1}{\sqrt{2}}\left(|E_e^A, E_g^B\rangle \pm |E_g^A, E_e^B\rangle\right). \tag{1.2}$$

We also consider the interaction Hamiltonian H_{int} in the Coulomb gauge and in the multipolar coupling scheme [10], [12]. In the electric dipole approximation, we have

$$H_{int} = -\boldsymbol{\mu}(A)\cdot\mathbf{E}(\mathbf{R_A}) - \boldsymbol{\mu}(\mathbf{B})\cdot\mathbf{E}(\mathbf{R_B}) \tag{1.3}$$

where we used $\mathbf{E}$ instead of $\mathbf{D}^{\perp}$ because, outside the atoms, the transverse displacement field coincides with the total (longitudinal plus transversal) field. The explicit expression for the electric field operator is

$$\mathbf{E}(\mathbf{r}) = \sum_{\mathbf{k},\lambda} i\left(\frac{2\pi\hbar ck}{V}\right)^{1/2}\left(\hat{\epsilon}_{\mathbf{k}_\lambda}\, a_{\mathbf{k}_\lambda} e^{i\mathbf{k}\cdot\mathbf{r}} - \hat{\epsilon}^*_{\mathbf{k}_\lambda}\, a^\dagger_{\mathbf{k}_\lambda} e^{-i\mathbf{k}\cdot\mathbf{r}}\right) \tag{1.4}$$

where $\hat{\epsilon}_{\mathbf{k}_\lambda}$ is the polarization unit vector, while $a_{\mathbf{k}_\lambda}$ and $a^\dagger_{\mathbf{k}_\lambda}$ are, respectively, the annihilation and creation field operators. We want to calculate the resonance interaction with the help of the perturbation theory. As we can see from Feynman diagrams, the possible diagrams describing the resonance interaction have at least two vertices and then we need at least a second-order expansion in the perturbation theory (M_{fi} is the second-order amplitude for the energy transfer between the two atoms)

$$M_{fi} = \sum_I \frac{\langle f|H_{int}|I\rangle\langle I|H_{int}|i\rangle}{E_i - E_I}. \tag{1.5}$$

In the above equation, assuming the field in its vacuum state $|0\rangle$ with no photons, we denoted with $|i\rangle$ and $|f\rangle$ the following initial and final states

$$\begin{aligned} |i\rangle &= |E_e^A, E_g^B; 0\rangle, \\ |f\rangle &= |E_g^A, E_e^B; 0\rangle. \end{aligned} \tag{1.6}$$

The intermediate states $|I\rangle$ are shown in Figure 1.3. The matrix elements of the interaction Hamiltonian related to the diagram (i) are

$$\langle I|H_{int}|i\rangle = \langle 1_{\mathbf{k},\lambda}; E_g^B, E_g^A|H_{int}|E_e^A, E_g^B; 0\rangle = i\sum_{\mathbf{k},\lambda}\left(\frac{2\pi\hbar ck}{V}\right)^{1/2} \hat{\epsilon}^*_{i,\mathbf{k}_\lambda}\,\mu_i^{ge}(A)\, e^{-i\mathbf{k}\cdot\mathbf{R_A}}, \tag{1.7}$$

$$\langle f|H_{int}|I\rangle = \langle 0; E_e^B, E_g^A|H_{int}|E_g^A, E_g^B; 1_{\mathbf{k},\lambda}\rangle = -i\sum_{\mathbf{k},\lambda}\left(\frac{2\pi\hbar ck}{V}\right)^{1/2} \hat{\epsilon}_{j,\mathbf{k}_\lambda}\,\mu_j^{eg}(B)\, e^{i\mathbf{k}\cdot\mathbf{R_B}} \tag{1.8}$$

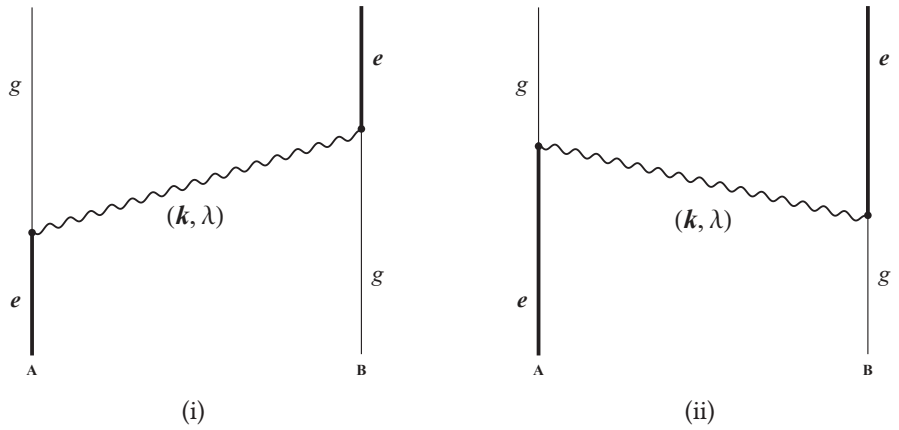

Figure 1.3 – Feynman diagrams involved in the calculation of the resonance interaction in the dipole approximation.

where we have introduced, respectively, the electric dipole matrix elements $\mu^{\mathbf{ge}}$ and $\mu^{\mathbf{eg}} = \mu^{\mathbf{ge}*}$ between the excited states and the ground states and vice versa. Then, the contribution to M given from the diagram (i) is

$$\sum_{\mathbf{k},\lambda} \left(\frac{2\pi\hbar ck}{V}\right) \hat{\epsilon}^*_{\mathbf{k}_\lambda}\, \hat{\epsilon}_{\mathbf{k}_\lambda}\, \mu^{ge}_i(A)\, \mu^{eg}_j(B)\, \frac{e^{i\mathbf{k}\cdot\mathbf{R}}}{E_{eg} - \hbar ck} \tag{1.9}$$

where $\mathbf{R} = \mathbf{R_B} - \mathbf{R_A}$ is the intermolecular distance and $E_{eg} = E_e - E_g$ is proportional to the atomic transition frequency. Proceeding similarly for the contribution of the diagram (ii), we finally get

$$M = \sum_{\mathbf{k},\lambda} \left(\frac{2\pi\hbar ck}{V}\right) \hat{\epsilon}^*_{i,\mathbf{k}_\lambda}\, \hat{\epsilon}_{j,\mathbf{k}_\lambda} \left[\mu^{ge}_i(A)\, \mu^{eg}_j(B)\, \frac{e^{i\mathbf{k}\cdot\mathbf{R}}}{E_{eg} - \hbar ck} + \mu^{ge}_j(A)\, \mu^{eg}_i(B)\, \frac{e^{-i\mathbf{k}\cdot\mathbf{R}}}{-E_{eg} - \hbar ck}\right]. \tag{1.10}$$

Exploiting the following property of the polarization unit vectors

$$\sum_{\lambda} \hat{\epsilon}_{i,\mathbf{k}_\lambda} \hat{\epsilon}^*_{j,\mathbf{k}_\lambda} = \left(\delta_{ij} - \hat{k}_i \hat{k}_j\right) \tag{1.11}$$

and transforming the sum over $\mathbf{k}$ in an integral

$$\sum_{\mathbf{k}} \longrightarrow \int \frac{V}{(2\pi)^3}\, k^2 dk\, d\Omega, \tag{1.12}$$

after some algebra and appropriate regularizations of the frequency integrals, we finally obtain

$$M = \mu^{ge}_i(A)\, \mu^{eg}_j(B)\, V_{ij}(K_e R) \tag{1.13}$$

where $V_{ij}(K_eR)$ is the retarded potential tensor (see [13])

$$V_{ij}(K_eR) = \frac{1}{R^3}\left[\left(\delta_{ij} - 3\hat{R}_i\hat{R}_j\right)\left(\cos(K_eR) + K_eR\sin(K_eR)\right) - \left(\delta_{ij} - \hat{R}_i\hat{R}_j\right) K_e^2R^2\cos(K_eR)\right] \tag{1.14}$$

and $K_e = E_{eg}/\hbar c$. We want to stress that the equation (1.14) is formally identical to the classical interaction, averaged in an oscillation cycle, between two dipoles oscillating at the same frequency.

Let us analyze the resonance interaction energy given by (1.13). In the limit of small intermolecular distances (*near zone*), i.e. for $K_eR \ll 1$ we recover the Coulombian interaction (1.1) between two static dipoles with a dependence with R^{-3} [14]. The opposite limit of large distance ($K_eR \gg 1$, *far zone*) the significant term in (1.14) has a dependence with R^{-1}. This is a quantum effect leading to a slower decreasing interaction between the atomic dipoles in the far zone, in the case of correlated states.

1.1.2 Dispersion interaction between molecules

We study in this subsection the dispersion interaction between two molecules both in their ground state. The result that we will now show takes into account the effects related to finite speed of light. The consequence of this is that, at relatively large distances, the interaction changes its dependence with the distance from R^{-6} (van der Waals) to R^{-7} (Casimir-Polder regime) [5].

Differently from the case of the resonance interaction we need a fourth-order expansion in the perturbative theory, as it is possible to see analyzing the Feynman diagrams. The second-order terms do not give contribution to the interatomic energy but only to the Lamb shift of the atoms and related effects [12], [15], [16]. The fourth-order interaction energy shift is given by

$$\begin{aligned}\Delta E = &\sum_{I,II,III} \frac{\langle 0|H_{int}|III\rangle\langle III|H_{int}|II\rangle\langle II|H_{int}|I\rangle\langle I|H_{int}|0\rangle}{\left(E_g - E_I\right)\left(E_g - E_{II}\right)\left(E_g - E_{III}\right)} \\ &- \sum_{I,II} \frac{\langle 0|H_{int}|II\rangle\langle II|H_{int}|0\rangle\langle 0|H_{int}|I\rangle\langle I|H_{int}|0\rangle}{\left(E_g - E_I\right)^2\left(E_g - E_{II}\right)}.\end{aligned} \tag{1.15}$$

According to perturbation theory developed by Rayleigh and Schrödinger, the second term in the above equation does not give any contribution for non-polar molecules so we focus only to the first term. Again, we use the multipolar Hamiltonian (1.3) in the electric dipole approximation. Atoms A and B, as mentioned, are both in their ground state. As an example, the states involved in the above equation are in the form

$$\begin{aligned}|0\rangle &= |E_g^A, E_g^B; 0\rangle, \\ |I\rangle &= |E_r^A, E_g^B; 1_{\mathbf{k}'}\rangle, \\ |II\rangle &= |E_g^A, E_g^B; 1_{\mathbf{k},\lambda}, 1_{\mathbf{k}',\lambda'}\rangle, \\ |III\rangle &= |E_r^A, E_g^B; 1_{\mathbf{k}',\lambda}\rangle.\end{aligned}$$

The unperturbed state denoted with $|0\rangle$ describes the state where both molecules are in the ground state g and the electromagnetic field is in its vacuum state. The possible intermediate states are represented in Figure 1.4.

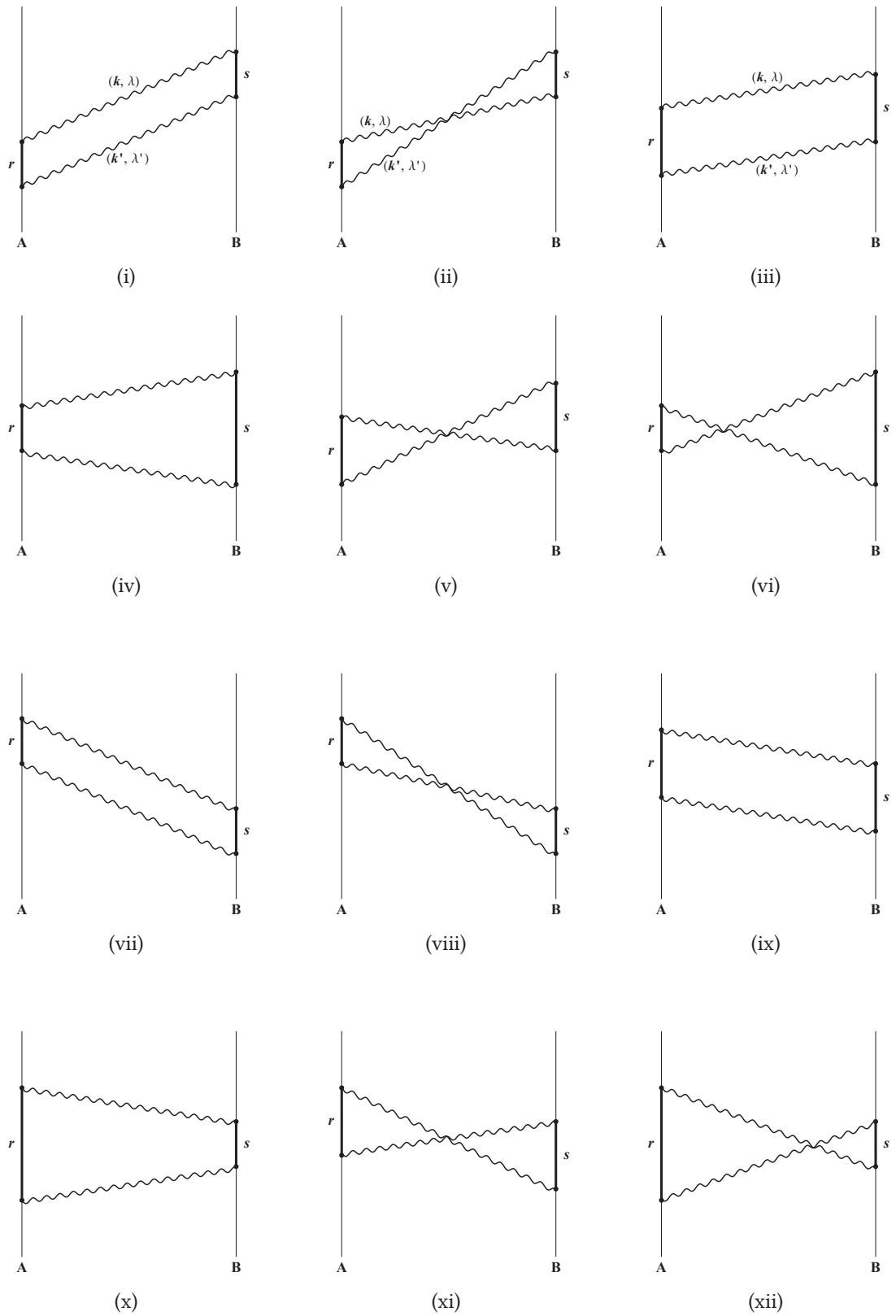

Figure 1.4 – Feynman diagrams involved in the calculation of the dispersion interaction between two ground-state molecules.

Let us consider, for example, the contribution to the energy shift given by the diagram (i) of Figure 1.4. Starting from

$$\begin{aligned}
\langle 0|H_{int}|III\rangle &= -i\left(\frac{2\pi\hbar ck}{V}\right)^{1/2} \hat{\epsilon}_{a,\mathbf{k}_\lambda}\, \mu_a^{gs}(B)\, e^{i\mathbf{k}\cdot\mathbf{R_B}},\\
\langle III|H_{int}|II\rangle &= -i\left(\frac{2\pi\hbar ck'}{V}\right)^{1/2} \hat{\epsilon}_{b,\mathbf{k}'_{\lambda'}}\, \mu_b^{sg}(B)\, e^{i\mathbf{k}'\cdot\mathbf{R_B}},\\
\langle II|H_{int}|I\rangle &= i\left(\frac{2\pi\hbar ck}{V}\right)^{1/2} \hat{\epsilon}^*_{i,\mathbf{k}_\lambda}\, \mu_i^{gr}(A)\, e^{-i\mathbf{k}\cdot\mathbf{R_A}},\\
\langle I|H_{int}|0\rangle &= i\left(\frac{2\pi\hbar ck'}{V}\right)^{1/2} \hat{\epsilon}^*_{j,\mathbf{k}'_{\lambda'}}\, \mu_j^{rg}(A)\, e^{-i\mathbf{k}'\cdot\mathbf{R_A}}
\end{aligned} \tag{1.16}$$

we obtain, using (1.11), the following contribution

$$\begin{aligned}
-\sum_{\mathbf{k},\mathbf{k}'}\sum_{r,s}&\left(\frac{2\pi\hbar ck}{V}\right)\left(\frac{2\pi\hbar ck'}{V}\right)\left(\delta_{ia}-\hat{k}_i\hat{k}_a\right)\left(\delta_{jb}-\hat{k}'_j\hat{k}'_b\right)\times\\
&\times\mu_i^{gr}\,\mu_j^{rg}\,\mu_a^{gs}\,\mu_b^{sg}\,\frac{e^{i(\mathbf{k}+\mathbf{k}')\cdot\mathbf{R}}}{\left(E_{sg}+\hbar ck\right)(\hbar ck+\hbar ck')\left(E_{rg}+\hbar ck'\right)}
\end{aligned} \tag{1.17}$$

where we omitted the labels (A) and (B) for the electric dipoles $\boldsymbol{\mu}$ (this is because the states r and s are unequivocally related, respectively, to A and B). For the other contributions of the diagrams in Figure 1.4 the procedure is analogous. If we consider that making the substitution $\mathbf{k}\to-\mathbf{k}$ and/or $\mathbf{k}'\to-\mathbf{k}'$, the exponential remain $e^{i(\mathbf{k}+\mathbf{k}')\cdot\mathbf{R}}$, the difference between the various terms are due only to the denominator in (1.17). These denominators D_l are listed in Table 1.1. For each diagram the contribution is

$$-\sum_{\mathbf{k},\mathbf{k}'}\sum_{r,s}\left(\frac{2\pi\hbar ck}{V}\right)\left(\frac{2\pi\hbar ck'}{V}\right)\left(\delta_{ia}-\hat{k}_i\hat{k}_a\right)\left(\delta_{jb}-\hat{k}'_j\hat{k}'_b\right)\mu_i^{gr}\,\mu_j^{rg}\,\mu_a^{gs}\,\mu_b^{sg}\,\frac{e^{i(\mathbf{k}+\mathbf{k}')\cdot\mathbf{R}}}{D_l}. \tag{1.18}$$

It is worth to note that the energies of the intermediate states are higher than the energy of the ground state and so the energy shift is negative. This can be interpreted as the molecules take energy from the quantum vacuum for a short period related to the Heisenberg time-energy uncertainty principle ($\Delta E\,\Delta t\geq\hbar$), so generating an attractive interaction.

We now need to sum over all contributions (1.18). As in the resonance case, transforming the sum over $\mathbf{k}$ and $\mathbf{k}'$ into integrals and using (1.11), after some algebra the energy shift can be cast as

$$\Delta E=-\frac{\hbar c}{\pi R^2}\int_0^\infty \alpha(A;iu)\alpha(B;iu)\left[1+\frac{2}{uR}+\frac{5}{u^2R^2}+\frac{6}{u^3R^3}+\frac{3}{u^4R^4}\right]u^4e^{-2uR}\,du \tag{1.19}$$

which is the result obtained by Casimir and Polder [5]. In the above equation we supposed that the molecules can rotate in every direction with the same probability and we

Diagram	Denominator
(i)	$\left(E_{sg}+\hbar ck\right)(\hbar ck+\hbar ck')\left(E_{rg}+\hbar ck'\right)$
(ii)	$\left(E_{sg}+\hbar ck'\right)(\hbar ck+\hbar ck')\left(E_{rg}+\hbar ck'\right)$
(iii)	$\left(E_{sg}+\hbar ck\right)\left(E_{rg}+E_{sg}\right)\left(E_{rg}+\hbar ck'\right)$
(iv)	$\left(E_{sg}+\hbar ck\right)\left(E_{rg}+E_{sg}\right)\left(E_{sg}+\hbar ck'\right)$
(v)	$\left(E_{sg}+\hbar ck'\right)\left(E_{rg}+E_{sg}+\hbar ck+\hbar ck'\right)\left(E_{rg}+\hbar ck'\right)$
(vi)	$\left(E_{sg}+\hbar ck'\right)\left(E_{rg}+E_{sg}+\hbar ck+\hbar ck'\right)\left(E_{sg}+\hbar ck\right)$
(vii)	$\left(E_{rg}+\hbar ck\right)(\hbar ck+\hbar ck')\left(E_{sg}+\hbar ck'\right)$
(viii)	$\left(E_{rg}+\hbar ck\right)(\hbar ck+\hbar ck')\left(E_{sg}+\hbar ck'\right)$
(ix)	$\left(E_{rg}+\hbar ck\right)\left(E_{rg}+E_{sg}\right)\left(E_{sg}+\hbar ck'\right)$
(x)	$\left(E_{rg}+\hbar ck\right)\left(E_{rg}+E_{sg}\right)\left(E_{rg}+\hbar ck'\right)$
(xi)	$\left(E_{rg}+\hbar ck\right)\left(E_{rg}+E_{sg}+\hbar ck+\hbar ck'\right)\left(E_{sg}+\hbar ck'\right)$
(xii)	$\left(E_{rg}+\hbar ck\right)\left(E_{rg}+E_{sg}+\hbar ck+\hbar ck'\right)\left(E_{rg}+\hbar ck\right)$

Table 1.1 – The D_l denominators appearing in (1.18).

introduced the isotropic dynamic polarizability

$$\alpha(k)=\frac{2}{3\,\hbar c}\sum_{e}\frac{k_{eg}\,|\mu^{eg}|^2}{k_{eg}^2-k^2}. \tag{1.20}$$

We now analyze the dispersion interaction in the two limit cases of *near zone* and *far zone*.

For small distances $k_{eg}R \ll 1$ (near zone) the virtual photons which significantly contribute to the energy shift are those with energy larger than the typical transition energies of the molecules of the system (that means high k and k'). This statement can be understood by means of the energy-time uncertainty principle. In fact, from this principle it follows that high-energy virtual photons are related to short "life-time"; so these photons do not travel for large distances from the atoms before being reabsorbed; thus they are important for the interaction at small distances and negligible for larger distances. From this analysis we deduce that only some denominators D_l (i.e. only some diagrams) contributes significantly. These denominators are the smaller ones. In particular the denominators which give relevant contribution to the interaction in near zone are D_{iii}, D_{iv}, D_{ix}, D_x because of the presence of the factor $(E_{rg}+E_{sg})$. In this way we can rewrite the shift energy obtaining

$$\Delta E \simeq -4\sum_{\mathbf{k},\mathbf{k}'}\sum_{r,\,s}\left(\frac{2\pi\hbar ck}{V}\right)\left(\frac{2\pi\hbar ck'}{V}\right)\left(\delta_{ia}-\hat{k}_i\hat{k}_a\right)\left(\delta_{jb}-\hat{k}'_j\hat{k}'_b\right)\mu_i^{gr}\,\mu_j^{rg}\,\mu_a^{gs}\,\mu_b^{sg}$$
$$\times\frac{e^{i(\mathbf{k}+\mathbf{k}')\cdot\mathbf{R}}}{(\hbar ck)\,(\hbar ck')\left(E_{rg}+E_{sg}\right)} \tag{1.21}$$

where the factor 4 is due to the fact that the four mentioned denominators under scrutiny give equal contributions. In the continuum limit we get

$$\Delta E \simeq -\frac{4}{\pi^2} \sum_{r,s} \frac{\mu_i^{gr}\,\mu_j^{rg}\,\mu_a^{gs}\,\mu_b^{sg}}{E_{rg}+E_{sg}} \iint \left(\delta_{ia}-\hat{k}_i\hat{k}_a\right)\left(\delta_{jb}-\hat{k}'_j\hat{k}'_b\right) e^{i\,\mathbf{k}\cdot\mathbf{R}}\, e^{i\,\mathbf{k}'\cdot\mathbf{R}}\, \frac{d^3k}{4\pi}\,\frac{d^3k'}{4\pi}. \tag{1.22}$$

After the angular integration and the integration over k and k' we can write

$$\Delta E \simeq -\frac{1}{R^6} \sum_{r,s} \frac{\mu_i^{gr}\,\mu_j^{rg}\,\mu_a^{gs}\,\mu_b^{sg}}{E_{rg}+E_{sg}} \left(\delta_{ia}-\hat{R}_i\hat{R}_a\right)\left(\delta_{jb}-\hat{R}_j\hat{R}_b\right) \tag{1.23}$$

This result is identical to that deduced considering a second-order perturbative expansion of the interaction Hamiltonian (1.1) which describes the interaction between two static dipoles. If, for example, we consider that the molecules freely rotate in every direction, the equation (1.23) becomes

$$\Delta E = -\frac{2}{3\,R^6} \sum_{r,s} \frac{|\boldsymbol{\mu}^{rg}|^2\,|\boldsymbol{\mu}^{sg}|^2}{E_{rg}+E_{sg}} \tag{1.24}$$

which has the typical R^{-6} dependence of London/van der Waals forces.

A similar expression of the above equation but written in terms of atomic polarizabilities can be deduced using the following identity

$$\frac{1}{E_{rg}+E_{sg}} = \frac{1}{\pi}\int_{-\infty}^{+\infty} \frac{E_{rg}\,E_{sg}}{\left(E_{rg}^2+u^2\right)\left(E_{sg}^2+u^2\right)}\,du. \tag{1.25}$$

As a consequence, using the definition of the dynamical polarizability in (1.20), introducing the imaginary frequency $u = -i\,\hbar\omega$, we finally get

$$\Delta E = -\frac{3\,\hbar c}{2\,\pi\,R^6} \int_{-\infty}^{+\infty} \alpha^A(iu)\,\alpha^B(iu)\,du. \tag{1.26}$$

Let us consider now the far zone case, i.e. $k_{eg}R \gg 1$. In this regime, with the same considerations done before for the near zone regime, the frequencies k e k' of the virtual photons which contribute significantly to the energy shift are much smaller than the frequency involved in the molecule transitions. Analyzing the denominators in Table 1.1, only the diagrams (and then the relative denominators) (i), (ii), (vii), (viii) give a significant contribution to the energy shift in the far zone. The reason is that the presence of the factor $(\hbar ck + \hbar ck')$ implies a more important contribution to ΔE than the remaining terms. The denominators relative to these diagrams are rewritten as $E_{rg}\,E_{sg}\,(\hbar ck + \hbar ck')$. In this way we can get the energy shift

$$\Delta E \simeq -4 \sum_{\mathbf{k},\mathbf{k}'} \sum_{r,\,s} \left(\frac{2\pi\hbar ck}{V}\right)\left(\frac{2\pi\hbar ck'}{V}\right)\left(\delta_{ia}-\hat{k}_i\hat{k}_a\right)\left(\delta_{jb}-\hat{k}'_j\hat{k}'_b\right)\mu_i^{gr}\,\mu_j^{rg}\,\mu_a^{gs}\,\mu_b^{sg}\,\times$$
$$\times\,\frac{e^{i(\mathbf{k}+\mathbf{k}')\cdot\mathbf{R}}}{E_{rg}\,E_{sg}\,(\hbar ck+\hbar ck')} \tag{1.27}$$

where the factor 4 is due to the identical contribution given from each diagram considered. Again,we assume that the molecules are freely rotating, so

$$\Delta E = -\frac{4}{9}\sum_{\mathbf{k},\mathbf{k}'}\sum_{r,s}\left(\frac{2\pi\hbar ck}{V}\right)\left(\frac{2\pi\hbar ck'}{V}\right)\left(1+\left(\hat{\mathbf{k}}\cdot\hat{\mathbf{k}}'\right)^2\right)\frac{|\boldsymbol{\mu}^{rg}|^2\,|\boldsymbol{\mu}^{sg}|^2}{E_{rg}\,E_{sg}}\frac{e^{i(\mathbf{k}+\mathbf{k}')\cdot\mathbf{R}}}{(\hbar ck+\hbar ck')}. \tag{1.28}$$

We introduce the isotropic static polarizability of the two atoms

$$\begin{aligned}\alpha(A) &= \frac{2}{3}\sum_{r}\frac{|\boldsymbol{\mu}^{rg}|^2}{E_{rg}},\\ \alpha(B) &= \frac{2}{3}\sum_{s}\frac{|\boldsymbol{\mu}^{sg}|^2}{E_{sg}}\end{aligned} \tag{1.29}$$

and going to the continuum limit, the energy shift becomes

$$\Delta E \simeq -\frac{\hbar c}{(2\pi)^4}\alpha(A)\,\alpha(B)\int\left(1+\left(\hat{\mathbf{k}}\cdot\hat{\mathbf{k}}'\right)^2\right)k^3\,k'^3\,\frac{e^{i(\mathbf{k}+\mathbf{k}')\cdot\mathbf{R}}}{(k+k')}\,dk\,dk'\;d\Omega\,d\Omega'. \tag{1.30}$$

After some standard algebraic calculation we finally obtain

$$\begin{aligned}\Delta E &\simeq -\frac{16\,\hbar c}{\pi^2}\,\frac{\alpha(A)\,\alpha(B)}{R^7}\int_0^\infty\frac{1}{(\eta^2+1)^6}\left(3\eta^4-2\eta^2+3\right)d\eta\\ &\simeq -\frac{23\,\hbar c}{4\,\pi}\,\frac{\alpha(A)\,\alpha(B)}{R^7}\end{aligned} \tag{1.31}$$

i.e. the standard attractive Casimir-Polder force having the well known R^{-7} dependence. This shows that, at large distance, the potential decreases more rapidly with the distance compared to the van der Waals potential [5].

1.1.3 Casimir-Polder interaction between two atoms at nonzero temperature

In the previous sections we discussed the Casimir-Polder interaction between molecules at zero temperature. However, these interactions are also present when the atoms/molecules interact with thermal radiation at a temperature different from zero. This means that real thermal photons are present in addition to the virtual ones. Thus, considering the Feynman diagrams in Figure 1.1, we must analyze also processes like that depicted in the diagram of Figure 1.1(ii). Using the perturbative approach adopted in the previous sections we can again calculate the Casimir-Polder force and obtain the energy shift due to the atom-field interaction. A condition to obtain this is the preparation of the uncoupled system in an energy eigenstate. A possibility is an incoherent superposition of energy eigenstates $|\psi\rangle$ with probabilities p_ψ described by the density matrix

$$\rho = \sum_{\psi} p_\psi|\psi\rangle\langle\psi|. \tag{1.32}$$

The energy shift is then defined as

$$\langle \Delta E \rangle = \sum_{\psi} p_{\psi} \langle \psi | H_{\text{int}} | \psi \rangle + \sum_{\psi} p_{\psi} \sum_{I \neq \psi} \frac{\langle \psi | H_{\text{int}} | I \rangle \langle I | H_{\text{int}} | \psi \rangle}{E_{\psi} - E_I} + \dots \tag{1.33}$$

Starting from this energy shift it is possible to calculate the Casimir-Polder interaction between two atoms at nonzero temperature [17]. However, here we want to show another approach to perform this calculation. There are many alternative models to explain the dispersion forces (see for example [18]-[23]), but our choice in this section falls on a simple and intuitive model. The key idea of this approach is the following: the field fluctuations induce instantaneous dipole moments in the two atoms, which are correlated because vacuum fluctuations are spatially correlated; the Casimir-Polder potential energy then arises from the classical interaction between the oscillating dipoles of the atoms induced and correlated by the vacuum fluctuations [24].

The induced dipole moments in the atoms are related to the fluctuating quantum field by the following relation (assuming isotropic atoms)

$$\mu_l(\mathbf{k}_\lambda) = \alpha(k) E_l(\mathbf{k}_\lambda, \mathbf{r}) \tag{1.34}$$

where we used the dynamical polarizability $\alpha(k)$ of the atoms introduced in (1.20). In the above equation $E_l(\mathbf{k}_\lambda, \mathbf{r})$ is the l component of the $\mathbf{k}_\lambda$ Fourier component of the electric field operator defined in (1.4). In the multipolar coupling it coincides with the transverse displacement field $D_l(\mathbf{k}_\lambda, \mathbf{r})$ [12]. The Casimir-Polder interaction energy in this approach is the following

$$\begin{aligned} W_{\text{AB}}(R) = &\sum_{\mathbf{k},\lambda} \langle \mu_l^{\text{A}}(\mathbf{k}_\lambda) \mu_m^{\text{B}}(\mathbf{k}_\lambda) \rangle V_{lm}(R) \\ &\sum_{\mathbf{k},\lambda} \alpha_{\text{A}}(k) \alpha_{\text{B}}(k) \langle E_l(\mathbf{k}_\lambda, \mathbf{r}_{\text{A}}) E_m(\mathbf{k}_\lambda, \mathbf{r}_{\text{B}}) \rangle V_{lm}(k, R) \end{aligned} \tag{1.35}$$

where $R = |\mathbf{r}_{\text{B}} - \mathbf{r}_{\text{A}}|$ is the interatomic distance while $V_{lm}(k, R)$ is the classical electromagnetic potential tensor, identical to that obtained in (1.14), between two oscillating dipoles at frequency $\omega = ck$.

As we can see in (1.35), we need to evaluate the spatial correlation function of the electric field $\langle E_l(\mathbf{k}_\lambda, \mathbf{r}_{\text{A}}) E_m(\mathbf{k}_\lambda, \mathbf{r}_{\text{B}}) \rangle$, that should be calculated on the state of the field that we are analyzing, i.e. the equilibrium thermal state at temperature T. This means that

$$\langle a^\dagger_{\mathbf{k}_\lambda} a_{\mathbf{k}_\lambda} \rangle = \frac{1}{e^{\hbar kc/k_B T} - 1} \tag{1.36}$$

where k_B is the Boltzmann constant. At this stage we have made the assumption $k_B T \ll \hbar\omega_0$, where ω_0 is a typical transition frequency of the atoms. In fact, we are considering situations where the atomic excitation is negligible. In a way similar to the cases previously considered, we go to the continuum limit exploiting the equation (1.36), and after some algebraic calculations we have

$$\sum_{\lambda} \int d\Omega_k \langle E_l(\mathbf{k}_\lambda, \mathbf{r}_{\text{A}}) E_m(\mathbf{k}_\lambda, \mathbf{r}_{\text{B}}) \rangle = \frac{8\pi^2 \hbar ck}{V} \coth\left(\frac{\hbar ck}{2k_B T}\right) \tau_{lm}(k, R) \tag{1.37}$$

where we have introduced the tensor

$$\tau_{lm}(kR) \equiv \frac{1}{4\pi}\int \left(\delta_{lm} - \hat{k}_l\hat{k}_m\right) e^{\pm i\mathbf{k}\cdot\mathbf{R}}\, d\Omega = \\ = \left(\delta_{lm} - 3\hat{R}_l\hat{R}_m\right)\left(\frac{\cos(kR)}{k^2R^2} - \frac{\sin(kR)}{k^3R^3}\right) + \left(\delta_{lm} - \hat{R}_l\hat{R}_m\right)\frac{\sin(kR)}{kR}. \tag{1.38}$$

Finally, after some algebraic manipulations, we obtain the general expression for the Casimir-Polder interaction energy [25]

$$W_{\mathrm{AB}}(R) = -\frac{\hbar c}{\pi R^3}\int dk\, k^3 \alpha_{\mathrm{A}}(k)\,\alpha_{\mathrm{B}}(k)\coth\left(\frac{\hbar c k}{2k_BT}\right) \\ \times\left[kR\sin(2kR) + 2\cos(2kR) - 5\frac{\sin(2kR)}{kR} - 6\frac{\cos(2kR)}{k^2R^2} + 3\frac{\sin(2kR)}{k^3R^3}\right]. \tag{1.39}$$

We notice that the temperature dependence of this interaction energy is inside the hyperbolic cotangent. Let us analyze this expression considering the two limiting cases of near and far zone.

In the near zone, since $kR \ll 1$, equation (1.39) reduces to

$$W_{\mathrm{AB}}(R) = -\frac{3\hbar c}{\pi R^6}\int dk\, \alpha_{\mathrm{A}}(k)\,\alpha_{\mathrm{B}}(k)\coth\left(\frac{\hbar c k}{2k_BT}\right)\sin(2kR) \tag{1.40}$$

which is identical to the expression obtained, for example, in [26].

In the far-zone regime we can use the static polarizabilities $\alpha_{\mathrm{A,B}} = \alpha_{\mathrm{A,B}}(0)$ introduced in (1.29) in place of the dynamical polarizabilities, and after the k integration we finally get

$$W_{\mathrm{AB}}(R) = \alpha_A\alpha_B\, k_BT\, D^R \coth\left(\frac{2\pi k_BTR}{\hbar c}\right) \tag{1.41}$$

where we have defined the following differential operator

$$D^r \equiv -\frac{1}{16r^2}\frac{\partial^4}{\partial r^4} + \frac{1}{4r^3}\frac{\partial^3}{\partial r^3} - \frac{5}{4r^4}\frac{\partial^2}{\partial r^2} + \frac{3}{r^5}\frac{\partial}{\partial r} - \frac{3}{r^6}. \tag{1.42}$$

From this expression two additional regimes of the far zone can be considered. A low-temperature regime $2\pi\, k_BT\, R/\hbar c \ll 1$ and an high-temperature regime $2\pi\, k_BT\, R/\hbar c \gg 1$. This means that a new distance scale $\lambda = \hbar c/2\pi\, k_BT$ appears when we consider the far zone case. For distance smaller than this distance scale, the Casimir-Polder energy in (1.41) has a distance-dependence as R^{-7}, the same of the Casimir-Polder far-zone interaction at zero temperature; for distances larger than the new distance scale, the interaction energy has a R^{-6} dependence reproducing the same dependence of the Casimir-Polder near-zone interaction at zero temperature [27] - [29].

1.2 Macroscopic manifestation of the vacuum fluctuations

We have seen that when we consider the atom-field interaction, even in the absence of real photons in the system, interactions between neutral atoms/molecules are originated. Until now we have studied molecular interactions so we have restricted our analysis to a microscopic point of view. The natural macroscopic consequence of these microscopic interactions is the well known and startling Casimir effect [6], [30]. According to it, two perfectly conducting slabs, which have null net charge, placed in the vacuum feel an attractive force, as a consequence of the vacuum fluctuations. The Casimir effect was then considered as an evidence of the existence of the quantum vacuum and of the related zero-point energy. However, Milonni and Schwinger obtained the same Casimir results without explicitly using the assumption of the vacuum fluctuations, but from the source fields [31], [32], [33] (see also the references [34], [35]). The common conclusion is that these effects are strictly related to the quantum nature of the system, the quantum nature of the matter for the source-field picture and the quantum nature of the fields in the vacuum fluctuation picture. They are then important cornerstone of Quantum Mechanics. Another point worth stressing is that, even if the Casimir effect can be considered as a macroscopic manifestation of the microscopic Casimir-Polder forces, it cannot be simply obtained as a sum of the van der Waals forces acting on the atoms composing the macroscopic bodies. The reason is related to the non-additive property of the van der Waals and Casimir-Polder forces [1, 36, 37].

In this section we present two examples of Casimir forces involving macroscopic bodies: the atom-wall Casimir-Polder interaction and the Casimir force between two parallel plates.

1.2.1 The atom-wall Casimir-Polder interaction

Let us analyze the physical system of an atom in front of a perfectly conducting wall in the vacuum. In the regime of small atom-wall distance d (relative to a typical wavelength transition of the atom) the interaction can be simply obtained considering the dipole-dipole interaction between the dipole and its image on the other side of the wall. This because, when the distance is small, the interaction is instantaneous and the retardation effects are negligible. Using the potential introduced in (1.1), we find that the energy interaction has a d^{-3} dependence. In the far zone, i.e. large atom-wall distance, the distance dependence of the interaction is different and the retardation effects become relevant, as for the far zone case of the two-atom system.

A simple derivation of the interaction energy for this case can be easily deduced from the classical potential energy of an electric dipole $U = -\mathbf{p} \cdot \mathbf{E}$. We denoted with $\mathbf{p}$ the electric dipole moment related to the electric field through the relation $\mathbf{p} = \alpha \mathbf{E}$, where α is the static polarizability. From this potential energy we can write the interaction energy

$$W = -\frac{1}{2}\alpha \mathbf{E}^2 \tag{1.43}$$

that found a formal quantum support in [38], [39]. We have inserted a factor 1/2 in the above equation because we are considering that the dipole moment is induced rather than permanent [14].

Equation (1.43) can be generalized to the Stark shift in the atom-wall system

$$W = -\frac{1}{2}\sum_{\mathbf{k},\lambda} \alpha(\omega)\mathbf{E}^2_{\mathbf{k}_\lambda}(\mathbf{r}_\mathrm{A}). \tag{1.44}$$

The quantities $\mathbf{k}$ and λ are, respectively, the wave vector and the polarization index and $\mathbf{E}_{\mathbf{k}_\lambda}(\mathbf{r}_\mathrm{A})$ is the $\mathbf{k}_\lambda$ Fourier component of the electric field evaluated at the position $\mathbf{r}_\mathrm{A}$ of the atom. The presence of the perfect conducting wall in the system impose specific boundary conditions, thus changing the vacuum field. Let us consider first a rectangular box with perfectly conducting surfaces, located in the half space opposite to that where the atom is placed. The sides of this parallelepiped are $L_x = L_y = L$ and L_z. In this situation, the components of the electric field satisfying the specific boundary conditions are

$$\begin{aligned}
E_x(\mathbf{r}) &= \left(\frac{16\pi\hbar\omega}{V}\right)^{1/2} \epsilon_x \cos(k_x x)\sin(k_y y)\sin(k_z z),\\
E_y(\mathbf{r}) &= \left(\frac{16\pi\hbar\omega}{V}\right)^{1/2} \epsilon_y \sin(k_x x)\cos(k_y y)\sin(k_z z),\\
E_z(\mathbf{r}) &= \left(\frac{16\pi\hbar\omega}{V}\right)^{1/2} \epsilon_z \sin(k_x x)\sin(k_y y)\cos(k_z z).
\end{aligned} \tag{1.45}$$

In the above equation we used that $\epsilon_x^2 + \epsilon_y^2 + \epsilon_z^2 = 1$, quantization volume $V = L^2 L_z$ and

$$k_x = \frac{l\pi}{L}, \quad k_y = \frac{m\pi}{L}, \quad k_z = \frac{n\pi}{L_z} \tag{1.46}$$

where $l, m, n \in \mathbb{N}$. Since we are in far zone regime we can replace the dynamical polarizability in (1.44) with the static one $\alpha(0)$. Then, calculating the electric field at the atom position $(L/2, L/2, d)$, (1.44) can be cast as

$$\begin{aligned}
W(d) = -\frac{1}{2}\alpha \sum_{\mathbf{k}} \frac{16\pi\omega_k}{V}\Bigg[&\epsilon_x^2 \cos^2\left(\frac{k_x L}{2}\right)\sin^2\left(\frac{k_y L}{2}\right)\sin^2(k_z z)\\
&+ \epsilon_y^2 \sin^2\left(\frac{k_x L}{2}\right)\cos^2\left(\frac{k_y L}{2}\right)\sin^2(k_z z)\\
&+ \epsilon_z^2 \sin^2\left(\frac{k_x L}{2}\right)\sin^2\left(\frac{k_y L}{2}\right)\cos^2(k_z z)\Bigg].
\end{aligned} \tag{1.47}$$

In the limit $L \to \infty$, the sinusoidal functions related to the components k_x and k_y can be replaced with their average value $1/2$ because they are rapidly oscillating. Then

$$W(d) = -\frac{2\pi\hbar\alpha}{V}\sum_{\mathbf{k}} \omega_k \left[\left(\epsilon_x^2 + \epsilon_y^2\right)\sin^2(k_z d) + \epsilon_z^2 \cos^2(k_z d)\right]. \tag{1.48}$$

We can define the interaction potential $V(d)$ as

$$V(d) = W(d) - W(\infty). \tag{1.49}$$

In the limit $d \to \infty$, also the k_z component in the sinusoidal functions in (1.48) can be replaced with their average value, obtaining

$$W(\infty) = -\frac{2\pi\hbar\alpha}{V}\sum_{\mathbf{k}}\omega_k\left[\frac{1}{2}\left(\epsilon_x^2+\epsilon_y^2+\epsilon_z^2\right)\right] = -\frac{2\pi\hbar\alpha}{V}\sum_{\mathbf{k}}\frac{1}{2}\omega_k. \tag{1.50}$$

We deduce then the potential energy

$$\begin{aligned} V(d) &= -\frac{2\pi\hbar\alpha}{V}\sum_{\mathbf{k}}\omega_k\left[\sin^2(k_z d)-\frac{1}{2}\right]\left(\epsilon_x^2+\epsilon_y^2-\epsilon_z^2\right) \\ &= \frac{\pi\hbar\alpha}{V}\sum_{\mathbf{k}}\omega_k\frac{2k_z^2}{k^2}\cos(2k_z d). \end{aligned} \tag{1.51}$$

In the continuum limit of allowed $\mathbf{k}$, we finally get

$$\begin{aligned} V(d) &= \frac{2\pi\hbar\alpha}{V}\frac{V}{8\pi^3}\int d^3k\,\frac{k_z^2}{k^2}\cos(2k_z d) \\ &= \frac{\alpha\hbar c}{2\pi}\int_0^{+\infty}dk\,k^3\int_0^{2\pi}d\theta\,\sin\theta\cos^2\theta\cos(2k\cos\theta d) \\ &= -\frac{3\alpha\hbar c}{8\pi d^4}. \end{aligned} \tag{1.52}$$

This is the same identical result obtained originally by Casimir in the far zone [6]. From (1.52), we notice that in the far zone, because of retardation effects, the distance-dependence of the atom-wall Casimir-Polder potential is as d^{-4} while in the near zone it is as d^{-3}. The atom-wall force can then be obtained by taking the derivative of $V(d)$ with respect to d, changed of sign.

1.2.2 The Casimir effect

We now consider the Casimir effect, originally obtained for the first time by Casimir in [6], consisting in an attractive force between two perfectly conducting metallic plates. In this subsection, however, we want to present a more general formula analyzing a more general problem, studied for the first time by Lifshitz [7], of two dielectric half-spaces, in thermal equilibrium at a finite temperature, placed in the vacuum and separated from a distance d. The Casimir effect for ideal metallic plates can be obtained as a limiting case dielectric $\to$ metal.

The Lifshitz calculation start from the Maxwell equations in the Fourier space

$$\nabla\times\mathbf{E} = i\frac{\omega}{c}\mathbf{B} \tag{1.53}$$

$$\nabla\times\mathbf{B} = -i\frac{\omega}{c}\varepsilon(\omega)\mathbf{E} - i\frac{\omega}{c}\mathbf{K} \tag{1.54}$$

where nonmagnetic dielectric media are considered. The dielectric constant considered in the two Maxwell equations above is in general complex, $\varepsilon(\omega) = \varepsilon'(\omega) + i\varepsilon''(\omega)$. This

means that both absorption and dispersion are possible. Moreover, we introduced a random fluctuating current $\mathbf{K}$. These two quantities are strictly related. In fact the use of a complex dielectric permittivity in Lifshitz's theory requires a random current $\mathbf{K}$. This is due to the fluctuation-dissipation theorem. From this theorem when an absorbing medium is considered, the dissipative nature of the medium requires a balancing coming from a fluctuating source in a way such that the correlations of the fluctuating field $\mathbf{K}$ are related to the dissipation. The correlation function that Lifshitz assumed is the following

$$\langle K_i(\mathbf{r},\omega)K_j(\mathbf{r}',\omega)\rangle = 2\hbar\varepsilon''(\omega)\delta_{ij}\delta^3(\mathbf{r}-\mathbf{r}'). \tag{1.55}$$

The above correlation function was used by Lifshitz to perform the calculation of $\langle g_i(\mathbf{k})g_j(\mathbf{k}')\rangle$ where $g_i(\mathbf{k})$ are the Fourier components of $\mathbf{K}$ and was used to write the solutions of the Maxwell equations for the field. After some calculations Lifshitz obtained the following formula for the Casimir force

$$\begin{aligned}\frac{F(d)}{A} = &-\frac{\hbar}{2\pi^2c^3}\int_1^{+\infty} dp p^2 \int_0^{+\infty} d\xi\xi^3\times \\ &\times\left[\left(\frac{s_1+\epsilon_1 p}{s_1-\epsilon_1 p}\frac{s_2+\epsilon_2 p}{s_2-\epsilon_2 p}e^{\frac{2\xi pd}{c}}-1\right)^{-1}+\left(\frac{s_1+p}{s_1-p}\frac{s_2+p}{s_2-p}e^{\frac{2\xi pd}{c}}-1\right)^{-1}\right]\end{aligned} \tag{1.56}$$

where $\epsilon_j = \epsilon_j(i\omega)$ and $s_j = \sqrt{p^2-1+\epsilon_j}$ for $j = 1,2$, being 1 and 2 the label for the two slabs. Taking the limit $\epsilon_1,\epsilon_2 \to +\infty$, i.e. perfect conducting plates, the well known Casimir force obtained in [6] is recovered. The power of the formula (1.56) also allows to deduce the Casimir-Polder force between two atoms making the assumption of very rarefied media and exploiting the expression for the dielectric permittivity $\epsilon(\omega) = 1 + 4\pi N\alpha(\omega)$ (where N denotes the number of atoms per unit volume).

We want to discuss briefly a different approach than the Lifshitz one, which allows us to write a more general expression compared to the Lifshitz formula [8]. It is well known from classical electromagnetism that the force density f in a medium, when electromagnetic fields are present, is related to the electromagnetic stress tensor T_{ij}

$$\begin{aligned} f_i = \partial_j T_{ij}, \quad T_{ij} = \frac{1}{4\pi}\left[E_iD_j + H_iH_j - \frac{1}{2}(\mathbf{E}\cdot\mathbf{D}+\mathbf{H}\cdot\mathbf{H})\,\delta_{ij}\right] \Rightarrow \\ f_i = \frac{1}{8\pi}\left[(\partial_i E_j)D_j - E_j(\partial_i D_j)\right]\end{aligned} \tag{1.57}$$

where we assume

$$\frac{1}{4\pi c}\frac{\partial}{\partial t}(\mathbf{D}\times\mathbf{H}) = 0 \tag{1.58}$$

i.e. that, under appropriate equilibrium conditions, the time variation of the momentum density of the field can be considered zero, and we suppose an isotropic media so that the stress tensor T_{ij} is symmetric. From a quantum point of view, we have to promote E_i and D_i to operators. Using the Fourier components of the field, symmetrizing and taking the

expectation values, the force density is

$$f_i(\mathbf{r}) = \frac{1}{8\pi}\,\mathrm{Re}\int_{-\infty}^{+\infty} d\omega \int_{-\infty}^{+\infty} d\omega' \Big\{ \langle \big[\partial_i E_j(\mathbf{r},\omega)\big] D_j(\mathbf{r},\omega')\rangle - \langle E_j(\mathbf{r},\omega)\big[\partial_i D_j(\mathbf{r},\omega')\big]\rangle \Big\}. \tag{1.59}$$

If we consider the Maxwell equations used by Lifshitz in (1.53) and (1.54), the Fourier component of the transverse displacement field is $\mathbf{D}(\mathbf{r},\omega) = \varepsilon(\mathbf{r},\omega)\mathbf{E}(\mathbf{r},\omega) + \mathbf{K}(\mathbf{r},\omega)$, that means

$$\langle E_j(\mathbf{r},\omega)\, D_j(\mathbf{r}',\omega')\rangle = \varepsilon(\mathbf{r},\omega)\langle E_j(\mathbf{r},\omega)\, E_j(\mathbf{r}',\omega')\rangle + \langle E_j(\mathbf{r},\omega)\, K_j(\mathbf{r}',\omega')\rangle. \tag{1.60}$$

We introduce, the dyadic Green function such that

$$-\nabla\times\nabla\times G(\mathbf{r},\mathbf{r}',\omega) + \frac{\omega^2}{c^2}\varepsilon(\mathbf{r},\omega)\, G(\mathbf{r},\mathbf{r}',\omega) = -4\pi\frac{\omega^2}{c^2}\delta^3(\mathbf{r}-\mathbf{r}'), \tag{1.61}$$

and we introduce in the first term of the right side of (1.60) the following form for the correlators [40]

$$\langle E_j(\mathbf{r},\omega)\, E_j(\mathbf{r}',\omega')\rangle = \frac{\hbar}{\pi}\Im\left[G_{jj}(\mathbf{r},\mathbf{r}',\omega)\delta(\omega-\omega')\right]. \tag{1.62}$$

where

$$E_j(\mathbf{r},\omega) = \frac{1}{4\pi}\int d^3r''\, G_{ji}(\mathbf{r},\mathbf{r}'',\omega)K_i(\mathbf{r}'',\omega). \tag{1.63}$$

We also assume that, similarly to (1.55), the operator $\mathbf{K}(\mathbf{r},\omega)$ has the following property, as a consequence of the fluctuation-dissipation theorem,

$$\langle K_i^\dagger(\mathbf{r},\omega)K_j(\mathbf{r}',\omega')\rangle = 0 \tag{1.64}$$

$$\langle K_i(\mathbf{r},\omega)K_j^\dagger(\mathbf{r}',\omega')\rangle = 4\hbar\varepsilon''(\omega)\delta_{ij}\delta(\omega-\omega')\delta^3(\mathbf{r}-\mathbf{r}'), \tag{1.65}$$

where we denoted with $\varepsilon''(\omega)$ the imaginary part of $\varepsilon(\omega)$. Then we have

$$\mathrm{Re}\langle E_j(\mathbf{r},\omega)\, D_j(\mathbf{r}',\omega')\rangle = \frac{\hbar}{\pi}\,\Im\left[\varepsilon(\mathbf{r}',\omega)\, G_{jj}(\mathbf{r},\mathbf{r}',\omega)\delta(\omega-\omega')\right] \tag{1.66}$$

and finally the density force reads

$$f_i(\mathbf{r}) = -\frac{\hbar}{8\pi^2}\,\Im\int_0^{+\infty} d\omega\; [\partial_i\varepsilon(\mathbf{r},\omega)]\, G_{jj}(\mathbf{r},\mathbf{r}',\omega). \tag{1.67}$$

This is a more general formula for the Casimir force and in the case of two half-space dielectrics, it has been used to deduce the Lifshitz formula (1.56). It also allows, for example, to calculate the force when a third dielectric material is placed between the two half-spaces [31], [41] - [43].

Many other methods have been developed over the years to calculate the Casimir force between macroscopic objects and in particular, in this thesis, in Chapter 4 we will use a very general method, based on the scattering operators, which allows us to derive the force between arbitrary objects with generic optical properties even in out of thermal equilibrium conditions.

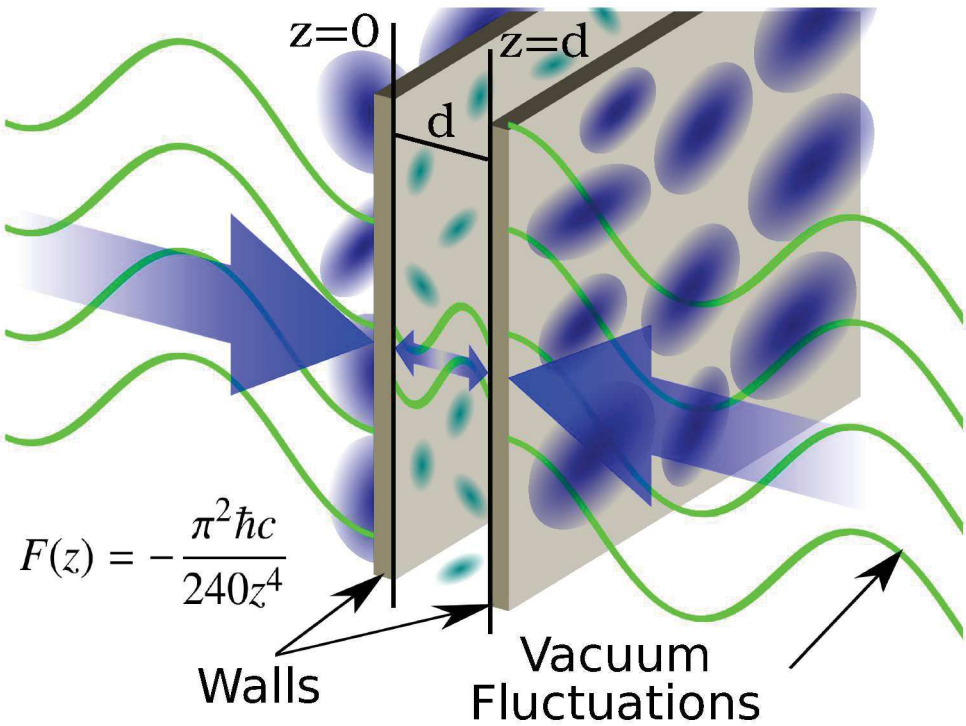

Figure 1.5 – Simple schematic representation of the Casimir effect. Here the attractive force between the slabs is due to the vacuum radiation pressure. The blue clouds depicts virtual photons of the vacuum and, roughly speaking, they are more outside the slabs than inside.

1.2.3 A physical insight about the Casimir effect

Casimir, for the eponymous effect, deduced the force between two perfectly conducting slabs calculating the zero-point energy difference between the case of slabs at infinite distance and the case when they are at finite distance. In this subsection we will deduce the same expression for the force using an alternative simple model which gives a more intuitive insight about the physical origin of the Casimir effect [44], [1]. In this model, the Casimir force is a consequence of the radiation pressure due to the quantum vacuum.

The system is composed by two parallel slabs whose positions are, respectively, $z = 0$ and $z = d$ (see Figure 1.5). The photons of the vacuum can be considered as if they carry a linear momentum which is $1/2\,\hbar\mathbf{k}$ for each virtual photon. With simple heuristic considerations we can state that the virtual photons in the zone external to the two slabs ($z < 0$, $z > d$) generate a radiation pressure which pushes the slabs to get close, while the virtual photons in the inside region ($0 < z < d$) tend to push away the slabs. If the surface density of photons "impinging" on the slabs were equal in the internal and external region the attraction and repulsion effects will compensate and no force would act on the slabs. However, in our case, we have, roughly speaking, that the virtual photons in the internal region are fewer than those in the external region due to the boundary conditions to the fields. This is because we are considering perfectly conducting slabs and then the photon density in the zone $0 < z < d$ is modified from the boundary conditions. For this reason we

can guess that the attractive effects exceed the repulsive ones.

To obtain a quantitative evaluation we should analyze the radiation pressure due to a perpendicular plane wave impinging on a slab. This will be twice the energy density u. More precisely, if we consider an incidence angle θ the radiation pressure under study is $P = 2u \cos^2\theta$. The square-cosine dependence is related to the fact that we have a factor $\cos\theta$ deriving from the momentum dependence on the incidence angle, and another factor derives because the surface element A and incidence angle are not perpendicular, so that factor $(\cos\theta)^{-1}$ arise. Each frequency mode $\omega = ck$ contributes to the radiation pressure and then

$$2\,\frac{1}{2}\left(\frac{1}{2\,V}\,\hbar\omega\right)\cos^2\theta = \frac{\hbar\omega}{2V}\,\frac{k_z^2}{k^2} \tag{1.68}$$

where V represents the quantization volume. In the above equation we have also added a factor $1/2$ which takes into account that for each mode k we can have incoming and outgoing propagation from the slabs and the energy is equal for each of these modes. If the slabs have infinite surfaces, we have a continuum spectrum for the x and y components of k while the values of k_z are discrete

$$k_z = \frac{n\pi}{d} \tag{1.69}$$

with $n \in \mathbb{N}$. Taking all the possible modes and summing each contribution to radiation pressure from the virtual photons in the internal region, we get the pressure acting on each slab

$$P_{int} = \frac{\hbar c}{\pi^2\,d}\sum_{n=1}^{\infty}\int_0^{\infty}\int_0^{\infty} dk_x\,dk_y\left(\frac{n\pi}{d}\right)^2\frac{1}{\sqrt{k_x^2+k_y^2+(n\pi/d)^2}}. \tag{1.70}$$

In (1.70) we have added a factor 2 due to the two different polarizations. The pressure P_{int}, as we mentioned, generates a repulsive force while the pressure P_{ext}, from the external virtual photons, generates an attraction between the slabs. In the external region all the components of k of the virtual photons have a continuous spectrum

$$P_{est} = \frac{\hbar c}{\pi^3}\int_0^{\infty}\int_0^{\infty}\int_0^{\infty} dk_x\,dk_y\,dk_z\,\frac{k_z^2}{\sqrt{k_x^2+k_y^2+k_z^2}}. \tag{1.71}$$

We notice that both P_{int} and P_{ext} are infinite but only their difference has a physical meaning (i.e only the difference is measurable), so we obtain

$$P_{int} - P_{ext} = \frac{\pi^2\,\hbar c}{4d^4}\left[\sum_{n=1}^{\infty} n^2\int_0^{\infty} dx\,\frac{1}{\sqrt{x^2+n^2}} - \int_0^{\infty} du\,u\int_0^{\infty} dx\,\frac{1}{\sqrt{x^2+u^2}}\right]. \tag{1.72}$$

With the help of the Eulero-Maclaurin formula [45], [46], after some algebra, we finally get the famous result originally obtained by Casimir for the force per unit area

$$P_{int} - P_{ext} = -\frac{\pi^2\,\hbar c}{240\,d^4}. \tag{1.73}$$

It must be said that, even if this approach allow us to give a simple and intuitive explanation of the Casimir effect, it gives good results only when rectangular plates are considered. For some other geometries the force deduced by this approach is not satisfactory or even wrong [47] - [50].

1.3 Casimir forces and Experiments

In this section we discuss and outline the experiments done to measure the Casimir forces. Accurate measures of the Casimir forces in different realistic situations are still under study. In fact, these effects are quite small when realistic conditions are considered and so the Casimir forces are very difficult to detect experimentally.

The situation is even more difficult when microscopic objects are involved in the experiment. In fact, the control of position, velocity, external forces acting on the atoms, etc... are all conditions that, when dealing with a microscopic system, are extremely difficult to obtain. Then is evident that there exists an intrinsic issue which makes extremely difficult the direct measurement of the van der Waals/Casimir-Polder forces. However indirect manifestations of these forces can be found in the measurement of macroscopic quantities, as for example suggested by van der Waals himself when he studied the modifications induced by his eponymous force in the equation of state of a gas.

One research field where accurate measurements of the van der Waals force has been obtained is about scattering experiments. There are two simple groups of experiments that can be made. In the first it is studied one atomic beam that is scattered from a a stationary gas which serves as target. For this case, the van der Waals interactions between the atoms deflect the atomic beam when this pass through the target gas and an attenuation of the beam is detected [51] - [53]. In the second case the scattering experiment concern two crossed atomic beams. Also in this case, the van der Waals interaction between the atoms of the two beams influences the scattering and the scattering spectrum of the incident beam as a function of the angle [54], [55].

The Casimir-Polder forces between an atom and a generic macroscopic body can be detected alternatively using scattering techniques. The main experimental configurations used deal with classical scattering and quantum scattering. In the classical scattering the experimental configuration is similar to that described above for an atomic beam and a target. In this case the target is a macroscopic body and the atomic beam is directed near the target body and its deflection, due to the Casimir-Polder interaction is observed and analyzed [56], [57]. The experimental setup based on quantum scattering exploits the property, which follows from the de Broglie hypothesis, that the matter can have a wave-like behavior. Then, for sufficiently small speeds, the reflection against a body of this matter-wave is studied. This reflection is certainly influenced by the Casimir-Polder interactions which can be then measured [58, 59]. The matter-wave behavior is also the basis for measuring the Casimir-Polder force by studying the diffraction of these matter-waves by gratings [60] - [62].

Another effective way to measure the Casimir-Polder forces is to consider trapped

atoms. When the atom is trapped it still has a motion, in particular an oscillatory motion. When a surface is near to the trapped atom this motion is modified by the Casimir-Polder interaction and the latter can be revealed in appropriate experiments. Using this configuration the Casimir-Polder have been measured, as well as its temperature modification or the possible repulsion force in an out of thermal equilibrium situation [63] - [66].

Many other methods to detect and observe indirectly the Casimir-Polder forces have been developed, for example spectroscopy, and we refer to [67] and the references therein for more details.

We now discuss the situation about experiments for the measurement of the Casimir force on macroscopic objects. A simple estimation of the magnitude of the Casimir force between two perfectly conducting slabs gives

$$\frac{F(d)}{A} = \frac{\pi^2}{240}\frac{\hbar c}{d^4} = \frac{0.013}{d^4}\ dynes/cm^2. \tag{1.74}$$

This result gives a force of 10^{-2} dyn (10^{-7} N in SI units) for plates of area $A = 1$ cm^2 at distance $d = 1\ \mu$m and the smallness of this values indicates why it is so difficult to measure such effects. However, the Casimir effect was detected for the first time by Sparnaay, in 1958 [68], only a few years later the theoretical prediction by Casimir. Sparnaay detected an attractive force between the two slabs at a distance between 0.5 μm and 2 μm. The experimental setup was very simple. It was made of a plate attached to a cantilever spring. Another plate was approached to the first one with the help of fine screws. The Casimir force was deduced by measuring the bending of the spring via a capacitor connected with the plates. However, because of residual electrostatic forces, the large experimental errors did not allow him to state that the Casimir effect was demonstrated but, as he said, the attractive force measured by him did not contradict the effect predicted by Casimir. After that experiment many other attempts was made to demonstrate the Casimir effect in the subsequent years.

Only in 1997 the Casimir effect was experimentally demonstrated and accurately measured, almost 50 years later the theoretical prediction! The measurement was given thanks to Lamoreaux and his work [69]. In this experiment Lamoreaux used an electromechanical system based on a torsion pendulum made of a slab and a sphere which reciprocal distances was in the range between 0.6 μm and 6 μm (the plate–sphere geometry was used because it avoids the need for a perfect parallel alignment). He was able to measure the Casimir force achieving a declared accuracy of 5%. The experimental results were in excellent agreement with the theoretical prediction by Casimir.

Just one year later, Mohideen and Roy [70] with an experimental setup based on an Atomic Force Microscope (AFM) measured the Casimir force between a slab and a sphere in a distance range between 0.1 μm and 0.9 μm, achieving a measurement accuracy of 1%.

The measurement of the Casimir effect in the configuration (parallel plates) proposed by Casimir himself was obtained only in relatively recent years. The reason is that the required perfect parallelism between the two slabs is very hard to achieve with good accuracy, particularly when the two plates are very close eac other In 2001, Bressi and collaborators [71] solved this issue aligning the slabs by means of microresonator with an accuracy un-

der the micron. In this way they were able to measure the Casimir force between parallel metallic plates with an accuracy of 15% in a distance range of the slabs of 0.5-3.0 μm.

Measurement of the Casimir forces concerning various geometries have been done. In recent years, for example, the configuration with gratings has been considered. For example in Reference [72] Chan and collaborators measured the Casimir force between a gold sphere and a silicon nanostructured surface (rectangular grating). In this case, in a range of distances between 150 nm and 500 nm, it has been shown that the attractive force is significantly different from the pairwise additive approximation (the latter approximation is a simple geometric approximation which calculates the modification of the force, due to the presence of "imperfections" of the surface, exploiting the force of the slab-slab configuration). This result demonstrates the strong dependence of the Casimir force on the shape of the interacting bodies.

In another example of sphere-grating configuration [73], the strong dependence from geometry of the Casimir force is also more interesting. In fact, using a setup made of a gold sphere in front of a metallic grating instead of a dielectric grating, the Casimir force, at distance scales below the plasma wavelength, shows a new unexpected regime. When a deep metallic lamellar grating, with sub-100 nm features, is considered then, for large inter-surfaces separations, it was found that the force is reduced beyond what would be expected by any existing theoretical prediction.

Also in view of the studies about the measurement of the Casimir force in realistic systems keeps on, going hand in hand with the possible technological applications which are, nowadays, always more concrete thanks to the micro-electromechanical (MEMS) devices. An important work concerning the Casimir force in these devices has been done by Chan, Aksyuk, Kleiman, Bishop and Capasso in [74] where they have showed that, when the distance between two surfaces is relatively small, the quantum effects acting on these devices becomes relevant and not negligible for the proper functioning of the device. The experimental setup is similar to that of Lamoreaux and, also in this case, there is a system made of a sphere in front of a slab. The sphere can rotate because of the Casimir force, thus acting as a torsion pendulum.

References

[1] P. W. Milonni, *The Quantum Vacuum. An Introduction to Quantum Electrodynamics*, Accademic Press, (1994).

[2] W. Greiner and J. Reinhardt, *Quantum Electrodynamics*, Springe-Verlag, Berlin Heidelberg New York (2003).

[3] J. D. van der Waals, *Over de Continuiteit van den Gas- en Vloeistoftoestand (on the continuity of the gas and liquid state)*, Ph.D. thesis, Universiteit Leiden, (1873).

[4] F. London, *Zur Theorie und Systematik der Molekularkräfte*, Z. Physik **63**, 245 (1930).

[5] H. B. G. Casimir and D. Polder, *The Influence of Retardation on the London-van der Waals Force* Phys. Rev. **73**, 360 (1948).

[6] H. B. G. Casimir, *On the attraction between two perfectly conducting plates*, Proc. Kon. Ned. Akad. Wetenschap **51**, 793 (1948).

[7] E. M. Lifshitz, *The Theory of Molecular Attractive Forces between Solids*, Sov. Phys. JETP **2**, 73 (1956).

[8] D. A. R. Dalvit, P. W. Milonni, D. C. Roberts, and F. S. S. Rosa in *Casimir Physics*, edited by D. A. R. Dalvit, P. W. Milonni, D. C. Roberts, F. S. S. Rosa, Springer, Berlin (2011).

[9] M. Bordag, G. L. Klimchitskaya, U. Mohideen, and V. M. Mostepanenko, *Advances in the Casimir Effect*, Oxford University Press, N.Y. (2009).

[10] D. P. Craig and T. Thirunamachandran, *Molecular Quantum Electrodynamics*, Academic Press, London, 1984.

[11] C. Cohen-Tannoudji, B. Diu and F. Laloe, *Quantum Mechanics*, Wiley, 1991.

[12] G. Compagno, R. Passante and F. Persico, *Atom-Field Interactions and Dressed Atoms*, Cambridge University Press, Cambridge, 1995.

[13] R. R. McLone and E. A. Power, *On the Interaction between two identical neutral dipole systems, one in an excited state and the other in the ground state*, Mathematika **11**, 91 (1965).

[14] J. D. Jackson, *Classical Electrodynamics*, Wiley and Sons, 1998.

[15] L. I. Schiff, *Quantum Mechanics*, McGraw-Hill and Kogakusha Company Ltd, Tokyo, 1955.

[16] E. Merzbacher, *Quantum Mechanics*, John Wiley and Sons, New York, 1961.

[17] S. Y. Buhmann, *Dispersion Forces I*, Springer, Berlin 2012.

[18] Y. S. Barash and V. L. Ginsberg, *Some problems in the theory of van der Waals forces*, Sov. Phys. Usp. **27**, 467 (1984).

[19] E. A. Power and T. Thirunamachandran, *Quantum electrodynamics with nonrelativistic sources. III. Intermolecular interactions*, Phys. Rev. A **28**, 2671 (1983).

[20] P. W. Milonni and M. L. Shih, *Source theory of the Casimir force*, Phys. Rev. A **45**, 4241 (1992).

[21] G. Compagno, R. Passante and F. Persico, *The role of the cloud of virtual photons in the shift of the ground state energy of a hydrogen atom*, Phys. Lett. A **98**, 253 (1983).

[22] L. Spruch, *Retarded or Casimir Long Range Potentials*, Phys. Today **39** (11), 37 (1986).

[23] G. Feinberg, J. Sucher and C.-K. Au, Phys. Rep. **180**, 83 (1989).

[24] E. A. Power and T. Thirunamachandran, *Casimir-Polder potential as an interaction between induced dipoles*, Phys. Rev. A **48**, 4761 (1993).

[25] R. Passante and S. Spagnolo, *Casimir-Polder interatomic potential between two atoms at finite temperature and in the presence of boundary conditions*, Phys. Rev. A **76**, 042112 (2007).

[26] P. W. Milonni and A. Smith, *van der Waals dispersion forces in electromagnetic fields*, Phys. Rev. A **53**, 3484 (1996).

[27] H. Wennerstrom, J. Daicic, B.W. Ninham, *Temperature dependence of atom-atom interactions*, Phys. Rev. A **60**, 2581 (1999).

[28] G. H. Goedecke, R.C. Wood, *Casimir-Polder interaction at finite temperature*, Phys. Rev. A **60**, 2577 (1999).

[29] G. Barton, *Long-range Casimir-Polder-Feinberg-Sucher intermolecular potential at nonzero temperature*, Phys. Rev. A **64**, 032102 (2001).

[30] B. DeWitt, "The Casimir Effect in Field Theory" in *Physics in the Making*, edited by A. Sarlemijn and M. J. Sparnaay, Elsevier, Amsterdam, 1989.

[31] J. Schwinger, L. L. DeRaad Jr. and K. A. Milton, *Casimir effect in dielectrics*, Ann. Phys. (New York) **115**, 1 (1978).

[32] P. W. Milonni, *Different Ways of Looking at the Electromagnetic Vacuum*, Physica Scripta **T21**, 102 (1988).

[33] P. W. Milonni, *Casimir forces without the vacuum radiation field*, Phys. Rev. A **25**, 1315 (1982).

[34] S. Rugh, H. Zinkernagel and T. Cao, *The Casimir Effect and the Interpretation of the Vacuum*, Studies in History and Philosophy of Modern Physics **30**, 111 (1999).

[35] I. R. Senitzky, *Radiation-Reaction and Vacuum-Field Effects in Heisenberg-Picture Quantum Electrodynamics*, Phys. Rev. Lett. **31**, 955 (1973).

[36] P. W. Milonni and P. B. Lerner, *Extinction theorem, dispersion forces, and latent heat*, Phys. Rev. A **46**, 1185 (1992).

[37] P. Barcellona and R. Passante, *A microscopic approach to Casimir and Casimir–Polder forces between metallic bodies*, Ann. Phys. **355**, 282 (2015).

[38] R. Passante, F. Persico, L. Rizzuto, *Spatial correlations of vacuum fluctuations and the Casimir–Polder potential*, Phys. Lett. A **316**, 29-32 (2003).

[39] R. Passante, E. A. Power and T. Thirunamachandran, *Radiation-molecule coupling using dynamic polarizabilities: Application to many-body forces*, Phys. Lett. A **249**, 77-82 (1998).

[40] F. S. S. Rosa, D. A. R. Dalvit, and P. W. Milonni, *Electromagnetic energy, absorption, and Casimir forces. II. Inhomogeneous dielectric media*, Phys. Rev. A **84**, 053813 (2011).

[41] I. E. Dzyaloshinskii and L. P. Pitaevskii, *Van der Waals Forces in an Inhomogeneous Dielectric*, Sov. Phys. JETP **9**, 1282 (1959).

[42] I. E. Dzyaloshinskii, E. M. Lifshitz and L. P. Pitaevskii, *The general theory of van der Waals forces*, Adv. Phys. **10**, 165 (1961).

[43] A. A. Abrikosov, L. P. Gorkov and I. E. Dzyaloshinskii, *Methods of Quantum Field Theory in Statistical Physics*, Dover, N. Y., (1975).

[44] P. W. Milonni, R. J. Cook and M. E. Goggin, *Radiation pressure from the vacuum: Physical interpretation of the Casimir force*, Phys. Rev. A **38**, 1621 (1988).

[45] M. Abramowitz and I. A. Stegun, *Handbook of Mathematical Functions*, Dover Books, New York, 1971.

[46] G. Arfken, *Mathematical Methods for Physicists*, Accademic Press, 1985.

[47] T. Boyer, *Quantum Electromagnetic Zero-Point Energy of a Conducting Spherical Shell and the Casimir Model for a Charged Particle* , Phys. Rev. **174**, 1764 (1968).

[48] V. Hushwater, *Repulsive Casimir force as a result of vacuum radiation pressure*, Am. J. Phy. **65**, 381 (1997).

[49] O. Kenneth, and I. Klich, *Opposites Attract: A Theorem about the Casimir Force*, Phys. Rev. Lett. **97**, 160401 (2006).

[50] S. K. Lamoreaux, *The Casimir force: background, experiments, and applications*, Rep. Prog. Phys. **68**, 201 (2005).

[51] P. Dehmer and L. Wharton, *Absolute Total Scattering Cross Sections for 7Li on He, Ne, Kr, and Xe*, J. Chem. Phys. **57**, 4821 (1972).

[52] V. Aquilanti, G. Liuti, F. Pirani, F. Vecchiocattivi and G. G. Volpi, *Absolute total elastic cross sections for collisions of oxygen atoms with the rare gases at thermal energies*, J. Chem. Phys. **65**, 4751 (1976).

[53] B. Brunetti, G. Luiti, E. Luzzatti, F. Pirani and G. G. Volpi, *The interaction of atomic and molecular nitrogen with argon by scattering measurements*, J. Chem. Phys. **79**, 273 (1983).

[54] D. Beck and H.J. Loesch, *Atom Atom Streuexperimente: Geschwindigkeitsabhängigkeit einiger totaler Streuquerschnitte*, Z. Phys. **195**, 444 (1966).

[55] C. H. Chen, P. E. Siska, Y. T. Lee, *Intermolecular potentials from crossed beam differential elastic scattering measurements VIII*, J. Chem. Phys. **59**, 601 (1973).

[56] D. Raskin, P. Kusch, *Interaction between a Neutral Atomic or Molecular Beam and a Conducting Surface*, Phys. Rev. **179**, 712 (1969).

[57] A. Shih, V. A. Parsegian, *Van der Waals forces between heavy alkali atoms and gold surfaces: Comparison of measured and predicted values*, Phys. Rev. A **12**, 835 (1975).

[58] M. J. Mehl, W. L. Schaich, *Quantum theory of neutral-atom scattering at long range from solid cylinders*, Phys. Rev. A **21**, 1177 (1980).

[59] H. Bender, P. W. Courteille, C. Marzok, C. Zimmermann, S. Slama, *Direct Measurement of Intermediate-Range Casimir-Polder Potentials*, Phys. Rev. Lett. **104**, 083201 (2010).

[60] R. E. Grisenti, W. Schöllkopf, J. P. Toennies, G. C. Hegerfeldt, T. Köhler, *Determination of Atom-Surface van der Waals Potentials from Transmission-Grating Diffraction Intensities*, Phys. Rev. Lett. **83**, 1755 (1999).

[61] J. C. Karam, N. Wipf, J. Grucker, F. Perales, M. Boustimi, G. Vassilev, V. Bocvarski, C. Mainos, J. Baudon, J. Robert, *Atom diffraction with a 'natural' metastable atom nozzle beam*, J. Phys. B: At. Mol. Opt. Phys. **38**, 2691 (2005).

[62] J. D. Perreault, A. D. Cronin, *Observation of Atom Wave Phase Shifts Induced by Van Der Waals Atom-Surface Interactions*, Phys. Rev. Lett. **95**, 133201 (2005).

[63] I. Carusotto, L. Pitaevskii, S. Stringari, G. Modugno, M. Inguscio, *Sensitive Measurement of Forces at the Micron Scale Using Bloch Oscillations of Ultracold Atoms*, Phys. Rev. Lett. **95**, 093202 (2005).

[64] J. M. Obrecht, R. J. Wild, M. Antezza, L. P. Pitaesvkii, S. Stringari, E. A. Cornell, *Measurement of the Temperature Dependence of the Casimir-Polder Force*, Phys. Rev. Lett. **98**, 063201 (2007).

[65] D. M. Harber, J. M. Obrecht, J. M. McGuirk, E. A. Cornell, *Measurement of the Casimir-Polder force through center-of-mass oscillations of a Bose-Einstein condensate*, Phys. Rev. A **72**, 033610 (2005).

[66] J. Schiefele, C. Henkel, *Bose-Einstein condensate near a surface: Quantum field theory of the Casimir-Polder interaction*, Phys. Rev. A **82**, 023605 (2010).

[67] S. Y. Buhmann, *Dispersion Forces I (Springer Tracts in Modern Physics, Volume 247)*, Springer, Berlin, 2012.

[68] M. J. Sparnaay, *Measurements of attractive forces between flat plates*, Physica **24**, 751 (1958).

[69] S. K. Lamoreaux, *Demonstration of the Casimir Force in the 0.6 to 6μm Range*, Phys. Rev. Lett. **78**, 5–8 (1997).

[70] U. Mohideen and A. Roy, *Precision Measurement of the Casimir Force from 0.1 to 0.9μm*, Phys. Rev. Lett. **81**, 4549–4552 (1998).

[71] G. Bressi, G. Carugno, R. Onofrio and G. Ruoso, *Measurement of the Casimir Force between Parallel Metallic Surfaces*, Phys. Rev. Lett. **88**, 41804 (2002).

[72] H. B. Chan, Y. Bao, J. Zou, R. A. Cirelli, F. Klemens, W. M. Mansfield, and C. S. Pai, *Measurement of the Casimir Force between a Gold Sphere and a Silicon Surface with Nanoscale Trench Arrays*, Phys. Rev. Lett. **101**, 030401 (2008).

[73] F. Intravaia, S. Koev, Il Woong Jung, A. A. Talin, P. S. Davids, R. S. Decca, V. A. Aksyuk, D. A. R. Dalvit and D. Lopez, *Strong Casimir force reduction through metallic surface nanostructuring*, Nat. Comm. **4**, 2515 (2013).

[74] H. B. Chan, V. A. Aksyuk, R. N. Kleiman, D. J. Bishop and F. Capasso, *Quantum Mechanical Actuation of Microelectromechanical Systems by the Casimir Force*, Science **291**, 1941 (2001).

Chapter 2

Effects of uniform acceleration on atom-field interactions

Contents

2.1 The Unruh effect **32**

2.2 Some known effects of uniform acceleration in quantum electrodynamics **35**

2.3 van der Waals interaction energy between two accelerated atoms . **39**

2.3.1 The model for the van der Waals interaction in the accelerated frame 40

2.3.2 Concluding remarks on the results 48

2.4 A fourth order method for the calculation of the Casimir-Polder force **50**

2.4.1 Perturbative calculation of the variation rates 52

2.4.2 The vacuum fluctuations contribution 54

2.4.3 The radiation reaction contribution 58

2.4.4 The van der Waals force between two atoms at rest 60

2.5 Thermal and non-thermal signatures of the Unruh effect in Casimir-Polder forces **65**

2.5.1 Thermal Casimir-Polder interactions 66

2.5.2 Unruh corrections to Casimir-Polder interactions 67

2.6 The resonance interaction between two uniformly accelerated identical atoms **70**

2.6.1 The scalar field case 72

2.6.2 The electromagnetic field case 75

2.6.3 Conclusions and Future Perspectives 78

References **79**

After having introduced the Casimir forces in the previous chapter, we consider some quantum electrodynamic effects related to the uniform acceleration of atoms in vacuum and show original results that we obtained on Casimir-Polder forces for accelerating atoms. The aim of this chapter is to understand how the dynamical out-of-equilibrium-condition, dictated from the uniform acceleration of the atoms, can modify the Casimir-Polder forces (or equivalently van der Waals forces). The class of physical systems that we are going to analyze are strictly related with one of the most intriguing phenomena in quantum field theory, the so-called Unruh effect [1, 2, 3, 4]. According to this effect, a uniformly accelerated detector in the Minkowski quantum vacuum experiences a thermal bath at a temperature proportional to its acceleration. In qualitative terms, as we will see forward in a dedicated section, this phenomenon originates from time-dependent Doppler shifts of the field detected by the accelerated detector [5]. Unfortunately, this effect is very tiny, and there is not yet an experimental evidence of it. In fact, an acceleration of the order of 10^{22} cm/s^2 would be necessary to obtain Unruh radiation corresponding to the temperature of 1 K [4]. The question of the perception of the quantum vacuum in accelerated frames remains a widely debated problem. In this chapter, after discussing briefly the physics behind the Unruh effect, we discuss some effects related to a uniform acceleration of atoms in the vacuum space, in the framework of quantum electrodynamics. After considering the radiative level shifts of a uniformly accelerated atom in vacuum, we focus on the atom-wall Casimir-Polder interaction for an accelerated atom, as well as on the van der Waals/Casimir-Polder interaction between two accelerating atoms. Also, we will discuss in detail the possibility of detecting the Unruh effect through these phenomena. Since the Lamb-shift and the Casimir-Polder interactions are directly related to vacuum field fluctuations [6, 7, 8], we are particularly interested to investigate if *thermal* effects due to the acceleration may produce observable effects in such physical systems. These effects can suggest new possibilities to detect the Unruh effect through a measurement of the Casimir-Polder interactions for atoms accelerating in the vacuum space.

The chapter is organized as follows. In the introductory Sections 2.1 and 2.2, we present and give a simple physical insight of the Unruh effect and shortly review some electrodynamic effects due to accelerated atoms. In Section 2.3 we start to show our results investigating the atom-atom van der Waals/Casimir-Polder force between two accelerating atoms through a physical model based on the spatial correlations of vacuum electromagnetic field and source field. In Section 2.4 we discuss and develop in detail a general statistical procedure for the calculation of the Casimir-Polder forces, extending to the fourth-order a method introduced by Dalibard, Dupont-Roc and Cohen-Tannoudji for second order effects. In Section 2.5 we exploit the new procedure that we developed in Section 2.4 to examine more rigorously the Casimir-Polder force between two ground-state atoms uniformly accelerating in the vacuum space. Finally in Section 2.6 we analyze the resonance interaction for two accelerated atoms, interacting with relativistic scalar field or with the electromagnetic field.

2.1 The Unruh effect

We start briefly presenting the Unruh effect, which plays a fundamental role in our original work presented in the following sections.

It is well known, in the literature, that a detector uniformly accelerating in the vacuum space behaves as an identical static detector immersed in a thermal radiation at temperature T proportional to its acceleration. Before Unruh's work, other works in astrophysical problems had suggested thermal effects of accelerating particles [9] - [12]. Hawking, in his studies on the black holes [13] - [14], predicted that a black hole radiates at a temperature $T = \hbar g/2\pi k_B c$ where g is the gravitational acceleration of the black hole and k_B is the Boltzmann constant. To find this result Hawking considered the effect of the gravity on the vacuum scalar field. Before the work of Hawking, Fulling had introduced an approach to deal with the quantum field theory in curved spaces [2]. However Unruh and Davies, with their independent works [1]-[3], were the first who directly showed the thermal effects due to acceleration in the background of the quantum field theory. They found that an observer moving with a uniform acceleration and interacting with the vacuum of the scalar field in the Minkowski space-time, feels a temperature given by the following expression

$$T = \frac{\hbar a}{2\pi c k_B} \tag{2.1}$$

where a is the observer's acceleration. Here a replaces the gravitational acceleration g in the analogous expression found by Hawking. This acceleration/temperature effect is called the *Unruh effect* or the *Unruh-Davies effect* or also the *Fulling-Unruh-Davies effect.* This effect is a striking manifestation of the fact that the quantum vacuum, and its particle content, is observer dependent.

A more general result of the Unruh effect, concerning not only with the scalar field but also to more generic spinor and vector field in a space-time of dimension d, has been found by Takagi [15]. When we will refer to (2.1) we will mean the *Hawking-Unruh temperature* because the results of Hawking and Unruh are identical on the basis of the equivalence principle and they differ only for the interpretation. In the first case we have a stationary detector on the event-horizon of a black hole with gravitational acceleration g, while in the second case we have an accelerated detector with uniform acceleration a in the vacuum space.

The methods usually used to deduce (2.1) are not particularly intuitive (see, for example, [1] - [4], [9] - [14], [16] - [18]). The reason is that these works use a formalism related to the quantization of the field in curved spaces. In this subsection we want to show the same famous result of Unruh using a simple and intuitive method proposed by Milonni and Alsing [5]. The key idea of this method is obtaining the Unruh effect from considerations on the Doppler shift of the vacuum field seen by an accelerated observer.

Let us suppose to have a plane wave with frequency ω_k and wave vector $\mathbf{k}$ which propagates along the $\pm x$ direction. We also suppose that the uniformly accelerated Rindler observer moves along the positive direction x. In the latter statement we mean with Rindler observer an observer which is comoving with the particle in an instantaneously inertial

reference frame. Since the observer is instantaneously inertial he will perceive the plane wave as having frequency ω'_k related to ω_k through the Lorentz transformation

$$\omega'_k(\tau) = \gamma(\tau)\,(\omega_k - k\,v(\tau)) \tag{2.2}$$

where we have assumed that the plane wave propagates along the positive x direction. Considered the motion of the observer we have

$$v(\tau) = c\tanh\left(\frac{a\tau}{c}\right), \quad \gamma(\tau) = \cosh\left(\frac{a\tau}{c}\right) \tag{2.3}$$

and this means that

$$\omega'_k(\tau) = \cosh\left(\frac{a\tau}{c}\right)\left(\omega_k - k\,c\tanh\left(\frac{a\tau}{c}\right)\right). \tag{2.4}$$

Since $\omega_k = ck$, the above equation reads

$$\omega'_k(\tau) = \omega_k e^{-a\tau/c}. \tag{2.5}$$

For a wave propagating along $-x$ the sign of $kv(\tau)$ in (2.2) changes and we get

$$\omega'_k(\tau) = \omega_k e^{a\tau/c}. \tag{2.6}$$

We notice that if we assume $a\tau/c \ll 1$, i.e non-relativistic motion, and we expand to first order the exponential in (2.5), (2.6) we obtain

$$\omega'_k(\tau) \simeq \omega_k\left(1 \mp \frac{a\tau}{c}\right) \tag{2.7}$$

which coincides with the non-relativistic Doppler effect ($a\tau \simeq v$). We want to stress the time-dependence of (2.5), (2.6) which implies, for the accelerated observer, a Doppler effect which is explicitly dependent on time.

Thus, because of the time-dependent Doppler effect, at each time, the Rindler observer see the wave oscillating with a different time-dependent frequency. Then, the accelerated observer will see the spectrum frequency proportional to

$$\left|\int_{-\infty}^{+\infty} e^{i\Omega\tau} e^{i\varphi(\tau)}\, d\tau\right|^2 \tag{2.8}$$

where

$$\varphi(\tau) = \int_0^\tau \omega'_k(\tau')\, d\tau'. \tag{2.9}$$

From equations (2.5) and (2.6) it follows that $\varphi(\tau)$ reads

$$\varphi_\pm(\tau) = \int_0^\tau \omega'_k(\tau')\, d\tau' = \left(\frac{\omega_k c}{a}\right) e^{\pm a\tau/c} \tag{2.10}$$

(the symbol ± denotes the two different cases where the wave propagates along $-x$ or x). The frequency spectrum $S(\Omega)$ is then proportional to

$$\left|\int_{-\infty}^{+\infty} e^{i\Omega\tau} \exp\left[i\left(\frac{\omega_k c}{a}\right)e^{\pm a\tau/c}\right] d\tau\right|^2 \tag{2.11}$$

The same spectrum (2.11) can be obtained considering that the plane waves ($\propto e^{i(kx\pm\omega_k t)}$), in the laboratory frame, are seen by the Rindler observer as

$$e^{i\varphi_\pm(\tau)} \equiv e^{i(kx\pm\omega_k t)} = \exp\left[i\left(\frac{\omega_k c}{a}\left(e^{\pm a\tau/c}-1\right)\right)\right]. \tag{2.12}$$

where we used

$$x(\tau) = \frac{c^2}{a}\left[\cosh\left(\frac{a\tau}{c}\right)-1\right], \quad t(\tau) = \frac{c}{a}\sinh\left(\frac{a\tau}{c}\right). \tag{2.13}$$

Thus, the spectrum $S(\Omega)$ is proportional to the squared module of the Fourier transform of (2.12). The term $e^{-i\omega_k c/a}$ in (2.12) is independent from τ, and in the Fourier transform integral gives only a proportionality factor. So we obtain again Eq. (2.11).

After some straightforward algebra we can evaluate the integral (2.11) and we finally get

$$\left|\int_{-\infty}^{+\infty} e^{i\Omega\tau} \exp\left[i\left(\frac{\omega_k c}{a}\right)e^{\pm a\tau/c}\right] d\tau\right|^2 = \frac{2\pi c}{\Omega a}\frac{1}{e^{2\pi c\Omega/a}-1}. \tag{2.14}$$

This result shows the Unruh-Hawking effect. In fact, we have obtained the Planck factor relative to the Bose-Einstein distribution for particles at temperature $T = \hbar a/2\pi k_B c$, which is indeed the Hawking-Unruh temperature. This simple, not formal, method gives us an intuitive physical insight on the origin of the Unruh effect. Despite its conceptual importance for connections with Hawking radiation [13, 14] and for its impact on cosmology, black hole physics, particle physics, and relativistic quantum information [19] - [21], experimental detection of the Unruh effect remains elusive, since an acceleration of the order of 10^{20}m/s^2 would be required in order to measure a temperature of 1K. Many experimental proposals for its measurements in circular accelerators [22], as well as in analogue models of condensed matter physics [23] have been also discussed. Other proposals concern, for example, detecting spin depolarization of accelerated electron [24], or accelerating particles by ultraintense laser pulses [25, 26] or laser filaments [27, 28]. However, despite the intense efforts the problem of detection of Unruh effect remains an open question because very high accelerations are required to obtain a Unruh temperature of some kelvin. On the other hand, a direct verification of the effect could allow a deeper understanding of some persisting controversies about the interpretation of this effect [29, 30, 31]. In this direction, it has been recently argued that interatomic van der Waals interactions between two uniformly accelerated atoms could be good candidates for detecting the Unruh effect, for reasonable values of the acceleration [32],[AN1].

Among the large number of open fundamental challenges in this field, a long-standing question concerns whether the effect of a relativistic acceleration is strictly equivalent to a

thermal field [33]. It has been recently shown, for example, that nonthermal features associated with uniform acceleration manifest on the radiative properties of single accelerated atoms [34] - [40],[AN3]. Also, recent works on entanglement generation or Casimir-Polder interactions between uniformly accelerated atoms, have shown that non-thermal effects of accelerations arise in a system of two or many particles [41, 42, 40],[AN3].

In this context, we have recently shown that the Casimir-Polder (CP) force between two uniformly accelerating atoms in their ground state exhibits a cross-over from a short distance thermal behavior to a long distance non-thermal behavior, with respect to a reference length identified with $z_a = \frac{c^2}{a}$, the characteristic scale for a breakdown of a local approximate description of the two-body system in terms of a Minkowskian space-time [40],[AN3]. Indeed, Casimir-Polder forces between neutral atoms arise from the retarded interaction among the dipoles induced and correlated by the zero-point quantum field fluctuations, and quanta mediating the interaction between the two atoms cannot disregard, for large distances, the non-inertial character of relativistic acceleration [32, 40],[AN1],[AN3]. All these consequences will be presented and discussed in detail in the next sections of this chapter.

2.2 Some known effects of uniform acceleration in quantum electrodynamics

In this Section, we introduce some physical configurations related to our study concerning with effects of a uniform acceleration in quantum electrodynamics [38],[AN2]. This will be the basis for our original work on this subject, which will be exposed in the next sections. We consider two different physical systems that are already studied in the literature. We first consider a hydrogen atom moving with a uniform acceleration and interacting with the quantum electromagnetic field in the vacuum state. We then consider the atom-wall Casimir-Polder interaction when the atom is uniformly accelerated. These two systems are good examples showing physical implications of the acceleration in quantum electrodynamics.

Let us now consider the physical system of a hydrogen atom uniformly accelerated in the quantum electromagnetic vacuum. The Hamiltonian describing the atom-field interaction in the instantaneous inertial frame of the atom, in the multipolar coupling scheme is [35, 34]

$$H(\tau) = H_{\mathrm{A}}(\tau) + H_{\mathrm{F}}(\tau) + H_{\mathrm{I}}(\tau)\,, \tag{2.15}$$

with

$$H_{\mathrm{A}}(\tau) = \hbar \sum_{n} \omega_n \sigma_{nn}(\tau), \tag{2.16}$$

$$H_{\mathrm{F}}(\tau) = \hbar \sum_{\mathbf{k}j} \omega_k a^{\dagger}_{\mathbf{k}} a_{\mathbf{k}} \frac{dt}{d\tau}, \tag{2.17}$$

$$H_{\mathrm{I}}(\tau) = -e \sum_{mn} \mathbf{r}_{mn} \cdot \mathbf{E}(x(\tau)) \sigma_{mn}(\tau)\,, \tag{2.18}$$

where τ is the proper time and $\sigma_{\ell m} = |\ell\rangle\langle m|$, $|n\rangle$ being a complete set of atomic states with energy ω_n. $\mu = e\mathbf{r}$ is the atomic electric dipole moment. Also, $x = (t, \mathbf{x})$ is the space-time coordinate of the atom and $\mathbf{k}j$ the wave vector ($j = 1, 2$ is the polarization index). We are interested in investigating the energy level shifts of the uniformly accelerated atom. Exploiting the general procedure in [43, 44, 46], that we will discuss and use in the following Section 2.4,we can split the energy shift of the atomic level of the accelerated atom in two parts,separating the contributions of vacuum fluctuations and radiation reaction field (indicated respectively with the subscripts *vf* and *rr*). These quantities, at second order in e, are [46]

$$(\delta E_a)_{\mathrm{vf}} = -\frac{ie^2}{\hbar} \int_{\tau_0}^{\tau} d\tau' C^{\mathrm{F}}_{\ell m}(x(\tau), x(\tau'))(\chi^{\mathrm{A}}_{\ell m})_a(\tau, \tau'), \tag{2.19}$$

$$(\delta E_a)_{\mathrm{rr}} = -\frac{ie^2}{\hbar} \int_{\tau_0}^{\tau} d\tau' \chi^{\mathrm{F}}_{\ell m}(x(\tau), x(\tau'))(C^{\mathrm{A}}_{\ell m})_a(\tau, \tau'), \tag{2.20}$$

where $C^{\mathrm{F(A)}}_{\ell m}$ and $\chi^{\mathrm{F(A)}}_{\ell m}$ are the symmetric correlation function and the linear susceptibility of the field (atom), respectively. Using the appropriate statistical functions of atom and field [15], after some algebra, we have [35]

$$\begin{aligned}(\delta E_a)_{\mathrm{vf}} &= \frac{e^2}{3\pi c^3} \sum_{b} |\langle a|\mathbf{r}(0)|b\rangle|^2 \int_0^{\infty} d\omega\, \omega^3 \left(1 + \frac{a^2}{c^2\omega^2}\right) \\ &\quad \times \coth\left(\frac{\pi c\, \omega}{a}\right) P\left(\frac{1}{\omega + \omega_{ab}} - \frac{1}{\omega - \omega_{ab}}\right),\end{aligned} \tag{2.21}$$

$$\begin{aligned}(\delta E_a)_{\mathrm{rr}} &= \frac{e^2}{3\pi c^3} \sum_{b} |\langle a|\mathbf{r}(0)|b\rangle|^2 \int_0^{\infty} d\omega\, \omega^3 \\ &\quad \times P\left(\frac{1}{\omega + \omega_{ab}} + \frac{1}{\omega - \omega_{ab}}\right),\end{aligned} \tag{2.22}$$

where the index a and the relative ket indicate a generic atomic state, $\omega_{ab} = \omega_a - \omega_b$, a is the acceleration of the atom, and the limit $\tau - \tau_0$ to infinity has been taken.

We first note from (2.22) that the radiation reaction contribution to the energy level shift does not depend on the atomic acceleration; it is identical to that obtained in the inertial frame. This result is expected on a physical ground: in fact, the field emitted by the atom propagates with the velocity of light, and it can act back on the atom only at the same time it is emitted. Thus, radiation reaction contribution is not influenced by the atomic motion.

As we shall discuss later in this section, the situation radically changes in the presence of a boundary, such as a reflecting mirror. On the other hand, the contribution of vacuum fluctuations depends explicitly on the acceleration, through the presence of the *thermal* term $\coth(\pi c\,\omega/a)$, linked to the Unruh temperature $T = \hbar a/2\pi c k_{\rm B}$, and of an extra term proportional to a^2. This result indicates that the atomic acceleration induces observable effects in the energy shifts.

The appearance of a nonthermal term proportional to a^2 is related to a similar term appearing in the correlation function of the electric field in the accelerated frame. It is possible to show that, for a ground-state hydrogen atom, thermal and non-thermal terms are comparable for $a \sim 10^{25}$ cm/s^2 [35]. This is also the typical acceleration required to detect the Unruh effect by measuring atomic level shifts.

The same physical arguments given above indicate that also the Casimir-Polder interaction between a uniformly accelerated atom and a perfectly reflecting plate could manifest the Unruh effect. Corrections to the atom-wall Casimir-Polder force due to the acceleration of the atom, have been calculated in the scalar field case [36]. It has been shown that such corrections are relevant only for accelerations of the order of 10^{24} cm/s^2, confirming the necessity of extremely high accelerations for a detection of the Unruh effect. This calculation has been extended to the more realistic case of a uniformly accelerated hydrogen atom interacting with the quantum electromagnetic field, in the presence of a perfectly reflecting mirror [37, 39]. Let us consider an atom moving with uniform acceleration in a direction parallel to the mirror at a distance z_0 from the mirror. In analogy with the case of an atom at rest near a plate, the atom-wall Casimir-Polder interaction can be obtained considering the z_0-dependent terms in the expression of the energy level shift. As before, we evaluate the contribution of vacuum fluctuations and of the radiation reaction field to the energy shift of the atomic level, in the presence of a conducting plate. After some lengthy algebra, it is found [39]

$$\begin{aligned}(\delta E_a)^{(b.c.)}_{\rm vf} = &-\frac{1}{8\pi^2 c^3}\sum_b \left(\mu^{ab}_\ell \mu^{ba}_m\right)\frac{1}{(2z_0)^3} P\int_0^\infty d\omega K_{\ell m}(\omega; z_0, a)\\ &\times \coth\left(\frac{\pi c\,\omega}{a}\right)\left(\frac{1}{\omega+\omega_{ab}} - \frac{1}{\omega-\omega_{ab}}\right)\end{aligned} \tag{2.23}$$

and

$$\begin{aligned}(\delta E_a)^{(b.c.)}_{\rm rr} = &\frac{1}{8\pi^2 c^3}\sum_b \left(\mu^{ab}_\ell \mu^{ba}_m\right)\frac{1}{(2z_0)^3} P\int_0^\infty d\omega\\ &\times K_{\ell m}(\omega; z_0, a)\left(\frac{1}{\omega+\omega_{ab}} + \frac{1}{\omega-\omega_{ab}}\right),\end{aligned} \tag{2.24}$$

where the superscript (b.c.) stands for *boundary conditions*, z_0 is the atom-wall distance and $K_{\ell m}(\omega; z_0, a)$ is a function containing a combination of sinusoidal functions, which takes

into account the presence of the conducting plate [39]

$$
\begin{aligned}
K_{\ell m}(\omega; z_0, a) = & \frac{\sigma_{\ell n}}{(1+a^2z_0^2)^{1/2}} \left\{ (\delta_{nm} - n_n n_m) \frac{(2\omega z_0)^2}{(1+a^2z_0^2)} \sin\left(2\frac{\omega}{a}\sinh^{-1}(az_0)\right) \right. \\
& + (\delta_{nm} - 3n_n n_m) \left[\frac{2\omega z_0}{(1+a^2z_0^2)^{3/2}} \cos\left(2\frac{\omega}{a}\sinh^{-1}(az_0)\right) - \frac{1}{(1+a^2z_0^2)^2} \sin\left(2\frac{\omega}{a}\sinh^{-1}(az_0)\right) \right] \\
& + a^2z_0^2 \left[(\delta_{nm} + 3\sigma_{nm}) \frac{2\omega z_0}{(1+a^2z_0^2)^{3/2}} \cos\left(2\frac{\omega}{a}\sinh^{-1}(az_0)\right) \right. \\
& \left. + (\delta_{nm} - 2\sigma_{nm}) \frac{2}{(1+a^2z_0^2)^2} \sin\left(2\frac{\omega}{a}\sinh^{-1}(az_0)\right) \right] \\
& \left. - \sigma_{nm} a^4 z_0^4 \frac{4}{(1+a^2z_0^2)^2} \sin\left(2\frac{\omega}{a}\sinh^{-1}(az_0)\right) \right\} + az_0[(\delta_{lm} - k_l k_m)az_0 + n_l k_m + k_l n_m] \\
& \times \left\{ \frac{(2\omega z_0)^2}{(1+a^2z_0^2)} \sin\left(2\frac{\omega}{a}\sinh^{-1}(az_0)\right) - \frac{2\omega z_0}{(1+a^2z_0^2)^{3/2}} \cos\left(2\frac{\omega}{a}\sinh^{-1}(az_0)\right) \right. \\
& \left. + \frac{1}{(1+a^2z_0^2)^2} \sin\left(2\frac{\omega}{a}\sinh^{-1}(az_0)\right) \right\} \\
& + a^3z_0^3[(\delta_{\ell m} - k_\ell k_m)az_0 + n_\ell k_m + k_\ell n_m] \left\{ \frac{4\omega z_0}{(1+a^2z_0^2)^{3/2}} \cos\left(2\frac{\omega}{a}\sinh^{-1}(az_0)\right) \right. \\
& \left. + \frac{4}{(1+a^2z_0^2)^2} \sin\left(2\frac{\omega}{a}\sinh^{-1}(az_0)\right) \right\}. \qquad (2.25)
\end{aligned}
$$

We now briefly comment the results obtained. Equation (2.23) clearly shows that the contribution of vacuum fluctuations contains not only a thermal correction due to the factor $\coth(\pi c\,\omega/a)$, but also an extra term proportional to the function $K_{\ell m}(\omega; z_0, a)$. This function modulates the Casimir-Polder interaction as a function of the atom-plate distance z_0 and of the atomic acceleration a. On the other hand, Equation (2.24) shows that the radiation reaction term is sensitive to the atomic acceleration. This behavior is not surprising. When a boundary is present, the field emitted by the atom can act back on the atom after a reflection on the conducting plate. Since the atom accelerates, in the time-interval between the emission and the subsequent absorption of the reflected field, the atom has moved from its position of a distance depending on its acceleration. This gives rise to a dependence of the radiation reaction contribution on the atomic acceleration. The expression for the total atom-wall Casimir-Polder interaction for the accelerated atom, is obtained by summing (2.23) and (2.24). It is easy to show that in order to reveal effects of acceleration on the atom-wall Casimir-Polder interaction, accelerations of the order of 10^{24}cm/s^2 are necessary, as in the case of the energy shift of an atom in the unbounded space [38],[AN2]. This makes very difficult to observe the effects of the acceleration through the Lamb shift or the atom-wall Casimir-Polder interactions. As we shall show with the results we obtained in the next sections, the situation seems different when we consider the van der Waals/Casimir-Polder interaction between two accelerated atoms.

2.3 van der Waals interaction energy between two accelerated atoms

As we have already seen van der Waals dispersion forces between two neutral atoms in the vacuum are related to fluctuations of the zero-point electromagnetic field, and thus they could be a good candidate for detecting an accelerated motion of the atoms and the Unruh effect. So in this section we will consider the effect of the acceleration on the dispersion interaction between two atoms, and we will show that new phenomena are present in this case, namely a change of the distance-dependence of the interaction energy and its explicit time-dependence [32],[AN1]. Using a simple model, some hints were already obtained on the effect of the acceleration on the dispersion force between accelerating atoms, exploiting the relation between acceleration and temperature given by the Unruh effect [47].

We consider the effect of a uniform acceleration on the van der Waals interaction energy between two ground-state atoms moving in the vacuum space with uniform acceleration. In particular, we are interested to investigate whether the (uniform) acceleration of the atoms yields a qualitative change of the properties of the force. The two atoms/molecules A and B move, in the laboratory system, with the same uniform acceleration a in the x direction, perpendicular to their distance, so that their separation is constant (see Figure 2.1). In order to obtain their van der Waals interaction, both in the near zone and in the far zone (Casimir-Polder regime) we use the following physical model: the interaction energy arises from the dipolar interaction between the (instantaneous) oscillating dipole moments of the atoms, induced and correlated by zero-point electromagnetic field fluctuations. In this model the dipolar fields are classical fields, and the quantum properties of the radiation are included in the spatial correlations of the electric field associated to vacuum fluctuations. This model has been used and proved valid in many cases: atoms at rest [8, 48], three-body dispersion forces [62], when boundary conditions are present [49] or in the presence of external radiation [50]. In the present case we need to generalize this model to the case of accelerating atoms, expressing the field generated by the atomic dipoles in the accelerated reference frame. An advantage of our method is that, even if the interaction energy is calculated for the accelerating atoms in their co-moving frame (the system in which the atoms are instantaneously at rest), all physical quantities relative to the atoms are given in terms of their known values in the laboratory frame.

We now obtain an explicit expression of the interaction energy and discuss in detail the near- and far-zone limits. Our results show that in the near zone a new term proportional to R^{-5} adds to the usual R^{-6} behavior, and in the far zone a term proportional to R^{-6} adds to the usual R^{-7} behavior, making the interaction of a longer range. We also find that the interaction energy has an explicit time dependence. In particular, we show that acceleration-dependent corrections to the R^{-7} (far zone) and R^{-6} (near zone) terms, proportional to a^2t^2/c^2, are present. This suggests that significant changes to the interaction between the two atoms could be obtained if sufficiently long times are considered, even for reasonable values of the acceleration, contrarily to other known manifestations of the Unruh effect, such as Lamb shift and atom-wall interaction for accelerated atoms previously

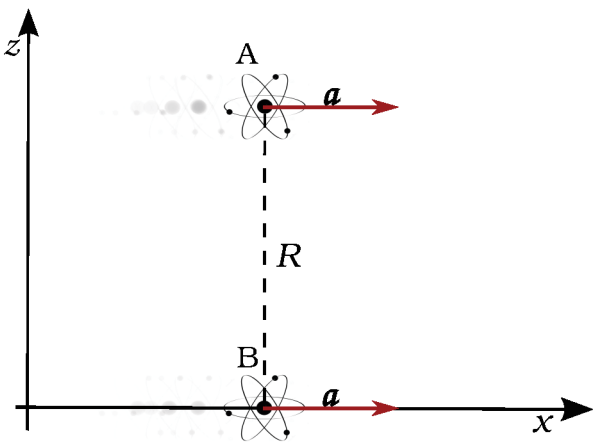

Figure 2.1 – A figure that depicts the geometrical configuration studied in Section 2.3.

discussed, which require extremely high accelerations. Although Lamb shift and atom-wall interactions have the same physical origin of the atom-atom interaction, the van der Waals interaction seems more sensitive to the acceleration because of the time-dependence of the interaction in this case.

In Subsection 2.3.1 we first introduce our physical model for the van der Waals interaction energy for the accelerating atoms, based on the method of correlated induced dipole moments, and evaluate the dipole fields of the accelerating atoms; we also introduce the important concept of *effective interaction distance*. After appropriate Lorentz transformation to the co-moving reference frame, we evaluate the interaction energy between the two atoms in the accelerated frame, in terms of physical quantities calculated in the laboratory frame. Finally, Subsection 2.3.2 is devoted to the discussion of our results and some concluding remarks.

2.3.1 The model for the van der Waals interaction in the accelerated frame

We first generalize the method of induced dipole moments, originally introduced for the calculations of van der Waals interactions between atoms at rest [8, 48], to the case of accelerated atoms. In this model, the interatomic interaction energy originates from the interaction of the instantaneous dipole moments of the two atoms. These dipoles are induced and correlated by the spatially correlated zero-point fluctuations of the quantum electromagnetic field. In this model the quantum nature of the dispersion interaction enters in the correlation function of zero-point fluctuations of the electric field, while the dipole fields are treated classically.

$\tilde{E}_i(\mathbf{k}\lambda, \mathbf{r}, t)$ indicates the $(\mathbf{k}\lambda)$ Fourier component ($\lambda = 1, 2$ is the polarization index) of the electric field at position $\mathbf{r}$, generated by atom A whose position is $\mathbf{R}_A$. This field, evaluated in the moving reference frame where atom B is instantaneously at rest (i.e. the co-moving frame), depends on the instantaneous (fluctuating) dipole moment of atom A

in the laboratory reference frame at the retarded time $t_r = t - \rho(t_r)/c$. $\rho(t_r)$ is an *effective interaction distance* given by the distance traveled by a light signal from its emission by atom A at time t_r to the time t when it is received by atom B. We shall evaluate this distance for the specific case of uniformly accelerated atoms at the end of this Section. In this model, the atoms are assumed having instantaneous oscillating dipole moments and their van der Waals interaction arises from the interaction between the field emitted by the fluctuating dipole of one atom with the dipole moment induced on the second atom. This field can be expressed as (summation over a repeated index is understood),

$$\tilde{E}_i(\mathbf{k}\lambda, \mathbf{R}_B, t) = -\mu_j^A \tilde{V}'_{ij}(k, \mathbf{R}, t_r), \tag{2.26}$$

where $\mathbf{R}_B$ is the position of atom B, $\mathbf{R} = \mathbf{R}_B - \mathbf{R}_A$ and μ_j^A is the dipole moment of atom A. $\tilde{V}'_{ij}(k, \mathbf{R}, t_r)$ is a tensor potential that will be defined explicitly in the next Subsection. From now onwards, a *tilde* indicates that the corresponding quantity is evaluated in the co-moving reference frame, where the atoms are instantaneously at rest. In the co-moving frame, the interaction of this field with the induced dipole moment of atom B is given by

$$-\tilde{\mu}_i^B \tilde{E}_i(\mathbf{k}\lambda, \mathbf{R}_B, t) = \tilde{\mu}_i^B \mu_j^A \tilde{V}'_{ij}(k, \mathbf{R}, t_r), \tag{2.27}$$

where $\tilde{\mu}_i^B$ is the dipole moment of atom B in the accelerated frame. Summation over $(\mathbf{k}\lambda)$ yields the interaction energy.

The Fourier $(\mathbf{k}\lambda)$ component $\mathbf{E}(\mathbf{k}\lambda; \mathbf{r})$ of the electric field, given by

$$E_j(\mathbf{k}\lambda; \mathbf{r}) = i\left(\frac{2\pi\hbar ck}{V}\right)^{1/2} \left(\hat{e}_j(\mathbf{k}\lambda) a_{\mathbf{k}\lambda} e^{i\mathbf{k}\cdot\mathbf{r}} - \hat{e}_j^*(\mathbf{k}\lambda) a_{\mathbf{k}\lambda}^\dagger e^{-i\mathbf{k}\cdot\mathbf{r}}\right) \tag{2.28}$$

($\hat{e}_j(\mathbf{k}\lambda)$ is the polarization unit vector), induces a dipole moment in the atom at position $\mathbf{r}$ given by

$$\mu^{ind}(\mathbf{k}\lambda; \mathbf{r}) = \alpha(k)\mathbf{E}(\mathbf{k}\lambda; \mathbf{r}), \tag{2.29}$$

where we are assuming an isotropic atom with dynamic polarizability $\alpha(k)$. As mentioned, the instantaneous dipole moment induced in one atom, let us say atom A, generates an electric field that then interacts with the other atom (B). This electric field is the field generated by atom A with position $\mathbf{R}_A$ at the retarded time $t_r = t - \rho(t_r)/c$, evaluated at the position of atom B. Because in our case both atoms are accelerating, we need the expression of the electric field generated by an oscillating dipole in motion. This expression, as well as that of the magnetic field, is known and it is usually separated in the two components $\mathbf{E}^{(pol)}$ and $\mathbf{E}^{(Roe)}$, called the polarization and Röntgen components, respectively. Because we are interested in the interaction between the two accelerating atoms in their co-moving system, that is a locally inertial frame, the electric field must be Lorentz-transformed to the co-moving system: thus, electric and magnetic fields are both necessary, because Lorentz transformations mix electric and magnetic fields. In the laboratory frame, these fields, for a dipole moving along an arbitrary trajectory $\mathbf{x}(t)$, are given in Ref. [51, 52] in terms of

the retarded time $t_r = t - r/c$. We use the general expressions in [51, 52] for the polarization and Röntgen components of the electric and magnetic fields in our case of a uniformly accelerated trajectory along x given by [53]

$$x(t) = \frac{c^2}{a}\left(\sqrt{\frac{a^2t^2}{c^2}+1}-1\right),$$
$$x(\tau) = \frac{c^2}{a}\left(\cosh\frac{a\tau}{c}-1\right), \tag{2.30}$$

where time t is related to the proper time τ by the relation

$$t = \frac{c}{a}\sinh\left(\frac{a\tau}{c}\right). \tag{2.31}$$

We also assume $\mathbf{x}(0) = 0$, $\dot{\mathbf{x}}(0) = 0$, and take into account that the two atoms are moving in a direction orthogonal to their distance, so that their distance does not change with time. We thus obtain the polarization and Röntgen components of the electric and magnetic fields for the uniformly accelerating dipole, evaluated at the position of the other dipole,

$$E_i^{(pol)}(\mathbf{r},t) = -\left(\frac{1}{\rho^3}\hat{T}_{ij}\mu_j(t_r) + \frac{1}{c\rho^2}\hat{T}_{ij}\dot{\mu}_j(t_r) + \frac{1}{c^3\rho}\hat{S}_{ij}\ddot{\mu}_j(t_r)\right), \tag{2.32}$$

$$E_i^{(Roe)}(\mathbf{r},t) = -\left(\frac{1}{c^2\rho^2}\dot{x}_i(t_r)\hat{\rho}_j\dot{\mu}_j(t_r) + \frac{1}{c^2\rho^2}\ddot{x}_i(t_r)\hat{\rho}_j\mu_j(t_r)\right.$$
$$\left. + \frac{1}{c^3\rho}\dot{x}_i(t_r)\hat{\rho}_j\ddot{\mu}_j(t_r) + \frac{1}{c^3\rho}\dddot{x}_i(t_r)\hat{\rho}_j\mu_j(t_r) + 2\frac{1}{c^3\rho}\ddot{x}_i(t_r)\hat{\rho}_j\dot{\mu}_j(t_r)\right), \tag{2.33}$$

$$B_i^{(pol)}(\mathbf{r},t) = -\frac{\epsilon_{ikj}}{c\rho^2}\hat{\rho}_k\dot{\mu}_j(t_r) - \frac{\epsilon_{ikj}}{c^2\rho}\hat{\rho}_k\ddot{\mu}_j(t_r), \tag{2.34}$$

$$B_i^{(Roe)}(\mathbf{r},t) = -\frac{1}{c\rho^2}\hat{T}_{ij}\epsilon_{jkl}\left(\frac{1}{\rho}\mu_k(t_r)\dot{x}_l(t_r) + \frac{1}{c}\mu_k(t_r)\ddot{x}_l(t_r) + \frac{1}{c}\dot{\mu}_k(t_r)\dot{x}_l(t_r)\right)$$
$$- \frac{1}{c^3\rho}\hat{S}_{ij}\epsilon_{jkl}\left(\mu_k(t_r)\dddot{x}_l(t_r) + 2\dot{\mu}_k(t_r)\ddot{x}_l(t_r) + \ddot{\mu}_k(t_r)\dot{x}_l(t_r)\right), \tag{2.35}$$

where $t_r = t - r/c$ is the retarded time, $\boldsymbol{\rho}(t) = \mathbf{r} - \mathbf{x}(t)$ and ϵ_{ilk} is the totally antisymmetric tensor. We have also defined the following tensors

$$\hat{T}_{ij} \equiv \delta_{ij} - 3\hat{\rho}_i\hat{\rho}_j, \tag{2.36}$$
$$\hat{S}_{ij} \equiv \delta_{ij} - \hat{\rho}_i\hat{\rho}_j. \tag{2.37}$$

Before obtaining the dispersion interaction energy for the two accelerating atoms, we need some considerations about the retarded time and the distance between the atoms to be used in the expressions above for the fields. The "effective interaction distance" $\rho(t_r)$ is the distance traveled by a light signal from one atom to the other one. For atoms at rest, it coincides with the interatomic distance ρ, while in the case of atoms moving at a constant velocity v, it is easy to show that $\rho(t_r) = \gamma\rho$. In our case the atoms are in an

accelerated motion: this makes evident that we should expect an explicit time-dependence of the interaction distance because $\gamma = (1 - v^2/c^2)^{-1/2}$ depends on time. By assuming that at $t = 0$ the atoms are at rest and have a uniform acceleration a, using (2.30) and simple geometrical considerations, it is possible to show that

$$\rho(t_r) = \rho + c\left(t - \frac{c \arctan(at/c)}{a}\right), \tag{2.38}$$

showing that indeed $\rho(t_r)$ depends on time and, as expected, it grows with time.

We now evaluate the interaction energy between the fluctuating atomic dipoles in accelerated motion. We assume a nonrelativistic motion for the atoms; because their acceleration is given, this assumption limits the timescale of validity of our results, as we shall discuss in more detail in the next Subsection. The potential energy will be evaluated in the co-moving frame of the accelerating atoms. All relevant physical quantities will be however expressed in terms of quantities measured in the laboratory reference frame and thus directly measurable; this makes our approach different with respect to results in the literature concerning other radiative processes in accelerated frames (such as Lamb shift, atom-wall interactions, etc), which are expressed in terms of physical quantities measured in the co-moving frame [35, 37, 39, 47].

In our approach, each Fourier component of vacuum field fluctuations induces an oscillating dipole in the atoms, that in the laboratory frame is of the form (in the $\mathbf{k}$ space)

$$\boldsymbol{\mu}^{A(B),ind}(\mathbf{k}, \lambda, t) = \boldsymbol{\mu}^{A(B),ind}(\mathbf{k}, \lambda) \cos(\omega t) \tag{2.39}$$

with $\omega = ck$. Using (2.27), the van der Waals interaction energy can be expressed as

$$\Delta\tilde{E} = \sum_{\mathbf{k},\lambda} \sum_{\mathbf{k}',\lambda'} \tilde{\mu}_i^{B,ind}(\mathbf{k}, \lambda) \mu_j^{A,ind}(\mathbf{k}', \lambda') \tilde{V}_{ij}{}'(\mathbf{R}, t). \tag{2.40}$$

We stress that in (2.40) the dipole moment of atom A is in the laboratory frame while that of atom B is still in the co-moving frame. We shall now transform the latter in the laboratory frame, in order to express the energy shift only in terms of quantities in this frame. Under a Lorentz transformation, the dipole moment transforms as a length; because the atoms move along the x direction, we have

$$\tilde{\boldsymbol{\mu}} = \gamma \mu_x \hat{\imath} + \mu_y \hat{\jmath} + \mu_z \hat{k}, \tag{2.41}$$

that shows that only the x component is different in the two reference frames.

Using the relation (2.29) between the induced dipole moment and the fluctuating vacuum field, we get

$$\Delta\tilde{E} = \sum_{\mathbf{k},\lambda} \sum_{\mathbf{k}',\lambda'} \alpha(A, k')\alpha(B, k) E_i(\mathbf{k}', \lambda'; \mathbf{R}_A) E_j(\mathbf{k}, \lambda; \mathbf{R}_B) \tilde{V}_{ij}(\mathbf{R}, t). \tag{2.42}$$

The Fourier components of the electric field operator in (2.42) are in the laboratory frame, because they come from relation (2.29) with the induced dipole moment in the laboratory system. The tensor $\tilde{V}_{ij}(\mathbf{R}, t)$ in (2.42) differs from the tensor $\tilde{V}_{ij}{}'(\mathbf{R}, t)$ in (2.40) because the γ factor in (2.41) has been included in it, that is

$$\tilde{V}_{xj}(\mathbf{R}, t) = \gamma \tilde{V}'_{xj}(\mathbf{R}, t), \qquad \tilde{V}_{yj}(\mathbf{R}, t) = \tilde{V}'_{yj}(\mathbf{R}, t), \qquad \tilde{V}_{zj}(\mathbf{R}, t) = \tilde{V}'_{zj}(\mathbf{R}, t). \tag{2.43}$$

In (2.42) a factor 2 should be added, taking into account that we should also consider an equal interaction energy obtained by exchanging the role of the two atoms. We shall include this factor 2 in the expression of the potential tensor $\tilde{V}_{ij}(\mathbf{R}, t)$ given in the following of this Section. We now take the vacuum expectation value of (2.42), taking into account that the electric field operators are in the laboratory frame. Thus we have

$$\langle 0|E_i(\mathbf{k}', \lambda'; \mathbf{R}_A)E_j(\mathbf{k}, \lambda; \mathbf{R}_B)|0\rangle = \frac{2\pi\hbar ck}{V}\,\hat{e}_i(\mathbf{k}, \lambda)\hat{e}^*_j(\mathbf{k}, \lambda)\, e^{-i\mathbf{k}\cdot(\mathbf{R}_B-\mathbf{R}_A)}\delta_{\mathbf{k}\mathbf{k}'}\delta_{\lambda\lambda'}. \tag{2.44}$$

In the continuum limit, $V \to \infty$, $\sum_{\mathbf{k}} \to V/(2\pi)^3 \int k^2 dk d\Omega$; performing polarization sum and angular integration,

$$\sum_{\lambda} \hat{e}_i(\mathbf{k}, \lambda)\hat{e}^*_j(\mathbf{k}, \lambda) = \delta_{ij} - \hat{k}_i\hat{k}_j, \tag{2.45}$$

$$\frac{1}{4\pi}\int \left(\delta_{ij} - \hat{k}_i\hat{k}_j\right) e^{\pm i\mathbf{k}\cdot\mathbf{R}}\, d\Omega = \left(\delta_{ij} - \hat{R}_i\hat{R}_j\right)\frac{\sin(kR)}{kR} + \left(\delta_{ij} - 3\hat{R}_i\hat{R}_j\right)\left(\frac{\cos(kR)}{k^2R^2} - \frac{\sin(kR)}{k^3R^3}\right), \tag{2.46}$$

we obtain

$$\langle \Delta\tilde{E}\rangle = 2\frac{\hbar c}{\pi}\int \left\{\hat{S}_{ij}\,\frac{\sin(kR)}{kR} + \hat{T}_{ij}\left(\frac{\cos(kR)}{k^2R^2} - \frac{\sin(kR)}{k^3R^3}\right)\right\}\tilde{V}_{ij}(\mathbf{R}, t)\, k^3\, dk. \tag{2.47}$$

In the approximation of a nonrelativistic motion, we have $\dot{x}(t) = at$, $\ddot{x}(t) = a$ and $\dddot{x}(t) = 0$. Using these expressions in (2.32-2.35), we obtain the electric and magnetic fields generated by the uniformly accelerating dipole in the laboratory frame. In order to obtain the expression of the tensor $\tilde{V}_{ij}(\mathbf{R}, t)$ in (2.47), we need the electric field in the co-moving frame. Thus we Lorentz-transform the fields according to the well-known relations

$$\begin{aligned}
\tilde{E}_x &= E_x \\
\tilde{E}_y &= \gamma(E_y - \beta B_z) \\
\tilde{E}_z &= \gamma(E_z + \beta B_y).
\end{aligned} \tag{2.48}$$

[54]. Using these transformations, the potential tensor $\tilde{V}_{ij}(\mathbf{R}, t)$ in (2.47) is obtained as

$$\begin{aligned}
\tilde{V}_{1j}(\mathbf{R}, t) = &-\frac{2\gamma(t)}{R}\left\{\frac{\hat{T}_{1j}}{R}\left[-\frac{1}{R}\mathcal{A}(R, t) + \frac{\omega}{c}\mathcal{B}(R, t)\right] + \hat{S}_{1j}\frac{\omega^2}{c^2}\mathcal{A}(R, t)\right. \\
&\left. + \hat{R}_j\frac{a}{c^2}\left[\left(\frac{1}{R} + \frac{\omega^2 t}{c}\right)\mathcal{A}(R, t) + \left(\frac{\omega t}{R} + \frac{2\omega}{c}\right)\mathcal{B}(R, t)\right]\right\},
\end{aligned} \tag{2.49}$$

$$\begin{aligned}
\tilde{V}_{2j}(\mathbf{R}, t) = &-\frac{2\gamma(t)}{R}\left\{\frac{\hat{T}_{2j}}{R}\left[-\frac{1}{R}\mathcal{A}(R, t) + \frac{\omega}{c}\mathcal{B}(R, t)\right] - \frac{\beta(t)}{c}\left[\hat{R}_l\varepsilon_{3lj}\omega\left(\frac{\omega}{c}\mathcal{A}(R, t) + \frac{1}{R}\mathcal{B}(R, t)\right)\right.\right. \\
&+ \hat{T}_{3l}\varepsilon_{lj1}\frac{a}{R}\left(-\left(\frac{1}{c} + \frac{t}{R}\right)\mathcal{A}(R, t) + \frac{t\omega}{c}\mathcal{B}(R, t)\right) \\
&\left.\left. + \hat{S}_{3l}\varepsilon_{lj1}\frac{a\omega}{c^2}\Big(\omega t\mathcal{A}(R, t) + 2\mathcal{B}(R, t)\Big)\right] + \hat{S}_{2j}\frac{\omega^2}{c^2}\mathcal{A}(R, t)\right\},
\end{aligned} \tag{2.50}$$

$$\tilde{V}_{3j}(\mathbf{R},t) = -\frac{2\gamma(t)}{R}\left\{\frac{\hat{T}_{3j}}{R}\left[-\frac{1}{R}\mathcal{A}(R,t)+\frac{\omega}{c}\mathcal{B}(R,t)\right]+\frac{\beta(t)}{c}\left[\hat{R}_l\varepsilon_{2lj}\omega\left(\frac{\omega}{c}\mathcal{A}(R,t)+\frac{1}{R}\mathcal{B}(R,t)\right)\right.\right.$$
$$+\hat{T}_{2l}\varepsilon_{lj1}\frac{a}{R}\left(-\left(\frac{1}{c}+\frac{t}{R}\right)\mathcal{A}(R,t)+\frac{t\omega}{c}\mathcal{B}(R,t)\right)$$
$$\left.\left.+\hat{S}_{2l}\varepsilon_{lj1}\frac{a\omega}{c^2}\Big(\omega t\mathcal{A}(R,t)+2\mathcal{B}(R,t)\Big)\right]+\hat{S}_{3j}\frac{\omega^2}{c^2}\mathcal{A}(R,t)\right\}, \tag{2.51}$$

where $\beta(t) = v(t)/c$, $\gamma(t) = (1-\beta^2(t))^{-1/2}$. We have used (2.36) and (2.37) with $\mathbf{R}$ in place of $\boldsymbol{\rho}$, and defined the functions

$$\mathcal{A}(R,t) = \cos(\omega t)\,\cos\left[\omega\left(t-\frac{R}{c}\right)\right], \tag{2.52}$$

$$\mathcal{B}(R,t) = \cos(\omega t)\,\sin\left[\omega\left(t-\frac{R}{c}\right)\right]. \tag{2.53}$$

Some considerations about the time-dependence of the potential tensor $\tilde{V}_{ij}(\mathbf{R},t)$ are now necessary. In the case of atoms at rest in the laboratory system, discussed in [8], the potential tensor is calculated, for each mode $(\mathbf{k},\lambda)$, after a time average on an oscillation period $2\pi/\omega$ of the dipoles. In that case, this is equivalent of taking a time-average of the quantities $\mathcal{A}(R,t)$ and $\mathcal{B}(R,t)$ in (2.52) and (2.53), respectively. In our case of accelerating atoms, extra time dependence is contained in the factors $\beta(t)$ and $\gamma(t)$ appearing in equations (2.49-2.51). We take the time-average of $\tilde{V}_{ij}(\mathbf{R},t')$ on a time t much larger than ω^{-1} (that is we take $\omega t \gg 1$ for a given ω) and keep the leading term in t only, which gives the main contribution to the time average. We thus consider the quantity

$$\langle\tilde{V}_{ij}(\mathbf{R},t)\rangle = \frac{1}{t}\int_0^t V_{ij}(\mathbf{R},t')dt'. \tag{2.54}$$

We take a nonrelativistic approximation; then

$$\beta(t) \simeq \frac{at}{c}; \qquad \gamma(t) \simeq 1+\frac{a^2t^2}{2c^2} \tag{2.55}$$

and keep only terms up to the second order in at/c. In order to evaluate (2.54) we need to calculate integrals of $\mathcal{A}(R,t')$ and $\mathcal{B}(R,t')$ and integrals of these functions multiplied by t' or t'^2, keeping only leading terms in t. After lengthy straightforward algebraic calculations, we finally obtain

$$\langle\tilde{V}_{ij}(\mathbf{R},t)\rangle = \left(1+\frac{a^2t^2}{6c^2}\right)\frac{1}{R^3}\left\{\hat{T}_{ij}\left[\cos(kR)+kR\sin(kR)\right]\hat{S}_{ij}\,k^2R^2\sin(kR)\right\}+Z_{ij}, \tag{2.56}$$

where $\mathbf{R} = (0,0,R)$ is along the z axis, and $\hat{T}_{ij} = \mathrm{diag}(1,1,-2)$ and $\hat{S}_{ij} = \mathrm{diag}(1,1,0)$ are diagonal 3x3 matrices. The 3x3 matrix Z_{ij} is defined below. Substituting (2.56) into (2.47), we obtain the van der Waals interaction energy shift of the two accelerating atoms

$$\langle\Delta\tilde{E}\rangle = \left(1+\frac{a^2t^2}{6c^2}\right)\Delta E^r + 2\frac{\hbar c}{\pi}\int\left\{\hat{S}_{ij}\frac{\sin(kR)}{kR}+\hat{T}_{ij}\left(\frac{\cos(kR)}{k^2R^2}-\frac{\sin(kR)}{k^3R^3}\right)\right\}Z_{ij}\,k^3\,dk \tag{2.57}$$

where

$$\Delta E^r = -\frac{\hbar c}{\pi R^3}\int_0^\infty k^3\, dk\, \alpha(A;k)\alpha(B;k) \times\left[kR\,\sin(2kR) + 2\,\cos(2kR) - 5\frac{\sin(2kR)}{kR} - 6\frac{\cos(2kR)}{k^2R^2} + 3\frac{\sin(2kR)}{k^3R^3}\right]$$
$$= -\frac{\hbar c}{\pi R^2}\int_0^\infty du\,\alpha(A;iu)\alpha(B;iu)\left[1+\frac{2}{uR}+\frac{5}{u^2R^2}+\frac{6}{u^3R^3}+\frac{3}{u^4R^4}\right]u^4e^{-2uR} \tag{2.58}$$

is the well-known van der Waals potential energy for two atoms at rest [7, 8]. In our result (2.57), t is the observation time and $\langle\Delta\tilde{E}\rangle$ is the interaction energy averaged between times 0 and t, as it follows from our averaging in (2.54); however, for sake of simplicity, we shall call it as the interaction energy at time t.

The result in (2.57) clearly shows that one effect of the uniform acceleration of the atoms is a correction to the potential energy proportional to a^2t^2/c^2 and a new term (that with the k integral), that we are now going to evaluate explicitly. We will show that this new term gives also a change of the R-dependence of the van der Waals potential energy when the two atoms are subjected to a uniform acceleration. From (2.57) and taking into account that $\hat{T}_{ij}$ and $\hat{S}_{ij}$ are diagonal matrices, we notice that only diagonal elements of the matrix Z_{ij} appearing in (2.56) are relevant. Their values are

$$Z_{11} = 0 \tag{2.59}$$

$$Z_{22} = \hat{T}_{33}\left[\frac{a^2t}{2c^3R^2}\cos(kR) + \frac{a^2t^2}{3c^2R^3}\cos(kR) + \frac{a^2t^2}{3c^2R^2}k\sin(kR)\right], \tag{2.60}$$

$$Z_{33} = \hat{T}_{22}\left[\frac{a^2t}{2c^3R^2}\cos(kR) + \frac{a^2t^2}{3c^2R^3}\cos(kR) + \frac{a^2t^2}{3c^2R^2}k\sin(kR)\right] + \hat{S}_{22}\left[\frac{a^2t}{c^3R}k\sin(kR) - \frac{a^2t^2}{3c^2R}k^2\cos(kR)\right]. \tag{2.61}$$

Substitution of (2.59-2.61) into (2.57), finally yields

$$\langle\Delta\tilde{E}\rangle = \Delta E^r + \frac{a^2t}{2c^3}\frac{\hbar c}{\pi R^3}\int_0^\infty \alpha(A;iu)\alpha(B;iu)\left(3+\frac{4}{uR}+\frac{2}{u^2R^2}\right)u^2\,e^{-2uR}\,du + \frac{a^2t^2}{6c^2}\frac{\hbar c}{\pi R^2}\int_0^\infty \alpha(A;iu)\alpha(B;iu)\left(-1+\frac{4}{uR}+\frac{8}{u^2R^2}+\frac{8}{u^3R^3}+\frac{4}{u^4R^4}\right)u^4\,e^{-2uR}\,du \tag{2.62}$$

The equation (2.62) is our main result for the van der Waals/Casimir-Polder interaction energy between uniformly accelerating atoms. It shows two terms correcting the van der Waals potential energy due to the atomic uniform acceleration: both are proportional to the square of the acceleration, and they explicitly depend on time as t and t^2, within our approximations. Because the potential for inertial atoms ΔE^r is negative (attractive interaction), Equation (2.62) shows that the effect of the acceleration is to reduce the interaction energy, and this reduction grows with time. This is consistent with the fact that the "effective interaction distance" $\rho(t_r)$ in (2.38) grows as time goes on, yielding a decrease of the

interaction energy between the accelerating atoms. However, as we shall discuss in more detail in Subsection 2.3.2, these corrections cannot turn the potential energy from attractive to repulsive, at least within our approximations.

We can consider two limiting cases of the van der Waals dispersion energy, the so-called *near zone* and *far zone*.

In the near zone, the interaction energy ΔE^r for atoms at rest is as R^{-6}. In this zone, we can approximate $uR \ll 1$ in (2.62), obtaining

$$\langle \Delta \tilde{E} \rangle \simeq -\left(1 - \frac{4a^2t^2}{9c^2}\right) \frac{3\hbar c}{2\,\pi R^6} \int_0^\infty \alpha(A; iu)\alpha(B; iu)\, du + \frac{a^2 t\, \hbar}{\pi\, c^2 R^5} \int_0^\infty \alpha(A; iu)\alpha(B; iu)\, du. \tag{2.63}$$

In the far zone we can approximate the atomic dynamical polarizabilities to their static value $\alpha^{A,B}(0)$, obtaining

$$\begin{aligned}\langle \Delta \tilde{E} \rangle =& \Delta E^r - \alpha^A(0)\alpha^B(0)\, \frac{\hbar c}{\pi R^3} \int_0^\infty \left\{ \frac{a^2 t}{2c^3 k} \left[3\sin(2kR) + 4\frac{\cos(2kR)}{kR} - 2\frac{\sin(2kR)}{k^2R^2} \right] \right. \\ &\left. + \frac{a^2t^2}{6c^2} \left[kR\, \sin(2kR) - 2\, \cos(2kR) + 3\frac{\sin(2kr)}{kR} + 2\frac{\cos(2kR)}{k^2R^2} - \frac{\sin(2kR)}{k^3R^3} \right] \right\} k^3\, dk\,,\end{aligned} \tag{2.64}$$

where in this case (far zone) the dispersion energy ΔE^r behaves as R^{-7}. Performing the k integrals, we finally get

$$\langle \Delta \tilde{E} \rangle \simeq -\frac{\hbar c}{\pi} \frac{\alpha^A(0)\alpha^B(0)}{R^7} \left(\frac{23}{4} - \frac{7}{24} \frac{a^2t^2}{c^2} \right) + \frac{11\hbar\, a^2 t}{8\pi\, c^2} \frac{\alpha^A(0)\alpha^B(0)}{R^6}. \tag{2.65}$$

These results clearly show the two new main features of the van der Waals interaction energy for accelerating atoms: a change of the dependence on the distance and an explicit time-dependence. In fact, from Equation (2.65) we can see that in the far zone an effect of the acceleration is to add a new (time-dependent) term behaving as R^{-6}, which has a longer range than the usual R^{-7} van der Waals energy in the Casimir-Polder regime for atoms at rest. A R^{-6} term in the atom-atom dispersion energy is known to occur when the interaction is calculated for atoms at rest at finite temperature [55], and this indicates the deep connection between our results and the Unruh effect. The near-zone result (2.63) also shows corrections giving an explicit time-dependence of the interaction energy proportional to the acceleration squared, and a new term proportional to acceleration and time, and decreasing as R^{-5}. The explicit time dependence as a^2t^2/c^2 in the first line of equations (2.63) and (2.65), for the near and far zone respectively, gives corrections to the interaction energy which grows with time and may become significant even for a reasonable value of the acceleration. In fact, it is possible to find time intervals such that, from one side the nonrelativistic approximation is still valid ($a^2t^2/c^2 \ll 1$), and on the other side the corrective term, although relatively small, is not negligible. For example, if $a^2t^2/c^2 \simeq 0.2$, we can still consider reasonable our approximation of a nonrelativistic motion of the atoms, and the correction to the van der Waals interaction energy from (2.63) and (2.65) is around ten

percent in the near zone and one percent in the far zone. These changes are small, but not negligible. Because only the product of acceleration and time is relevant for our correction to the dispersion energy (and not the absolute value of the acceleration, as in the correction to the Lamb shift or the atom-wall interaction energy [35, 37, 39, 56]), this should be achievable even with reasonable accelerations, provided a sufficiently long time is taken. Also, the corrections as R^{-6} and R^{-5} in the second lines of (2.63) and (2.65), respectively, give a change to the van der Waals interaction of a few percent, using the same value of the acceleration considered above and an interatomic distance R such that $aR/c^2 \sim 0.1$, for which our use of a locally inertial system is valid (see also the discussion at the end of next Subsection). These new results we found suggest a new possibility for detecting the Unruh effect, or in general effects related to accelerated motion in quantum electrodynamics, without necessity of extremely high accelerations as in the case of other quantum-electrodynamic effects recently discussed in the literature [4, 35, 37, 39].

2.3.2 Concluding remarks on the results

In the previous subsection we have considered the van der Waals interaction energy between two ground-state atoms (or polarizable bodies) moving in the vacuum with the same uniform acceleration. The acceleration is assumed orthogonal to the separation between the atoms, so that their distance is constant. We have shown that the main effects of the acceleration are twofold: an explicit time-dependence of the the interatomic interaction and a qualitative change of its dependence from the interatomic distance, which depends on the acceleration squared, making the interaction of longer range. In particular, in the near zone a new term as R^{-5} adds to the usual R^{-6} behavior, while in the far zone a R^{-6} term adds to the usual R^{-7} van der Waals energy in the Casimir-Polder regime.

We now discuss some physical consequences of our results as well as the limits of our approximations.

Our result (2.62) for the van der Waals dispersion interaction energy for two uniformly accelerating atoms, and approximated in (2.63) and (2.65) for the near- and far-zone respectively, clearly shows how the accelerated motion of the atoms affects the interaction energy and changes its distance dependence. The latter is an important point showing that the effect of the accelerated motion is not only a correction to the strength of the potential energy, but also a qualitative change of its properties. This also suggests, in perspective, the intriguing possibility of detecting signatures of the Unruh effect in interacting atomic systems, in particular when their properties, even at the macroscopic level, may critically depend on the form of the interaction among the atoms. The time dependence of the interaction in (2.62) is related to the effective interaction distance given by (2.38), which grows with time for the accelerated atoms, making larger the "effective distance" traveled by the virtual photons exchanged between the atoms, as time goes on. A similar effect is not present in cases previously considered for the Lamb shift of an accelerated hydrogen atom [56, 35] or the atom-surface Casimir-Polder interaction for an atom accelerating parallel to an infinite conducting plate [39]: in these cases, the field fluctuations perceived by the atom are time-independent and the atom-surface "effective distance" is constant, and thus

a time-dependence is not expected and the corrections depend on the absolute value of the acceleration only. We have also shown that taking appropriate values of the product of acceleration and time, the relative change of the van der Waals interaction, with parameters such that all our approximations are valid, can be in the range 1-10 percent, and thus not negligible.

In our model, we have neglected the possibility that the atoms are excited due to their acceleration. It is known that accelerated atoms have a finite probability of being spontaneously excited [56, 57, 58]. In principle, this could add another source of change of the distance dependence of the dispersion interaction between the atoms, because this interaction behaves differently if one or both atoms are excited [59]. The excitation probability, however, behaves as $1/(e^{2\pi c\omega_0/a}-1)$, ω_0 being a main atomic transition frequency [56, 57, 58]. It is thus very small (exponentially) when $a \ll c\omega_0$. Taking a typical value for $\omega_0 \sim 10^{15}\,\mathrm{s}^{-1}$, we expect that this contribution be negligible for $a \ll 10^{23}\,\mathrm{m/s}^2$. Since we can obtain a significant change of the van der Walls energy for much smaller accelerations (making negligible the excitation probability, which decreases exponentially with decreasing accelerations), provided we consider a sufficiently long time (see discussion above), atomic excitation induced by acceleration can be neglected in our case. Moreover, the contribution of the atomic excitation to the interatomic potential energy is a higher-order effect. In fact, the van der Waals interaction is a fourth-order effect, both for ground- and excited-state atoms [59]. Because the atomic excitation probability due to acceleration is a second-order effect, its contribution to the van der Waals interaction starts from sixth-order in the atom-field interaction.

Finally, we wish to make some considerations on the sign of the interaction energy of the accelerated atoms, which determines the attractive or repulsive character of the electric van der Waals force between two ground-state atoms (for atoms at rest it is always attractive). Equations (2.63) and (2.65) show that the accelerated motion reduces the potential energy between the atoms; this reduction grows with time, in agreement with the increasing effective interaction distance given by (2.38). One interesting question is to investigate whether the terms related to the acceleration in (2.63) and (2.65) can turn the van der Waals force to a repulsive character, thus making the interaction energy positive. In the near zone, analyzing equation (2.63), we see that the R^{-6} term changes sign when at/c is of the order of one; however, this is not compatible with our nonrelativistic approximation. On the other hand, the new (positive) R^{-5} term becomes comparable with the usual (negative) R^{-6} term for an interatomic distance $R \sim c^3/(a^2 t)$ and, due to our nonrelativistic approximation $at/c \ll 1$, this would require $R \gg c^2/a$. This situation, however, would require a different treatment of our problem, by quantizing the field in a curved space-time; in fact, our use of a locally inertial system for the accelerated atoms is valid only when the dimension of the system is much less than c^2/a [17, 60, 61]. In other words, an interatomic distance larger than c^2/a cannot thus be considered by adopting the locally inertial frame we have used. Similar considerations hold for the far-zone potential energy in (2.65), too. In our model there is not relative motion between the two atoms, so it seems that our results have no relation to the quantum friction (for discussion on quantum friction see Chapter 3). We can then conclude that, within our approximations, the attractive character of the van der

Waals interaction is preserved also for the accelerated atoms. However, our results show that the van der Waals interaction between the two atoms is significantly affected by their uniformly accelerated motion and the time-dependence of the interaction energy could allow to detect the accelerated motion without necessity of the extremely high accelerations. As a possible future perspective it could be very interesting analyze if the same effects can rise for atoms at rest under the influence of gravity and then if the equivalence principle can be invoked.

2.4 A fourth order method for the calculation of the Casimir-Polder force

In this section we present and extend a more rigorous approach to study the same problem faced in the previous section. As for the works presented in Section 2.2 we exploit the general procedure by Dalibard, Dupont-Roc and Cohen-Tannoudji (DDC) [43, 44]. However here we develop and extend, for the first time, the method up to order four in the coupling constant [45],[AN6]. This allows us to calculate the interaction energy between two atoms separating it into vacuum fluctuations and radiation reaction field contributions. These general equations then can be used to several physical situations and, in particular, we will use them to evaluate the interaction energy between the atoms in three very different cases: atoms at rest, atoms at rest in a thermal bath and atoms accelerated in the same direction in the vacuum.

Let us start describing the general method. The total Hamiltonian of a physical system interacting with a reservoir (see Figure 2.2) can be simply written as

$$H = H_S + H_R + V \tag{2.66}$$

where H_S and H_R are, respectively, the Hamiltonian of the system and of the reservoir. The system and the reservoir interact through a coupling potential that we indicated with V and it can be written in the form

$$V = g \sum_i R_i S_i. \tag{2.67}$$

In this equation g is a coupling constant and S_i (R_i) are Hermitian operators of the system (reservoir). Using the Heisenberg equations we can calculate the rate of variation of an arbitrary observable G and in particular the contribution given by the coupling is

$$\begin{aligned}\left(\frac{dG(t)}{dt}\right)_{\text{coupling}} &= \frac{i}{\hbar} g \sum_i [R_i(t) S_i(t), G(t)] \\ &= \frac{i}{\hbar} g\, R_i(t) \sum_i [S_i(t), G(t)].\end{aligned} \tag{2.68}$$

Let us now write the operator of the reservoir $R_i(t)$ as sum of a free part and a source part $R_i(t) = R_i^f(t) + R_i^s(t)$ where $R_i^f(t)$ represents its free evolution between time t_0 to time t

$$R_i^f(t) = e^{i(t-t_0)\, H_R(t_0)/h} R_i(t_0) e^{-i(t-t_0)\, H_R(t_0)/h}. \tag{2.69}$$

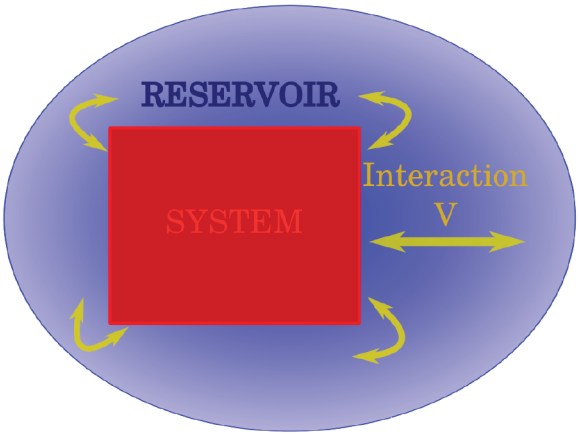

Figure 2.2 – The representative picture of a general physical system S immersed in a reservoir R, and that interacts with the reservoir by a linear interaction V.

It is the solution of the Heisenberg equation for R_i to zeroth-order in g. $R_i^s(t)$ is instead the solution of the Heisenberg equation for R_i to order 1 and higher in g. Splitting the operator $R_i(t)$ in this way and following the procedure suggested in [44], based on the chosen operator ordering which is symmetric in our case, we get two contributions to the variation rate of the observable G

$$\begin{aligned}\left(\frac{dG}{dt}\right)_{\mathrm{rf}} &= \frac{ig}{2\hbar}\sum_i \left\{[S_i(t), G(t)], R_i^f(t)\right\},\\ \left(\frac{dG}{dt}\right)_{\mathrm{sr}} &= \frac{ig}{2\hbar}\sum_i \left\{[S_i(t), G(t)], R_i^s(t)\right\}.\end{aligned} \tag{2.70}$$

The first equation is the *reservoir fluctuations* contribution that can be interpreted as due to the fluctuations of the reservoir; only the free part of R_i give a contribution to this term. The second equation is the *self reaction* contribution due to the influence of the system on the reservoir which reacts back on the system itself (this term depends on the reservoir operators only through the source part).

If we consider the following identity

$$\left\{Z_i, [S_i, G]\right\} = \left[\frac{1}{2}\{Z_i, S_i\}, G\right] + \frac{1}{2}\left\{[Z_i, S_i], G\right\} + S_i G Z_i - Z_i G S_i \tag{2.71}$$

we can write the rates in (2.70) as the sum of a term linked to an effective Hamiltonian H_{eff} and a term relative to relaxation. The latter is the non Hamiltonian part of the evolution of $G(t)$ [44] and takes into account phenomena like the spontaneous decay and the atomic

dissipation that, from now on, will be neglected. Then, for the two effective Hamiltonians, we have

$$H_{\rm rf}^{\rm eff}(t) = \frac{g}{4}\sum_i \left\{R_i^f(t), S_i(t)\right\}$$
$$H_{\rm sr}^{\rm eff}(t) = \frac{g}{4}\sum_i \left\{R_i^s(t), S_i(t)\right\}. \tag{2.72}$$

We are interested, in this section and in the following ones, to calculate the Casimir-Polder interaction energy between atoms. To obtain it we will make an average of the two effective Hamiltonians in the reservoir state. If the coupling constant g is relatively small we can perform a perturbative expansion in g. In our case we need a perturbative expansion up to fourth-order in the coupling constant. We thus need to extend this method to the fourth-order because the van der Waals/Casimir-Polder interaction is a fourth-order effect [59] (in [44] the rates are calculated up to order two in the coupling constant).

2.4.1 Perturbative calculation of the variation rates

We are interested to evaluate the average of the two rates of an arbitrary system observable, given by (2.70), using a perturbative expansion. At first we suppose that the reservoir and the system start to interact at time t_0. In mathematical terms, this means that the density operator at $t = t_0$ is factorized in a part relative to the system and in a part relative to the reservoir.

Considering the general Hamiltonian (2.66), let us write the Heisenberg equation for an arbitrary operator $O(t)$:

$$\begin{aligned}\frac{d}{dt}O(t) &= \frac{i}{\hbar}[H(t), O(t)]\\ &= \frac{i}{\hbar}[H_S(t) + H_R(t), O(t)] + \frac{i}{\hbar}[V(t), O(t)].\end{aligned} \tag{2.73}$$

Since the interaction term V depends on the coupling constant we can use this equation for our perturbative expansion in g. Let $|\alpha\rangle$ and $\langle\beta|$ ($|a\rangle, \langle b|$) indicate eigenstates of H_R (H_S) with eigenvalues E_α, E_β ($\varepsilon_a, \varepsilon_b$). A basis of operators for the spaces of R and S is

$$Q_{\alpha\beta} = |\alpha\rangle\langle\beta| \tag{2.74}$$
$$q_{ab} = |a\rangle\langle b|. \tag{2.75}$$

These operators have a free evolution Bohr frequency given by $\Omega_{\alpha\beta} = (E_\alpha - E_\beta)/\hbar$ for $Q_{\alpha\beta}$ and $\omega_{ab} = (\varepsilon_a - \varepsilon_b)/\hbar$ for q_{ab}. For example, the Heisenberg equation for the operator $Q_{\alpha\beta}$ is

$$\begin{aligned}\frac{d}{dt}Q_{\alpha\beta}(t) &= i\Omega_{\alpha\beta}Q_{\alpha\beta}(t)\\ &\quad + \frac{ig}{\hbar}\sum_i S_i(t)[R_i(t), Q_{\alpha\beta}(t)].\end{aligned} \tag{2.76}$$

We can write the general solution of this equation as

$$Q_{\alpha\beta}(t) = Q^f_{\alpha\beta}(t) + Q^s_{\alpha\beta}(t) \tag{2.77}$$

where

$$Q^f_{\alpha\beta}(t) = Q_{\alpha\beta}(t_0)e^{i\Omega_{\alpha\beta}(t-t_0)} \tag{2.78}$$

is the part of $Q_{\alpha\beta}(t)$ having a free evolution (zeroth-order in g), while

$$Q^s_{\alpha\beta}(t) = \frac{ig}{\hbar}\int_{t_0}^{t} dt'\, e^{i\Omega_{\alpha\beta}(t-t')} \times \sum_i S_i(t')[R_i(t'), Q_{\alpha\beta}(t')] \tag{2.79}$$

is the source part; it is of first order or higher in the coupling constant g. An analogous solution can be written for the operator $q_{ab}(t)$:

$$q^s_{ab}(t) = \frac{ig}{\hbar}\int_{t_0}^{t} dt'\, e^{i\omega_{ab}(t-t')} \times \sum_i R_i(t')[S_i(t'), q_{ab}(t')] \tag{2.80}$$

Now, starting from (2.79) we can perform our perturbative expansion in g by iteration. In fact, if we replace in (2.79) each operator with its free part, we get the first-order approximation of $Q^s_{\alpha\beta}(t)$. In a similar way we get the expansion of the operator $q_{ab}(t)$.

$$Q^s_{\alpha\beta}(t) \simeq \frac{ig}{\hbar}\int_{t_0}^{t} dt' \sum_i S^f_i(t')[R^f_i(t'), Q^f_{\alpha\beta}(t)] \tag{2.81}$$

$$q^s_{ab}(t) \simeq \frac{ig}{\hbar}\int_{t_0}^{t} dt' \sum_i R^f_i(t')[S^f_i(t'), q^f_{ab}(t)]. \tag{2.82}$$

Where we have used (2.78) and an analogous expression for $q^f_{ab}(t)$.

The expansion can be generalized to any reservoir (system) operator $R\,(S)$, by exploiting its expansion in terms of $Q_{\alpha\beta}(t)$ ($q_{ab}(t)$). In fact, we can write

$$\begin{aligned} R(t) &= \sum_{\alpha\beta} Q_{\alpha\beta}(t)\langle\alpha|R|\beta\rangle = R^f(t) + R^s(t), \\ S(t) &= \sum_{ab} q_{ab}(t)\langle a|S|b\rangle = S^f(t) + S^s(t), \end{aligned} \tag{2.83}$$

where

$$\begin{aligned} R^f(t) &= \sum_{\alpha\beta} Q^f_{\alpha\beta}(t)\langle\alpha|R|\beta\rangle, & R^s(t) &= \sum_{\alpha\beta} Q^s_{\alpha\beta}(t)\langle\alpha|R|\beta\rangle, \\ S^f(t) &= \sum_{ab} q^f_{ab}(t)\langle a|S|b\rangle, & S^s(t) &= \sum_{ab} q^s_{ab}(t)\langle a|S|b\rangle. \end{aligned} \tag{2.84}$$

Thus, at first order we have

$$R^s(t) \simeq \frac{ig}{\hbar}\int_{t_0}^{t} dt' \sum_i S_i^f(t')[R_i^f(t'), R^f(t)] \tag{2.85}$$

$$S^s(t) \simeq \frac{ig}{\hbar}\int_{t_0}^{t} dt' \sum_i R_i^f(t')[S_i^f(t'), S^f(t)]. \tag{2.86}$$

After we have found the expansion for each reservoir and system operator at the first order, we can use it to find the higher-order terms of the perturbative expansion by a recursive calculation.

2.4.2 The vacuum fluctuations contribution

The equation obtained in (2.72) and (2.84) are very general and can be used for many physical systems. Because we are interested in the Casimir-Polder interaction energy between two accelerating atoms, for the sake of simplicity, we will first consider a pair of two-level atoms (with the same transition frequency ω_0) interacting with the massless scalar field in its vacuum state. Then the free Hamiltonians of the two-level atoms A and B, that evolve with respect to the proper time τ, are (from now on in this section we use units such that $c = \hbar = 1$)

$$H_A = \omega_0\sigma_3^A(\tau), \quad H_B = \omega_0\sigma_3^B(\tau) \tag{2.87}$$

where we introduced the operator $\sigma_3^{A/B} = (1/2)\left(|e_{A/B}\rangle\langle e_{A/B}| - |g_{A/B}\rangle\langle g_{A/B}|\right)$ (Dicke notation [66]).

The free Hamiltonian of the quantum scalar field is

$$H_F(\tau) = \int d^3k\, \omega_k a_{\mathbf{k}}^\dagger a_{\mathbf{k}} \frac{dt}{d\tau} \tag{2.88}$$

where $a_{\mathbf{k}}$ and $a_{\mathbf{k}}^\dagger$ are the bosonic annihilation and creation operators of the scalar field $\phi(x)$.

The atoms and the field are coupled in a linear way through the following interaction Hamiltonian

$$H_A^{\text{int}} = \lambda\sigma_2^A(\tau)\phi[x_A(\tau)], \quad H_B^{\text{int}} = \lambda\sigma_2^B(\tau)\phi[x_B(\tau)] \tag{2.89}$$

where λ is the atom-field coupling constant and we have introduced the operators $\sigma_2^{A/B} = (i/2)(\sigma_-^{A/B} - \sigma_+^{A/B})$, indicating with $\sigma_-^{A/B} = |g_{A/B}\rangle\langle e_{A/B}|$ and $\sigma_+^{A/B} = |e_{A/B}\rangle\langle g_{A/B}|$ the atomic lowering and raising operators.

We now want to expand the effective Hamiltonian previously introduced up to order four in λ. Let us start calculating the vacuum fluctuations contribution. The vacuum fluctuations Hamiltonian as a function of the proper time τ relative to atom A is (see equation (2.72))

$$H_{\text{vf}}^{\text{A}}(\tau) = \frac{\lambda}{4}\left\{\phi^f[x_A(\tau)], \sigma_2^A(\tau)\right\} \tag{2.90}$$

(we get the same term for the atom B by interchanging the label A and B). To expand this vacuum fluctuations term up to order four, we must expand the operator $\sigma_2^A(\tau)$ up to order three. Since in the physical problem we are considering the system S is composed by two subsystems, that relative to atom A and that relative to atom B, we have $S = S_A \otimes S_B$. Then we define two basis for the operators relative to the system S, one for the subsystem S_A and one for the subsystem S_B, in a way similar to (2.75)

$$q_{aa'} = |a\rangle\langle a'| \tag{2.91}$$

$$q_{bb'} = |b\rangle\langle b'|. \tag{2.92}$$

Now we expand σ_2^A. Let us first write $q^s_{aa'}(\tau)$:

$$q^s_{aa'}(\tau) = i\lambda \int_{\tau_0}^{\tau} d\tau' \phi[x_A(\tau')][\sigma_2^A(\tau'), q^f_{aa'}(\tau)]. \tag{2.93}$$

Using the (2.84) we can write for $\sigma_2^{A,s}(\tau)$

$$\sigma_2^{A,s}(\tau) = i\lambda \int_{\tau_0}^{\tau} d\tau' \phi[x_A(\tau')][\sigma_2^A(\tau'), \sigma_2^{A\,f}(\tau)]. \tag{2.94}$$

We can find a similar expression for $\sigma_2^{B,s}(\tau)$ exchanging the label A with the label B in (2.94) while for the field operator we can write

$$\begin{aligned}\phi^s[x_{A/B}(\tau)] = i\lambda \int_{\tau_0}^{\tau} d\tau' \Big\{ &\sigma_2^A(\tau')[\phi[x_A(\tau')], \phi^f[x_{A/B}(\tau)]] \\ &+\sigma_2^B(\tau')[\phi[x_B(\tau')], \phi^f[x_{A/B}(\tau)]]\Big\}.\end{aligned} \tag{2.95}$$

Looking at (2.94), we have three possibilities to work out the third-order term of $\sigma_2^A(\tau)$. We can use $\sigma_2^A(\tau')$ with his second-order term and replace the free part for the field operator; we can replace the two operator, $\sigma_2^A(\tau')$ and $\phi[x_A(\tau')]$, with their respective first-order term; we can replace the field operator in (2.94) with his second-order term and use the free part for $\sigma_2^A(\tau')$.

Let us start with the first case mentioned. Keeping in mind the (2.83) and using recursively the (2.94) we can write the following contribution

$$\lambda\, T(\tau) + \lambda^2 \int_{\tau_0}^{\tau} d\tau'\, T'(\tau') + O(\lambda^3). \tag{2.96}$$

where $T(\tau)$ is a function of free operators only (so the first term on the right side of (2.96) is a term at first order in λ) and

$$\begin{aligned}T'(\tau') \propto \int_{\tau_0}^{\tau'} \int_{\tau_0}^{\tau} d\tau' d\tau'' \phi[x_A(\tau')]\phi[x_A(\tau'')] \\ \times \Big[[\sigma_2^A(\tau''), \sigma_2^A(\tau')], \sigma_2^{A,f}(\tau)\Big].\end{aligned} \tag{2.97}$$

As we already said, the Casimir-Polder interaction is a fourth-order effect then we can neglect the term with $T(\tau)$ in (2.96). For this reason, from now on, we will neglect all the terms such that the effective Hamiltonian is of order different from the fourth.

Then, to expand the term in (2.96) of $\sigma_2^A(\tau)$ up to third order we have to take the first-order expansion of $T'(\tau')$. Since we will average the Hamiltonian (2.90) in the ground state of the atoms A and B we have to keep in mind that

$$\langle g_{a/b}|\left[\sigma_2^{A/B}(\tau)\right]^{2n+1}|g_{a/b}\rangle = 0 \tag{2.98}$$

$$\langle g_{a/b}|\left[\sigma_2^{A/B}(\tau)\right]^{2n}|g_{a/b}\rangle \neq 0 \tag{2.99}$$

where $n \in \mathbb{N}$ and $|g_{a/b}\rangle$ is the ground state of the atom A (B). Also considering that we are interested to calculate an interaction energy between the atoms A and B our expression for the energy must have an interatomic-distance dependence and contain both operators relative to atom A and atom B. Terms which have atomic operators relative only to one of the two atoms could be considered as describing Lamb shift. So any expansion up to first-order of (2.97) will not give a contribution for the interaction energy.

We consider now the second case. That is we take the two operators at first order. Let us first consider the first-order expansion of $\sigma_2^A(\tau')$. We can obtain it similarly to what we have done in (2.82), i.e. replacing all the operators in the integral with the respective free operators. In this way we can easily see that the contribution given in (2.94) by this term would have three operators σ_2^A (at three different times) and therefore it is zero. This because of the average on the ground states of the atoms given by (2.98).

We now consider the third case where we do an expansion up to order two of the field operator and show that it gives a nonzero contribution. Using (2.95), we can cast the equation (2.94) as follows

$$\sigma_2^{A,s}(\tau) = (i\lambda)^2 \int_{\tau_0}^{\tau}\int_{\tau_0}^{\tau'} d\tau' d\tau'' \sigma_2^B(\tau'')\Big[\phi[x_B(\tau'')], \phi[x_A(\tau')]\Big]\Big[\sigma_2^{A^f}(\tau'), \sigma_2^{A^f}(\tau)\Big]. \tag{2.100}$$

where we have neglected a term containing three operators σ_2^A for the reasons before discussed. Analyzing (2.100), we have three possible expansions to get the third-order term. We start expanding $\sigma_2^B(\tau'')$ and using their free part for the other operators, to obtain the contribution

$$\begin{aligned}(i\lambda)^3 \int_{\tau_0}^{\tau}\int_{\tau_0}^{\tau'}\int_{\tau_0}^{\tau''} d\tau' d\tau'' d\tau''' \\ \times\phi^f[x_B(\tau''')]\Big[\sigma_2^{B^f}(\tau'''), \sigma_2^{B^f}(\tau'')\Big]\Big[\phi^f[x_B(\tau'')], \phi^f[x_A(\tau')]\Big]\Big[\sigma_2^{A^f}(\tau'), \sigma_2^{A^f}(\tau)\Big].\end{aligned} \tag{2.101}$$

Considering the Hamiltonian (2.90), we must calculate the following expectation value of the energy shift relative to the term in (2.101)

$$\langle\Big\{\phi^f[x_A(\tau)], \phi^f[x_B(\tau''')][\phi^f[x_B(\tau'')], \phi^f[x_A(\tau')]]\Big\}\rangle. \tag{2.102}$$

In order to compute expectation values as that in (2.102), Wick's theorem is very useful. According to this theorem it can be shown that, in our case, if we have four operators $\hat{A}$, $\hat{B}$, $\hat{C}$, $\hat{D}$, the expectation value for the product of the four operators on a state $|\psi\rangle$ can be expressed as

$$\begin{aligned}\langle\psi|\hat{A}\hat{B}\hat{C}\hat{D}|\psi\rangle = \langle\psi|\hat{A}\hat{B}|\psi\rangle\langle\psi|\hat{C}\hat{D}|\psi\rangle + \langle\psi|\hat{A}\hat{C}|\psi\rangle\langle\psi|\hat{B}\hat{D}|\psi\rangle + \langle\psi|\hat{A}\hat{D}|\psi\rangle\langle\psi|\hat{B}\hat{C}|\psi\rangle \\ -2\langle\psi|\hat{A}|\psi\rangle\langle\psi|\hat{B}|\psi\rangle\langle\psi|\hat{C}|\psi\rangle\langle\psi|\hat{D}|\psi\rangle. \end{aligned} \tag{2.103}$$

From this expression we can easily deduce the following identities

$$\begin{aligned}\langle[\hat{A},\hat{B}]\hat{C}\hat{D}\rangle &= \langle\hat{C}\hat{D}\rangle\left(\langle\hat{A}\hat{B}\rangle - \langle\hat{B}\hat{A}\rangle\right), \\ \langle\hat{A}[\hat{B},\hat{C}]\hat{D}\rangle &= \langle\hat{A}\hat{D}\rangle\left(\langle\hat{B}\hat{C}\rangle - \langle\hat{C}\hat{B}\rangle\right), \\ \langle\hat{A}\hat{B}[\hat{C},\hat{D}]\rangle &= \langle\hat{A}\hat{B}\rangle\left(\langle\hat{C}\hat{D}\rangle - \langle\hat{D}\hat{C}\rangle\right). \end{aligned} \tag{2.104}$$

With the help of the identities (2.104), we can then write the expression in (2.102) as follows

$$\begin{aligned}\langle\{\phi^f[x_A(\tau)],\phi^f[x_B(\tau''')]\}\rangle\langle[\phi^f[x_B(\tau'')],\phi^f[x_A(\tau')]]\rangle \\ =2\,C^F_{AB}(\tau,\tau''')(-2)\chi^F_{AB}(\tau',\tau'') \end{aligned} \tag{2.105}$$

where we have introduced, respectively, the field symmetric correlation function and the field susceptibility

$$C^F_{AB}(\tau,\tau') = \frac{1}{2}\langle 0|\{\phi^f[x_A(\tau)],\phi^f[x_B(\tau')]\}|0\rangle, \tag{2.106}$$

$$\chi^F_{AB}(\tau',\tau') = \frac{1}{2}\langle 0|[\phi^f[x_A(\tau)],\phi^f[x_B(\tau')]]|0\rangle. \tag{2.107}$$

The other possible contributions given by (2.100) can be obtained doing the expansion up to order one of the field operator $\phi[x_B(\tau'')]$ and replacing the others operators with their free part, or expanding the field operator $\phi[x_A(\tau')]$ at first order and substituting the others operators with their free part. In this way we obtain the following two contributions

$$\begin{aligned}\langle\Big\{\phi^f[x_A(\tau)],\Big[\Big[\phi^f[x_B(\tau''')],\phi^f[x_B(\tau'')]\Big],\phi^f[x_A(\tau')]\Big]\Big\}\rangle, \\ \langle\Big\{\phi^f[x_A(\tau)],\Big[\phi^f[x_B(\tau''')],\Big[\phi^f[x_B(\tau'')],\phi^f[x_A(\tau')]\Big]\Big]\Big\}\rangle. \end{aligned} \tag{2.108}$$

It is easy to see that, using the identities (2.104), the terms above vanish. We are thus able to write the fourth-order energy shift given by vacuum fluctuations contribution

$$\left(\delta E^A_a\right)_{vf} = 4i\lambda^4\int_{\tau_0}^{\tau}d\tau'\int_{\tau_0}^{\tau'}d\tau''\int_{\tau_0}^{\tau''}d\tau'''\,C^F_{AB}(\tau,\tau''')\chi^F_{AB}(\tau',\tau'')\chi^B_b(\tau'',\tau''')\chi^A_a(\tau,\tau') \tag{2.109}$$

where we introduced the linear susceptibilities of the two atoms

$$\begin{aligned}\chi^A_a(\tau,\tau') &= \frac{1}{2}\langle a|[\sigma_2^{Af}(\tau),\sigma_2^{Af}(\tau')]|a\rangle, \\ \chi^B_b(\tau,\tau') &= \frac{1}{2}\langle b|[\sigma_2^{Bf}(\tau),\sigma_2^{Bf}(\tau')]|b\rangle. \end{aligned} \tag{2.110}$$

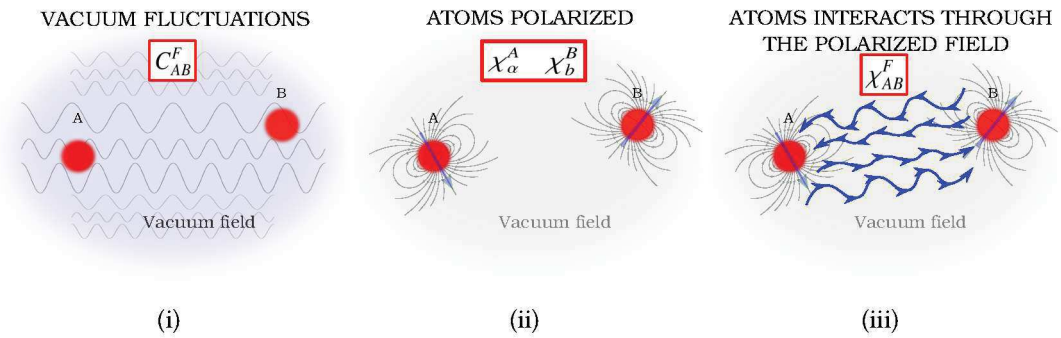

Figure 2.3 – The schematic picture describes a possible physical interpretation of the equation (2.109) giving the vacuum fluctuations contribution to the Casimir-Polder interaction.

Let us analyze the physical meaning of the expression (2.109) that we have obtained. The physical origin of the interaction energy generated by the vacuum fluctuations term can be thought in the following way: the field has nonlocal fluctuations, represented by the C^F function expressed in (2.106), which polarize the atoms inducing and correlating their dipole moments (expressed by $\chi^{A/B}$ in (2.107)); finally, these induced dipole moments polarize the field ($\chi^{A/B}$) causing the interatomic interaction (see Figure 2.3). This physical picture is also consistent with the paradigmatic interpretation of Casimir-Polder forces by Power and Thirunamachandran in [8], and often used to calculate also many-body Casimir-Polder forces [62, 63, 64].

2.4.3 The radiation reaction contribution

We now consider the radiation reaction contribution to the interaction energy. The radiation reaction Hamiltonian relative to atom A is

$$H^{\mathrm{A}}_{\mathrm{rr}}(\tau) = \frac{\lambda}{4}\Big\{\phi^s[x_A(\tau)], \sigma^A_2(\tau)\Big\}. \tag{2.111}$$

We get a similar term for the atom B simply changing the label A with B. To obtain the fourth-order expansion of (2.111), our starting point is equation (2.95) which allows us to write

$$\begin{aligned} H^{\mathrm{A}}_{\mathrm{rr}}(\tau) = \frac{\lambda}{4}(i\lambda)\int_{\tau_0}^{\tau} d\tau' \Big\{ &\Big\{\sigma^A_2(\tau), \sigma^A_2(\tau')\Big\}\Big[\phi[x_A(\tau')], \phi^f[x_A(\tau)]\Big] \\ &+\Big\{\sigma^A_2(\tau), \sigma^B_2(\tau')\Big\}\Big[\phi[x_B(\tau')], \phi^f[x_A(\tau)]\Big]\Big\}. \end{aligned} \tag{2.112}$$

Analyzing this equation, we can split its calculation in two parts: a first part from the term containing σ^A_2 and a second part from the term containing σ^B_2. Then let us start by calculating of the first term.

At first sight, we have many possible contributions for the first addend of (2.112). However, taking into account (2.94) and by considerations similar to those made before, we can

deduce that the operators σ_2^A in the first addend of (2.112) can be replaced with their relative free parts. Thus to obtain the contribution of the first part of (2.112) we must expand $\phi[x_A(\tau')]$ to order two. Using (2.95), we can write

$$H_{\rm rr}^{\rm A,1}(\tau) = \frac{\lambda}{4}(i\lambda)^2 \int_{\tau_0}^{\tau} d\tau' \Big\{\sigma_2^{Af}(\tau), \sigma_2^{Af}(\tau')\Big\}\Big[\sigma_2^B(\tau'')\Big[\phi[x_B(\tau'')], \phi^f[x_A(\tau')]\Big], \phi^f[x_A(\tau)]\Big] \tag{2.113}$$

where we have neglected the part of (2.95) with σ_2^A because it would give Lamb shift terms or vanishing terms, due to (2.98). Now, to obtain the fourth-order expansion we have two possibilities, expanding σ_2^B or expanding $\phi(x_B)$. When we expand $\phi[x_B(\tau'')]$, it is easy to show that for the field operators we have two terms of the form

$$\Big[[\hat{A}, \hat{B}], \hat{C}\Big]\hat{D} - \hat{D}\Big[[\hat{A}, \hat{B}], \hat{C}\Big]. \tag{2.114}$$

With the help of the identities (2.104) we obtain that the two addends in (2.114). This means that only the expansion of $\sigma_2^B(\tau'')$ gives a nonzero term for equation (2.113). So, using (2.104), we finally get

$$\Big(\delta E_a^{\rm A,1}\Big)_{\rm rr}(\tau) = 4i\lambda^4 \int_{\tau_0}^{\tau} d\tau' \int_{\tau_0}^{\tau'} d\tau'' \int_{\tau_0}^{\tau''} d\tau''' \, \chi_{AB}^F(\tau, \tau''')\chi_{AB}^F(\tau', \tau'')\chi_b^B(\tau'', \tau''') \, C_a^A(\tau, \tau') \tag{2.115}$$

where we have introduced the symmetrical correlation functions for the atom A/B

$$C_a^A(\tau, \tau') = \frac{1}{2}\langle a|\{\sigma_2^{Af}(\tau), \sigma_2^{Af}(\tau')\}|a\rangle, \tag{2.116}$$

$$C_b^B(\tau, \tau') = \frac{1}{2}\langle b|\{\sigma_2^{Bf}(\tau), \sigma_2^{Bf}(\tau')\}|b\rangle. \tag{2.117}$$

We should remember that (2.115) is only one contribution from the radiation reaction Hamiltonian (2.112). We still must compute the terms given by the expansion of σ_2^B in (2.112). However, the procedure is very similar to the previous ones yielding the vacuum fluctuation energy shift and (2.115). After lengthy but straightforward algebra, we can obtain this second contribution of the radiation reaction Hamiltonian. Adding the two contributions of $H_{\rm rr}^A$, we can finally write the complete radiation reaction energy shift

$$\begin{aligned}
\Big(\delta E_a^A\Big)_{rr} = {} & 4i\mu^4 \int_{\tau_0}^{\tau} d\tau' \int_{\tau_0}^{\tau'} d\tau'' \int_{\tau_0}^{\tau''} d\tau''' \; C_a^A(\tau, \tau')\chi_b^B(\tau'', \tau''')\chi_{AB}^F(\tau, \tau''')\chi_{AB}^F(\tau', \tau'') \\
& -4i\mu^4 \int_{\tau_0}^{\tau} d\tau' \int_{\tau_0}^{\tau'} d\tau'' \int_{\tau_0}^{\tau''} d\tau''' \, C_a^A(\tau''', \tau)\chi_b^B(\tau'', \tau')\chi_{AB}^F(\tau''', \tau'')\chi_{BA}^F(\tau', \tau) \\
& -4i\mu^4 \int_{\tau_0}^{\tau} d\tau' \int_{\tau_0}^{\tau'} d\tau'' \int_{\tau_0}^{\tau''} d\tau''' \, C_b^B(\tau', \tau''')\chi_a^A(\tau'', \tau)\chi_{BA}^F(\tau''', \tau'')\chi_{BA}^F(\tau', \tau) \\
& +4i\mu^4 \int_{\tau_0}^{\tau} d\tau' \int_{\tau_0}^{\tau'} d\tau'' \int_{\tau_0}^{\tau} d\tau''' \; C_{AB}^F(\tau''', \tau'')\chi_{AB}^F(\tau, \tau')\chi_b^B(\tau'', \tau')\chi_a^A(\tau''', \tau).
\end{aligned} \tag{2.118}$$

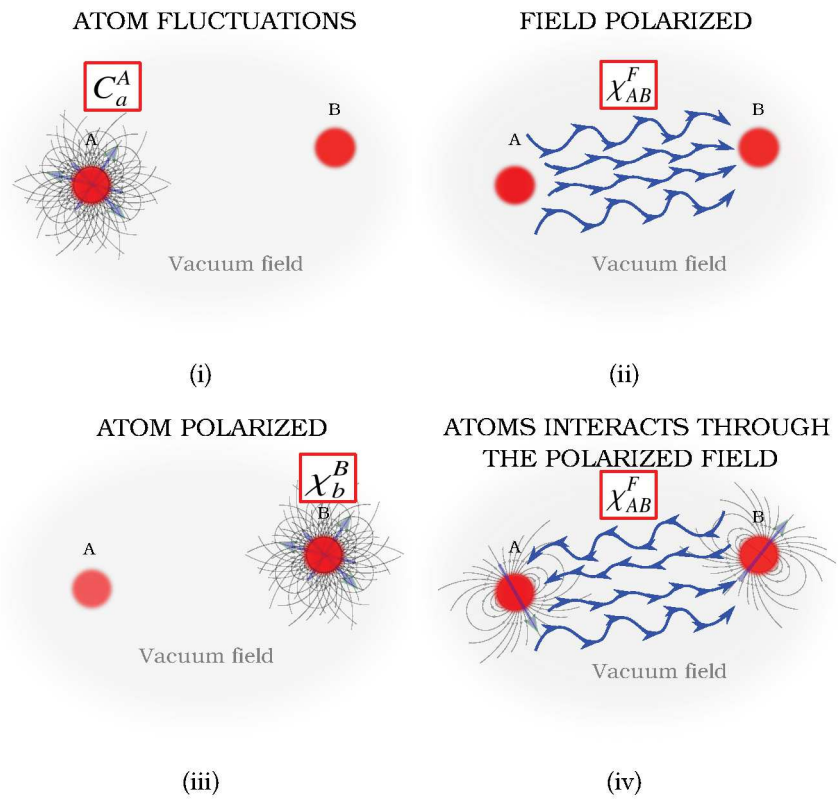

Figure 2.4 – A schematic figure that gives a possible intuitive interpretation of the equation (2.118) giving the radiation reaction contribution to the Casimir-Polder interaction.

For general symmetrical functions of the field as the following one

$$C_{AB}^F(\tau,\tau') = \int d\omega f(\omega)\left(e^{-i\omega(\tau-\tau')} + e^{i\omega(\tau-\tau')}\right) \tag{2.119}$$

the last term of the (2.118) is null. This can be easily proved performing first the integral on $d\tau'''$ and then the integral on $d\omega$. Symmetrical functions assume a form like that in (2.119) for many commons physical systems, for example the case of two atoms at rest.

As we did for the vacuum fluctuation term (2.109), we can now give a physical interpretation of the radiation reaction contribution that we have obtained in (2.118). One of the two atoms fluctuates (C_a^A/C_b^B) and polarizes the field (χ_{AB}^F). This produces a polarization of the other atom (C_b^B/C_a^A), the field reacts to this change and is polarized (χ_{AB}^F), generating the interaction between the two atoms (see Figure 2.4).

2.4.4 The van der Waals force between two atoms at rest

Now we can use the equations (2.109) and (2.118) to calculate, as example, the van der Waals/Casimir-Polder interaction energy for two identical two-level atoms at rest interacting with the scalar field. As a first step, we need to evaluate the statistical functions of the

field in a particular trajectory. In this section, to show the utility of the method we have developed and of our results (2.109) and (2.118) we study the van der Waals force between two atoms at rest. The atom A is fixed at the origin while the B atom is placed at a distance z. In this physical system, the statistical functions of the field can be calculated starting from (2.106) and (2.107); we get

$$\begin{aligned} C^F_{AB}(\tau,\tau') &= \frac{1}{8\pi^2 z}\int d\omega \sin(\omega z)\left(e^{-i\omega(\tau-\tau')} + e^{i\omega(\tau-\tau')}\right), \\ \chi^F_{AB}(\tau,\tau') &= \frac{1}{8\pi^2 z}\int d\omega \sin(\omega z)\left(e^{-i\omega(\tau-\tau')} - e^{i\omega(\tau-\tau')}\right). \end{aligned} \tag{2.120}$$

For the statistical functions of the atoms instead we have

$$\begin{aligned} C^A_a(\tau,\tau') &= \frac{1}{8}\left(e^{-i\omega_0(\tau-\tau')} + e^{i\omega_0(\tau-\tau')}\right), \\ \chi^A_a(\tau,\tau') &= \frac{1}{8}\left(e^{i\omega_0(\tau-\tau')} - e^{-i\omega_0(\tau-\tau')}\right) \end{aligned} \tag{2.121}$$

where we assume for simplicity that the atoms A and B are identical.

We first evaluate the vacuum fluctuations contribution. Using equations (2.120) and (2.121) we can cast equation (2.109) as follows

$$\begin{aligned} \left(\delta E^A_a\right)_{vf} = &-\frac{i\lambda^4}{1024\,\pi^4 z^2}\int_0^\infty d\omega \int_0^\infty d\omega' \sin(\omega z)\sin(\omega' z)\int_0^T du' \int_0^{T-u'} du'' \int_0^{T-u'-u''} du''' \\ &\times\left(e^{i\omega_0 u'} - e^{-i\omega_0 u'}\right)\left(e^{i\omega(u'''+u''+u')} + e^{-i\omega(u'''+u''+u')}\right)\left(e^{i\omega' u''} - e^{-i\omega' u''}\right)\left(e^{i\omega_0 u'''} - e^{-i\omega_0 u'''}\right) \end{aligned} \tag{2.122}$$

where we did the substitutions

$$\begin{aligned} u''' &= \tau'' - \tau''', \\ u'' &= \tau' - \tau'', \\ u' &= \tau - \tau', \\ T &= \tau - \tau_0. \end{aligned} \tag{2.123}$$

Moreover, we will consider the limits $\tau \to +\infty$ and $\tau_0 \to -\infty$, so that $T \to +\infty$. We start performing the integration over $d\tau'''$. All time integrands are integrals of exponential functions of the form

$$\lim_{\eta\to 0}\int_0^D du\, e^{\pm(\Omega\pm i\eta)u} = \left(e^{\pm(\Omega\pm i\eta)D} - 1\right)\left(\pm\frac{1}{i(\Omega\pm i\eta)}\right) \tag{2.124}$$

where Ω is in general sum of two of the three frequencies ω, ω', ω_0, and D is one of the three values T, $T-u'$, $T-u'-u''$. We added a pure imaginary part η in the argument of the exponentials; we will let it go to zero after the integration. The sign of η is chosen in a way such that when the u goes to infinity we have a decaying exponential that regularizes

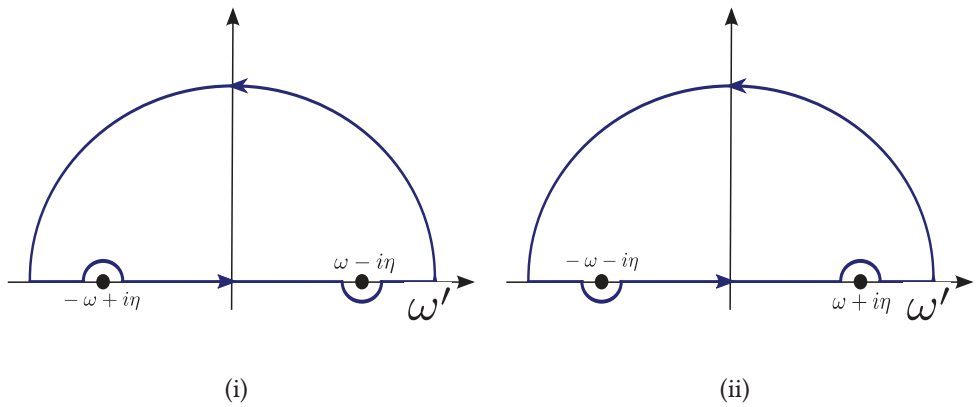

Figure 2.5 – Integration contours used to evaluate the integral over ω'. The contour (a) has been used for the term in the first row of (2.126) and the contour (b) for the term in the second row of (2.126).

our integral. This allows to easily deal with the poles in the frequency integration. Using (2.124), after the first time integration we get

$$e^{-i\omega(u'+u'')}\left(\frac{1}{i(\omega-\omega_0-i\eta)}-\frac{1}{i(\omega+\omega_0-i\eta)}\right)+e^{i\omega(u'+u'')}\left(\frac{1}{i(\omega-\omega_0+i\eta)}-\frac{1}{i(\omega+\omega_0+i\eta)}\right). \tag{2.125}$$

In the equation above we neglected the terms coming from the exponentials in the right hand side of (2.124), because in the integrand of (2.122) they yield the exponential factor $\exp(\pm i\omega T)$. Thus, making the integration over ω and considering that T goes to ∞, from the Riemann-Lebesgue lemma we can assert that these terms are vanishing. We want to stress that, consequently, we have no more explicit time dependence. We can do the same analysis for the integrations over τ'' and τ' getting the expression

$$\begin{aligned}&\left(\frac{1}{i(\omega-\omega_0-i\eta)}-\frac{1}{i(\omega+\omega_0-i\eta)}\right)^2\left(\frac{1}{i(\omega-\omega'-i\eta')}-\frac{1}{i(\omega+\omega'-i\eta')}\right)+\\&+\left(\frac{1}{i(\omega-\omega_0+i\eta)}-\frac{1}{i(\omega+\omega_0+i\eta)}\right)^2\left(\frac{1}{i(\omega-\omega'+i\eta')}-\frac{1}{i(\omega+\omega'+i\eta')}\right).\end{aligned} \tag{2.126}$$

We can now work out the ω' integral in the above equation. Analyzing the poles of the integrand we can use the two integration contours in Figure 2.5, respectively for the term in the first row and for the second row of (2.126), and then the limit of $\eta'\to 0$. The path is chosen according to the sign of η which suggests how avoid the pole. The integral over ω' is

$$\int_0^{+\infty} d\omega'\,\sin(\omega' z)\frac{2\omega'}{\omega^2-\omega'^2}=\frac{1}{2i}\int_{-\infty}^{+\infty} d\omega' e^{i\omega' z}\frac{2\omega'}{\omega^2-\omega'^2}=\pi\cos(\omega z)\quad \text{for } z>0 \tag{2.127}$$

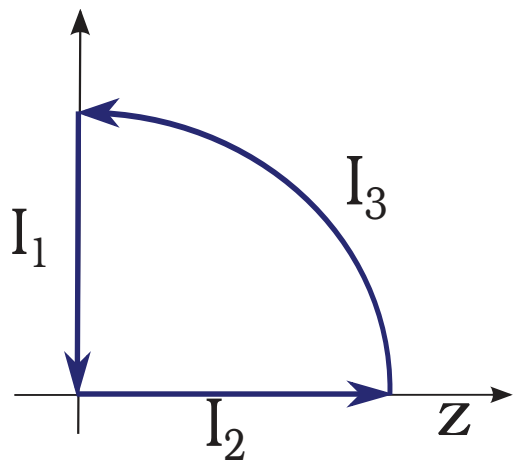

Figure 2.6 – Integration contour in the complex plane used to calculate the frequency integral in (2.128).

where we have exploited the parity of the function that multiply $\sin(\omega' z)$ and the residue theorem.

For the last integral over $d\omega$ we have to deal with the poles at $\pm\omega_0$. These poles are closely related to the dynamic polarizability of the two atoms $\alpha(\omega) \propto 1/(\omega_0^2 - \omega^2)$. When we consider the generalization that includes the possibility of absorption we can see that a linewidth parameter appears in the definition of the polarizability [65]. This means that the poles of the polarizability are always in the lower complex plane (the imaginary part is always negative). When we perform our integrations and the limit $\eta \to 0$ we must take into account that the poles have a negative imaginary part. So the energy shift for the vacuum fluctuations contribution becomes

$$E_{\mathrm{CP}}^{(\mathrm{vf})} = \frac{\lambda^4}{1024\,\pi^3\,z^2}\int_0^{+\infty} d\omega\,\sin(2\omega z)\frac{4\omega_0^2}{(\omega^2-\omega_0^2)^2} = \frac{\lambda^4}{1024\,\pi^3\,z^2}\,\Im\left(i\int_0^{+\infty} d\omega e^{i2\omega z}\frac{4\omega_0^2}{(\omega^2-\omega_0^2)^2}\right). \tag{2.128}$$

To calculate the integral above it is useful to transform it in an integration in the complex plane with the path shown in Figure 2.6. It is simple to see that the integral over I_3 is null. Since there are not singularities inside our closed integration contour, we have $I_2 = -I_1$. Thus we calculate only the integral over I_1 (that is done by the substitution $\omega = i\,u$ in (2.128)).

We will evaluate this integral in the two regimes of near and far zone, introduced in Chapter 1. In the far zone we know that only photons with low frequency ($\omega \ll \omega_0$) contributes significantly to the interaction and then we simply get

$$E_{\mathrm{CP}}^{(\mathrm{vf})} \simeq -\frac{1}{512\pi^3}\frac{\lambda^4}{\omega_0^2 z^3}. \tag{2.129}$$

In the near zone case, we know that only the high frequency photons are relevant for the

interaction ($\omega \gg \omega_0$), so

$$I_1 = \int_0^{+\infty} d\omega e^{-2\omega z} \frac{4\omega_0^2}{(\omega^2 - \omega_0^2)^2} \simeq \int_0^{+\infty} d\omega \frac{4\omega_0^2}{(\omega^2 - \omega_0^2)^2} \tag{2.130}$$

and we obtain

$$E_{\mathrm{CP}}^{(\mathrm{vf})} \simeq -\frac{1}{1024\pi^3} \frac{\lambda^4}{\omega_0 z^2}. \tag{2.131}$$

To compute the complete interaction energy it remains to work out the radiation reaction contribution in (2.118). We have already seen that the last row vanishes for symmetrical statistical correlation functions of the field and this is our case. The term in the first row is pretty similar to that from vacuum fluctuations that we have already calculated. After analogous analysis and time integrals calculations, we can cast this term as follows

$$\begin{aligned} &\frac{i\lambda^4}{1024\,\pi^4 z^2} \int_0^{\infty} d\omega \int_0^{\infty} d\omega' \sin(\omega z) \sin(\omega' z) \\ &\quad \times \left[\left(\frac{1}{(\omega + \omega_0 - i\eta)^2} - \frac{1}{(\omega - \omega_0 - i\eta)^2} \right) \left(\frac{1}{i(\omega + \omega' - i\eta')} - \frac{1}{i(\omega - \omega' - i\eta')} \right) + \right. \\ &\quad \left. + \left(\frac{1}{(\omega + \omega_0 + i\eta)^2} - \frac{1}{(\omega - \omega_0 + i\eta)^2} \right) \left(\frac{1}{i(\omega + \omega' + i\eta')} - \frac{1}{i(\omega - \omega' + i\eta')} \right) \right]. \end{aligned} \tag{2.132}$$

The integral over ω' is the same in (2.127). Considering again that the poles of the polarizability are in the lower complex plane and performing the integral over ω in the complex plane using the contour of Figure 2.6, we get

$$\begin{aligned} \int_0^{+\infty} d\omega \sin(2\omega z) \frac{\omega\omega_0}{(\omega^2 - \omega_0^2)^2} &= \Im \left(\int_0^{+\infty} d\omega\, e^{i2\omega z} \frac{\omega\omega_0}{(\omega^2 - \omega_0^2)^2} \right) \\ &= \Im \left(\int_0^{+\infty} i\, du\, e^{-2uz} i \frac{u\omega_0}{(u^2 - \omega_0^2)^2} \right) = 0. \end{aligned} \tag{2.133}$$

The last integral above is zero because the integrand is a real function so the imaginary part of the integral will be null. It means that the first term in (2.118) is zero.

We still need to calculate the other two remaining terms of the radiation reaction contribution in equation (2.118). Their calculation is similar and for brevity we will show only the computation for the term in the second row of (2.118). Starting with the integration over τ''' we get terms of the following form

$$\begin{aligned} &e^{i\omega_0(u''+u')} \left(\frac{2\omega}{\omega^2 - \omega_0^2} \right), \quad e^{-i\omega(T-u')} \frac{e^{\pm i\omega_0 T}}{i(\omega \mp \omega_0)} \left(e^{i(\omega+\omega_0)u''} - e^{i(\omega-\omega_0)u''} \right), \\ &\qquad e^{i\omega(T-u')} \frac{e^{\pm i\omega_0 T}}{i(\omega \pm \omega_0)} \left(e^{-i(\omega-\omega_0)u''} - e^{-i(\omega+\omega_0)u''} \right). \end{aligned} \tag{2.134}$$

For terms as the first in (2.134), using previous considerations on the poles of the polarizability, it is possible to perform the integration over ω without performing the time integrations first. Hence we have

$$\int_0^{+\infty} d\omega \sin(\omega z) \frac{2\omega}{\omega^2 - \omega_0^2} = \Im\left(\int_0^{+\infty} d\omega\, e^{i\omega z} \frac{2\omega}{\omega^2 - \omega_0^2}\right) = \Im\left(\int_0^{+\infty} i\, du\, e^{-uz} i \frac{2u}{u^2 - \omega_0^2}\right) = 0. \tag{2.135}$$

For the other terms in (2.134), the ones contain the parameter T, after the time integrations, we obtain expressions containing $e^{\pm i\omega T}$, $e^{\pm i\omega' T}$ and other terms proportional to

$$\pm \frac{\sin(\omega z)\sin(\omega' z)}{(\omega \pm \omega_0)^2} \left(\frac{2\omega'}{\omega'^2 - \omega_0^2}\right). \tag{2.136}$$

Terms containing $e^{\pm i\omega T}$ and $e^{\pm i\omega' T}$ vanish because of the Riemann-Lebesgue lemma, while the others are null when we integrate over ω' (see equation (2.135)). Thus the second and third terms of (2.118) are zero.

We can finally conclude that in the case considered here the radiation reaction contribution to the Casimir-Polder interaction energy is zero. The interaction energy is given exclusively by the vacuum fluctuations contribution; in the regimes of far and near zone the expressions of this energy are, respectively, the (2.129) and (2.131). This last result it is not too surprising if we think to the physical interpretation of Casimir-Polder forces given by Power and Thirunamachandran in [8] (equivalent to that given for the vacuum contribution in (2.109)), and often used to calculate consistently the Casimir-Polder forces for many physical situations.

2.5 Thermal and non-thermal signatures of the Unruh effect in Casimir-Polder forces

In this Section, we present our original results aiming at bridging the Casimir forces and the Unruh effect, showing that both thermal and non-thermal features associated to a relativistic uniformly accelerated motion can be probed through the Casimir-Polder force between two accelerating atoms. In order to inspect the hallmarks of relativistic accelerations on Casimir-Polder forces, we start using the general formula (2.72), which allows for the computation of Casimir-Polder forces in generic stationary conditions from first principles, extended to fourth order in perturbation theory (see equations (2.109) and (2.118)) [45],[AN6]. In particular, we consider the interaction energy, arising from quantum vacuum fluctuations, among two atoms moving with a uniform proper acceleration a in the same direction and separated by a constant distance z, perpendicular to their trajectories, and linearly coupled to a scalar field [40],[AN3]. We show that the Casimir-Polder force between the two accelerating atoms displays a novel transition in its distance dependence at a new length scale, z_a, given by the inverse of the atomic acceleration (hereafter we use natural units $\hbar = c = k_B = 1$.). Such a transition is a cross-over in the interaction energy,

from a Casimir-Polder potential for $az \ll 1$, where the static zero-temperature interaction (as z^{-2} and z^{-3} in the nonretarded and retarded regimes, respectively) receives a small thermal-like correction due to acceleration at the Unruh temperature $T_U = a/2\pi$, to a non-thermal interaction energy for $az \gg 1$, characterized by a z^{-4} power law decay. This result should be compared with the Casimir-Polder force between two static atoms interacting with the scalar field at temperature T, where at the thermal wavelength $\lambda^{th.} \sim 1/T$ the interaction shows a transition from the z^{-3} quantum regime to the z^{-2} thermal classical regime. The new characteristic length $z_a \sim 1/a$ is associated with the breakdown of the approximate description of the system in terms of a local inertial frame, and it indicates that the Casimir-Polder interaction is strongly reshaped by the presence of the non-inertial space-time background, associated to the relativistic accelerated motion of the two atoms. This phenomenology is a non-trivial extension of the Unruh thermal response detected by a single accelerated observer to a system of two accelerated particles [40],[AN3].

2.5.1 Thermal Casimir-Polder interactions

We consider the same Hamiltonian of a pair of two-level atoms (A,B), interacting with the scalar field, that we introduced in Section 2.4, characterized by the same transition frequency ω_0 and linearly coupled to a massless scalar field $\phi(x)$ by the coupling constant λ. This Hamiltonian, in the Dicke notation [66] and in natural units ($\hbar = c = 1$), is

$$H = \omega_0\sigma_3^A(\tau) + \omega_0\sigma_3^B(\tau) + \int d^3k\omega_{\mathbf{k}}a_{\mathbf{k}}^\dagger a_{\mathbf{k}}\frac{dt}{d\tau} + \lambda\sigma_2^A(\tau)\phi(x^A(\tau)) + \lambda\sigma_2^B(\tau)\phi(x^B(\tau)), \quad (2.137)$$

where σ_i ($i = 1, 2, 3$) are the Pauli matrices, $a_{\mathbf{k}}$, $a_{\mathbf{k}}^\dagger$ are the annihilation and creation operators of the massless scalar field $\phi(x)$ with the linear dispersion relation $\omega_{\mathbf{k}} = |\mathbf{k}|$. The Hamiltonian (2.137) is expressed in terms of the same proper time τ of the two atoms (assuming a background flat spacetime), and the interaction term is evaluated on a generic stationary trajectory $x(\tau)$ of the two atoms. The distance z between the atoms, perpendicular to their acceleration, is constant. Quantum fluctuations of the field, as well as radiation source fields, can induce an effective interaction among the two atoms at fourth order in the atom-field interaction. Following the procedure developed in the previous section, we use (2.109) and (2.118) as our starting point.

Since we want to focus on the relation between Casimir-Polder interactions and Unruh effect and to consider the connection between the latter and thermal effects we start our analysis calculating the Casimir-Polder energy in the case of a finite temperature T. For the thermal Casimir-Polder interaction, following procedures and considerations analogous to that done in Section 2.4.4, it is possible to show that the radiation reaction contribution is negligible compared to the vacuum fluctuation contribution for all the cases considered in this section. Specifically, at small temperatures, i.e. for $T \ll \omega_0$, or, in the case of two uniformly accelerating atoms, for $a \ll \omega_0$. Thus we concentrate on the vacuum fluctuations contribution only.

A simple generalization of (2.109) allows us to obtain the scalar Casimir-Polder force at finite temperature T, in terms of the thermal correlation function and susceptibility for a

scalar field

$$\begin{aligned} C^F_{th.}(\phi^f(x_A(\tau)),\phi^f(x_B(\tau'))) &= \frac{1}{8\pi^2}\frac{1}{z}\int_0^\infty d\omega\,\sin(\omega z)\coth\Big(\frac{\omega}{2T}\Big)(e^{-i\omega(\tau-\tau')}+e^{i\omega(\tau-\tau')}),\\ \chi^F_{th.}(\phi^f(x_A(\tau)),\phi^f(x_B(\tau'))) &= \frac{1}{8\pi^2}\frac{1}{z}\int_0^\infty d\omega\,\sin(\omega z)(e^{-i\omega(\tau-\tau')}-e^{i\omega(\tau-\tau')}). \end{aligned} \tag{2.138}$$

The explicit computation is performed in the limit of small temperatures, $T \ll \omega_0$, following a general method originally introduced by Lifshitz [68, 69, 70]. In view of the comparison with the Casimir-Polder force between two accelerated atoms, which is the main point of this section, it is important to stress that at finite temperatures, the massless thermal wavelength $\lambda^{th.} \sim 1/T$ separates a quantum regime from a classical thermal regime. Indeed, for distances $z \ll \lambda^{th.}$ we find the expression for the static scalar Casimir-Polder force in near and far zone plus subleading thermal corrections proportional to $-\frac{\lambda^4}{z}(\frac{T}{\omega_0})^2$; on the other hand, for distances larger than the typical length scales associated to quantum effects, i.e. for $z \gg \lambda^{th.}$, the Casimir-Polder force manifests again a classical thermal behavior similar to that in the near zone

$$E^{th.}_{CP} = -\frac{1}{512\pi^3}\frac{\lambda^4}{\omega_0^2}\frac{T}{z^2}, \tag{2.139}$$

as it has been already noticed for the electromagnetic case [55, 70].

2.5.2 Unruh corrections to Casimir-Polder interactions

We now apply the method we have developed in Section 2.4 to the case of two atoms moving with the same uniform acceleration, perpendicular to their separation. In this case, a modification of their Casimir-Polder interaction is expected, because the two atoms perceive modified vacuum fluctuations, as the Unruh effect would suggest [47, 32],,[AN1]. It is important to stress that for the accelerated case here analyzed we will focus our attention only on vacuum fluctuations contribution because it can be shown, with a calculation similar to that performed in Section 2.4.4 that the radiation reaction contribution is negligible compared to the vacuum fluctuations contribution.

An atom moving with uniform relativistic acceleration a in the $\hat{x}$ direction follows the worldline (we remember that we are using natural units $\hbar = c = k_B = 1$)

$$t(\tau) = \frac{1}{a}\sinh(a\tau) \quad x(\tau) = \frac{1}{a}\cosh(a\tau) \quad y(\tau) = z(\tau) = 0. \tag{2.140}$$

We are now going to show how interatomic Casimir-Polder interactions allow to distinguish the effect of a relativistic acceleration from a thermal behavior. Even if such a thermal character have been envisaged in a large number of situations [4, 56, 71, 72], departures from thermal predictions for accelerating atoms have been shown in the Lamb shift and in the spontaneous excitation of accelerating atoms, coupled to the electromagnetic field, in vacuum space [15, 35] or in front of a conducting plate [36, 39, 57, 73].

In such a situation it is convenient to introduce a new set of coordinates, necessary to cover the Minkowski spacetime (t, x) accessible to accelerated observers. They are defined

in two regions, the Rindler wedges, which are causally disconnected, and where a Rindler metric can be defined accordingly [4, 16].

We consider two uniformly accelerating atoms, moving along the worldlines (2.140) with the same uniform acceleration $a \ll \omega_0$, and separated by a distance z orthogonal to the acceleration direction $\hat{x}$. We now show that, at short distances, Casimir-Polder interactions can probe thermal Unruh-like effects, while at larger distances they reveal a non-thermal behavior due to the intrinsically non-inertial nature of the Rindler metric. As done in (2.138) for the thermal Casimir-Polder force, we first obtain the correlation function and susceptibility of the scalar field in the accelerated background

$$\begin{aligned} C^F_{acc.}(\phi^f(x_A(\tau)), \phi^f(x_B(\tau'))) &= \frac{1}{8\pi^2}\frac{1}{\mathcal{N}(z,a)}\int_0^\infty d\omega f(\omega,z,a)\coth\Big(\frac{\pi\omega}{a}\Big)(e^{-i\omega(\tau-\tau')} + e^{i\omega(\tau-\tau')}), \\ \chi^F_{acc.}(\phi^f(x_A(\tau)), \phi^f(x_B(\tau'))) &= \frac{1}{8\pi^2}\frac{1}{\mathcal{N}(z,a)}\int_0^\infty d\omega f(\omega,z,a)(e^{-i\omega(\tau-\tau')} - e^{i\omega(\tau-\tau')}), \end{aligned} \tag{2.141}$$

where $f(\omega,z,a) = \sin(\frac{2\omega}{a}\sinh^{-1}(\frac{az}{2}))$ and $\mathcal{N}(z,a) = z\sqrt{1+(az/2)^2}$. A close comparison between (2.141) and (2.138) shows that for $az \ll 1$ the correlation function (2.141) has a thermal-like behavior set by the Unruh temperature T_U. Hence, the vacuum fluctuations contribution (2.109) to the Casimir-Polder interaction exhibits, at the lowest order in az, the same thermal-like correction $\sim -\frac{\lambda^4}{z}(\frac{T_U}{\omega_0})^2$, found for the Casimir-Polder interaction at finite temperature. At higher orders in az, equation (2.141) shows that the correction due to the accelerated atomic motion starts to differ significantly from a thermal-like correction. (A similar behavior of the correlation functions (2.141) can be extrapolated from the Lamb shift and spontaneous emission corrections of an accelerated atom near a conducting plate obtained in [36, 39, 73]) This discrepancy suggests a strong breakdown of the common analogy between acceleration and finite temperature for the Casimir-Polder potential at distances $z \gg z_a \sim 1/a$ ($z_a \sim c^2/a$ when units with $c \neq 1$ are considered), resulting in a novel power law behavior of the Casimir-Polder interaction,

$$E^{acc.}_{CP} = -\frac{1}{512\pi^4}\frac{\lambda^4}{\omega_0^2}\frac{z_a}{z^4}. \tag{2.142}$$

Our result (2.142) shows that the Casimir-Polder interaction energy between two accelerated atoms decreases faster with the distance than in both near and far zones [40],[AN3]. This can be guessed from the following heuristic argument: since both atoms are accelerating, the distance traveled by a scalar photon emitted by one atom to reach the other atom increases with time, and this results in an overall decrease of the interaction strength among them (see Section 2.3). A more precise comparison between our result in (2.142) and the results obtained in 2.3 is not straightforward because in the latter case the interaction energy is time-dependent and valid in a well-defined time interval, while the present result involves a time average of the interaction energy, as it is evident from (2.109). In fact, considerations similar to those used after (2.125) show that in the present case there is not time dependence of the force, due to our time-averaging procedure.

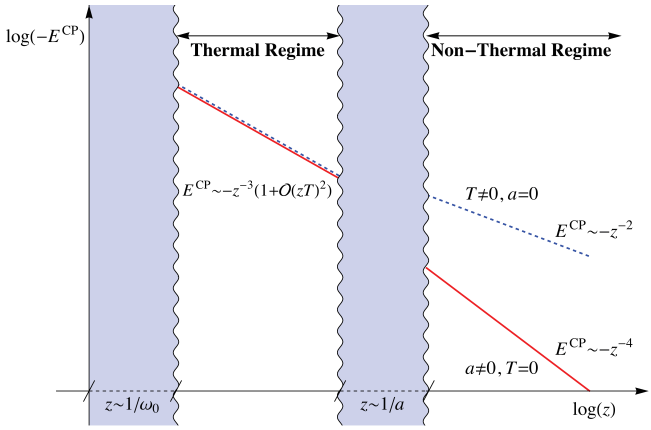

Figure 2.7 – Comparison between the Casimir-Polder interaction between two atoms (scalar case) moving with relativistic uniform acceleration a and constant separation z (red continuous line), and the static interaction for atoms at rest at temperature $T = a/2\pi$ and same distance (blue dashed line), in far zone, $z \gg 1/\omega_0$. While for short distances, $z \ll 1/a$, both potentials display the same thermal-like behavior, at distances larger than the characteristic length scale $1/a$, the thermal and the accelerated Casimir-Polder potentials exhibit a sharply different power law decay with the interatomic distance.

We can consider the behavior described by (2.142) as a new quantum regime, as opposed to the classical thermal regime given by (2.139) which, on the contrary, destroys the quantum retarded z^{-3} Casimir-Polder interaction. Also, we wish to stress that the distance z_a is the characteristic length scale for the breakdown of the local inertial frame approximation [60]: for distances smaller than z_a, it is possible to find a local inertial frame where the correlation functions of the scalar field are fairly well described by the their thermal Minkowski analogue, and the only net effect of acceleration is embodied in the Unruh thermal analogy; on the other hand, signals spreading over distances larger than z_a must take into account the non-inertial character of relativistic acceleration, encoded in the non-Minkowskian metric. Consequently, field quantization in Rindler spacetime will strongly affect the nature of vacuum fluctuations (C_F) and field susceptibility (χ_F), ultimately leading to the novel power law behavior of the Casimir-Polder potential (2.142). This phenomenology is in sharp contrast with the *classical* effect outlined above for the Casimir-Polder interaction at finite temperature (see equation (2.139)) and it is summarized in Fig. 2.7. It should be noted that such an effect cannot be detected by a single uniformly accelerated *point-like* detector in the unbounded space, as in [4, 56], since in this case it is always possible to find a local set of Minkowski coordinates in the neighborhood of a point-like detector. With this respect, our result can be seen as a non-trivial extension of the Unruh thermal response detected by a single accelerating observer, to a system of two relativistic accelerated systems. Finally, we wish to point out that the qualitative change of Casimir-Polder force described by equation (2.142) is ultimately grounded on the non-inertial character of the accelerated background and it is expected to manifest ubiquitously also for other fields, as well as for multi-level atoms.

In conclusion, we have shown how Casimir-Polder forces among two uniformly accelerating atoms can probe non-thermal effects beyond the Unruh analogy between uniform acceleration and finite temperature. We have shown that for interatomic distances above the characteristic length scale associated to a local inertial description of the system, the Casimir-Polder energy shows a different power law dependence with the distance, compared to the corresponding potential at finite temperature [40],[AN3].

A qualitative change of the interatomic potential may also affect some macroscopic properties of an accelerated many-atoms system, as the following example would suggest (analogous ideal experiments were envisaged in [74] for an accelerating box filled with photons). Let us consider a box filled with atoms with a given proper density and moving with finite acceleration a. The qualitative change of the interaction between the atoms from a marginal long-range z^{-3} to a short-range z^{-4} at the acceleration-dependent scale z_a given by (2.142), could manifest in a change of its thermodynamical properties (for example in the equation of state of the gas), if the average interatomic distance is larger than $\sim 1/a$, since the thermodynamics of long-range and short-range interacting systems is sharply different. (We adopt the definition of long-range interacting systems, $U(z) \simeq 1/z^{\alpha}$, with $\alpha \leq d$ where d is dimensionality of the system, relevant for thermodynamics [75]). This density/acceleration cross-over is of quantum origin, and it could have also consequences on the thermodynamics of the Universe during the stages of its evolution.

Also, we wish to stress that our new expressions for the fourth-order vacuum fluctuations and radiation reaction contributions to energy shifts have a general validity (see [45],[AN6]), and they could be straightforwardly applied to investigate electromagnetic dispersion interactions involving accelerating atoms [76, 15, 35, 39, 32],[AN1] or atoms in circular motion, which could be relevant to detect the Unruh effect [24]. Furthermore, they can be easily employed to compute dispersion forces between two atoms outside a Schwarzschild black hole or in de Sitter spacetime, where Casimir forces could provide new physical insights into problems of cosmological interest (similarly to recent calculations of the Lamb Shift in curved backgrounds [77, 78]).

2.6 The resonance interaction between two uniformly accelerated identical atoms

In this section we show our results obtained in the investigation of the resonance interaction between two uniformly accelerated identical atoms, one excited and the other in its ground state, prepared in a correlated (symmetric or antisymmetric) state [79],[AN7]. We show that this interaction exhibits, similarly to the ground-state accelerated atoms considered in the previous section, a pure non-thermal behavior, carrying no signature of Unruh thermal fluctuations on the interatomic force. Nevertheless, we show that the relativistic acceleration still causes a qualitative change of the distance-dependence of the interaction between the two atoms, as a consequence of the metric effects associated to relativistic accelerations.

We have seen in Chapter 1 that resonant interactions between atoms occur when one or more atoms are in their excited state and an exchange of real photons between the atoms is

involved [80, 81]. If the two atoms are prepared in an uncorrelated state, resonant Casimir-Polder interaction requires a fourth-order perturbation theory. In this case, the interaction scales as R^{-2} for large interatomic separations, $R \gg \lambda$ (R being the interatomic distance and λ the wavelength associated to the atomic transition). These effects have been recently discussed in the literature mainly focusing on the spatially oscillating behavior of the force [82, 83, 84]. On the other hand, resonant interactions can occur also when the two atoms are prepared in a correlated (symmetric or antisymmetric) state, and in this case they manifest as a second-order effect in the electric charge. Such interactions are of very long range, showing a R^{-1} dependence in the far-zone limit, and can be much larger than the usual dispersion interactions. It should be noted that decoherence effects induced by the environment can destroy the entanglement between the atoms, and this poses serious limits on the observability of such resonant effects. Recently, the possibility to control (for example to enhance) resonant forces between atoms placed in nano-structured materials (such as a photonic crystal) has been discussed [85]. Also, such effects have been investigated in relation to the resonant energy transfer between molecules, and it has been discussed that they can play a fundamental role in biological systems [86, 87, 88].

We shall now consider two identical atoms, one in the excited state and the other in the ground state, prepared in a correlated (symmetric or antisymmetric) state and uniformly accelerating in vacuum, and investigate the effect of the atomic acceleration on the resonance interaction between the two atoms. We first consider the atoms interacting with a relativistic scalar field and then we generalize our investigation to the electromagnetic field case. Since the atoms are prepared in a correlated state, our calculation requires only a second-order perturbation theory. We shall show that also for this system that new features appear as a consequence of the acceleration; specifically a different scaling of the interaction energy with the distance and a new dependence on the acceleration, if compared to the "Unruh-thermal" Casimir-Polder interaction case.

Following the procedure adopted in Section 2.4, we separate the contributions of vacuum fluctuations and radiation reaction to the resonant energy shift of the two atoms. We develop the method at second order in perturbation theory as in [43, 44, 56, 46]. We show that, in both cases considered, the resonance interaction is exclusively related to the radiation reaction contribution. Thus, Unruh thermal fluctuations do not affect the interatomic interaction. Beyond a characteristic length associated to the breakdown of a local inertial description of the system of two atoms, non-thermal effects, present in the radiation reaction corrections, change qualitatively the distance-dependence of the resonance interaction. Thus our approach permits to highlight non-thermal signatures of the atomic acceleration, through the second order resonant interaction between atoms.

The section is organized as follows. In Section 2.6.1 we introduce the model and we discuss the resonance interaction between two accelerated atoms interacting with the scalar field in the vacuum state. In Section 2.6.2 we generalize our procedure to the more realistic case of atoms interacting with the electromagnetic field. Section 2.6.3 is finally devoted to conclusions and perspectives. Details of some calculation are given in the Appendix A

2.6.1 The scalar field case

Let us consider two identical atoms A and B modeled as point-like systems with two internal energy levels, $\pm\frac{1}{2}\hbar\omega_0$, associated with the eigenstates $|g\rangle$ and $|e\rangle$, respectively, and separated by a distance z. We assume the two atoms accelerating with the same uniform acceleration along two parallel trajectories, $x_A(\tau)$ and $x_B(\tau)$, and interacting locally with a real massless scalar field in its vacuum state. Also we assume that ω_0 includes any direct modification of the atomic transition frequency due to the accelerated motion. The Hamiltonian describing the atom-field interacting system in the instantaneous inertial frame of the two atoms is (τ is a proper time) (2.137)

$$H(\tau) = \hbar\omega_0\sigma_3^A(\tau) + \hbar\omega_0\sigma_3^B(\tau) + \sum_{\mathbf{k}} \hbar\omega_k a_{\mathbf{k}}^\dagger a_{\mathbf{k}} \frac{dt}{d\tau} + \lambda\Big\{\sigma_2^A(\tau)\phi\Big[x_A(\tau)\Big] + \sigma_2^B(\tau)\phi\Big[x_B(\tau)\Big]\Big\} \tag{2.143}$$

where σ_i ($i = 1, 2, 3$) are the atomic pseudospin operators,, and $a_{\mathbf{k}}^\dagger$, $a_{\mathbf{k}}$ are the bosonic operators of the scalar field

$$\phi(\mathbf{x}, t) = \sum_{\mathbf{k}} \sqrt{\frac{\hbar}{2V\omega_k}} \left[a_{\mathbf{k}}(t)e^{i\mathbf{k}\cdot\mathbf{x}} + a_{\mathbf{k}}^\dagger(t)e^{-i\mathbf{k}\cdot\mathbf{x}}\right]. \tag{2.144}$$

We want to calculate the resonant energy shift of the system of the two accelerated atoms, using the procedure of Section 2.4. Since the resonant interaction is a second-order effect in the coupling constant, we use our expansion of the (2.72) simply up to second order. Then we can derive, after some algebra, the effective Hamiltonians $H_{vf,sr}$ at second order in the coupling for one of the two atoms. We obtain

$$\left(H_A^{eff}\right)_{vf} = -i\frac{\lambda^2}{2\hbar}\int_{\tau_0}^{\tau} d\tau' C^F(x_A(\tau), x_A(\tau'))\left[\sigma_{2,A}^f(\tau), \sigma_{2,A}^f(\tau')\right]$$

and

$$\begin{aligned}\left(H_A^{eff}\right)_{sr} = & - i\frac{\lambda^2}{2\hbar}\int_{\tau_0}^{\tau} d\tau' \chi^F(x_A(\tau), x_A(\tau'))\left\{\sigma_{2,A}^f(\tau), \sigma_{2,A}^f(\tau')\right\} \\ & - i\frac{\lambda^2}{2\hbar}\int_{\tau_0}^{\tau} d\tau' \chi^F(x_A(\tau), x_B(\tau'))\left\{\sigma_{2,A}^f(\tau), \sigma_{2,B}^f(\tau')\right\}\end{aligned} \tag{2.145}$$

where the statistical functions for the scalar field have been introduced in (2.106) and (2.107).

The resonant interaction between two atoms moving on the stationary trajectories $x_A(\tau)$ and $x_B(\tau)$, is then obtained evaluating the expectation value of effective Hamiltonians (2.145) and (2.145), on the correlated state of the two atoms, and taking into account only the terms depending on the atomic separation.

In order to do that, we suppose the system prepared in one of the correlated states

$$|\,\psi_\pm\rangle = \frac{1}{\sqrt{2}}\left(|\,g_A, e_B; 0_{\mathbf{k}}\rangle \pm |\,e_A, g_B; 0_{\mathbf{k}}\rangle\right), \tag{2.146}$$

where, as mentioned before, g (e) indicates the ground (excited) state of the atom, and $|\,0_{\mathbf{k}}\rangle$ the scalar field vacuum state. In such states the atomic excitation is delocalized among the two atoms. The symmetrical state is called a superradiant state, because in the Dicke model its decay rate is larger than that of the individual atoms, yielding a collective spontaneous decay [66]. On the contrary, the antisymmetric combination is called a subradiant state, because its decay rates is inhibited. Different methods to obtain super- and sub-radiant states for two-level systems, have been proposed (see for example [89, 90]). On the other hand, it has been recently shown that entanglement between accelerated systems can be induced by the Unruh bath [41, 42]. This is relevant for our problem, because resonance interactions require the atoms prepared in a correlated (symmetric or antisymmetric) state, and decoherence induced by the environment could pose serious limits on the observability of such effects.

To obtain the resonant energy shift for the system considered, we now evaluate the expectation values of H^{eff}_{vf} and H^{eff}_{sr} on the state (2.146). After some algebra, we get

$$\begin{aligned}(\delta E)_{vf} &= (\delta E_A)_{vf} + (\delta E_B)_{vf} \\ &+ \lim_{(\tau-\tau_0)\to\infty}\left(-\frac{i\lambda^2}{\hbar}\int_{\tau_0}^{\tau} d\tau' C^F(x_A(\tau), x_A(\tau'))\chi_A(\tau,\tau')\right) + (A \leftrightarrows B\,\text{terms})\end{aligned} \tag{2.147}$$

$$\begin{aligned}(\delta E)_{sr} &= (\delta E_A)_{sr} + (\delta E_B)_{sr} = \lim_{(\tau-\tau_0)\to\infty}\left(-\frac{i\lambda^2}{\hbar}\int_{\tau_0}^{\tau} d\tau' \chi^F(x_A(\tau), x_A(\tau'))C_A(\tau,\tau')\right) \\ &+ \lim_{(\tau-\tau_0)\to\infty}\left(-\frac{i\lambda^2}{\hbar}\int_{\tau_0}^{\tau} d\tau' \chi^F(x_A(\tau), x_B(\tau'))C_{A,B}(\tau,\tau')\right) + (A \leftrightarrows B\,\text{terms})\end{aligned} \tag{2.148}$$

were we have introduced the atomic statistical functions

$$C_{A,B}(\tau,\tau') = \frac{1}{2}\langle\psi_\pm|\left\{\sigma^f_{2,A}(\tau), \sigma^f_{2,B}(\tau')\right\}|\psi_\pm\rangle \tag{2.149}$$

$$\chi_{A,B}(\tau,\tau') = \frac{1}{2}\langle\psi_\pm|\left[\sigma^f_{2,A}(\tau), \sigma^f_{2,B}(\tau')\right]|\psi_\pm\rangle. \tag{2.150}$$

$$\tag{2.151}$$

It is clear that, at the order considered, the only contribution to the resonant interaction between the two atoms arises from the second term of (2.148). In fact, the (second order) vacuum fluctuations contribution (2.147) is exclusively related to nonlocal field correlations (expressed by $C^F(x_A(\tau), x_A(\tau'))$) evaluated on the trajectory of each atom (A or B), as if the other were absent; therefore (2.147) describes only the contribution of vacuum fluctuations to the Lamb-shift of each atom. Similarly, the first term of (2.148) describes the self-reaction contribution to the Lamb shift of each atom. On the contrary, the second term of (2.148) is the only relevant for the resonance interaction; it describes the interaction of each atom with the field it emits modified by the presence of the other atom (as expressed by $\chi^F(x_A(\tau), x_B(\tau'))$). It depends on the distance between the two atoms, and therefore it contributes to the interatomic interaction. It turns out that the resonance interaction is entirely due to the radiation reaction contribution, δE_{sr}, vacuum field fluctuations having no role at the order considered. This is indeed expected on a physical ground, because

resonant interactions are second order effects, originating from the exchange of photons between two correlated atoms. Atomic correlations are not induced by the (correlated) vacuum fluctuations, as in the dispersive interactions, but they are given by the atomic state considered.

The procedure outlined above is general and valid for any arbitrary stationary trajectory. We now focus on the specific situation of the atoms moving along the trajectories (2.152) with the same uniform acceleration a,

$$\begin{aligned} &t(\tau) = \frac{c}{a}\sinh\frac{a\tau}{c}, \;\; x_{A/B}(\tau) = \frac{c^2}{a}\cosh\frac{a\tau}{c}, \\ &y_{A/B}(\tau) = 0, \;\; z_A(\tau) = z_A \;\; , z_B(\tau) = z_B. \end{aligned} \tag{2.152}$$

We first evaluate the the linear susceptibility of the scalar field and the atomic correlation function. We have

$$\chi^F(x_A(\tau), x_B(\tau')) = -\frac{\hbar}{8\pi^2c^2}\frac{1}{z\sqrt{N(z,a)}}\int_0^\infty d\omega g(\omega,z,a), \left(e^{i\omega(\tau-\tau')} - e^{-i\omega(\tau-\tau')}\right) \tag{2.153}$$

and

$$C_{A,B}(\tau',\tau) = \pm\frac{1}{8}\left(e^{i\omega_0(\tau-\tau')} + e^{-i\omega_0(\tau-\tau')}\right) \tag{2.154}$$

where we have defined

$$N(z,a) = 1 + (za/2c^2)^2, \qquad g(\omega,z,a) = \sin\left[\frac{2\omega c}{a}\sinh^{-1}\left(\frac{za}{2c^2}\right)\right]. \tag{2.155}$$

Now, substituting (2.153) and (2.154) in (2.148) and taking into account only $z-$dependent terms, we finally obtain the resonance interaction between the two accelerated atoms

$$\delta E = (\delta E_A)_{sr} + (\delta E_B)_{sr} = \mp\frac{\lambda^2}{16\pi^2c^2}\frac{1}{z\sqrt{N(z,a)}}\int_0^\infty d\omega g(\omega,z,a)\left(\frac{1}{\omega+\omega_0} + \frac{1}{\omega-\omega_0}\right) \tag{2.156}$$

where $\mp$ signs refer, respectively, to the energy shift for the symmetric and antisymmetric states. The integral above can be computed analytically, giving

$$\delta E = \mp\frac{\lambda^2}{16\pi c^2}\frac{1}{z\sqrt{N(z,a)}}\cos\left(\frac{2\omega_0 c}{a}\sinh^{-1}\left(\frac{za}{2c^2}\right)\right). \tag{2.157}$$

Equation (2.157) is the main result of this section. Since the interaction is entirely due to the radiation reaction contribution, the effect of relativistic acceleration will leave no thermal signatures on the resonance interaction; its only effect comes from the normalization factor $N(z,a)$ and the function $g(\omega,z,a)$. Most importantly, the factor $N(z,a)$ yields a deviation from the inertial character of the metric. Indeed, as discussed in previous section, we can identify a new characteristic length scale, $z_a = c^2/a$, associated to the breakdown of the approximate description of the system in terms of a local inertial frame. For distances smaller

than z_a, it is possible to find a local inertial frame where the linear susceptibility of field is fairly well described by its static counterpart; on the other hand, signals spreading over distances larger then z_a, cannot disregard the non-inertial character of relativistic acceleration, encoded in the non-Minkowskian Rindler metric. Accordingly, we expect that relativistic accelerations can deeply modify the qualitative behaviour of the resonant interaction energy. In fact, in the limit $z \gg c^2/a$, we get

$$\delta E \simeq \mp \frac{\lambda^2}{8\pi} \frac{1}{z^2 a} \cos\left(\frac{2\omega_0 c}{a} \log\left(\frac{za}{c^2}\right)\right), \tag{2.158}$$

while for $z \ll c^2/a$ we recover the static result

$$\delta E = \mp \frac{\lambda^2}{16\pi c^2} \frac{1}{z} \cos\left(\frac{\omega_0 z}{c}\right) \tag{2.159}$$

Thus, the resonance interaction strongly bears signatures of the relativistic acceleration, resulting in a new power law decaying as z^{-2} compared to the usual z^{-1} of the static case (see equation (2.159)). This result should be compared with that obtained in Section 2.5, where it was shown that, as a consequence of the metric effects, the scalar Casimir-Polder interaction between two uniformly accelerated atoms, was characterized by a new z^{-4} power law decay, for distances $z \gg c^2/a$. Also, equation (2.158) exhibits a global overall pre-factor depending on the inverse of the acceleration, while the "thermal-Unruh" analogy would have suggested the presence of a Unruh term at temperature $T_U = a/2\pi$, directly proportional to acceleration [40],[AN3]. Therefore, our result shows that it is possible to single out metric effects associated to relativistic accelerations from the usual "Unruh thermal-like" effects.

The limit $z \ll c^2/a$ gives back the expression of the resonant interaction in the static case. For typical interatomic distances ($z \sim 10^{-6}$m), this is valid also for high acceleration values, thus suggesting that the resonance interaction is almost insensitive to the atomic acceleration in the limit $z \ll z_a$. Actually, such a behavior can be expected from the following qualitative considerations. Resonance interactions arise from the exchange of real photons between the atoms. Then, if the distance between the atoms is much smaller then z_a, in the time spent by the real photon emitted by one atom to reach the other atom ($t \sim z/c$), the accelerating atoms move of a distance (x) smaller than their interatomic distance z. The photon mediating the interaction then cannot discern the atomic motion, and the interaction appears to be the static one.

Finally, it is worth to note from (2.158), that the static resonance interaction decreases as z^{-1} for any interatomic distance. This is a consequence of the scalar model we have considered and of the fact that the resonance interaction is essentially the interaction of an atom with the field emitted by the other atom. The situation is quite different in the case of electromagnetic field, as we are going to discuss in the next subsection.

2.6.2 The electromagnetic field case

We now extend our previous investigation to the case of two uniformly accelerated atoms interacting with the electromagnetic field in the vacuum state.

To describe our system, we adopt the Hamiltonian in the multipolar coupling scheme and in the dipole approximation

$$H = H_A + H_B + \sum_{\mathbf{k}j} \hbar\omega_k a^\dagger_{\mathbf{k}j} a_{\mathbf{k}j} \frac{dt}{d\tau} - \mu_A(\tau)\cdot\mathbf{E}(x_A(\tau)) - \mu_B(\tau)\cdot\mathbf{E}(x_B(\tau)) \tag{2.160}$$

where $\mathbf{E}(x(\tau))$ is the electric field operator and $\mu = e\mathbf{r}$ the atomic dipole moment operator.

As already discussed, the resonant interaction energy is related only to the radiation reaction contribution and it is obtained from the expectation value of the effective Hamiltonian $(H_A^{eff})_{sr} + (H_B^{eff})_{sr}$ on the states $|\psi_\pm\rangle$

$$\delta E = -\frac{e^2}{2}\int_{\tau_0}^{\tau} d\tau' \chi^F_{\ell m}(x_A(\tau), x_B(\tau'))C^{A/B}_{\ell m}(\tau,\tau') + (A \leftrightarrows B \text{ terms}) \tag{2.161}$$

In order to calculate this quantity, we first obtain the field and atomic statistical functions. The susceptibility of the electromagnetic field in the accelerated frame can be obtained from the two-point field correlation function in the proper reference frame of the two accelerated atoms (Rindler noise) [15]. After lengthy calculations involving Lorentz transformations of the electromagnetic field, we obtain

$$\begin{aligned} g_{\ell m}(x_A(\tau), x_B(\tau')) = \langle 0|E_\ell(x_A(\tau))E_m(x_B(\tau'))|0\rangle &= \frac{\hbar a^4}{4\pi c^7}\frac{1}{\left(\sinh^2\frac{a(\tau-\tau'-i\epsilon)}{2c} - \left(\frac{za}{2c^2}\right)^2\right)^3} \\ &\times\left\{\left[\delta_{\ell m} - \frac{za}{4c^2}n_\ell k_m\right]\sinh^2\frac{a(\tau-\tau')}{2c}\right. \\ &\left. + \left(\frac{za}{2c^2}\right)^2[\delta_{\ell m} - 2n_\ell n_m]\left[1 + 2(\delta_{\ell m} - k_\ell k_m)\sinh^2\frac{a(\tau-\tau')}{2c}\right]\right\} \end{aligned} \tag{2.162}$$

$(\ell, m = x, y, z)$. $\mathbf{n} = (0,0,1)$ is the unit vector along the z direction and $\mathbf{k} = (1,0,0)$ is the unit vector along the direction x of acceleration. A simple calculation shows that the only nonzero components of $g_{\ell m}$ are the xx, yy, zz, and xz components. In particular, $g_{\ell\ell}(x_A(\tau), x_B(\tau')) \neq g_{mm}(x_A(\tau), x_B(\tau'))$ (for $\ell \neq m$); Therefore, the Rindler noise evaluated on the atomic trajectories of the two accelerated atoms, is not isotropic and displays a non-diagonal component. A similar anisotropy is not present in the case of a single uniformly accelerated atom in the unbounded space, where it is possible to show that the Rindler noise is isotropic. Actually, we have two distinct spatial directions, namely the direction of the acceleration and the direction of distance vector between the two atoms; in this sense, the anisotropic aspect of the Rindler function can be ascribed to the spatial extent of the two-particles system considered. From Eq (2.162), we can obtain the linear susceptibility of electromagnetic field in the proper reference frame. Its expression, as an integral over frequencies, is

$$\begin{aligned} \chi_{\ell m}(x_A(\tau), x_B(\tau)) = \frac{ia^4}{\pi c^7}\frac{1}{\sqrt{N(z,a)}}&\left\{M_{\ell m}\left[c_1(z,a)]\frac{d^2}{dT^2} + c_2(z,a)\frac{d}{dT} + c_3(z,a)\right]F(T,u)\right. \\ &\left. + Q_{\ell m}\left[c_4(z,a)\frac{d}{dT} + c_5(z,a)\right]F(T,u)\right\} \end{aligned} \tag{2.163}$$

where $M_{\ell m}(z,a)$, $Q_{\ell m}(z,a)$ and the coefficients $c_i(z,a)$ ($i = 1, ...5$) are given in the Appendix A, and we have defined

$$F(T,u) = \int_0^\infty d\omega \sin(\omega T)(e^{i\omega u} - e^{-i\omega u}), \quad u = \tau - \tau'$$
$$T = \frac{2c}{a}\sinh^{-1}\left(\frac{za}{2c^2}\right) \tag{2.164}$$

The symmetric correlation function for the atoms is

$$C^{A/B}_{\ell m}(\tau,\tau') = \frac{1}{2}\langle\psi_\pm|\left\{r^A_\ell(\tau), r^B_m(\tau')\right\}|\psi_\pm\rangle = \pm\frac{1}{4}\left(e^{i\omega_0(\tau-\tau')} + e^{-i\omega_0(\tau-\tau')}\right)(r^A_{12})_\ell(r^B_{21})_m \tag{2.165}$$

The resonance interaction between the two accelerated atoms is now obtained substituting Eqs. (2.163) and (2.165) into Equation (2.161), and taking the limits $\tau_0 \to -\infty$, $\tau \to \infty$. After some algebraic manipulation (details are given in the Appendix A), we obtain

$$\delta E = \pm(\mu^A_{21})_\ell(\mu^B_{12})_m\left(V_{\ell m}(\omega_0,z,a) + (\frac{za}{2c^2})^2\frac{1}{N(z,a)}U_{\ell m}(\omega_0,z,a)\right) \tag{2.166}$$

where the explicit expressions of $V_{\ell m}(\omega_0,z,a)$ and $U_{\ell m}(\omega_0,z,a)$ are given in the Appendix A. These quantities explicitly depend on the atomic acceleration and can be interpreted as a generalization of the static interaction potential to the case of accelerated atoms.

The expression given above is valid for any value of az/c^2. As before, we now investigate the two cases, $z \ll c^2/a$ and $z \gg c^2/a$.

It is easy to show that, for $za \ll 1$, the linear susceptibility (2.163) is fairly well described by its static counterpart. Therefore, at the lowest order in za, we recover the usual expression of the resonance interaction in the static case [80]

$$\delta E = \pm(\mu^A_{21})_\ell(\mu^B_{12})_m V_{\ell m}(\omega_0,z) \tag{2.167}$$

where $V_{\ell m}(\omega_0,z)$ is the well-known tensor potential

$$V_{\ell m} = \frac{1}{z^3}\left\{(\delta_{\ell m} - 3n_\ell n_m)\left[\cos\left(\frac{\omega_0 z}{c}\right) + \frac{\omega_0 z}{c}\sin\left(\frac{\omega_0 z}{c}\right)\right] - (\delta_{\ell m} - n_\ell n_m)\frac{z^2\omega_0^2}{c^2}\cos\left(\frac{\omega_0 z}{c}\right)\right\} \tag{2.168}$$

In particular, in the far-zone limit ($R \gg \lambda$), the resonance interaction decreases as $\sim 1/z$, while in the near-zone ($R \ll \lambda$), $\delta E \sim z^{-3}$ [80].

On the other hand, at higher orders in az, we expect that the corrections due to the atomic acceleration cause a qualitative change of the resonance interaction, scaling with a different power law. In particular, it is interesting to consider the situation when one of the two dipoles is oriented along the x direction and the other along the z direction. A similar situation was not present in the case of scalar field considered before, since it is clearly related to the peculiar anisotropic nature of the Rindler noise of the electromagnetic field.

In this case, the only non-zero contribution to the resonant interaction comes from the anisotropic term $W_{\ell m}(\omega_0, z, a)$ in (2.166), and we find

$$\delta E_{CP} = \pm\mu_z^A \mu_x^B \frac{1}{2z^3} \cos\left(\frac{2c\omega_0}{a} \ln\left(\frac{az}{c^2}\right)\right) \tag{2.169}$$

Our result (2.169) shows that, for specific orientations of the two dipole moments, the resonance interaction between two accelerated atoms decreases with the distance as z^{-3}. This also shows that it is possible to control the effect of atomic acceleration by an appropriate choice of the orientation of the dipole moments. A comparison with the case of the scalar field discussed in the previous section shows that the emergence of a qualitative change of the resonance interaction behavior comes not only from the presence of the metric factor, $N(z, a)$, but also from the anisotropic structure of the field susceptibility, related to the vector nature of the electromagnetic field and to the fact that our two-atom system is spatially extended.

2.6.3 Conclusions and Future Perspectives

In this section we have investigated the resonance interaction between two uniformly accelerated atoms, one excited and the other in ground state, prepared in correlated (symmetrical or anti-symmetrical) state [79],[AN7]. We have considered the contributions of vacuum fluctuation and radiation reaction field to the resonance interaction, and shown that the Unruh thermal fluctuations do not affect the interatomic interaction, which is exclusively modified by radiation-reaction corrections. We have discussed that beyond a characteristic length scale associated to the breakdown of the approximate description by a local inertial frame of the system of the atoms, non-thermal effects change qualitatively the distance-dependence of the resonance interaction. Specifically, we have shown that these non-thermal effects related to the non-inertial character of acceleration result in a different scaling with the distance and a different dependence on acceleration, if compared to the usual thermal case. The merit of our approach is the simplicity in highlighting non-thermal features, exploiting atomic entanglement as condition to have resonant second-order interactions. Our results open the way for new future developments. First of all, it is known that the Unruh bath does not induce full decoherence and can even create entanglement during the time evolution of a pair of accelerating atoms [42]; this limits the description presented in this work up to time scales of the order of inverse of acceleration but it poses the intriguing question on the fate of the resonant interaction in the long-time limit, since for its existence a minimum of entanglement among the two atoms is required. Moreover, since the basic set-up we have considered in this work is the pillar to build the Dicke model, one might ask which is the impact of the change of interatomic potential on its phase transition (sub or superradiant transition phase). Understanding it the qualitative change of interatomic interactions in accelerated systems, can modify macroscopic phenomena, such as thermodynamics phase transitions, is one promising direction to highlight non-thermal signatures of relativistic accelerations in a many-body context.

References

[1] W. G. Unruh, Phys. Rev. D **14**, 870 (1976).

[2] S. A. Fulling, Phys. Rev. D **7**, 2850 (1973).

[3] P. C. W. Davies, J. Phys. A **8**, 609 (1975).

[4] L. C. B. Crispino, A. Higuchi, and G. E. A. Matsas, Rev. Mod. Phys. **80**, 787 (2008).

[5] P. M. Alsing, P. W. Milonni, Am. J. Phys. **72**, 1524-1529 [arXiv:0710.5373] [quant-ph] (2004).

[6] T A Welton, Phys. Rev. **74**, 1157 (1948).

[7] H. B. G. Casimir, D. Polder, Phys. Rev. **73**, 360 (1948).

[8] E. A. Power, T. Thirunamachandran, Phys. Rev. A **48**, 4761 (1993).

[9] G. B. Gibbons and M. J. Perry, Phys. Rev. Lett. **36**, 985 (1976).

[10] P. Candelas and D. Deutsch, Phys. Rev. Lett. **38**, 1372 (1977).

[11] P. Candelas and D. W. Sciama, Proc. R. Soc. Lond. A **354**, 79 (1977).

[12] W. Troost and H. Van Dam, Phys. Lett. B **71**, 149 (1977).

[13] S. W. Hawking, Nature (London) **248**, 30-31 (1974).

[14] S. W. Hawking, Commun. Math. Phys. **43**, 199–220 (1975).

[15] S. Takagi, Prog. Theor. Phys. Suppl. **88**, 1 (1986).

[16] N. D. Birrell and P. C. W. Davies, *Quantum fields in curved space*, Cambridge University Press, Cambridge (1983).

[17] S. A. Fulling, *Aspects of Quantum Field Theory in Curved Space-Time*, Cambridge University Press, Cambridge 1989.

[18] R. M. Wald, *Quantum Field Theory in Curved Spacetime and Black Hole Thermodynamics*, The University of Chicago Press, Chicago, (1994).

[19] P. C. W. Davies, Chaos **11**, 539 (2001).

[20] G.J. Milburn, P.M. Alsing, Phys. Rev. Lett. **91**, 180404 (2003).

[21] I. Fuentes-Schuller and R. B. Mann, Phys. Rev. Lett. **95**, 120404 (2005).

[22] K. K. Ng, L. Hodgkinson, J. Louko, R. B. Mann, and E. Martín-Martínez, Phys. Rev. D **90**, 064003 (2014).

[23] A. Retzker, J.I. Cirac, M.B. Plenio and B. Reznik, Phys. Rev. Lett. **101**, 110402 (2008).

[24] J. S. Bell and J. M. Leinaas, Nucl. Phys. B **212**, 131 (1983).

[25] P. Chen and T. Tajima, Phys. Rev. Lett. **83**, 256 (1999).

[26] R. Schützhold, G. Schaller, and D. Habs, Phys. Rev. Lett. **97**, 121302 (2006).

[27] W. G. Unruh and R. Schützhold, Phys. Rev. D **86**, 064006 (2012).

[28] F. Belgiorno, S. L. Cacciatori, M. Clerici, V. Gorini, G. Ortenzi, L. Rizzi, E. Rubino, V. G. Sala, and D. Faccio, Phys. Rev. Lett. **105**, 203901 (2010).

[29] D. A. T. Vanzella and G. E. A. Matsas, Phys. Rev. Lett. **87**, 151301 (2001).

[30] N.B. Narozhny, A.M. Fedotov, B.M. Karnakov, V.D. Mur, V. A. Belinskii, Phys. Rev. D, **65**, 025004 (2001).

[31] G.W. Ford , R.F. O'Connell, Phys. Lett. A **350**, 17 (2006).

[32] A. Noto and R. Passante, Phys. Rev. D **88**, 025041 (2013).

[33] D. Buchholz, S. Solveen, Class.Quantum Grav. **30**, 085011 (2013).

[34] Hongwei Yu, and Zhiying Zhu, Phys Rev. D **74**, 044032 (2006).

[35] R. Passante, Phys. Rev. A **57** 1590 (1998).

[36] L. Rizzuto, Phys. Rev. A **76**, 062114 (2007).

[37] Z. Zhu and H. Yu, Phys. Rev. A **82**, 042108 (2010).

[38] J. Marino, A. Noto, R. Passante, L. Rizzuto and S. Spagnolo, Phys. Scr. **T160**, 014031 (2014).

[39] L. Rizzuto and S. Spagnolo, Phys. Rev. A **79**, 062110 (2009).

[40] J. Marino, A. Noto, R. Passante, Phys. Rev. Lett. **113**, 020403 (2014).

[41] Jiawei Hu and Hongwei Yu, Phys. Rev. A **91** 012327 (2015).

[42] F. Benatti, R. Floreanini, Phys. Rev. A 70, 012112, (2004).

[43] J. Dalibard, J. Dupont-Roc, C. Cohen-Tannoudji, J. Physique **43**, 1617 (1982).

[44] J. Dalibard, J. Dupont-Roc, C. Cohen-Tannoudji, J. Physique **45**, 637 (1984).

[45] A. Noto, J. Marino and R. Passante, in preparation (2015).

[46] J. Audretsch and R. Müller, Phys. Rev. A **52**, 629 (1995).

[47] J. Marino and R. Passante, in: *Quantum Field Theory under the Influence of External Conditions (QFEXT09)*, edited by K.A. Milton and M. Bordag, World Scientific, Singapore 2010, p. 328.

[48] R. Passante, F. Persico, L. Rizzuto, Phys. Lett. A **316**, 29 (2003).

[49] S. Spagnolo, R. Passante, and L. Rizzuto, Phys. Rev. A **73**, 062117 (2006).

[50] A. Salam, J.Phys.: Conf. Ser. **161**, 012040 (2009).

[51] E. A. Power, T. Thirunamachandran, Proc. R. Soc. Lond. A **457**, 2757 (2001).

[52] T. Thirunamachandran, J. Phys. B **39**, S725 (2006).

[53] W. Rindler, *Introduction to Special Relativity*, Oxford University Press, Oxford (1991).

[54] J. D. Jackson, *Classical Electrodynamics*, Wiley (1998).

[55] G. Barton, Phys. Rev. A **64**, 032102 (2001).

[56] J. Audretsch and R. Müller, Phys. Rev. A **50**, 1755 (1994).

[57] Z. Zhu, H. Yu, and S. Lu, Phys. Rev. D **73**, 107501 (2006).

[58] G. Barton and A. Calogeracos, J. Phys. A **41**, 164030 (2008).

[59] E. A. Power and T. Thirunamachandran, Phys. Rev. A **47**, 2539 (1993).

[60] C. W. Misner, K. S. Thorne, and J. A. Wheeler, *Gravitation*, W.H. Freeman and Co, San Francisco (1973).

[61] J.W. Maluf and F. F. Faria, Ann. Phys. (Berlin) **17**, 326 (2008).

[62] M. Cirone and R. Passante, J. Phys. B **30**, 5579 (1997).

[63] A. Salam, Phys. Rev. A **73**, 013406 (2006).

[64] L. Rizzuto, R. Passante, and F. Persico, Phys. Rev. Lett. **98**, 240404 (2007).

[65] K. D. Bonin and V. V. Kresin, *Electric-Dipole Polarizabilities of Atoms, Molecules and Clusters*, World Scientific Publishing Company, (1997).

[66] R. H. Dicke, Phys. Rev. 93, 99 (1954).

[67] G. W. Gibbons and E. P. S. Shellard, Science **295**, 1476 (2002);

[68] E. M. Lifshitz, Zh. Eksp. Teor. Fiz. **29**, 94 (1956).

[69] P. W. Milonni and M. L. Shih, Phys. Rev. A **45**, 4241 (1992).

[70] G. H. Goedecke and R. Wood, Phys. Rev. A **60**, 2577 (1999).

[71] D. W. Sciama, P. Candelas, and D. Deutsch, Adv. Phys. **30**, 327 (1981).

[72] H. Hu and Z. Zhu, Phys. Lett. B, **645**, 459-465 (2007).

[73] H. Yu and S. Lu, Phys. Rev. D **72**, 064022 (2005).

[74] W. G. Unruh and R. M. Wald, Phys. Rev. D **25**, 942 (1982); Phys. Rev. D **29**, 1047 (1984).

[75] A. Campa, T. Dauxois, S. Ruffo, Physics Reports **480**, 57159 (2009).

[76] T. Y. Boyer, Phys. Rev. D **29**, 1089 (1984).

[77] W. Zhou, H. Yu, Phys. Rev.D **82**, 104030 (2010)

[78] W. Zhou, H. Yu, Phys. Rev. D **82**, 124067 (2010).

[79] L. Rizzuto, M. Lattuca, J. Marino, A. Noto, S. Spagnolo and R. Passante, in preparation (2015).

[80] D. P. Craig and T. Thirunamachandran *Molecular Quantum Electrodynamics*, Dover Publ., Mineola, NY (1998).

[81] A. Salam *Molecular Quantum Electrodynamics*, John Wiley and Sons, Hoboken, New Jersey, (2010).

[82] P. R. Berman, Phys. Rev. A, **91**, 042127 (2015).

[83] M. Donaire, R. Guerout, and A. Lambrecht, Phys. Rev. Lett., **115**, 033201 (2015).

[84] P. Barcellona, R. Passante, L. Rizzuto and S. Y. Buhmann, in preparation (2015).

[85] R. Incardone, T. Fukuta, S. Tanaka, T. Petrosky, L. Rizzuto, R. Passante, Phys. Rev. A **89**, 062117 (2014).

[86] G. Juzelinuas, D.L. Andrews, Adv. Chem. Phys., **112**, 357 (2000).

[87] J. Preto, M. Pettini, Phys. Lett. A, **377**, 587 (2013).

[88] S. Ravets, H. Labuhn, D. Barredo, L.Béguin, T. Lahaye, A. Browaeys, Nat. Phys., **10**, 914 (2014).

[89] K. Lalumière, B. C. Sanders, A. F. van Loo, A. Fedorov, A. Wallraff, and A. Blais, Phys. Rev. A **88**, 043806 (2013).

[90] A.F. van Loo, A. Fedorov, K. Lalumière, B.C. Sanders, A. Blais, and A. Wallraff, Science **342**, 1494 (2013).

Chapter 3

Dynamical Casimir-Polder effect

Contents

3.1 The dynamical Casimir effect and the quantum friction 85

3.2 Experimental setups for DCE 90

3.3 Optomechanical Rydberg atoms excitation via dynamic Casimir-Polder coupling 92

3.3.1 Experimental proposal 96

References 99

Zero-point fluctuations are among the most striking consequences of the quantum description of the electromagnetic field. They are at the origin of the Casimir-Lifshitz force, a long-range quantum electromagnetic interaction between neutral polarizable bodies, and they are also responsible for the Casimir-Polder forces between an atom and a surface or between two atoms (van der Waals forces) [1] - [8].

When boundary conditions are set in motion with nonuniform acceleration in the vacuum, or when material properties are changed nonadiabatically, a dynamical Casimir effect is realized, and a parametric excitation of vacuum fluctuations may lead to the emission of real photons [9] - [15]. Similarly, a dynamical Casimir-Polder effect occurs when physical parameters of an atom near a conducting plate are rapidly changed [16].

Another rapidly growing research field is that of quantum optomechanics, which deals with systems where mechanical degrees of freedom are coupled to cavity fields [17]. Such systems have been experimentally and theoretically investigated, for example, for realizing sensitive force detectors, cooling macroscopic mirrors or obtaining quantum superposition states for macroscopic objects [18]. Significant experimental progress has been obtained in precision trapping of cold atoms near a nanoscale optical cavity, allowing to probe cavity near fields [19]. The effect of quantum fluctuations of the position of a cavity mirror on Casimir and Casimir-Polder interactions has been also demonstrated [20, 21].

In this Chapter, after an overview of the Dynamical Casimir effect that we discuss briefly, we propose a new optomechanical Rydberg atoms-surface coupling based on a novel aspect of the dynamical Casimir-Polder (CP) effect, able to affect the internal atomic state [22],[AN4]. It is a new near-field effect, not related to the excitation of atoms by the few

real photons expected in the dynamical Casimir effect [23] - [27]. Specifically, when considering a gas of dilute Rydberg atoms trapped in front of a substrate whose refractive index is changed in time (dynamical mirror) at a frequency corresponding to one of atomic transition frequencies. Due to the effective periodical change of the atom-mirror distance, the optomechanical coupling between the wall and the Rydberg atoms yields a periodic perturbation on the atoms, which can be excited to upper levels [22]. On the experimental side, this scheme may largely profit from recent progresses in the realization of dynamical mirrors [28], and in the cigar-shape trapping of Rydberg atoms and their preparation in long-lived excited states [29].

It is worth saying that recently a micromechanical atom-wall system has been realized with a trapped Rb Bose Einstein Condensate (BEC) close to a dielectric substrate, and the collective oscillations of the gas have been used to measure the CP force [30, 31]. In particular, this allowed measurement of the more elusive thermal component of this interaction [32]. Theoretical predictions of the thermal component of the Casimir-Polder force can be found in [33, 34]. Differently from that case, where the *external* degrees of freedom of an atomic gas have been used *to detect* the CP force, here we *use* the CP force to couple a substrate to the *internal* atomic degrees of freedom.

This Chapter has the following structure. The first two sections are introductory and pave the way to the original results that we show in the last section. In particular, in Section 3.1 we present and discuss two effects due to moving bodies and vacuum fluctuations, the dynamical Casimir effect and the quantum friction. After the analysis on the physical origin of these effects we present in Section 3.2 some experiments, presented in literature, related to them. Finally, in the last Section 3.3, we present and discuss our original work about a new effect between an atom and an oscillating mirror due to the dynamical atom-mirror Casimir-Polder force. We discuss the possibility to detect this new effect and we also present an original experimental proposal.

3.1 The dynamical Casimir effect and the quantum friction

The Dynamical Casimir Effect (DCE) is an effect related to photon generation from the vacuum due to accelerating nonuniformly neutral bodies in free space, as suggested for the first time by Moore [9]. In general this effect is related to quick changes of the system geometry or of the optical properties of neutral macroscopic objects. Although Casimir did not write anything about this effect, the presence of the Casimir's name in the DCE is due to the close connection between the DCE and vacuum fluctuations. This effect can be physically explained stating that it is the parametric amplification of the electromagnetic quantum fluctuations in systems having non adiabatic time-dependent parameters.

From Quantum Electrodynamics we know that any quantum observable associated to the electromagnetic field has fluctuations. Also the vacuum radiation pressure fluctuates. Thus, if we consider a body at rest in the vacuum, we can find a fluctuating force acting on it which generates a quantum Brownian motion. Due to the fluctuation-dissipation

theorem this yields dissipative effects too [35]. The force on a body at rest is zero as well as we consider a uniform motion in vacuum, due to the relativity principle. If we consider a mirror moving with a 1D nonuniform motion, it has been found [36] that the Casimir dissipative force is proportional to the second-order derivative of its velocity. In this way we can understand that there is a relation between the Casimir dissipation and the emission of photons by the accelerated neutral mirror. Exploiting energy conservation, we find that the power dissipated because of the motion of the mirror is equal to the total radiated power in the DCE.

Other simple considerations can be made to understand the DCE. These considerations start from the analogy between the quantum electromagnetic field and a set of quantum harmonic oscillators. Let us write the Hamiltonian of the free field in a cavity

$$H_0 = \sum_n^{\infty} \hbar\omega_n \left(\frac{1}{2} + a_n^\dagger a_n\right) \tag{3.1}$$

where a_n and $a_n^\dagger$ are, respectively, the annihilation and creation bosonic operators of the field mode at the given frequency ω_n. When we consider the possibility of the interaction between the system and the environment, we must add an interaction term $H_I(t)$ (in general function of time). Usually we can consider that this interaction is relatively weak and we can expand the $H_I(t)$ term in series with respect to powers of the bosonic operators a_n, $a_n^\dagger$. The linear term of this expansion can be interpreted as describing field excitations due to external currents and/or charges. The second-order terms, proportional to $a_n a_n^\dagger$, $a_n^\dagger a_n$, $a_n a_n$, $a_n^\dagger a_n^\dagger$ with time-dependent coefficients, can be considered as terms arising from possible time-dependent changes of the system geometry or optical properties of the cavity. The latter can generate field excitations that can be interpreted as an amplification of the initial fluctuations of the field. So the photon creation from vacuum of the DCE can be read as an excitation of the vacuum due to the time-dependent dependence of the interaction Hamiltonian.

It must be said that the DCE and its analogues, when realistic situations are considered, are very tiny effects due to the small number of emitted photons. Nevertheless (as we will see in Section 3.2) they have been recently observed in superconducting circuits [37], in Josephson metamaterials [38] and in Bose-Einstein condensates [39] and many experimental setups have been proposed and realized to measure them.

We discuss now a simple 1D model to show the dynamical Casimir effect. We consider an electrically neutral point-like mirror in nonuniform motion and coupled to a massless scalar field $\Phi(x,t)$. The motion of the mirror is described by its position $Q(t)$. Following [7], the idea to show the DCE in this model is to calculate the vacuum radiation-pressure-force $F(t)$ by making simple considerations. If we consider a non-relativistic motion, we know that the force must be proportional to some velocity derivative of the moving mirror. At the same time this force is a quantum effect, so we expect that it is proportional to $\hbar$. In addition its expression should be consistent with the Lorentz invariance of the vacuum filed

state. In a 1D space, after a dimensional analysis, we deduce that

$$F(t) \propto \frac{\hbar \dddot{Q}(t)}{c^2} \tag{3.2}$$

where the dot indicates a time derivative. We see that the third time derivative of the position is involved: it follows that a nonuniform motion is necessary.

We now calculate the dimensionless factor in the above equation. We treat the motion of the mirror as a small perturbation and we use the Dirichlet boundary conditions on the mirror

$$\Phi(Q(t), t) = 0 \tag{3.3}$$

to first order in $Q(t)$. In the frequency domain we can write the Fourier transform $\phi(x, \omega)$ of the field as a sum of an unperturbed field $\phi_0(x, \omega)$, corresponding to a static mirror fixed at $x = 0$, plus a perturbation $\delta\phi(x, \omega)$

$$\phi(x, \omega) = \phi_0(x, \omega) + \delta\phi(x, \omega). \tag{3.4}$$

The boundary condition for $\phi_0(0, \omega) = 0$ at $x = 0$ is automatically fulfilled, while for $\delta\phi(x, \omega)$ we make a Taylor expansion around $x = 0$. At first order in Q we get

$$\delta\phi(0, \omega) = -\int_{-\infty}^{+\infty} \frac{d\omega_i}{2\pi} q(\omega_0 - \omega_i)\partial_x\phi_0(0, \omega_i) \tag{3.5}$$

where we have introduced the Fourier transform $q(\Omega)$ of $Q(t)$. The key element generating the photon emission is already in this equation. This element is the frequency $\Omega = \omega_0 - \omega_i$. In fact, as we are going to show, since in the integral in (3.5) the function $q(\Omega)$ is translated by ω_0, the only frequencies that contribute to the dissipative Casimir force are the negative frequencies in the range $[-\Omega, 0]$. In order to show this point we must calculate the force. We take the Fourier transform of the component T_{11} of the energy-momentum tensor

$$T_{11} = \frac{1}{2}\left[\frac{1}{c^2}(\partial_t\Phi)^2 + (\partial_x\Phi)^2\right] \tag{3.6}$$

and consider the expansions given by (3.4) and (3.5). After averaging over the vacuum state, the force is given by

$$f(\Omega) = \chi(\Omega)q(\Omega) \tag{3.7}$$

where

$$\chi(\Omega) = 2i\frac{\hbar}{c^2}\int_{-\infty}^{+\infty} \frac{d\omega_i}{2\pi}(\Omega + \omega_i)|\omega_i|. \tag{3.8}$$

Analyzing the above expression for $\chi(\Omega)$, using an appropriate regularization of the integral, we can see that, due to the "translation" of the frequency Ω_i, the contribution given

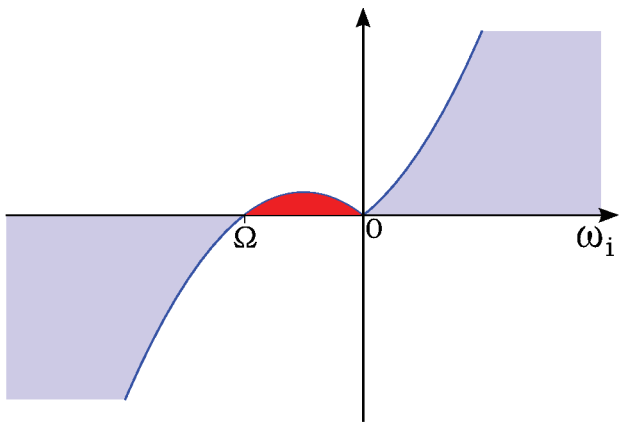

Figure 3.1 – This figure shows the reason why only the frequencies in the interval $-\Omega \leq \omega_i \leq 0$ contribute to the integral (3.8).

by the integral in the integration interval $[-\infty, -\Omega]$ is opposite to that from the interval $[0, +\infty]$, as it can be seen in Figure 3.1. Thus follows

$$f(\Omega) = i\frac{\hbar\Omega^3}{6\pi c^2}q(\Omega) \tag{3.9}$$

which gives the prefactor $\frac{1}{6\pi}$ (it is positive as expected for a dissipative force). The fact that only frequencies in the interval $[-\Omega, 0]$ contribute to the dissipative force is not totally unexpected. In fact, from qualitative considerations, we expect that the frequencies $|\omega_i| \gg \Omega$ do not contribute because, roughly speaking, the mirror motion at frequency Ω is quasi-static. The dissipative Casimir force is due to low-frequencies modes for which the motion can be considered non-adiabatic.

From a physical point of view, the "translation" mentioned before can be interpreted, with the help of Figure 3.1, as a mixing of negative and positive frequencies in the interval $[-\Omega, 0]$. This mixing remembers the action of a Bogoliubov transformation on the bosonic operators a_n, $a_n^\dagger$, coupling output annihilation operators to input creation operators (input and output in this case indicate, respectively, the situation at $t < 0$ before the mirror motion starts and the situation at $t \geq 0$ after its motion has started). It is important to stress the connection between negative (positive) frequencies and the creation (annihilation) operators. Thus, we can conclude that the dissipative Casimir force, related with the motion of the mirror, due only to the field frequencies in $[-\Omega, 0]$, generates photon so yielding the dynamical Casimir effect. We can also deduce that, as long as the mirror motion allows to use perturbation theory, the frequency of the emitted photons is bounded from the frequency $-\Omega$. Another important aspect that we can figure out from the symmetry of the integrand in (3.8) in the interval $[-\Omega, 0]$, is that photon emission occurs in pairs (this situation is depicted in Figure 3.1 and highlighted in the red zone of this figure).

The result in (3.9) was obtained by Ford and Vilenkin in [36] for a non-relativistic motion of the mirror. The general case of relativistic mirror motion, was developed by Fulling and Davies [40].

We have seen the close connection between the DCE and the dissipative Casimir force. The latter seems acting as a radiation reaction force (generated from the vacuum!) and this can be seen from the equation (3.2) which has the same form of the radiation reaction force of classical electrodynamics.

We can give an order of magnitude for the rate of photon emission in the DCE in a 3D space. We expect that, when we analyze a plate in the xy plane with surface A and moving along the z direction, the 3D dissipative Casimir force should depend linearly on the surface A. Following the same method described above and with appropriate changes for the electromagnetic case, we get

$$F(t) = -\frac{\hbar A}{30\pi^2 c^4}\frac{d^5 Q(t)}{dt^5}. \tag{3.10}$$

Since from the energy conservation we know that the total radiated energy is the negative of the work done by the dissipative Casimir force on the moving mirror, we can write

$$E = -\int_{-\infty}^{+\infty} dt F(t)\dot{Q}(t). \tag{3.11}$$

For simplicity we examine one oscillating mirror with frequency Ω and amplitude Q_0, whose motion is exponentially damped over a time scale $T \gg 1/\Omega$. For this simple case we obtain

$$E = \frac{\hbar T A Q_0^2 \Omega^6}{120\pi^2 c^4}. \tag{3.12}$$

In order to obtain the number of emitted photons N we can exploit the fact that the spectrum is symmetrical with respect to the frequency $\Omega/2$, writing $E = N\hbar\Omega/2$. We finally obtain

$$\frac{N}{T} = \frac{1}{15}\frac{A}{\lambda_0^2}\left(\frac{\nu_{\max}}{c}\right)^2 \Omega. \tag{3.13}$$

In the above equation we introduced $\nu_{\max} \equiv \Omega Q_0$ and $\lambda_0 \equiv 2\pi c/\Omega$. If, for examples, we use in (3.13) physical parameters compatible with possible actual experimental setups, such as $A \sim \lambda_0^2 \sim 10\ \mathrm{cm}^2$ $\nu_{\max}/c \sim 10^{-7}$ and $\Omega/2\pi \sim 10$ GHz, we find that the photon emission rate is of the order of 10^{-5}, which means one photon pair every about two days. Of course this is a very small effect. However, many situations have been studied to amplify the photon emission effect [10], [41], [42]. Typically, a second mirror or a cavity with moving walls are considered to significantly enhance the photon emission rate by a resonance effect [43] (see also [42] and reference therein).

In the context of quantum effects due to motion of bodies in the electromagnetic vacuum there is another effect, stronly related to the DCE, that we wish to mention, the quantum friction. It predicts the possibility that a force, which tends to work against the relative motion, can be experienced between two electrically neutral and polarizable bodies in parallel relative motion, then a non-contact "friction " is originated. This effect is expected to be present even at zero temperature and when the surfaces of the moving bodies are flat and

perfectly smooth. It has been also predicted for an atom moving parallel in front of a surface [44]. Differently to what we have seen with the DCE, here the friction effect due to the quantum vacuum can take place also when the motion of the bodies is uniform. The reason is that, even if the two bodies are in uniform motion, the relative shear motion can not be removed changing the frame of reference. From an energy conservation point of view, the energy lost during the quantum friction is balanced by the external energy necessary to keep the body a constant velocity.

A simple qualitative explanation of the quantum friction can be given thinking that the electric dipoles generated from the quantum vacuum in one of the surfaces (a similar picture to that given before for the Casimir-Polder interaction) induce image electric dipoles on the other surface which lags behind because of the relative motion. We have that when the shear motion of the two bodies is considered, the van der Waals-like attraction experienced between the two bodies is related to the relative velocity (roughly speaking the photons exchanged for the interaction carry the motion information) and the generation of a friction force follows. Many scientists consider the quantum friction as a purely quantum effect with no classical analogue and they do not unanimously agree on the interpretation. This effect is still debated in the literature [45, 46].

3.2 Experimental setups for DCE

In this section we present a short overview about the possibility to observe the DCE in a laboratory experiment. We already discussed in Section 3.1 that the rate of photon emission by DCE in the presence of an accelerating mirror is small. The experimental observation of such phenomenon is a formidable technological and scientific challenge. The dynamical Casimir effect is considered as a direct manifestation of the existence of the vacuum fluctuations. As a consequence, the detection of the photon emission due to the DCE is also considered an important contribute to fundamental physics and a milestone which provides further relevance to Quantum Electrodynamics.

Many efforts have been done recently to find promising systems to detect the DCE. In particular the photon emission generated in a resonant time-dependent cavity has been widely considered. For these configurations the photon emission rate is strongly amplified compared to the simple and ideal situation of a single accelerating mirror [47]. In these setups, the average number of photons created is

$$\langle N \rangle = \sinh^2(\eta\omega\varepsilon t) \tag{3.14}$$

so it grows exponentially with time [23, 48]. In the above expression, ω represents the frequency of the resonant mode of the cavity, η is a parameter related to the geometry of the cavity (its order of magnitude is 1) and ε indicates the relative amplitude of the oscillations involved, i.e. $\varepsilon = a/\lambda = a\omega/2\pi c$ where a is the amplitude of the mirror oscillation. Notwithstanding this exponentially growing time dependence of the average number of emitted photons, the observation of these photons in realistic laboratory conditions is arduous, due to cavity losses and the presence of thermal photons.

Let us first analyze other important aspects involved in realistic laboratory situations. If, for example, we consider a cavity of length $L_0 \simeq 10^{-2}$ m, in order to exploit the resonance condition, and thus amplify the photon emission, the order of magnitude of the oscillation frequencies (either mirror oscillation or conductivity oscillation) is of about 10 GHz. Achieving these frequencies from a mechanical point of view is not feasible. An alternative method could be dealing with surface vibrations without having a motion of the mirror center-of-mass. These kind of systems lead to amplitude values ε which need a minimum quality factor Q of 10^8. In spite of the fact that greater values of the Q-factor has been achieved experimentally, the presence of oscillating walls complicates a lot the situation decreasing the value of the Q-factor, making then very difficult the observation of the dynamical effect.

We now report the main aspects of recent experiments on the DCE. Considering all these difficulties related to mechanical oscillations of the mirror, some scientists thought to other experimental setups for the DCE revelation where a mobile boundary condition is somehow simulated. The first observation of photon emission related to the DCE has been made in 2011 in a superconducting circuit [37]. The experimental setup was made by an open transmission line terminated by a superconducting quantum interference device (SQUID). In the SQUID two Josephson junctions were present and connected in parallel to form a loop. The key idea was to use a time-dependent magnetic flux to control the effective inductance of the SQUID, placed at the end of a transmission line. This generates a time-dependent boundary condition for the phase field (the time integral of the electric field) which can be seen as a transmission line with a variable length. The change in the electrical length of the transmission line simulates a time-dependent boundary condition, as the idealized moving mirror already discussed. The effective velocity of the simulated effective mirror, defined as the rate of change of the electrical length, can be very large, thus increasing the rate of photon emission. This means that a non-relativistic approach as that in Section 3.1 it is not possible and a fully relativistic approach is necessary. The theoretical prediction for this case gives a photon production rate several orders of magnitude larger than in other systems. The involved photons exhibited two-mode squeezing correlations, which are characteristic of photons generated in correlated pairs.

Similarly to this experiment in a superconducting circuit, a recent work in 2013 has demonstrated the DCE with the help of Josephson metamaterials [38]. The considered setup was a Josephson metamaterial, made of an array of 250 SQUIDs, forming the signal line of a superconducting coplanar waveguide. This metamaterial is embedded into a low-quality-factor cavity. Here the DCE was produced by modulating, through an external magnetic field, the refraction index of this material near its quantum ground state. This setup, compared with the superconducting circuit setup described above, allows for an enhancement of the DCE. This is possible because the presence of a cavity in this system produces a resonance effect avoiding the problem of uncontrolled resonances which affect the detection of photon emission in [37].

Another indirect observation of the DCE is that presented in [39]. In this work an acoustic analog of the dynamical Casimir effect is described. Through the modulation of the speed of sound in a Bose-Einstein Condensate, correlated pairs of elementary excitations

are produced, both phonon-like and particle-like. The idea inspiring this work starts from the study of an interacting Bose gas. Keeping in mind that the change in the interaction strength of the gas is analogous to an optical index change (for example the speed of sound changes) an acoustic analog of the dynamical Casimir effect is realized by changing the scattering length in the gas. From a microscopic point of view, the ground state of such a gas is the vacuum of Bogoliubov quasi-particles. When the interaction strength is changed the old vacuum state is mapped into a new state where pairwise excitations appears and it can be seen as pairs of the new quasi-particles. Also, the confining potential of the BEC can be modified (it means changing of the density of the BEC) and the same effect occurs. However there is a substantial difference between the results related to this experiment and the standard configuration of the DCE. In fact, in this acoustic analog of the DCE the effect of the temperature is not negligible. It seems that the pair generation does not arise from the vacuum but rather from the thermal noise marking a fundamental difference with the DCE which is predicted also at zero temperature.

We now briefly describe the *motion induced radiation* (MIR) experiment [49, 50, 51], which is related to the our work we will describe in the next section. In the MIR experiment, the difficulty to reach sufficiently high frequencies of mechanical oscillation is bypassed using an effective dynamical mirror. The main idea in this approach is to change the length of the cavity by modifying the reflectivity of one of the slabs present in the cavity walls. This is possible exploiting the property of some semiconductors that, when irradiated with short laser pulses, change their optical properties becoming a reflector or a transparent medium. With the help of this kind of system it is possible to reach greater oscillation amplitudes $\varepsilon \simeq 10^{-4}$ mm and high oscillation frequency of the order of tens of GHz, allowing much smaller values of the Q-factor. However, in this system dissipative effects can be significant. The change of the optical properties by laser impulses is due to creation of electron-hole pairs in the semiconductor slab. Thus, the charge carriers of the irradiated semiconductor must have a very short recombination time and a very high mobility. This kind of material has been built [49] and then the photon emission by DCE for this experiment could be measured in a pure quantum electrodynamics framework. It must be said that the MIR experiment is still in the making.

3.3 Optomechanical Rydberg atoms excitation via dynamic Casimir-Polder coupling

In this section, we focus on the main issue of this Chapter. We describe our original work concerning with the study of a new dynamical Casimir-Polder effect. It is based on the optomechanical coupling of an oscillating mirror (dynamical mirror) with a diluite gas of Rydberg atoms, mediated by the dynamical atom-mirror Casimir-Polder force in the non-retarded near-field regime [22],[AN4]. This coupling may produce a near-field resonant atomic excitation whose probability scales as $\propto (d^2\ a\ n^4\ t)^2/z_0^8$, where z_0 is the average atom-surface distance, d the atomic dipole moment, a the mirror's effective oscillation amplitude, n the initial principal quantum number of the Rydberg atoms, and t the time. We

propose an experimental configuration to realize this system with a cold Rydberg atoms gas trapped at a distance $\sim 2 \cdot 10\,\mu$m from a semiconductor substrate, whose dielectric constant is periodically driven by an external laser pulse, hence realizing an effective mechanical mirror motion due to the periodic change of the substrate from transparent to reflecting. For a parabolic gas shape, this effect is predicted to excite about $\sim 10^2$ atoms of a dilute gas of 10^3 trapped Rydberg atoms with initial principal number $n = 75$ after about $0.5\,\mu$s, hence high enough to be detected in typical Rydberg gas experimental conditions.

To describe our system we now consider a fixed Rydberg atom near a perfectly conducting plate; the plate is forced to move harmonically around its equilibrium position. We model the atom as a two-level system. The mirror's position coincides with the plane $z = 0$ at $t = 0$, and the atom-mirror distance is $z(t)$. We first analyze the case of a fixed mirror at a distance z from the atom; we assume that this distance is much smaller than a main transition wavelength $\lambda_0 = 2\pi c/\omega_0$ of the Rydberg atom, ω_0 being the corresponding transition angular frequency. The atom-mirror Casimir-Polder (CP) interaction energy is thus in its near-zone nonretarded regime, where electrostatic (longitudinal field) contributions are dominant [1, 30]. We assume the atom prepared in a long-lived Rydberg state and treat it as a stable state, assuming to study the system for times shorter than its lifetime (Rydberg atoms in circular states can have a very long lifetime). As we saw in Chapter 1, for typical short wavelength atomic transitions, there is a thermal regime dominating at large separations. For long wavelength transitions (molecular or Rydberg states, as in this section) and for the conditions considered in this section, this thermal regime is absent [34, 52]. The CP interaction energy between a ground-state atom and a fixed perfectly conducting mirror, within dipole approximation and in the nonretarded regime, is (*cgs* units) [53, 54]

$$V(z) = -\frac{\langle d_x^2\rangle + \langle d_y^2\rangle + 2\langle d_z^2\rangle}{16z^3} = -\frac{1}{16}\frac{\sigma_{ij}\langle d_i d_j\rangle}{z^3}, \tag{3.15}$$

where the sum over repeated indices is used, and the average of the squared components of the atomic dipole moment operator $\mathbf{d}$ are taken on the atomic state considered. The atom-mirror distance z is along the $\hat{z}$ direction. We have also defined the diagonal matrix $\sigma = \mathrm{diag}(1, 1, 2)$.

The expression (3.15) of the atom-wall interaction for an ideal conductor is a very good approximation in our case, since we shall consider atom-wall distances of the order of $2 \cdot 10^{-3}$ cm, much larger than the plasma wavelength of a typical metal (of the order of $\lambda \sim 10^{-5}$ cm), where real-conductor corrections are known to be negligible [55].

It is well known that in the near-zone limit, the atom-wall nonretarded interaction (3.15) is well described by the interaction between the atomic dipole and its image [54]. In order to describe the interaction of the atom with the oscillating mirror, we adopt a semiclassical model: we obtain the atom-wall interaction as the interaction energy between the atomic dipole and an effective classical field due to the image atom (Figure 3.2). Using the method of image charges [56], we can describe the near-zone atom-wall interaction by the coupling term $H_I = -\mathbf{d}\cdot\mathbf{E}(\mathbf{r})/2$, where $\mathbf{d}$ is the atomic dipole moment operator and $\mathbf{E}(\mathbf{r})$ is the electric field generated by the image dipole $\tilde{d} = (-d_x, -d_y, d_z)$ at the atom's position $\mathbf{r} = (0, 0, z)$. The factor $1/2$ takes into account that, when the atomic dipole is moved from infinity to its final

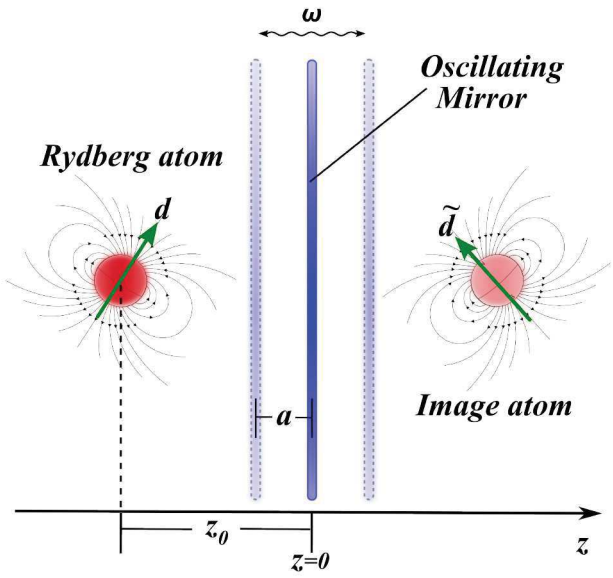

Figure 3.2 – Schematic figure that represents the system of a Rydberg atom in front of a mirror, oscillating with a frequency is ω, at an average distance z_0. The mirror oscillates around the $z = 0$ position with an amplitude a. The Casimir-Polder interaction is described as a force between the induced dipole of the Rydberg atom and the image dipole.

position, the image dipole moves symmetrically in the opposite direction [57]. Comparing H_I with equation (3.15), the effective electric field acting on the atom, due to the image atom at a distance $2z$, is

$$E_i(\mathbf{r}) = \frac{1}{8}\frac{\sigma_{ij}d_j}{z^3}\,. \tag{3.16}$$

Quantum mechanically, a fluctuating field is indeed acting on the atom, due to vacuum fluctuations modified by the presence of the conducting wall. Its effect on the atom is equivalent to the action of the effective field (3.16). The effective semiclassical interaction Hamiltonian, quadratic in the atomic dipole moment operator, is then

$$H_I = -\left(\frac{\sigma_{ij}}{16z^3}\right)d_i d_j\,, \tag{3.17}$$

whose average on the atomic state coincides with (3.15).

We now assume that the plate oscillates harmonically around its equilibrium position $z = 0$, so that the atom-wall distance changes as $z(t) = z_0[1 - \frac{a}{z_0}\sin\omega t]$, where z_0 is the average atom-mirror distance and ω the mirror's oscillation angular frequency. We also assume the oscillation amplitude a such that $a \ll z_0$, and that the atom-wall Casimir-Polder interaction follows instantaneously the plate oscillation. The latter assumption is fully consistent with our near-zone hypothesis, because the interaction is non-retarded in this case. From (3.17), the effective interaction Hamiltonian between the atom and the oscillating mirror will then take the form $H_I(t) = H_s + V_I(t)$, where H_s is a time-independent

term yielding the usual z_0^{-3} near-zone static Casimir-Polder potential (3.15), and

$$V_I(t) \simeq -d_i d_j \left(\frac{3\sigma_{ij}}{16 z_0^3} \frac{a}{z_0} \sin \omega t \right) , \tag{3.18}$$

is a time-dependent term linked to the plate oscillation. The approximation $\frac{1}{z^3(t)} \simeq \frac{1}{z_0^3}(1 + \frac{3a}{z_0} \sin \omega t)$ has been used. The perturbation (3.18) can induce transitions in the atom. Applying time-dependent perturbation theory with $V_I(t)$ as the perturbation operator, we can easily obtain the probability amplitude for the transition $|g\rangle \to |e\rangle$ from the atomic initial state g to a more excited state e,

$$c_e(z_0, t) = \frac{i}{\hbar} \frac{3\sigma_{ij}(d_i d_j)^{eg}}{16 z_0^3} \frac{a}{z_0} \int_0^t dt' e^{i\omega_0 t'} \sin \omega t' , \tag{3.19}$$

where $\hbar\omega_0 = E_e - E_g$ and $(d_i d_j)^{eg} = \langle e \mid d_i d_j \mid g \rangle$. Under resonance conditions ($\omega \simeq \omega_0$), the atomic excitation probability $P_e(z_0, t) = |c_e(z_0, t)|^2$ is given by

$$P_e(z_0, t) \simeq \frac{9}{2^{10}\hbar^2} \left(\frac{a}{z_0} \right)^2 \frac{\mid \sigma_{ij}(d_i d_j)^{eg} \mid^2}{z_0^6} t^2. \tag{3.20}$$

We now estimate the order of magnitude of the excitation probability $P_e(t)$. For a Rydberg atom, the matrix element of the product of components of the atomic dipole moment appearing in (3.20) is related to the electron charge e, the Bohr radius a_0 and the principal quantum number n through the relation $\mid \sigma_{ij} d_i d_j \mid \sim e^2 a_0^2 n^4$ [58, 59]. Thus the excitation probability approximately becomes

$$P_e(z_0, t) \simeq \left(3 \cdot 10^{-19} \mathrm{cm}^6 \mathrm{s}^{-2} \right) \frac{a^2}{z_0^8} n^8 t^2. \tag{3.21}$$

The condition $P_e(z_0, t) \ll 1$ must be satisfied for the validity of our perturbative approach, and this sets an upper limit to the acceptable values of time t, once the other parameters have been fixed. For $n = 75$, yielding a frequency of about 30 GHz for the transition $n = 75 \to 77$, $a/z_0 \simeq 10^{-1}$ and $z_0 \simeq 2 \cdot 10^{-3}$ cm, the single-atom excitation probability is $P_e(t) \simeq \left(5 \cdot 10^{10}\, \mathrm{s}^{-2} \right) t^2$. This shows that, by taking a time of the order of $2\,\mu$s (well compatible with achievable trapping times of Rydberg atoms [60, 61]), the probability is of the order of 20%.

If we consider now a trapped Rydberg gas instead of a single atom, if the trap size is comparable with the atom-mirror distance, equation (3.21) could not be sufficiently accurate, and the actual profile of the atomic trap should be taken into account. If $\rho(z)$ is the atomic linear density in the direction z orthogonal to the surface, the number of excited atoms, neglecting interactions among them, can be written as

$$N_e(t) = \int_0^\infty dz \rho(z) P_e(z, t) . \tag{3.22}$$

If the gas profile is cigar-shaped, as shown in Figure 3.3, parallel to the mirror, as a first approximation we may use a parabolic profile in the three dimensions. Let N be the number

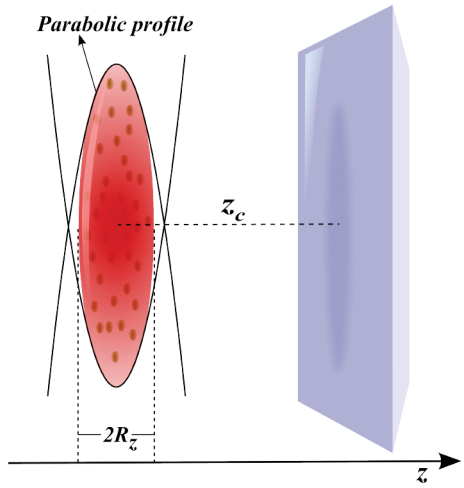

Figure 3.3 – The geometry of a gas with a cigar-shaped profile. z_c is the distance between the trap center and the wall, while $2R_z$ is the width of the gas profile along z.

of Rydberg atoms in the gas, z_c and $2R_z$ (with $R_z < z_c$) respectively the trap center-wall distance and the width of the gas profile along z, the atomic linear density in the z direction is given by

$$\rho(z) = \frac{3N}{4R_z^3}\left[R_z^2 - (z - z_c)^2\right] \tag{3.23}$$

for $-R_z < z - z_c < R_z$, and $\rho(z) = 0$ for $z - z_c < -R_z$ or $z - z_c > R_z$. Then from (3.21), (3.22) and (3.23), the number of excited atoms at time t is

$$\begin{aligned} N_e(t) &\simeq \left(10^{-20}\mathrm{cm}^6\,\mathrm{s}^{-2}\right) \\ &\times \frac{3 + 42\bar{z}_c^2 + 35\bar{z}_c^4}{(\bar{z}_c^2 - 1)^6}\frac{Na^2n^8t^2}{R_z^8}, \end{aligned} \tag{3.24}$$

where $\bar{z}_c = z_c/R_z$. Other gas profiles (gaussian, for example) could be directly used in (3.22) in order to refine our estimate to specific experimental setups. We stress that the Rydberg gas density is sufficiently low to make negligible the van der Waals interaction between the Rydberg atoms, compared to the atom-wall interaction; this should prevent the Rydberg excitation blockade mechanism.

3.3.1 Experimental proposal

In Figure 3.4 we show our possible experimental scheme to realize the proposed optomechanical coupling [22],[AN4]. The required dynamic mirror is based on a semiconductor layer whose conductivity is changed by a train of laser pulses [62] impinging on its rear surface, covered by a metal mesh that acts as a *rear* mirror. On the opposite side of the semiconductor, a high reflectivity interferential dielectric Bragg mirror, tuned to the the incident laser wavelength, prevents light that has not been absorbed in the semiconductor to enter the Rydberg atoms region. The thickness of the rear metal mesh should assure a good

reflectivity at all field frequencies relevant for the Casimir-Polder interaction at the considered atom-mirror distance z_0. In the figure a parallel-line structure mesh is shown, even if more complex patterns can be designed. To optimize the dynamical mirror, the size of the non-metallic areas in the mesh could be further reduced well below the incident laser wavelength. The laser beam would then be transmitted through the rear mirror by exploiting the EOT (extraordinary optical transmission) effect [63]. In the devised scheme, a is comparable with the thickness of the semiconductor layer, of the order of a few micrometers, which is in turn comparable with α^{-1}, the absorption length of near infrared light in direct band gap semiconductors. For example, $\alpha^{-1} \sim 1\,\mu$m in GaAs excited at the band gap photon energy that corresponds to $\lambda \sim 800$ nm.

The Rydberg atoms are prepared in an initial state characterized by a principal quantum number n, which determines the required oscillation frequency of the mirror in order to obtain a resonance effect for the transition to a higher energy level. We could assume that the initial state of the Rydberg atom is a circular state (maximum angular momentum quantum numbers), yielding a very long lifetime of the initial state. Angular momentum selection rules for the transition give $\Delta\ell = 0, \pm 2$. A possible transition worth to consider in our case is that with $\Delta\ell = 2$. By tuning the mirror oscillation frequency we can set also $\Delta n = 2$. Such a transition brings the Rydberg atom to a final state with maximum azimuthal quantum number, that is a long-lived state too, because only one decay channel by a dipole transition is allowed [59]. This should make easier the detection of the atomic excitation. If, as mentioned, an initial $n = 75$ state is prepared, the atom should be promoted to the upper level with $n = 77$ when the moving mirror oscillates at a frequency of approximately 30 GHz. A MOPA (master oscillator power amplifier) laser system [64] with a seed oscillator operating at 30 GHz delivers the pulses at the required repetition rate, and with an energy/pulse (few μJ) sufficient to excite a plasma mirror in the semiconductor layer. Lower mirror oscillation frequencies (thus lower repetition rates) would be allowed for initial states with a higher principal number. A limitation to higher values of n is however set by the detection technique of the excited states, which would rely on the selective field ionization [59] (in experiments using Rydberg states with $n = 30 - 85$, a field control at the mV/cm level has been demonstrated feasible [65]). On the other hand, the difficulties in obtaining higher frequencies of the wall vibration become ever more stringent for decreasing initial quantum numbers.

The non-harmonicity of the atom-wall distance in the presented experimental scheme can be easily included by using the atom-mirror distance $z(t) = z_0[1 - \frac{a}{z_0} f(t)]$, where $f(t)$ is the appropriate function describing the mirror's motion. In this case, equation (3.19) becomes

$$\begin{aligned} c_e(z_0, t) &= -\frac{1}{\sqrt{2\pi}\hbar} \frac{3\sigma_{ij}(d_i d_j)^{eg}}{16 z_0^3} \frac{a}{z_0} \\ &\quad \times \int_{-\infty}^{\infty} d\omega g(\omega) \frac{e^{-i(\omega-\omega_0)t} - 1}{\omega - \omega_0}, \end{aligned} \tag{3.25}$$

where $g(\omega)$ is the Fourier transform of $f(t)$. Once its form is obtained for the specific experimental setup considered, the squared modulus of equation (3.25) gives the corresponding

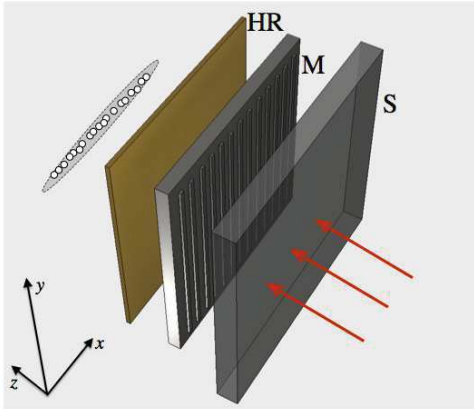

Figure 3.4 – Schematic figure representing the system: The trapped Rydberg atoms interact with the dynamical mirror (M), made by a semiconductor layer whose rear surface is covered by a metallic mesh. The semiconductor layer is illuminated by a multigigahertz repetition rate laser that induces a periodical variation of its dielectric properties. This dynamical mirror is sandwiched between a transparent bulk dielectric (S) that acts as thermal sink, and a Bragg high reflectivity mirror (HR).

atomic excitation probability, generalizing equation (3.20).

In our experimental proposal, the optomechanical coupling with the moving surface could be optimized with a quasi-one-dimensional Rydberg gas prepared in a magneto-optic trap. Such a Rydberg gas has been recently obtained in a trap with a density of 10^{10} atoms/cm^3 and number of atoms reaching the order of 10^6, whose distance from a surface could be controlled with a few micrometers precision [29, 60]. Lower densities are preferable in our case, in order to reduce possible interactions among the atoms. The average atom-wall distance we consider, in the range $20 - 50$ micrometers, is much less than a typical transition wavelength of the Rydberg atom (of the order of 1 cm for the transition mentioned above), so that the near-zone Casimir-Polder interaction between the atoms and the mirror is relevant in this case, as we have assumed.

Trapping a sample of about $N \sim 10^3$ ^{87}Rb atoms in a cigar-like shape with $R_\perp \sim 5 \cdot 10^{-2}$ cm and $R_z \sim 10^{-3}$ cm at a distance $z_c = 2 \cdot 10^{-3}$ cm from a surface for times up to $10\,\mu$s, is also realistic using actual Rydberg atoms trapping techniques.

From (3.24), with the values given above and for $a = 2 \cdot 10^{-4}$cm, we obtain that about 100 atoms in the sample of 10^3 are excited after $0.5\,\mu$s (atoms in the sample closer to the wall are more likely excited, due to the strong dependence of the excitation probability with the atom-wall distance). Hence a considerable number of trapped atoms can be excited in a quite short time interval, making possible to detect the dynamical effect we have proposed.

The atom density considered in the estimate above is such that the long-range atom-atom van der Waals interaction, which scales as r^{-6} with the interatomic distance r, can be neglected. In fact, the closest atom-atom distance is around 10^{-3} cm and the average atom-wall distance is $2 \cdot 10^{-3}$ cm. Using known expressions for atom-atom and atom-wall interactions [66], it is possible to show that the atom-wall interaction energy is some three

orders of magnitude larger than the interaction energy between one atom and its closest atom. Interatomic interactions can be thus neglected for the gas density we have considered. Similarly, it is easy to check that quadrupolar interactions [66, 67] are several orders of magnitude smaller than dipolar ones, and can be therefore neglected. This is also expected on a physical basis, because in our case the size of the Rydberg atoms, $\sim 10^{-5}$ cm, is much smaller than the average relevant atom-wall and atom-atom distances.

Finally, we can compare our excitation probability of the Rydberg atoms with that due to absorption of the real photons emitted by dynamical Casimir effect. Using known results for the number of emitted photons by an oscillating wall [36], [68], with the same parameters given above for our proposed experiment, the number density (for unit area) of real photons emitted is $\sim 10^{-1}/\text{cm}^2$. Then the number of photons that can excite our trapped atomic sample, which has a front area of $\sim 10^{-5}\text{cm}^2$, is $\sim 10^{-6}$. This is an upper limit for the single-atom excitation probability by the real photons (far field) emitted by the oscillating wall under resonance condition; it is thus negligible compared to our near-field excitation probability ($\sim 10\%$). The number of emitted photons could be increased by a resonant cavity [23], but also in this case the atomic excitation probability by photon absorption is order of magnitudes smaller than our near-field effect.

Summing up, we proposed a new optomechanical dynamical coupling between Rydberg atoms and a substrate, based on the dynamical Casimir-Polder effect [22],[AN4]. In particular, we have analyzed a dilute sample of Rydberg atoms trapped in the proximity (tens of micrometers) of an oscillating reflective mirror. This effect could be observed using currently available experimental techniques.

It shows how quantum vacuum fluctuations may be used to realize an optomechanical coupling between a macroscopic body and an elementary or mesoscopic quantum system, and to change the internal state of that system.

References

[1] P. W. Milonni, *The Quantum Vacuum: An Introduction to Quantum Electrodynamics*, Academic Press, San Diego, (1994).

[2] G. Compagno, R. Passante, and F. Persico, *Atom-Field Interactions and Dressed Atoms*, Cambridge University Press, Cambridge, (1995).

[3] H. B. G. Casimir, Proc. K. Ned. Akad. Wet. B **51**, 793 (1948).

[4] H. B. G. Casimir and D. Polder, Phys. Rev. **73**, 360 (1948).

[5] I. E. Dzyaloshinskii, E. M. Lifshitz, and L. P. Pitaevskii, Adv. Phys. **10**, 165 (1961).

[6] M. Bordag, G. L. Klimchitskaya, U. Mohideen, and V. M. Mostepanenko, *Advances in the Casimir Effect*, Oxford Science Publication, Oxford, (2009), and references therein.

[7] *Casimir Physics*, edited by D. Dalvit, P. Milonni, D. Roberts, and F. de Rosa, Springer, Heidelberg, (2011).

[8] A. Canaguier-Durand, P. A. Maia Neto, A. Lambrecht, and S. Reynaud, Phys. Rev. Lett. **104**, 040403 (2010).

[9] G. T. Moore, J. Math. Phys. **11**, 2679 (1970).

[10] V. V. Dodonov, Phys. Scr. **82**, 038105 (2010).

[11] J. T. Mendonça and A. Guerreiro, Phys. Rev. A **72**, 063805 (2005).

[12] R. Golestanian and M. Kardar, Phys. Rev. A **58**, 1713 (1998).

[13] M. F. Maghrebi, R. Golestanian, and M. Kardar, Phys. Rev. D 87, 025016 (2013).

[14] A. Lambrecht, M. T. Jaekel, and S. Reynaud, Phys. Rev. Lett. **77**, 615 (1996).

[15] I. Carusotto, M. Antezza, F. Bariani, S. De Liberato, and C. Ciuti, Phys. Rev. A **77**, 063621 (2008).

[16] R. Messina, R. Vasile, and R. Passante, Phys. Rev. A **82**, 062501 (2010); H. R. Haakh, C. Henkel, S. Spagnolo, L. Rizzuto, and R. Passante, Phys. Rev. A **89**, 022509 (2014).

[17] P. Meystre, Ann. Physik **525**, 215 (2013).

[18] M. Aspelmeyer, T. J. Kippenberg, and F. Marquardt, arXiv: 1303.0733.

[19] J. D. Thompson, T. G. Tiecke, N. P. de Leon, J. Feist, A. V. Akimov, M. Gullans, A. S. Zibrov, V. Vuletić, and M. D. Lukin, Science **340**, 1020 (2013).

[20] S. Butera and R. Passante, Phys. Rev. Lett. **111**, 060403 (2013).

[21] F. Armata and R. Passante, Phys. Rev. D **91**, 025012 (2015).

[22] M. Antezza, C. Braggio, G. Carugno, A. Noto, R. Passante, L. Rizzuto, G. Ruoso, and S. Spagnolo, Phys. Rev. Lett. **113**, 023601 (2014).

[23] V. V. Dodonov, Phys. Lett. A **207**, 126 (1995).

[24] T. Kawakubo and K. Yamamoto, Phys. Rev. A **83**, 013819 (2011).

[25] A. M. Fedotov, N. B. Narozhny, and Y. E. Lozovik, Phys. Lett. A **274**, 213 (2000).

[26] N. B. Narozhny, A. M. Fedotov, and Y. E. Lozovik, Phys. Rev. A **64**, 053807 (2001).

[27] A. Belyanin, V. Kocharovsky, V. Kocharovsky, and F. Capasso, Phys. Rev. Lett. **88**, 053602 (2002).

[28] A. Agnesi, C. Braggio, G. Carugno, F. Della Valle, G. Galeazzi, G. Messineo, F. Pirzio, G. Reali, and G. Ruoso, Rev. Sci. Instr. **82**, 115107 (2011).

[29] A. Reinhard, K. C. Younge, T. Cubel Liebisch, B. Knuffman, P. R. Berman, and G. Raithel, Phys. Rev. Lett. **100**, 233201 (2008).

[30] M. Antezza, L. P. Pitaevskii, and S. Stringari, Phys. Rev. A **70**, 053619 (2004).

[31] M. Antezza, J. Phys. A: Math. Gen. **39**, 6117 (2006).

[32] J. M. Obrecht, R. J. Wild, M. Antezza, L. P. Pitaevskii, S. Stringari, and E. A. Cornell, Phys. Rev. Lett. **98**, 063201, 2007.

[33] M. Antezza, L. P. Pitaevskii, and S. Stringari, Phys. Rev. Lett. **95**, 113202 (2005).

[34] M.-P. Gorza and M. Ducloy, Eur. Phys. J. D. **40**, 343 (2006).

[35] H.B. Callen, T.A. Welton, Phys. Rev. **83**, 34–40 (1951).

[36] L. H. Ford and A. Vilenkin, Phys. Rev. D **25**, 2569 (1982).

[37] C. M. Wilson, G. Johansson, A. Pourkabirian, M. Simoen, J. R. Johansson, T. Duty, F. Nori and P. Delsing, Nature, **479**, 376 (2011).

[38] P. Lähteenmäki, G. S. Paraoanu, J. Hassel, and P. J. Hakonen, Proc. Nat. Acad. Sci. **110**, 4234 (2013).

[39] J.-C. Jaskula, G. B. Partridge, M. Bonneau, R. Lopes, J. Ruaudel, D. Boiron, and C. I. Westbrook, Phys. Rev. Lett **109**, 220401 (2012).

[40] S.A. Fulling, P.C.W. Davies, Proc. R. Soc. A **348**, 393–414 (1976).

[41] V. V. Dodonov, Adv.Chem.Phys. **119**, 309-394 (2001).

[42] V. V. Dodonov, J. Phys.: Conf. Ser. **161**, 012027 (2009).

[43] G. A. Askar'yan, Sov. Phys. – JETP **15**, 1161–2 (1962).

[44] J. F. Annett and P. M. Echenique, Phys. Rev. B **34**, 6853 (1986).

[45] T. G. Philbin and U. Leonhardt, New J. Phys. **11**, 033035 (2009).

[46] J. B. Pendry, New J. Phys. **12**, 033028 (2010).

[47] C. K. Law, Phys. Rev. Lett. **73**, 1931 (1994).

[48] V. V. Dodonov and A. B. Klimov, Phys. Rev. A **53**, 2664–82 (1996).

[49] A. Agnesi, C. Braggio, G. Bressi, G. Carugno, G. Galeazzi, F. Pirzio, G. Reali, G. Ruoso and D. Zanello, J. Phys. A: Math. Gen. **41**, 164024 (2008).

[50] A. Agnesi, C. Braggio, G. Bressi, G. Carugno, F. Della Valle, G. Galeazzi, G. Messineo, F. Pirzio, G. Reali, G. Ruoso, D. Scarpa and D. Zanello, J. Phys.: Conf. Ser. **161**, 012028 (2009).

[51] C. Braggio, G. Carugno, F. Della Valle, G. Galeazzi, A. Lombardi, G. Ruoso and D. Zanello, New J. Phys. **15** 013044 (2013).

[52] S. Å. Ellingsen, S. Y. Buhmann, and S. Scheel, Phys. Rev. Lett. **104**, 223003 (2010).

[53] S. Y. Buhmann, *Dispersion Forces I (Springer Tracts in Modern Physics, Volume 247)*, Springer, Berlin, 2012.

[54] S. M. Barnett, A. Aspect, and P.W. Milonni, J.Phys. B **33**, L143 (2000).

[55] F. Intravaia, C. Henkel, and M. Antezza, in: *Casimir Physics*, edited by D. Dalvit, P. Milonni, D. Roberts and F. Rosa, Springer-Verlag, Berlin 2011, p. 345.

[56] J. D. Jackson, *Classical Electrodynamics*, Wiley, New York (1975).

[57] E. A. Power and T. Thirunamachandran, Am. J. Phys. **50**, 8 (1982).

[58] J. A. Crosse, S. Å. Ellingsen, K. Clements, S. Y. Buhmann, and S. Scheel, Phys. Rev. A **82**, 010901(R) (2010).

[59] T. F. Gallagher, Rep. Prog. Phys. **51**, 143 (1988).

[60] M. Viteau, M. G. Bason, J. Radogostowicz, N. Malossi, D. Ciampini, O. Morsch, and E. Arimondo, Phys. Rev. Lett. **107**, 060402 (2011).

[61] P. Pillet, T. Vogt, M. Viteau, A. Chotia, J. Zhao, D. Comparat, T. F. Gallagher, D. Tate, A. Gaëtan, V. Miroshnychenko, T. Wilk, A. Browaeys, and P. Grangier, J. Phys. Conf. Ser. **194** 012066 (2009).

[62] A. Agnesi, C. Braggio, G. Bressi, G . Carugno, F. Della Valle, G. Galeazzi, G. Messineo, F. Pirzio, G. Reali, G. Ruoso, D. Scarpa, and D. Zanello, J. Phys: Conf. Ser. **161**, 012028 (2009).

[63] F. J. Garcia-Vidal, L. Martin-Moreno, T. W. Ebbesen, L. Kuipers, Rev. Mod. Phys., **82**, 729 (2010).

[64] A. Agnesi, C. Braggio, L. Carrà, F. Pirzio, S. Lodo, G. Messineo, D. Scarpa, A. Tomaselli, G. Reali, C. Vacchi, Opt. Express **16**, 15811 (2008).

[65] M. Viteau, J. Radogostowicz, M. G. Bason, N. Malossi, D. Ciampini, O. Morsch, and E. Arimondo, Opt. Express **19**, 6007 (2011).

[66] E. A. Power and T. Thirunamachandran, Phys. Rev A **53**, 1567 (1996); Phys. Rev A **25**, 2473 (1982).

[67] J. M. Hutson, P. W. Fowler, and A. Zaremba, Surface Science **175**, L775 (1986).

[68] P. A. Maia Neto and L. A. S. Machado, Phys. Rev A **54**, 3420 (1996).

[69] J. B. Pendry, J. Phys.: Condens. Matter **9**, 10301–10320 (1997).

Chapter 4

Casimir-Lifshitz force out of thermal equilibrium between dielectric gratings

Contents

4.1 A scattering-matrix approach to Casimir-Lifshitz force out of thermal equilibrium . . . 106

4.1.1 Correlation functions of the total field . . . 110

4.1.2 The force between two slabs . . . 114

4.2 Methods for the diffraction by gratings . . . 119

4.2.1 The Fourier Modal Method . . . 119

4.2.2 Some other methods for the diffraction by gratings . . . 128

4.3 OTE Casimir-Lifshitz force between two dielectric gratings . . . 132

4.3.1 Numerical results . . . 139

4.3.2 Dependence on geometrical parameters . . . 143

4.3.3 Modulation of the attractive-repulsive transition . . . 146

4.3.4 Concluding remarks . . . 147

References . . . 148

Casimir-Lifshitz force is an interaction between polarizable bodies originating from the fluctuations of the electromagnetic field. We already saw that it was first theoretically derived by Casimir in 1948 for an idealized configuration of two infinite conducting plates at zero temperature and generalized later by Lifshitz and collaborators in the case of bodies having arbitrary optical properties and finite temperature [1] - [3]. The Casimir-Lifshitz interaction, experimentally verified for several geometries [4], results from two contributions, one originating from vacuum fluctuations and present also at zero temperature, the other one from purely thermal fluctuations. The latter becomes relevant when the distance separating the bodies is larger than the thermal wavelength $\lambda_T = \hbar c/k_\mathrm{B}T$, of the order of

8 μm at ambient temperature. This explains why it has been only very recently experimentally observed at thermal equilibrium [5].

Nevertheless, the situation completely changes for systems out of thermal equilibrium. It was first theoretically predicted in 2005 that the atom-surface interaction (usually referred to as Casimir-Polder force) is qualitatively and quantitatively modified with respect to thermal equilibrium [6, 7]. New power-law behaviors appear: the force, which depends on the temperatures involved in the systems, can turn into repulsive (being only attractive at thermal equilibrium) and it is strongly tunable by modifying the temperatures. This prediction was verified in 2007, providing the first experimental observation of thermal effects [8]. These results paved the way to a renewed interest in Casimir-Lifshitz effects out of thermal equilibrium. In fact, these effects have been studied for two slabs [9, 10] and in presence of atoms [11] - [16], and more recently several different approaches have been developed to deal with the problem of the force out of thermal equilibrium and heat transfer between two [17] - [24] or more [25] - [28] arbitrary bodies. The physics of the electromagnetic field out of thermal equilibrium has also stimulated the study of other effects, such as the manipulation of atomic populations [29, 30] and entanglement [31, 32].

In parallel with the interest in the absence of thermal equilibrium, Casimir-Lifshitz interactions have been studied in several different geometries, with particular interest to the sphere-plane configuration, the most studied experimentally. More recently, nanostructured surfaces have been theoretically considered in the contexts of both force [33] - [43] and heat transfer [44, 45, 46]. Experimentally, the force have been measured between a sphere and a dielectric [47, 48] or a metallic grating [49].

The problem we discuss in this Chapter concerns with the results obtained from the calculation of the Casimir-Lifshitz force out of thermal equilibrium in presence of dielectric gratings, computation made in our work [39],[AN5] for the first time in literature. This physical system has been analyzed in order to study the combination of non-equilibrium and geometrical effects, that we show in detail. In particular we consider a system made of two different gratings having different temperatures, immersed in an environmental bath at a third temperature. Our calculations can be relevant both to imagine new experiments measuring the Casimir-Lifshitz force out of thermal equilibrium and in the more general context of the manipulation of the force in micro- and nano-electromechanical systems [50, 51].

The Chapter is structured as follows. In the first two sections we present the methods, already developed in literature, that we have used to get our original results presented in the last section of this chapter. In particular, in Section 4.1 we introduce the method used to calculate the force between two arbitrary objects out of thermal equilibrium and we also show, for example, its application to the case of two slabs. In Section 4.2 we focus our attention on the issue of finding the scattering operators for the gratings, necessary to calculate the Casimir-Lifshitz force in our approach. Here we discuss shortly some usual methods developed for the scattering problem in gratings and we aim to develop and solve the problem of the scattering upon a single 1D lamellar dielectric grating by means of the Fourier Modal Method. In Section 4.3, we apply the results of the previous sections in order to calculate the force out of thermal equilibrium between two different gratings. We explore the

behavior of the force as a function of the three temperatures and of the geometrical parameters of the gratings, with a specific attention to the appearance and features of repulsion and finally we give some conclusive remarks.

4.1 A scattering-matrix approach to Casimir-Lifshitz force out of thermal equilibrium

In this section we show how to derive an expression for the Casimir-Lifshitz force out of thermal equilibrium between two bodies at two different temperatures immersed in external radiation, an environment, characterized by another temperature. We see that this derivation, deduced in [19], is also strictly related to the heat transfer problem. In particular we focus our attention to cast the average values of the electromagnetic field in terms of the scattering operators. Finally we numerically apply the general expression found to the simple and well known configuration of two slabs, by calculating the heat transfer and the force out of thermal equilibrium [19].

Let us start introducing in detail the general system considered. We analyze two bodies, labeled with indexes 1, 2, with arbitrary geometries and material properties. The geometry of the system is represented in Figure 4.1. We assume that the two bodies are separated by a geometrical planar surface. This assumption is useful because it allows us to use a plane-wave decomposition and can be in principle relaxed by an appropriate change of basis. In addition, it is an assumption verified in most experimental configurations. So we can define three different zones A, B, C, enclosed respectively in $z_1 \leq z \leq z_2$, $z_2 \leq z \leq z_3$, $z_3 \leq z \leq z_4$.

Our physical system is considered in a configuration out of thermal equilibrium (OTE). This means that each body is supposed to be in local thermal equilibrium with a constant temperature T_i. We also assume that the two bodies are immersed in a radiation bath coming from bounding walls far from the system and having temperature T_{e}, in general different from the temperatures of the two bodies (see also [19]). The whole system is considered in a stationary regime so that the three temperatures involved are constant in time.

The procedure that we use is based on a mode decomposition of the fields. Each mode $(\omega, \mathbf{k}, p, \phi)$ is identified by the direction of propagation $\phi = \{+, -\}$ along the z axis, by the polarization index p (assuming the values $p = 1, 2$ which respectively correspond to transverse electric (TE) and transverse magnetic (TM) modes), by the frequency ω and the transverse wave vector $\mathbf{k} = (k_x, k_y)$. In this description, the z component of the wave vector k_z is a dependent variable defined as

$$k_z = \sqrt{\frac{\omega^2}{c^2} - \mathbf{k}^2}. \tag{4.1}$$

while the complete wave vector $\mathbf{K}$ is

$$\mathbf{K}^{\phi} = (\mathbf{k}, \phi k_z) = (k_x, k_y, \phi k_z). \tag{4.2}$$

We see that when $k \leq \frac{\omega}{c}$, k_z is real so the corresponding wave is propagative. Instead when $k > \frac{\omega}{c}$, k_z becomes imaginary and the corresponding wave is evanescent. In the latter case ϕ represents the direction along which the amplitude of the evanescent wave decays.

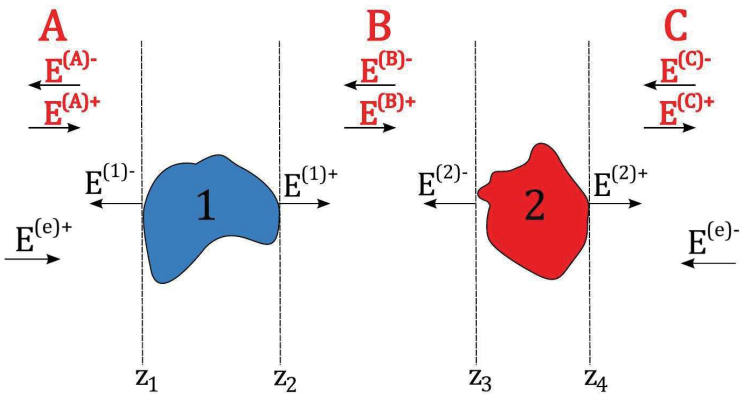

Figure 4.1 – The geometry of the system. We define three different zones A, B, and C useful when we consider the scattering. The width of the zone B defines a distance between the two bodies $z_2 \leq z \leq z_3$.

We consider now the expression for the electric field. We first decompose it with respect to frequency and we work only with positive frequencies

$$\mathbf{E}(\mathbf{R}, t) = 2\,\mathrm{Re}\left[\int_0^{+\infty} \frac{d\omega}{2\pi} \exp(-i\omega t)\mathbf{E}(\mathbf{R}, \omega)\right]. \tag{4.3}$$

Then we decompose the single-frequency component $\mathbf{E}(\mathbf{R}, \omega)$ with respect to the parallel wave vector $\mathbf{k}$, the direction of propagation ϕ and the polarization p

$$\mathbf{E}(\mathbf{R}, \omega) = \sum_{\phi,p} \int \frac{d^2\mathbf{k}}{(2\pi)^2} \exp(i\mathbf{K}^\phi \cdot \mathbf{R})\hat{\boldsymbol{\epsilon}}_p^\phi(\mathbf{k}, \omega)E_p^\phi(\mathbf{k}, \omega). \tag{4.4}$$

In general, from now on, the sum on ϕ runs over the values $\{+, -\}$ and the sum on p over the values $\{1, 2\}$. The polarization vectors $\hat{\boldsymbol{\epsilon}}_p^\phi(\mathbf{k}, \omega)$ appearing in (4.4) are defined in the following standard way

$$\begin{aligned} \hat{\boldsymbol{\epsilon}}_{\mathrm{TE}}^\phi(\mathbf{k}, \omega) &= \hat{\mathbf{z}} \times \hat{\mathbf{k}} = \frac{1}{k}(-k_y\hat{\mathbf{x}} + k_x\hat{\mathbf{y}}) \\ \hat{\boldsymbol{\epsilon}}_{\mathrm{TM}}^\phi(\mathbf{k}, \omega) &= \frac{c}{\omega}\hat{\boldsymbol{\epsilon}}_{\mathrm{TE}}^\phi(\mathbf{k}, \omega) \times \mathbf{K}^\phi = \frac{c}{\omega}(-k\hat{\mathbf{z}} + \phi k_z\hat{\mathbf{k}}) \end{aligned} \tag{4.5}$$

where $\hat{\mathbf{x}}$, $\hat{\mathbf{y}}$ and $\hat{\mathbf{z}}$ are, respectively, the unit vectors along the directions x, y and z while $\hat{\mathbf{k}} = \mathbf{k}/k$.

Using Maxwell's equations we can easily find the expression of the single-frequency component of the magnetic field and we get

$$\mathbf{B}(\mathbf{R}, \omega) = \frac{1}{c}\sum_{\phi,p} \int \frac{d^2\mathbf{k}}{(2\pi)^2} \exp(i\mathbf{K}^\phi \cdot \mathbf{R})\hat{\boldsymbol{\beta}}_p^\phi(\mathbf{k}, \omega)E_p^\phi(\mathbf{k}, \omega) \tag{4.6}$$

where

$$\hat{\boldsymbol{\beta}}_p^\phi(\mathbf{k}, \omega) = (-1)^p\hat{\boldsymbol{\epsilon}}_{S(p)}^\phi(\mathbf{k}, \omega) \tag{4.7}$$

and the function S is defined as $S(1) = 2$ and $S(2) = 1$.

The starting point for our calculation of the OTE Casimir-Lifshitz force and the heat transfer on each body are the following integrals

$$\begin{aligned} \mathbf{F} &= \int_{\Sigma} \langle \mathbb{T}(\mathbf{R}, t)\rangle_{\text{sym}} \cdot d\mathbf{\Sigma} \\ H &= -\int_{\Sigma} \langle \mathbf{S}(\mathbf{R}, t)\rangle_{\text{sym}} \cdot d\mathbf{\Sigma}. \end{aligned} \tag{4.8}$$

These are surface integrals of the quantum symmetrized average of the Maxwell stress tensor $\mathbb{T}$ (having cartesian components T_{ij}, with $i, j = x, y, z$) and the Poynting vector $\mathbf{S}$ through a closed surface Σ enclosing the body under study. In classical electromagnetism, for bodies immersed in vacuum, the definitions of these two quantities in SI units are the following

$$\begin{aligned} T_{ij}(\mathbf{R}, t) = \epsilon_0\Big[E_i(\mathbf{R}, t)E_j(\mathbf{R}, t) + c^2 B_i(\mathbf{R}, t)B_j(\mathbf{R}, t) - \frac{1}{2}\Big(E^2(\mathbf{R}, t) + c^2 B^2(\mathbf{R}, t)\Big)\delta_{ij}\Big], \\ \mathbf{S}(\mathbf{R}, t) = \epsilon_0 c^2 \mathbf{E}(\mathbf{R}, t) \times \mathbf{B}(\mathbf{R}, t). \end{aligned} \tag{4.9}$$

and the quantum symmetrized average value $\langle AB\rangle_{\text{sym}}$ is defined as

$$\langle AB\rangle_{\text{sym}} = \frac{1}{2}\Big(\langle AB\rangle + \langle BA\rangle\Big) \tag{4.10}$$

being $\langle A\rangle$ an ordinary quantum average value. From the expressions in (4.9) we see that, for the calculation of the integrals in (4.8), the following products of the fields are involved

$$E_i(\mathbf{R}, t)E_j(\mathbf{R}, t), \quad B_i(\mathbf{R}, t)B_j(\mathbf{R}, t) \tag{4.11}$$

and, keeping in mind the passage to quantum operators, as a further step their symmetrized quantum average. In this last stage the terms like EE and $E^\dagger E^\dagger$ have null quantum average and only the terms $EE^\dagger$ are relevant. So it is convenient to introduce the following expression of the operator $C^{\phi\phi'}$, defined in terms of the correlation functions of the field amplitudes. With ϕ and ϕ' we indicate the propagation direction of the field in region where $\bar{z}$ is located

$$\begin{aligned} \langle E_p^{\phi}(\mathbf{k}, \omega)E_{p'}^{\phi'\dagger}(\mathbf{k}', \omega')\rangle_{\text{sym}} &= \frac{1}{2}\langle E_p^{\phi}(\mathbf{k}, \omega)E_{p'}^{\phi'\dagger}(\mathbf{k}', \omega') + E_{p'}^{\phi'\dagger}(\mathbf{k}', \omega')E_p^{\phi}(\mathbf{k}, \omega)\rangle \\ &= 2\pi\delta(\omega - \omega')\langle p, \mathbf{k}|C^{\phi\phi'}|p', \mathbf{k}'\rangle. \end{aligned} \tag{4.12}$$

In the above equation, we stress that, generally, two modes of the field propagating in opposite directions do not necessarily commute and the conservation of frequency has been inserted. The latter is due to the time invariance since no dynamics is considered in the system under scrutiny.

From now on, the calculation concerns the heat transfer and the force acting on body 1. We have chosen as enclosing surface Σ a closed box as that pictured in Figure 4.2. This box has one side of length D and a square base of side L parallel to the xy plane. According to the

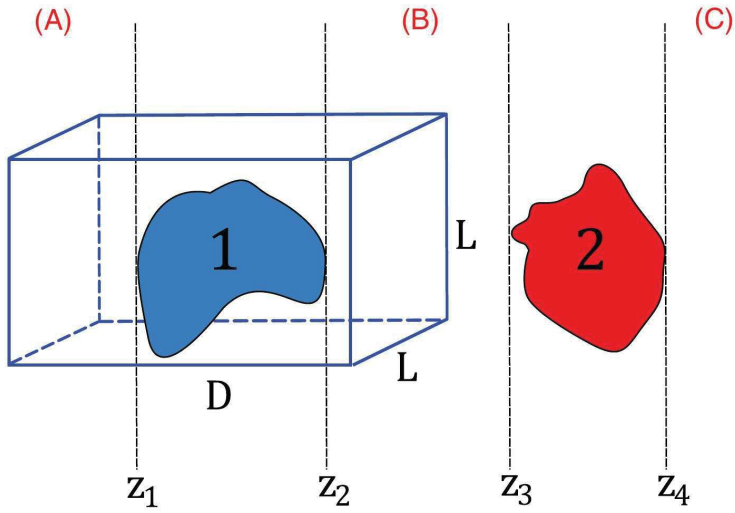

Figure 4.2 – The enclosing box chosen for the calculation of the fluxes.

definition of T_{ij} (S_{ij}), the m component of the force (m = x,y,z) (the heat transfer) is given in this case by the flux of T_{mz} (S_z) through the two surfaces orthogonal to the z axis, plus the fluxes of T_{mx} (S_x) and T_{my} (S_y) through the surfaces of the parallelepiped orthogonal to the x and y axes, respectively. Taking the limit $L \to +\infty$, we can see how the surface of the two faces of the box which are orthogonal to the z axis diverges more rapidly (as L^2) than the other four surfaces (as L). Then we see that for the calculation of the fluxes in (4.8) one simply needs to calculate the flux of T_{mz} (S_z) on the surface (which is now a plane with infinite area) in region A and to subtract this result from the flux of T_{mz} (S_z) through the plane in region B. In addition, as a consequence of the arbitrariness of the box, the two fluxes calculated in region A and the region B, must not depend on the z coordinates of the respective planes, in spite of the fact that the stress tensor depends, in general, on z.

Then we only need the flux of T_{zz} and S_z through two planes $z = \bar{z}$ on the two sides of the body. From now on, we use a more compact notation for the expressions relative to force and heat flux and we introduce an index m whose value $m = 1$ is associated to the heat flux and $m = 2$ to the force. In this way we have

$$\varphi_m(\bar{z}) = \int_{z=\bar{z}} d^2\mathbf{r} \begin{cases} \langle S_z \rangle_{\text{sym}} & m = 1 \\ \langle T_{zz} \rangle_{\text{sym}} & m = 2 \end{cases} \tag{4.13}$$

Using the expressions of the fields given in (4.4) and in (4.6), after some simple algebra (see [19] for details), the *generalized flux* reads

$$\varphi_m(\bar{z}) = -(-1)^m 2\epsilon_0 c^2 \sum_p \int \frac{d^2\mathbf{k}}{(2\pi)^2} \left(\sum_{\phi=\phi'} \int_{ck}^{+\infty} \frac{d\omega}{2\pi} + \sum_{\phi\neq\phi'} \int_0^{ck} \frac{d\omega}{2\pi} \right) \left(\frac{\phi k_z}{\omega} \right)^m \langle p, \mathbf{k} | C^{\phi\phi'} | p, \mathbf{k} \rangle. \tag{4.14}$$

We observe that with the knowledge of the generalized flux above and thanks to the explicit expression of the correlators in any region of our system, we can calculate the force and

the heat transfer for our considered system. We also note that $C^{\phi\phi'}$ is the only quantity in (4.14) depending on the position $\bar{z}$ of the plane where we calculate the flux. Moreover, analyzing the equation (4.14) we can see that the flux have two separate contributions, coming from the propagative and evanescent sectors. The first is given by the correlators between the field propagating in a direction ϕ and itself. The second involves the correlators of counterpropagating fields.

If we introduce the following definitions

$$\langle p, \mathbf{k}|\mathcal{P}_n^{(\mathrm{pw/ew})}|p', \mathbf{k}'\rangle = k_z^n \langle p, \mathbf{k}|\Pi^{(\mathrm{pw/ew})}|p', \mathbf{k}'\rangle \tag{4.15}$$

where $\Pi^{(\mathrm{pw})}$ ($\Pi^{(\mathrm{ew})}$) are the projector on the propagative (evanescent) sector and defining the trace operator

$$\mathrm{Tr}\,\mathcal{A} = \sum_p \int \frac{d^2\mathbf{k}}{(2\pi)^2} \int_0^{+\infty} \frac{d\omega}{2\pi} \langle p, \mathbf{k}|\mathcal{A}|p, \mathbf{k}\rangle \tag{4.16}$$

we have

$$\varphi_m(\bar{z}) = -(-1)^m 2\epsilon_0 c^2 \sum_{\phi\phi'} \mathrm{Tr}\Big\{\Big(\frac{\phi}{\omega}\Big)^m C^{\phi\phi'}\Big[\delta_{\phi\phi'}\mathcal{P}_m^{(\mathrm{pw})} + (1-\delta_{\phi\phi'})\mathcal{P}_m^{(\mathrm{ew})}\Big]\Big\}. \tag{4.17}$$

where $\delta_{\phi\phi'}$ is the Kronecker delta.

4.1.1 Correlation functions of the total field

To go on with the computation of the generalized flux (4.17) we need to find the correlation functions of the total field in any region of the system. This results from the source fields present in our system, i.e the fields $E^{(i)\phi}$ emitted by the body i and propagating in direction ϕ and the counterpropagating fields emitted by the environment $E^{(\mathrm{e})}\phi$, (Figure 4.1). We have to consider then all the possible scattering processes undergone by our system. In this way we can make explicit the connection between total and source fields by introducing the reflection and transmission operators associated to each body.

To define these scattering operators let us analyze a body placed in the region $z_1 < z < z_2$. We assume that an external field is impinging on our body, either from its left or from its right side. The body will scatter the incoming field. In this way new components of the field on both sides of the body are produced. The field coming from the left (right) will produce a reflected field propagating toward the left (right) on the left (right) side and a transmitted field that propagates toward the same direction of the incoming one (see Figure 4.3). We will use the notations $\mathcal{R}^{(i)\phi}$ and $\mathcal{T}^{(i)\phi}$ to indicate, respectively, the reflection and transmission operators of body i, where ϕ describes the direction of propagation of the outgoing field.

For example, let us consider an incoming field coming from the left side. In this way we have

$$\mathbf{E}^{(\mathrm{in})+}(\mathbf{R}, t) = \mathbf{E}^{(\mathrm{re})-}(\mathbf{R}, t) + \mathbf{E}^{(\mathrm{tr})+}(\mathbf{R}, t). \tag{4.18}$$

We already noted the conservation of the frequency for the system here considered. We get a definition of the operators $\mathcal{R}^-$ and $\mathcal{T}^+$ that connect each mode of the outgoing fields

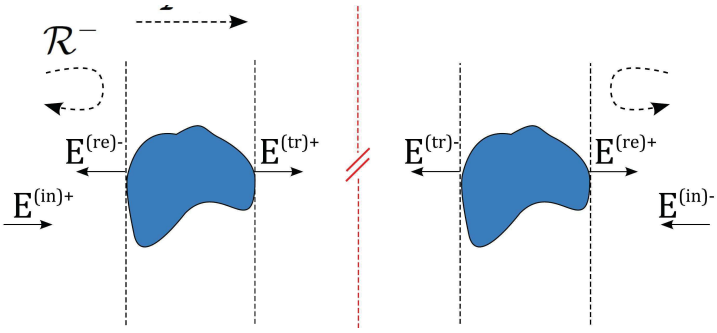

Figure 4.3 – A schematic figure to define the scattering operators.

to all modes of the incoming field at the same frequency ω

$$\mathbf{E}_p^{(\mathrm{re})-}(\mathbf{k},\omega) = \sum_{p'} \int \frac{d^2\mathbf{k}'}{(2\pi)^2} \langle p,\mathbf{k}|\mathcal{R}^-|p',\mathbf{k}'\rangle E_{p'}^{(\mathrm{in})+}(\mathbf{k}',\omega) \tag{4.19}$$

$$\mathbf{E}_p^{(\mathrm{tr})+}(\mathbf{k},\omega) = \sum_{p'} \int \frac{d^2\mathbf{k}'}{(2\pi)^2} \langle p,\mathbf{k}|\mathcal{T}^+|p',\mathbf{k}'\rangle E_{p'}^{(\mathrm{in})+}(\mathbf{k}',\omega). \tag{4.20}$$

We want to remark that the frequency dependence is implicitly contained in the scattering operators. Obviously an analogous definition of the operators $\mathcal{R}^+$ and $\mathcal{T}^-$ can be given in a similar way.

Making use of the scattering operators we introduced, it is possible to get the self-consistent system of equations giving the total field in each region. We simply need the amplitudes $E_p^{(1)+}(\mathbf{k},\omega)$, $E_p^{(2)-}(\mathbf{k},\omega)$ and $E_p^{(3)\pm}(\mathbf{k},\omega)$. In each region (A,B) of Figure 4.1 the field propagates in both directions. We gather all the modes and denote the amplitudes with the symbol $E^{(\gamma)\phi}$, where $\gamma = A,\ B$, and we write the system of equations

$$\begin{cases} E^{(\mathrm{A})+} = E^{(\mathrm{e})+} \\ E^{(\mathrm{A})-} = E^{(1)-} + \mathcal{R}^{(1)-}E^{(\mathrm{e})+} + \mathcal{T}^{(1)-}E^{(\mathrm{B})-} \\ E^{(\mathrm{B})+} = E^{(1)+} + \mathcal{R}^{(1)+}E^{(\mathrm{B})-} + \mathcal{T}^{(1)+}E^{(\mathrm{e})+} \\ E^{(\mathrm{B})-} = E^{(2)-} + \mathcal{R}^{(2)-}E^{(\mathrm{B})+} + \mathcal{T}^{(2)-}E^{(\mathrm{e})-}. \end{cases} \tag{4.21}$$

In the equations above the products between scattering operators and fields must be considered as matrix-vector products. Besides, we used a more compact notation where the ω dependence of all operators and field amplitudes is omitted. We also introduce the following operators

$$\begin{aligned} U^{(1,2)} &= \sum_{n=0}^{+\infty} (\mathcal{R}^{(1)+}\mathcal{R}^{(2)-})^n = (\mathbb{1} - \mathcal{R}^{(1)+}\mathcal{R}^{(2)-})^{-1}, \\ U^{(2,1)} &= \sum_{n=0}^{+\infty} (\mathcal{R}^{(2)-}\mathcal{R}^{(1)+})^n = (\mathbb{1} - \mathcal{R}^{(2)-}\mathcal{R}^{(1)+})^{-1}. \end{aligned} \tag{4.22}$$

describing the infinite series of multiple reflections in the *cavity* formed by bodies 1 and 2.

Now, using the scattering operators defined above and performing simple algebraic manipulations on (4.21), we obtain the total fields in regions A and B

$$E^{(\mathrm{A})+} = E^{(\mathrm{e})+}, \tag{4.23}$$

$$\begin{aligned} E^{(\mathrm{A})-} &= \mathcal{T}^{(1)-}U^{(2,1)}\mathcal{R}^{(2)-}E^{(1)+} + E^{(1)-} + \mathcal{T}^{(1)-}U^{(2,1)}E^{(2)-} + \mathcal{R}^{(1)-}E^{(\mathrm{e})+} \\ &+ \mathcal{T}^{(1)-}U^{(2,1)}\mathcal{R}^{(2)-}\mathcal{T}^{(1)+}E^{(\mathrm{e})+} + \mathcal{T}^{(1)-}U^{(2,1)}\mathcal{T}^{(2)-}E^{(\mathrm{e})-}, \end{aligned} \tag{4.24}$$

$$E^{(\mathrm{B})+} = U^{(1,2)}\Big[E^{(1)+} + \mathcal{R}^{(1)+}E^{(2)-} + \mathcal{T}^{(1)+}E^{(\mathrm{e})+} + \mathcal{R}^{(1)+}\mathcal{T}^{(2)-}E^{(\mathrm{e})-}\Big], \tag{4.25}$$

$$E^{(\mathrm{B})-} = U^{(2,1)}\Big[\mathcal{R}^{(2)-}E^{(1)+} + E^{(2)-} + \mathcal{R}^{(2)-}\mathcal{T}^{(1)+}E^{(\mathrm{e})+} + \mathcal{T}^{(2)-}E^{(\mathrm{e})-}\Big]. \tag{4.26}$$

In this way we have found an expression of the total field in each region as a function of the source fields $E^{(i)\phi}$ ($i = 1, 2$, $\phi = +, -$) and the environmental field $E^{(\mathrm{e})\phi}$.

We can now return to develop an explicit expression for the correlators related to the scattering operators. If we consider an identical system to that we are considering here but at thermal equilibrium, the correlators of the total electromagnetic field outside the body can be deduced from the fluctuation-dissipation theorem [27]. This expression relates the correlators with the Green function of the system and with the thermal population density

$$N(\omega, T) = \frac{\hbar\omega}{2}\coth\Big(\frac{\hbar\omega}{2k_BT}\Big) = \hbar\omega\Big[\frac{1}{2} + n(\omega, T)\Big], \quad n(\omega, T) = \frac{1}{e^{\frac{\hbar\omega}{k_BT}} - 1}. \tag{4.27}$$

However, when we consider the out of thermal equilibrium configuration, the fluctuation-dissipation theorem, strictly speaking, is not applicable. Though, if we assume that a local temperature can be defined for each body and that it remains constant in time, the correlators of the field emitted by each body can still be deduced using the fluctuation-dissipation theorem at the local temperature. This is possible because the assumption made leads to think that the part of the total field emitted by each body is the same as if the body were at thermal equilibrium with the environment at its temperature. It is like saying that the emission of each body is not significantly influenced by the modification due to the external radiation impinging on the body. It should be said, however, that the limits of validity of this hypothesis, already used in literature, require further experimental and theoretical investigations.

Now it remains to find the connection between the Green function and the scattering operators. We will not go into the details of the calculation; it is discussed in [19] and here we present only the result. Similarly to what we have done in (4.12) we define the following matrices

$$\begin{aligned} \langle E_p^{(i)\phi}(\mathbf{k}, \omega)E_{p'}^{(i)\phi'\dagger}(\mathbf{k}', \omega')\rangle_{\mathrm{sym}} &= 2\pi\delta(\omega - \omega')\langle p, \mathbf{k}|C^{(i)\phi\phi'}|p', \mathbf{k}'\rangle, \\ \langle E_p^{(\mathrm{e})\phi}(\mathbf{k}, \omega)E_{p'}^{(\mathrm{e})\phi'\dagger}(\mathbf{k}', \omega')\rangle_{\mathrm{sym}} &= 2\pi\delta(\omega - \omega')\langle p, \mathbf{k}|C^{(\mathrm{e})\phi\phi'}|p', \mathbf{k}'\rangle. \end{aligned} \tag{4.28}$$

In addition we introduce the useful function

$$f_\alpha(\mathcal{R}) = \begin{cases} \mathcal{P}_{-1}^{(\mathrm{pw})} - \mathcal{R}\mathcal{P}_{-1}^{(\mathrm{pw})}\mathcal{R}^\dagger + \mathcal{R}\mathcal{P}_{-1}^{(\mathrm{ew})} - \mathcal{P}_{-1}^{(\mathrm{ew})}\mathcal{R}^\dagger \\ \qquad\qquad\qquad\qquad\qquad\qquad \alpha = -1 \\ \mathcal{P}_m^{(\mathrm{pw})} + (-1)^m\mathcal{R}^\dagger\mathcal{P}_m^{(\mathrm{pw})}\mathcal{R} + \mathcal{R}^\dagger\mathcal{P}_m^{(\mathrm{ew})} \\ +(-1)^m\mathcal{P}_m^{(\mathrm{ew})}\mathcal{R} \\ \qquad\qquad\qquad\qquad\qquad\qquad \alpha = m \in \{1,2\} \end{cases} \tag{4.29}$$

. In this way we can write the correlation functions of the source fields as follows

$$C^{(i)\phi\phi} = \frac{\omega}{2\varepsilon_0 c^2} N_i\Big(f_{-1}(\mathcal{R}^{(i)\phi}) - \mathcal{T}^{(i)\phi}\mathcal{P}_{-1}^{(\mathrm{pw})}\mathcal{T}^{(i)\phi\dagger}\Big), \tag{4.30}$$

$$C^{(i)\phi,-\phi} = \frac{\omega}{2\varepsilon_0 c^2} N_i\Big(-\mathcal{R}^{(i)\phi}\mathcal{P}_{-1}^{(\mathrm{pw})}\mathcal{T}^{(i)-\phi\dagger} - \mathcal{T}^{(i)\phi}\mathcal{P}_{-1}^{(\mathrm{pw})}\mathcal{R}^{(i)-\phi\dagger} + \mathcal{T}^{(i)\phi}\mathcal{P}_{-1}^{(\mathrm{ew})} - \mathcal{P}_{-1}^{(\mathrm{ew})}\mathcal{T}^{(i)-\phi\dagger}\Big), \tag{4.31}$$

$$C^{(\mathrm{e})\phi\phi'} = \delta_{\phi\phi'}\frac{\omega}{2\varepsilon_0 c^2} N_{\mathrm{e}}\mathcal{P}_{-1}^{(\mathrm{pw})}, \tag{4.32}$$

where for $\alpha \in \{1, 2, \mathrm{e}\}$ we have defined $N_\alpha = N(\omega, T_\alpha)$.

At this stage we have found the expression of the total field in each region in terms of the source fields. Since this relation is always linear, we can write it under the general form

$$E^{(\gamma)\phi} = \sum_{i=1}^{3}\sum_{\alpha=+,-} A_{i\alpha}^{(\gamma)\phi}E^{(i)\alpha} + \sum_{\alpha=+,-} B_\alpha^{(\gamma)\phi}E^{(\mathrm{e})\alpha}, \tag{4.33}$$

where $\gamma \in \{\mathrm{A,B,C}\}$. From this general expression we can derive the general expression of the correlation functions of the total field in the region γ

$$C_\gamma^{\phi\phi'} = \sum_{i=1}^{3}\sum_{\alpha,\alpha'=+,-} A_{i\alpha}^{(\gamma)\phi}C^{(i)\alpha\alpha'}A_{i\alpha'}^{(\gamma)\phi'\dagger} + \sum_{\alpha=+,-} B_\alpha^{(\gamma)\phi}C^{(\mathrm{e})}B_\alpha^{(\gamma)\phi'\dagger}, \tag{4.34}$$

where $C^{(\mathrm{e})} = C^{(\mathrm{e})\phi\phi}$. Since $A_{i\alpha}^{(\gamma)\phi}$ and $B_\alpha^{(\gamma)\phi}$ are the coefficients of the decomposition derived in (4.23)-(4.26), knowing the source correlation functions obtained in (4.12), we are able to derive the correlators of the total field in any region. We are now ready to calculate the fluxes in the region A and B and derive our final expression of the OTE force and of the heat transfer of our system in terms of the scattering operators.

Finally exploiting the results obtained in the limit case of thermal equilibrium (see [19] and the more general case in [28] for more details), it is convenient to separate the force as the sum of two terms

$$F_{1z} = F_{1z}^{(\mathrm{eq})}(T_1) + \Delta_2 \tag{4.35}$$

where

$$F_{1z}^{(\mathrm{eq})}(T_1) = -2\,\mathrm{Re}\,\mathrm{Tr}\Big[k_z\omega^{-1}N(\omega, T_1)\Big(U^{(1,2)}\mathcal{R}^{(1)+}\mathcal{R}^{(2)-} + U^{(2,1)}\mathcal{R}^{(2)-}\mathcal{R}^{(1)+}\Big)\Big], \tag{4.36}$$

is the force acting on body 1 if the system were at the thermal equilibrium at temperature T_1, while Δ_2 is a nonequilibrium term that depends on the three temperatures of the system. The latter is null when all the three temperatures of the system are the same. It is important to note that the equilibrium force contains both the zero-temperature term and the thermal correction. In addition it has a dependence only on the intracavity reflection operators $\mathcal{R}^{(1)+}$ and $\mathcal{R}^{(2)-}$, i.e., the operators that describe the reflection produced by each body on the side of the other one.

With this separation of the force and indicating the heat transfer as $H = \Delta_{1,1}$, after lenghty algebraic manipulations, we can write the expression for heat transfer and the OTE Casimir-Lifshitz force

$$\begin{aligned}\Delta_m = &-(-1)^m \hbar \,\mathrm{Tr}\Big\{\omega^{2-m}\Big[n_{e1}\Big[U^{(2,1)}\mathcal{T}^{(2)-}\mathcal{P}^{(\mathrm{pw})}_{-1}\mathcal{T}^{(2)-\dagger}U^{(2,1)\dagger}\Big(f_m(\mathcal{R}^{(1)+}) - \mathcal{T}^{(1)-\dagger}\mathcal{P}^{(\mathrm{pw})}_{m}\mathcal{T}^{(1)-}\Big)\\ &+(-1)^m\Big(U^{(1,2)}\mathcal{T}^{(1)+}\mathcal{P}^{(\mathrm{pw})}_{-1}\mathcal{T}^{(1)+\dagger}U^{(1,2)\dagger} - \mathcal{P}^{(\mathrm{pw})}_{-1}\Big)f_m(\mathcal{R}^{(2)-})\\ &+\Big(\mathcal{R}^{(2)-}\mathcal{P}^{(\mathrm{pw})}_{-1}\mathcal{R}^{(2)-\dagger} - \mathcal{R}^{(12)-}\mathcal{P}^{(\mathrm{pw})}_{-1}\mathcal{R}^{(12)-\dagger}\Big)\mathcal{P}^{(\mathrm{pw})}_{m}\Big]\\ &+n_{21}U^{(2,1)}\Big(f_{-1}(\mathcal{R}^{(2)-}) - \mathcal{T}^{(2)-}\mathcal{P}^{(\mathrm{pw})}_{-1}\mathcal{T}^{(2)-\dagger}\Big)U^{(2,1)\dagger}\Big(f_m(\mathcal{R}^{(1)+}) - \mathcal{T}^{(1)-\dagger}\mathcal{P}^{(\mathrm{pw})}_{m}\mathcal{T}^{(1)-}\Big)\Big]\Big\}\end{aligned}$$

where we introduced

$$\mathcal{R}^{(12)-} = \mathcal{R}^{(1)-} + \mathcal{T}^{(1)-}U^{(2,1)}\mathcal{R}^{(2)-}\mathcal{T}^{(1)+} \tag{4.37}$$

and

$$n_{ij} = n(\omega, T_i) - n(\omega, T_j), \quad \text{i,j=1, 2, e.} \tag{4.38}$$

This expression gives the heat transfer ($m = 1$) and the non-equilibrium contribution to the force ($m = 2$) on body 1 for an arbitrary set of the two bodies having arbitrary geometry, dielectric properties and temperatures and immersed in a thermal bath having a third different temperature. The equation (4.35) and the equation (4.37) are the starting point for our original calculation discussed in this chapter. We want to conclude this derivation saying that it is also possible to generalize the method developed here to the case of three body in an OTE configuration [28].

4.1.2 The force between two slabs

In this subsection we shortly analyze, as example for an application of the expressions found above, the OTE Casimir-Lifshitz force and the heat transfer for the case of two slabs. These cases, already studied in literature (see references [9], [52] and [19]), are presented here to show the power and the applicability of the method introduced in this Section. Moreover, since the two slabs case has been deeply studied in Casimir physics [53], this system is a very good example to understand some aspects of the OTE Casimir-Lifshitz force and make a comparison with the thermal configuration.

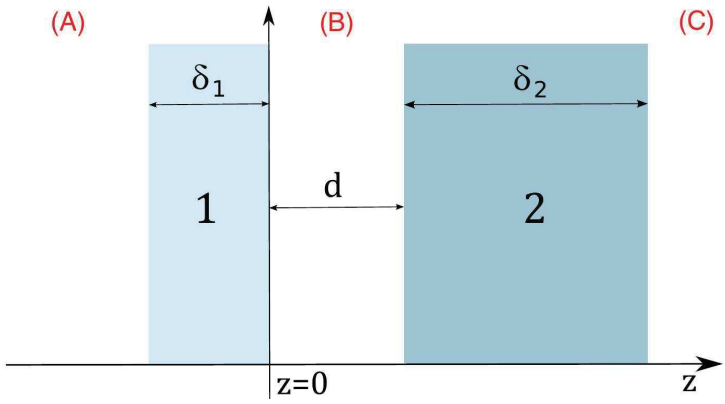

Figure 4.4 – A figure that represents the geometry of the system of two slabs studied in this subsection.

We consider two parallel homogeneous dielectric slabs, labeled $i\,(i = 1, 2)$ of finite thickness δ_i placed at a distance d (see Figure 4.4). At first we analyze the reflection and transmission operators $\mathcal{R}^{(1)+}$ and $\mathcal{T}^{(1)+}$. For the case of homogeneous slab, as that we are considering here, these operators are diagonal and can be written as

$$\langle p, \mathbf{k}|\mathcal{R}^{(1)+}|p', \mathbf{k}'\rangle = (2\pi)^2\delta(\mathbf{k}-\mathbf{k}')\delta_{pp'}\rho_{1p}(\mathbf{k},\omega), \tag{4.39}$$

$$\langle p, \mathbf{k}|\mathcal{T}^{(1)+}|p', \mathbf{k}'\rangle = (2\pi)^2\delta(\mathbf{k}-\mathbf{k}')\delta_{pp'}\tau_{1p}(\mathbf{k},\omega), \tag{4.40}$$

where we introduced the modified Fresnel coefficients, respectively the reflection and transmission ones, considering the finite thickness of the slabs:

$$\rho_{1p}(\mathbf{k},\omega) = r_{1p}(\mathbf{k},\omega)\frac{1-e^{2ik_{z1}\delta_1}}{1-r_{1p}^2(\mathbf{k},\omega)e^{2ik_{z1}\delta 1}}, \tag{4.41}$$

$$\tau_{1p}(\mathbf{k},\omega) = \frac{t_{1p}(\mathbf{k},\omega)\bar{t}_{1p}(\mathbf{k},\omega)e^{i(k_{z1}-k_z)\delta_1}}{1-r_{1p}^2(\mathbf{k},\omega)e^{2ik_{z1}\delta 1}}. \tag{4.42}$$

In the equations above we defined the z component of the wave vector $\mathbf{k}$ inside the slab 1 and we used the standard Fresnel coefficients for the vacuum-medium configuration

$$k_{z1} = \sqrt{\varepsilon_1(\omega)\frac{\omega^2}{c^2} - \mathbf{k}^2}, \tag{4.43}$$

$$r_{1,\mathrm{TE}} = \frac{k_z - k_{z1}}{k_z + k_{z1}}, \quad r_{1,\mathrm{TM}} = \frac{\varepsilon_1(\omega)k_z - k_{z1}}{\varepsilon_1(\omega)k_z + k_{z1}}, \tag{4.44}$$

$$t_{1,\mathrm{TE}} = \frac{2k_z}{k_z + k_{z1}}, \quad t_{1,\mathrm{TM}} = \frac{2\sqrt{\varepsilon_1(\omega)}k_z}{\varepsilon_1(\omega)k_z + k_{z1}}, \tag{4.45}$$

and we have also introduced the Fresnel coefficients for the medium-vacuum transmission

$$\bar{t}_{1,\mathrm{TE}} = \frac{2k_{z1}}{k_z + k_{z1}}, \quad \bar{t}_{1,\mathrm{TM}} = \frac{2\sqrt{\varepsilon_1(\omega)}k_{z1}}{\varepsilon_1(\omega)k_z + k_{z1}}. \tag{4.46}$$

The transmission operator $\mathcal{T}^{(1)-}$ and the scattering operators $\mathcal{R}^{(2)-}$, $\mathcal{T}^{(2)-}$ of body 2 can be found from geometrical considerations of the system and solving the problem of the scattering operators change when we perform a translation from a frame of reference $O \to \tilde{O}$. Let us discuss this translation transformation and let us introduce the operator $\mathcal{S}^{\phi\phi'}$ in the following way

$$\mathcal{S}^{++} = \mathcal{T}^{+}, \quad \mathcal{S}^{+-} = \mathcal{R}^{+}, \tag{4.47}$$

$$\mathcal{S}^{-+} = \mathcal{R}^{-}, \quad \mathcal{S}^{--} = \mathcal{T}^{-}. \tag{4.48}$$

This operator simply connects the outgoing modes propagating in direction ϕ to the incoming modes propagating in direction ϕ'. If we indicate with $\mathbf{R}_S$ the translation vector, from the definition of the electric field (4.4), we can write

$$\mathbf{E}(\mathbf{R},\omega) = \sum_{\phi,p} \int \frac{d^2\mathbf{k}}{(2\pi)^2} \exp(i\mathbf{K}^{\phi}\cdot(\mathbf{R}-\mathbf{R}_S))\hat{\epsilon}_p^{\phi}(\mathbf{k},\omega)E_p^{\phi}(\mathbf{k},\omega)\exp(i\mathbf{K}^{\phi}\cdot\mathbf{R}_S) \tag{4.49}$$

and we obtain the amplitude $\tilde{E}_p^{\phi}(,\omega)$ in the translated frame $\tilde{O}$

$$\tilde{E}_p^{\phi}(\mathbf{k},\omega) = \exp(i\mathbf{K}^{\phi}\cdot\mathbf{R}_S)E_p^{\phi}(,\omega). \tag{4.50}$$

We deduce then

$$\tilde{E}_p^{(\mathrm{out})\phi}(\mathbf{k},\omega) = \exp(i\mathbf{K}^{\phi}\cdot\mathbf{R}_S)\sum_p \int \frac{d^2\mathbf{k}'}{(2\pi)^2}\langle p,\mathbf{k}|\mathcal{S}^{\phi\phi'}|p',\mathbf{k}'\rangle \exp(-i\mathbf{K}'^{\phi'}\cdot\mathbf{R}_S)\tilde{E}_{p'}^{(\mathrm{in})\phi'}(\mathbf{k},\omega) \tag{4.51}$$

and from this we finally have

$$\langle p,\mathbf{k}|\tilde{\mathcal{S}}^{\phi\phi'}|p',\mathbf{k}'\rangle = \exp\left[-i(\mathbf{K}^{\phi}-\mathbf{K}'^{\phi'})\cdot\mathbf{R}_S\right]\langle p,\mathbf{k}|\mathcal{S}^{\phi\phi'}|p',\mathbf{k}'\rangle. \tag{4.52}$$

So if we consider a translation of d along the z axis, as in the case of two slabs we are considering, we obtain the following relations

$$\langle p,\mathbf{k}|\tilde{\mathcal{R}}^{+}|p',\mathbf{k}'\rangle = \exp\left[i(k_z+k_z')d\right]\langle p,\mathbf{k}|\mathcal{R}^{+}|p',\mathbf{k}'\rangle, \tag{4.53}$$

$$\langle p,\mathbf{k}|\tilde{\mathcal{R}}^{-}|p',\mathbf{k}'\rangle = \exp\left[-i(k_z+k_z')d\right]\langle p,\mathbf{k}|\mathcal{R}^{-}|p',\mathbf{k}'\rangle, \tag{4.54}$$

$$\langle p,\mathbf{k}|\tilde{\mathcal{T}}^{+}|p',\mathbf{k}'\rangle = \exp\left[i(k_z-k_z')d\right]\langle p,\mathbf{k}|\mathcal{T}^{+}|p',\mathbf{k}'\rangle, \tag{4.55}$$

$$\langle p,\mathbf{k}|\tilde{\mathcal{T}}^{-}|p',\mathbf{k}'\rangle = \exp\left[-i(k_z-k_z')d\right]\langle p,\mathbf{k}|\mathcal{T}^{-}|p',\mathbf{k}'\rangle \tag{4.56}$$

and we are able to get all the scattering operators to which we are interested.

We note that for the physical system that we are considering, the matrix element of the scattering operators between two generic states is proportional to a Dirac delta function, as we can see from (4.39) and (4.40). This delta function comes from the translational invariance along x and y dictated by the particular geometry under scrutiny. We can deduce that the force acting on the body 1 is formally divergent as well as the heat transfer. However this is not an issue of concern because the body 1, a slab, has an infinite surface so this

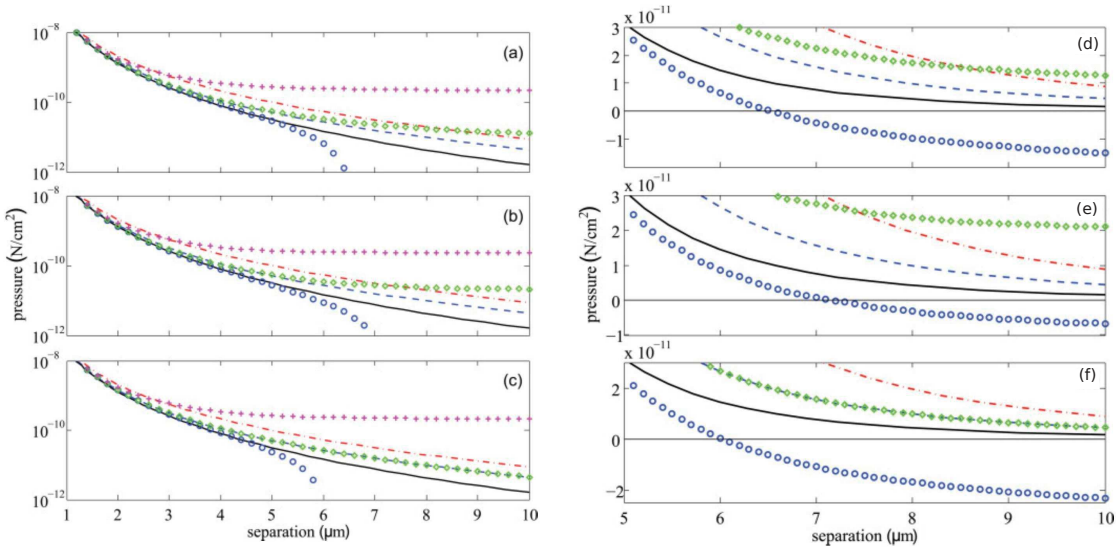

(i) (ii)

Figure 4.5 – In this figure, coming from [19], it is plotted the pressure acting on a fused silica slab of thickness $\delta_1 = 2\,\mu$m placed in front of a second silicon slab of thickness $\delta_2 = 1000\,\mu$m. Lines: pressures of the equilibrium state at $T = 0$ K (black solid), 300 K (blue dashed), and 600 K (red dash-dotted). Symbols: pressures of the nonequilibrium state where $T_3 = 0$ K (blue circles), 300 K (green diamonds), and 600 K (magenta plus). $T_1 = 300$ K and $T_2 = 0$ K in (a), $T_1 = 0$ K and $T_2 = 300$ K in (b), and $T_1 = T2 = 300$ K in (c). (d), (e) and (f) are the same plots of those on the left but with linear pressure scale.

divergence is not surprising. In fact, we can consider the force density or the heat transfer per unit area which are instead finite quantities. We can then calculate the pressure and heat transfer density on body 1 and make our physical considerations on these quantities.

We have now all the ingredients for the calculation of the pressure and of the heat transfer density. We present and discuss the case of a slab made of fused silica with a thickness of 2μm placed in front of a silicon slab with thickness of $1000\,\mu$m. It is numerically evaluated and studied in reference [19].

Let us start with the results of the pressure, for different configurations of temperatures, shown in Figure 4.5 (see the caption for the temperature configurations). In these three plots, the pressure as a function of the distance (range from 1 to 10 μm) is shown. For each of them both the pressure of the non-thermal-equilibrium state and the pressure of the thermal-equilibrium state (at the environment temperature) are reported. The remarkable point of these group of plots is that the transition from an equilibrium to a nonequilibrium configuration change significantly the qualitative and quantitative behavior of the interaction. Moreover, the environmental temperature can be considered as a parameter to tune the interaction. In particular in the plot (c) of Figure 4.5, where the two bodies are in relative thermal equilibrium ($T_1 = T_2$), the environmental temperature assumes an important

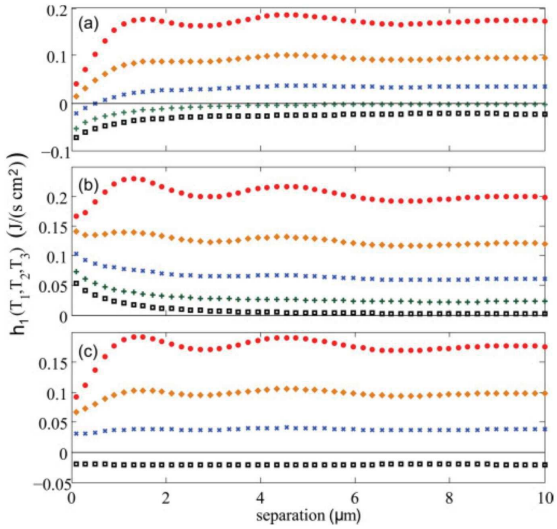

Figure 4.6 – Figure from [19] where is plotted the radiative heat transfer per unit surface between a fused silica slab of thickness $\delta_1 = 2\,\mu$m placed in front of a second silicon slab of thickness $\delta_2 = 1000\,\mu$m. The temperatures of the slabs are $T_1 = 300$ K and $T_2 = 0$ K in (a), $T_1 = 0$ K and $T_2 = 300$ K in (b), and $T_1 = T_2 = 300$ K in (c). Symbols: $T_e = 0$ K (black squares), 300 K (green plus), 400 K (blue crosses), 500 K (brown diamonds), and 600 K (red circles).

role since it can modify the force. This point stresses the fact that the environmental temperature should be carefully controlled also in experiments where the force is measured at the relative equilibrium between the two bodies. In the second group of plots of Figure 4.5 (plots (d), (e), (f)) we see the same features already described but the transition of the force from attractive to repulsive becomes evident thanks to the linear scale used; also, it can be seen more easily what are the distances where the transition occurs (around 6 μm).

We turn now to the results of the heat transfer density pictured in Figure 4.6. We have three different configurations, corresponding to the three different choices of the slab temperatures T_1 and T_2 listed in the caption. IN each case we have a plot for the heat transfer when the environmental temperature T_e has the values (0,300,400,500,600) K. We can immediately stress the importance of the environmental radiation, as we already seen for the pressure. In fact, the heat transfer h1 shows an oscillating behavior with an amplitude that increases when the temperature T_e takes higher values. It can be shown (see [19]) that these oscillations are due to the propagative sector. We also wish to stress that the occurrence of a change of sign in the heat transfer. The higher is the value of T_e, the smaller is the distance at which this change of sign occurs.

4.2 Methods for the diffraction by gratings

In this section we focus our attention on the description of the diffraction of light in presence of periodic media, in particular diffraction gratings. Gratings are optical devices having a periodic structure (1D or 2D periodicity) which, when impinged by electromagnetic radiation, split and diffract the incident rays of the radiation in several beams. There are several applications in science and in technology related to diffraction by gratings and also in nature we find many examples of these systems (butterfly wings for example). For this reason several methods have been developed over the years, each of these more suitable in some specific physical situations [54]. We dwell on describe the Fourier Modal Method which, thanks to its simplicity, versatility, numerical stability and rapidity has been chosen for the calculation of our original work showed in this chapter, the OTE Casimir-Lifshitz force between two dielectric gratings. We also briefly discuss other two methods strictly related to the Fourier Modal Method, the adaptive spatial resolution method and the C-method. The latter is important for possible future applications to the calculation of the force between two gratings when they are made of metal. The C-method instead is interesting because, besides the FMM and the modal method that for brevity is not described here, is a one of the few methods used to calculate the Casimir-Lifshitz force between gratings with continuous profile.

4.2.1 The Fourier Modal Method

We start presenting and discussing the Fourier Modal Method (FMM), the method we have used to obtain our original results showed in the next section. It is the most used and popular method to describe the diffraction by gratings. With this approach, based on a Rayleigh expansion of the fields in the homogeneous zones, the problem of the search for solutions of the fields in the grating region simply translates in an eigenvalue problem. This is possible after an appropriate expansion of the fields into Floquet-Fourier series and the periodic permittivity in the grating region into Fourier series. The method is relatively simple. We need to know the Maxwell equations, the Fourier series and basic concepts of geometry and algebra. It is also a quick method with respect to numerical convergence and the code necessary to implement it in a computer calculation requires relative few steps in programming and it can be easily written in several different programming languages (Matlab, Mathematica, C, Fortran). Moreover, it is a versatile method because the range of systems that can be treated with it is very wide.

Before discussing the FMM we want to state the paradigm of the diffraction problem. We want to find the distribution, in near and far field, of the electromagnetic waves after an incident electromagnetic wave irradiates a grating (with known geometrical and optical properties). This means that we must solve a boundary value problem. The FMM faces this problem through the following steps. At first the geometrical space where the grating is placed is divided in three zones (see Figure 4.7). In the upper semi-infinite transparent region with dielectric constant ε_1 the incident plane wave comes from infinity; in the middle region, i.e. the grating region, the dielectric constant $\varepsilon_2(x)$ is periodic and in the lower semi-

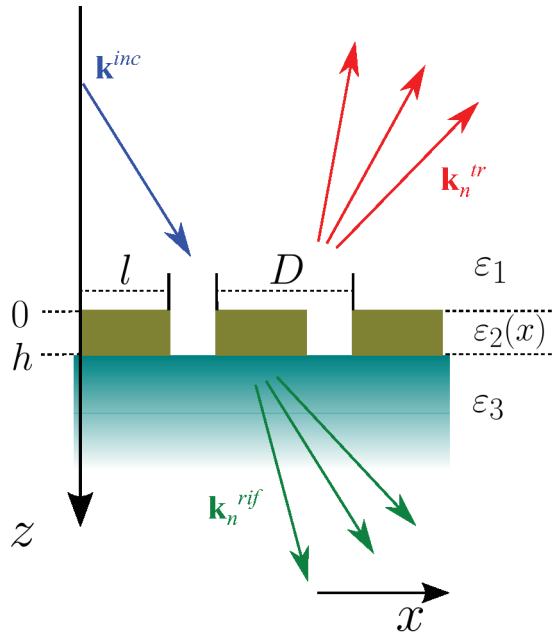

Figure 4.7 – The figure illustrates the system analyzed in this subsection. A rectangular (or lamellar) grating illuminated by a monochromatic plane wave.

infinite region there is a medium that may be opaque and has dielectric constant ε_3. After the partition of the space, the electromagnetic fields and the permittivity are expanded in Floquet-Fourier series. With the help of the Maxwell equations an eigenvalue problem is solved to find the fields in the grating region. At this stage the electromagnetic boundary conditions are applied to the total fields at the interfaces between the regions defined before and the resulting linear system of equations is solved to find the unknowns coefficients. Finally, using the formalism of the S-matrix the scattering operators of the system can be deduced.

We start the description of the FMM analyzing in more detail the physical system in Figure 4.7. The three regions are labeled, from top to bottom, 1, 2, 3. The origin of the coordinate system is placed at the start of one of the grooves. The grating is supposed to be infinite in the xy plane and is composed of two media, medium a and medium b, with permittivities ε_a and ε_b. In particular we have that $\varepsilon_2(x)$ is

$$\varepsilon_2(x) = \begin{cases} \varepsilon_a & 0 \leq x < l \\ \varepsilon_b & l \leq x < D. \end{cases} \tag{4.57}$$

Since, in several optical problems and in particular in the main problem we face in this chapter the magnetic permeabilities are approximately equal to that of the vacuum for all the media we will consider from now on $\mu = 1$. The four values of ε introduced can be different from each other but usually in the applications (as well as for the system considered in our work on the OTE Casimir-Lifshitz force) we have that in the region 1 there is air and

that $\varepsilon_1 = \varepsilon_b$ while $\varepsilon_a = \varepsilon_3$. The zones with ε_a and ε_b are called, respectively, ridges and grooves of the grating. The geometrical parameters describing the grating are the period, indicated with D, the groove depth h and the ridge width l. It is also useful to introduce the filling factor defined as $f = l/D$. From now on we will consider that the wave vector $\mathbf{k}^{(\mathrm{in})}$ stays on the xz plane

$$\mathbf{k}^{(\mathrm{in})} = k_0 \sqrt{\varepsilon_1}\,(\sin\theta\,\hat{\mathbf{x}} + \cos\theta\,\hat{\mathbf{z}}) \tag{4.58}$$

where k_0 is the wave number of the vacuum. The conical case (i.e. the case where the incident wave vector stays in a plane different from the xz plane) is easily found with a generalization and it is treated in the next section. As a consequence of this y invariance of $\mathbf{k}^{(\mathrm{in})}$ we have that also the fields $\mathbf{E}$ and $\mathbf{H}$ are independent of y. The grating problem, from the properties of the Maxwell equations thus, becomes scalar and it is necessary to find only one component of the electric/magnetic field, the other ones are then easily determined from it with the help of the Maxwell equations (for our system we have $\partial_t = -i\omega$)

$$\begin{cases} \cancel{\partial_y E_z} - \partial_z E_y = i\omega\mu_0 H_x \\ \partial_x E_y - \cancel{\partial_y E_x} = i\omega\mu_0 H_z, \qquad \text{TE case} \\ \partial_z H_x - \partial_x H_z = -i\omega\varepsilon\varepsilon_0 E_y \end{cases} \tag{4.59}$$

$$\begin{cases} \cancel{\partial_y H_z} - \partial_z H_y = -i\omega\varepsilon\varepsilon_0 E_x \\ \partial_x H_y - \cancel{\partial_y H_x} = -i\omega\varepsilon\varepsilon_0 E_z, \qquad \text{TM case} \\ \partial_z E_x - \partial_x E_z = i\omega\mu_0 H_y \end{cases} \tag{4.60}$$

This means that we can consider only two different cases, the transverse electric (*TE*) case and the transverse magnetic *TM* case (see Figure 4.8). For the first case we must determine the y-component of the electric field while for the second one we must determine the y-component of the magnetic field.

Let us now introduce the following useful compact notation:

$$u^{(\mathrm{i})}(x,z) = \begin{cases} E_y^{(\mathrm{i})}(x,z) & \text{TE} \\ H_y^{(\mathrm{i})}(x,z) & \text{TM} \end{cases} \tag{4.61}$$

where $i = 1, 2, 3$ indicates one of the three regions. In this notation we get from the equations (4.59) and (4.60) the following wave equations valid in the grating region

$$\frac{\partial^2 u^{(2)}}{\partial x^2} + \frac{\partial^2 u^{(2)}}{\partial z^2} + k^2 \varepsilon^{(2)}(x)\, u^{(2)}(x,z) = 0 \qquad \text{TE}, \tag{4.62}$$

$$\frac{\partial}{\partial x}\left(\frac{1}{\varepsilon^{(2)}}\frac{\partial u^{(2)}}{\partial x}\right) + \frac{1}{\varepsilon^{(2)}}\frac{\partial^2 u^{(2)}}{\partial z^2} + k^2 \varepsilon^{(2)}(x)\, u^{(2)}(x,z) = 0 \qquad \text{TM}. \tag{4.63}$$

Since the electric permittivity is periodic in the grating region, from the Floquet-Bloch theorem we deduce that the fields are pseudo-periodic

$$u^{(2)}(x + D, z) = e^{i k_x D}\, u^{(2)}(x,z) \tag{4.64}$$

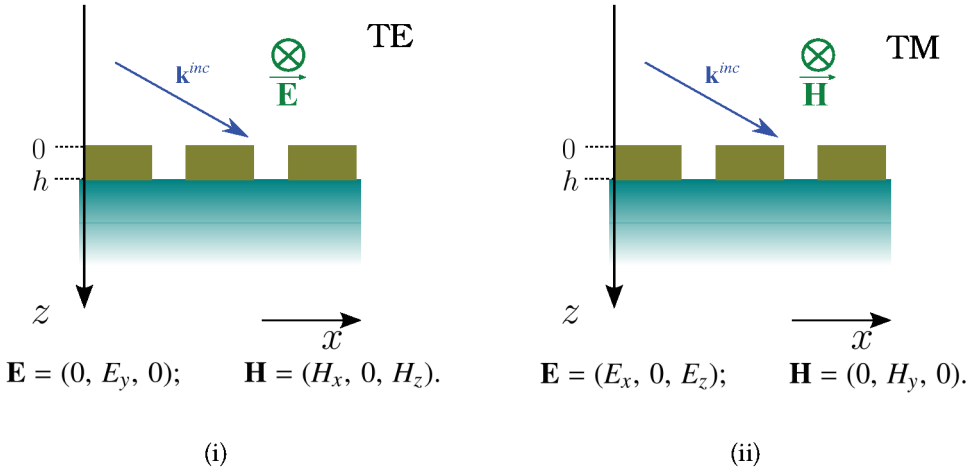

Figure 4.8 – A schematic representation of the two cases of TE (i) and TM (ii).

and we can state that the function

$$v^{(2)}(x,z) = \frac{u^{(2)}(x,z)}{e^{ik_x x}} \tag{4.65}$$

is periodic. As a consequence, by using a Fourier series expansion it follows that

$$v^{(2)}(x,z) = \sum_n u_n(z) e^{i\frac{2\pi}{D}n\,x} \qquad \Rightarrow$$
$$u^{(2)}(x,z) = \sum_n u_n(z) e^{ik_x x} e^{i\frac{2\pi}{D}n\,x} = \sum_n u_n(z) e^{ik_{x,n}x} \tag{4.66}$$

where we have defined

$$k_{x,n} = k_x + n\frac{2\pi}{D}, \qquad n \in \mathbb{N}. \tag{4.67}$$

Using the expression of the fields in (4.66) in one m-th homogenous zone ($m = 1, 3$) and inserting it in the Helmholtz equation we get

$$\sum_n \left[\frac{d^2 u_n^{(\mathrm{m})}}{dz^2} + \left(\varepsilon_m k^2 - k_{x,n}^2\right) u_n^{(\mathrm{m})} \right] e^{in\frac{2\pi}{D}x}. \tag{4.68}$$

We deduce that

$$\frac{d^2 u_n^{(\mathrm{m})}}{dz^2} + \left(\varepsilon_m k^2 - k_{x,n}^2\right) u_n^{(\mathrm{m})} = 0. \tag{4.69}$$

The solutions of this well known differential equation are

$$v_n^{(\mathrm{m})}(z) = A_n\, e^{-ik_{z,n}^{(\mathrm{m})} z} + B_n\, e^{ik_{z,n}^{(\mathrm{m})} z} \tag{4.70}$$

where we introduced the definition

$$k_{z,n}^{(m)} = \sqrt{\varepsilon^{(i)}(\omega)\frac{\omega^2}{c^2} - k_{x,n}^2}, \tag{4.71}$$

$$\mathrm{Re}\left(k_{z,n}^{(m)}\right) \geq 0 \qquad \text{and} \qquad \mathrm{Im}\left(k_{z,n}^{(m)}\right) \geq 0. \tag{4.72}$$

Finally we obtain the well known Rayleigh expansion for the field in the homogenous zones

$$u^{(\mathrm{m})}(x,z) = \sum_{n\in\mathbb{Z}} \left[A_n\, e^{ik_{x,n}x + ik_{z,n}z} + B_n\, e^{ik_{x,n}x - ik_{z,n}z}\right]. \tag{4.73}$$

In particular we use the following notation for the Rayleigh expansion

$$u^{(1)}(x,z) = \sum_{n\in\mathbb{Z}} \left(I_n e^{ik_{z,n}^{(1)}z} + R_n e^{-ik_{z,n}^{(1)}z}\right) e^{ik_{x,n}x}, \tag{4.74}$$

$$u^{(3)}(x,z) = \sum_{n\in\mathbb{Z}} \left(T_n e^{ik_{z,n}^{(3)}(z-h)}\right) e^{ik_{x,n}x} \tag{4.75}$$

where we added a phase factor $e^{-ik_{z,n}h}$ in the zone 3, useful for the following calculations and that we can remove later on, and we indicated with I_n the known coefficients of the incident wave. R_n, T_n are, respectively, the unknown reflection and transmission coefficients.

We can turn now to analyze the field in the grating region. Let us start with the TE case. Exploiting the expansions in Fourier series made in (4.66) for the fields and for the electric permittivity

$$\varepsilon_p = \frac{1}{D}\int_0^D dx\, \varepsilon^{(2)}(x) e^{-i\frac{2\pi}{D}p\,x} \tag{4.76}$$

we can cast the wave equation (4.62) as follows

$$\frac{\partial^2}{\partial x^2}\left(\sum_n u_n(z)e^{ik_{x,n}x}\right) + \frac{\partial^2}{\partial z^2}\left(\sum_n u_n(z)e^{ik_{x,n}x}\right) + k^2\left(\sum_p \varepsilon_p e^{i\frac{2\pi}{D}p\,x}\right)\left(\sum_n u_n(z)e^{ik_{x,n}x}\right) = 0. \tag{4.77}$$

The above equation can be rewritten exploiting the rules of Fourier Factorization. If we consider a function $h(x) = g(x)f(x)$, where $g(x)$ and $f(x)$ are periodic piecewise-continuous-functions, and assuming that all three functions have the same period, to compute the Fourier coefficients of $h(x)$ in terms of the Fourier coefficients g_n and f_m, we use the following rules [55], [56]:

(1) $h_{n,\Omega} = \sum_{m\in\Omega} g_{n-m} f_m, \quad n \in \Omega$, with $g(x)$ discontinuous and $f(x)$ continuous

(2) $h_{n,\Omega} = \sum_{m\in\Omega} \left[\!\left[\frac{1}{g}\right]\!\right]^{-1}_{\mathrm{nm}} f_m, \quad n \in \Omega$, with $g(x)$ and $f(x)$ discontinuous and $h(x)$ continuous at some point x_0 (4.78)

where Ω indicates a set of integers in the range $m_1 < m < m_2$ for some fixed m_1 and m_2. We have also introduced the Toeplitz matrix $[\![a]\!]$, defined by the relation $[\![a]\!]_{ij} = a_{i-j}$, a_n being the n-th Fourier component of a.

$$[\![\varepsilon]\!] = \begin{pmatrix} \dots & \varepsilon_{-1} & \varepsilon_{-2} & \varepsilon_{-3} & \dots \\ \varepsilon_1 & \varepsilon_0 & \varepsilon_{-1} & \varepsilon_{-2} & \varepsilon_{-3} \\ \varepsilon_2 & \varepsilon_1 & \varepsilon_0 & \varepsilon_{-1} & \varepsilon_{-2} \\ \varepsilon_3 & \varepsilon_2 & \varepsilon_1 & \varepsilon_0 & \varepsilon_{-1} \\ \dots & \varepsilon_3 & \varepsilon_2 & \varepsilon_1 & \dots \end{pmatrix} \tag{4.79}$$

If we are not in one of the two cases mentioned in (4.78), there is not a general rule to compute the Fourier coefficients of $h(x)$. Usually the approach used is to rearrange $g(x)$, $f(x)$ as a sum of terms that fulfill one of the two cases listed above. Having in mind these rules we obtain from (4.77) that

$$\left(\sum_p \varepsilon_p e^{i\frac{2\pi}{D}p\,x}\right)\left(\sum_n u_n(z) e^{ik_{x,n}x}\right) = \sum_n \left(\sum_p \varepsilon_{n-p} u_p\, e^{ik_{x,n}x}\right) \tag{4.80}$$

and we can deduce the equation

$$\sum_n \left(\frac{d^2 u_n(z)}{dz^2} - k_{x,n}^2 u_n(z) + k^2 \sum_p \varepsilon_{n-p} u_p(z)\right) e^{ik_{x,n}x} = 0. \tag{4.81}$$

Using a matrix notation

$$\mathcal{U} = [\dots, u_{-2}, u_{-1}, u_0, u_1, u_2, \dots]^T \qquad \alpha = \mathrm{diag}\,(\dots, k_{x,-1}, k_{x,0}, k_{x,1}, \dots) \tag{4.82}$$

we get the following differential equation

$$\frac{d^2\mathcal{U}}{dz^2} = \left(\alpha^2 - k^2 [\![\varepsilon]\!]\right)\mathcal{U}(z) \equiv \mathbb{A}\mathcal{U}(z). \tag{4.83}$$

If we look for solutions of the form

$$\mathcal{U}(z) = e^{\mathbb{X}z}\mathcal{U}_0' \tag{4.84}$$

then

$$\mathbb{X}^2 e^{\mathbb{X}z}\mathcal{U}_0' = \mathbb{A} e^{\mathbb{X}z}\mathcal{U}_0' \Rightarrow \mathbb{X} = \pm\,\mathbb{A}^{1/2} = \pm\left(\mathbb{P}\mathbb{D}^2\mathbb{P}^{-1}\right)^{1/2} = \pm\,\mathbb{P}\mathbb{D}\mathbb{P}^{-1}, \tag{4.85}$$

giving

$$e^{\mathbb{X}z} = e^{\pm\mathbb{P}\mathbb{D}\mathbb{P}^{-1}z} = \mathbb{P}e^{\pm\mathbb{D}z}\mathbb{P}^{-1} \tag{4.86}$$

where $\mathbb{P}$ and $\mathbb{D}^2$ are respectively the eigenvectors and eigenvalues matrices of the matrix $\mathbb{X}$. For the fields we then get

$$\begin{cases} \mathcal{U}(z) = \mathbb{P}\left(e^{\mathbb{D}z}\mathcal{A} + e^{-\mathbb{D}z}\mathcal{B}\right) & \mathrm{Re}(\mathbb{D}) \leq 0 \\ \partial_z\mathcal{U}(z) = \mathbb{P}\mathbb{D}\left(e^{\mathbb{D}z}\mathcal{A} - e^{-\mathbb{D}z}\mathcal{B}\right) & \mathrm{Re}(\mathbb{D}) \leq 0 \end{cases} \tag{4.87}$$

using the following definitions $\mathbb{P}\mathbb{D} \equiv \mathbb{P}'$,

$$\mathcal{A} = [\ldots, a_{-1}, a_0, a_1, \ldots]^T \tag{4.88}$$

$$\mathcal{B} = [\ldots, b_{-1}, b_0, b_1, \ldots]^T. \tag{4.89}$$

We see from the equation (4.83) that the problem to find the solutions of the fields in the grating region has been reduced to an eigenvalue problem. Numerically the matrix $\mathbb{A}$ has to be truncated to $N \times N$. The number of eigensolutions is N, but there are $2N$ eigensolutions for the physical problem when we take the square root of the eigenvalues of $\mathbb{A}$. The truncation number N determines the accuracy of the numerical results. When we increase N, the results become more accurate but at the expense of more memory and computer time. As a consequence N should be chosen large enough to include all propagating orders and sufficiently many evanescent orders on both side of the propagating orders. The choice of how large N can be, depends on the specific problem and a general criterion cannot be given. However, in general, a metallic grating requires a larger N than a dielectric grating does. Then, we conclude that it is necessary to run a few convergence tests for the specific problem under study. In general a good and reasonable criterion for a convergence test is to consider the minimum N showing stable numerical results for the quantities of interest.

The last step is to impose the boundary conditions at the interfaces of the system, in this case at $z = 0$ and $z = h$. This is realized by matching the Fourier coefficients of the tangential components of the total fields. For the TE case it means to impose the continuity of E_y and H_x, that in our notations means $u(x, z)$ and $\partial_z u(x, z)$. At the $z = 0$ interface we have

$$\forall\ 0 \le x \le D, \qquad \begin{cases} E_y^{(1)}(x, 0) = E_y^{(2)}(x, 0) \\ H_x^{(1)}(x, 0) = H_x^{(2)}(x, 0) \end{cases} \tag{4.90}$$

$$\begin{cases} \sum_n \left(\delta_{0n} e^{ik_{z,n}^{(1)}0} + R_n e^{-ik_{z,n}^{(1)}0}\right) e^{ik_{x,n}x} = \sum_n \left[\sum_p \mathbb{P}_{np}\left(a_p\, e^{\mathbb{D}_p 0} + b_p\, e^{-\mathbb{D}_p 0}\right)\right] e^{ik_{x,n}x} \\ \sum_n ik_{z,n}^{(1)} \left(\delta_{0n} e^{ik_{z,n}^{(1)}0} - R_n e^{-ik_{z,n}^{(1)}0}\right) e^{ik_{x,n}x} = \sum_n \left[\sum_p \mathbb{P}'_{np}\left(a_p\, e^{\mathbb{D}_p 0} - b_p\, e^{-\mathbb{D}_p 0}\right)\right] e^{ik_{x,n}x} \end{cases} \tag{4.91}$$

and for the $z = h$ interface

$$\forall\ 0 \le x \le D, \qquad \begin{cases} E_y^{(2)}(x, h) = E_y^{(3)}(x, h) \\ H_x^{(2)}(x, h) = H_x^{(3)}(x, h) \end{cases} \tag{4.92}$$

$$\begin{cases} \sum_n \left[\sum_p \mathbb{P}_{np}\left(a_p\, e^{\mathbb{D}_p h} + b_p\, e^{-\mathbb{D}_p h}\right)\right] e^{ik_{x,n}x} = \sum_n \left(T_n e^{ik_{z,n}^{(3)}(h-h)} + 0\, e^{-ik_{z,n}^{(3)}(h-h)}\right) e^{ik_{x,n}x} \\ \sum_n \left[\sum_p \mathbb{P}'_{np}\left(a_p\, e^{\mathbb{D}_p h} - b_p\, e^{-\mathbb{D}_p h}\right)\right] e^{ik_{x,n}x} = \sum_n ik_{z,n}^{(3)} \left(T_n\, e^{ik_{z,n}^{(3)}(h-h)} - 0\, e^{-ik_{z,n}^{(3)}(h-h)}\right) e^{ik_{x,n}x}. \end{cases} \tag{4.93}$$

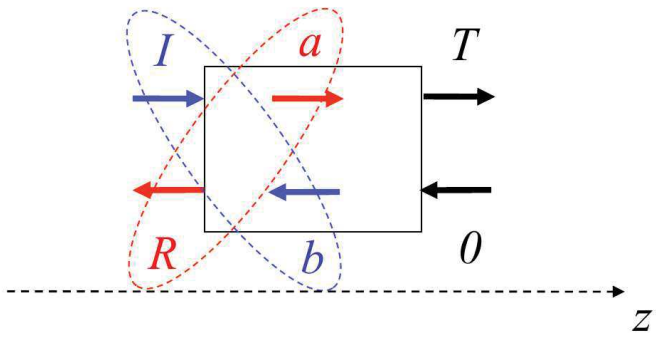

Figure 4.9 – Schematic figure that depicts the defined directions for $\mathcal{A}$, $\mathcal{B}$ at the interface $z = 0$.

It is convenient to write these boundary conditions in a more compact form through the matrix notation. In this way we can write

$$z = 0; \qquad \begin{cases} \mathcal{I} + \mathcal{R} = \mathbb{P}(\mathcal{A} + \mathcal{B}) \\ i\,\mathbb{K}_1\,(\mathcal{I} - \mathcal{R}) = \mathbb{P}'(\mathcal{A} - \mathcal{B}) \end{cases} \tag{4.94}$$

and

$$z = h; \qquad \begin{cases} \mathbb{P}(\phi\mathcal{A} + \phi^{-1}\mathcal{B}) = 0 + \mathcal{T} \\ \mathbb{P}'(\phi\mathcal{A} - \phi^{-1}\mathcal{B}) = i\,\mathbb{K}_3\,(-0 + \mathcal{T}) \end{cases} \tag{4.95}$$

where we have introduced the following vectors

$$\mathcal{I} = [\ldots, 0, 0, I_0, 0, 0, \ldots]^T, \quad \mathcal{R} = [\ldots, R_{-1}, R_0, R_1, \ldots]^T, \quad \mathcal{T} = [\ldots, T_{-1}, T_0, T_1, \ldots]^T, \tag{4.96}$$

and operators

$$\mathbb{K}_i = \mathrm{diag}\left(k_{z,n}^{(i)}\right), \quad \phi = e^{\mathbb{D}h}. \tag{4.97}$$

We exploit the well known S-matrix formalism to find the reflection and transmission matrices of the grating. We define the S-matrix which relates the electric field amplitudes of the incident wave to the amplitudes of the reflected and transmitted electric field

$$\begin{pmatrix} \mathcal{R} \\ \mathcal{T} \end{pmatrix} = \mathbb{S}\begin{pmatrix} \mathcal{I} \\ 0 \end{pmatrix} = \begin{pmatrix} \mathbb{R} & \mathbb{T}' \\ \mathbb{T} & \mathbb{R}' \end{pmatrix}\begin{pmatrix} \mathcal{I} \\ 0 \end{pmatrix}. \tag{4.98}$$

$\mathbb{S}$ is a block matrix composed by the reflection and transmission matrix $\mathbb{R}$ and $\mathbb{T}$. The matrices $\mathbb{R}'$ and $\mathbb{T}'$ are respectively the reflection and transmission matrices for the analogous problem of diffraction when the incident wave is coming from the region 3. If we analyze equation (4.94) and we consider the convention defined in Figure 4.9 for the signs used for $\mathcal{A}$ and $\mathcal{B}$, we can cast the boundary conditions at $z = 0$ as

$$\begin{pmatrix} \mathcal{R} \\ \mathcal{A} \end{pmatrix} = \begin{pmatrix} -\mathbb{1} & \mathbb{P} \\ i\,\mathbb{K}_1 & \mathbb{P}' \end{pmatrix}^{-1} \begin{pmatrix} \mathbb{1} & -\mathbb{P} \\ i\,\mathbb{K}_1 & \mathbb{P}' \end{pmatrix}\begin{pmatrix} \mathcal{I} \\ \mathcal{B} \end{pmatrix} \equiv \mathbb{S}_1 \begin{pmatrix} \mathcal{I} \\ \mathcal{B} \end{pmatrix}. \tag{4.99}$$

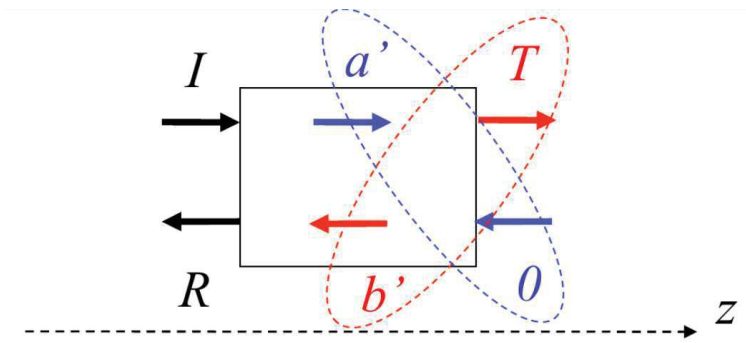

Figure 4.10 – Schematic figure that depicts the directions for $\mathcal{A}'$, $\mathcal{B}'$ at the interface $z = h$.

In the same way, defining $\phi\mathcal{A} = \mathcal{A}'$ and $\phi^{-1}\mathcal{B} = \mathcal{B}'$, considering the Figure 4.10 and the equation (4.95), we cast the boundary conditions at $z = h$ as

$$\begin{pmatrix}\mathcal{B}\\ \mathcal{T}\end{pmatrix} = \begin{pmatrix}\phi & \mathbb{0}\\ \mathbb{0} & \mathbb{1}\end{pmatrix}\begin{pmatrix}-\mathbb{P} & \mathbb{1}\\ \mathbb{P}' & i\,\mathbb{K}_1\end{pmatrix}^{-1}\begin{pmatrix}\mathbb{P} & -\mathbb{1}\\ \mathbb{P}' & i\,\mathbb{K}_3\end{pmatrix}\begin{pmatrix}\phi & \mathbb{0}\\ \mathbb{0} & \mathbb{1}\end{pmatrix}\begin{pmatrix}\mathcal{A}\\ 0\end{pmatrix} \equiv \mathbb{S}_2\begin{pmatrix}\mathcal{A}\\ 0\end{pmatrix}. \tag{4.100}$$

Defining the associative operation $\mathbb{A} = \mathbb{B} \circledast \mathbb{C}$ for square matrices as follows

$$\mathbb{A}_{11} = \mathbb{B}_{11} + \mathbb{B}_{12}(\mathbb{1} - \mathbb{C}_{11}\mathbb{B}_{22})^{-1}\mathbb{C}_{11}\mathbb{B}_{21}, \tag{4.101}$$
$$\mathbb{A}_{12} = \mathbb{B}_{12}(\mathbb{1} - \mathbb{C}_{11}\mathbb{B}_{22})^{-1}\mathbb{C}_{12}, \tag{4.102}$$
$$\mathbb{A}_{21} = \mathbb{C}_{21}(\mathbb{1} - \mathbb{B}_{22}\mathbb{C}_{11})^{-1}\mathbb{B}_{21}, \tag{4.103}$$
$$\mathbb{A}_{22} = \mathbb{C}_{22} + \mathbb{C}_{21}(\mathbb{1} - \mathbb{B}_{22}\mathbb{C}_{11})^{-1}\mathbb{B}_{22}\mathbb{C}_{12}, \tag{4.104}$$

we get the final expression of the S-matrix as $\mathbb{S} \equiv \mathbb{S}_1 \circledast \mathbb{S}_2$.

We have found the S-matrix, therefore the reflection and transmission matrices, in the transverse electric case. We turn now to the transverse magnetic case and discuss it briefly. The procedure to find the solutions of the fields in the grating region and the S-matrix are quite similar to the TE case. It is not difficult to see that, starting from (4.63) and using the compact matrix notation, we obtain the following differential equation

$$\frac{d^2\mathcal{U}}{dz^2} = \left[\!\left[\frac{1}{\varepsilon}\right]\!\right]^{-1}\left(\alpha\left[\!\left[\frac{1}{\varepsilon}\right]\!\right]\alpha - k^2\mathbb{1}\right)\mathcal{U}(z) \equiv \mathbb{A}\mathcal{U}(z) \tag{4.105}$$

where we used the second of the rules defined in (4.78) for the Fourier factorization. From this differential equation we find the solutions

$$\begin{cases}\mathcal{U}(z) = \mathbb{P}\left(e^{\mathbb{D}z}\mathcal{A} + e^{-\mathbb{D}z}\mathcal{B}\right) & \mathrm{Re}(\mathbb{D}) \le 0\\ \partial_z\mathcal{U}(z) = \left[\!\left[\frac{1}{\varepsilon}\right]\!\right]\mathbb{P}\mathbb{D}\left(e^{\mathbb{D}z}\mathcal{A} - e^{-\mathbb{D}z}\mathcal{B}\right) & \mathrm{Re}(\mathbb{D}) \le 0.\end{cases} \tag{4.106}$$

To find the scattering operators, i.e. the S-matrix, for the TM case we apply again the boundary conditions at the interfaces $z = 0$ and $z = h$. In this particular situation, we

impose the continuity of the fields $H_y = u(x, z)$ and $E_x = \frac{1}{\varepsilon}\partial_z u(x, z)$. Proceeding analogously to the TE case, we obtain the same formally identical matrix $\mathbb{S}$ where we have to do the substitutions

$$\mathbb{K}_i \to \frac{\mathbb{K}_i}{\varepsilon_i}, \quad \mathbb{P}' \to \left[\!\left[\frac{1}{\varepsilon}\right]\!\right]\mathbb{P}'. \tag{4.107}$$

4.2.2 Some other methods for the diffraction by gratings

To conclude this section we briefly present some other methods to study the diffraction by gratings. At first we discuss concisely the possible application of the FMM to the case of gratings different from the rectangular one and one possible improvement of the FMM, especially for the case of metallic gratings. We start discussing the common extension of the FMM for gratings with smooth profile, i.e. the so-called *staircase approximation*. The main idea of this approach is to divide the grating region in many subregions as, for example, in the situation represented in the Figure 4.11. In each subregion we have a rectangular grating and then we can apply the FMM. With this idea we replaced the resolution of the original grating problem with this new "approximated" problem of the modified grating. This staircase approximation seems reasonable because, as the number of layers increase and tends to infinity, the layer thickness goes to zero, and we recover the initial original grating. Unfortunately we must also consider the physical problems introduced with this approximation. Several numerical evaluations show that, for 1D periodic gratings, the approximation is quite good for TE polarization but not for TM polarization, especially if we consider highly conducting metallic gratings [57]. We can explain this because when we analyze, at the sharp edge of a wedge made of nonmagnetic media with different dielectric constants, the transverse component of the electric field to the edge direction we see that it is, if nonzero, infinite, as it is known from classical electromagnetism. When we then do the staircase approximation we introduce many artificial edges. For the TE case we do not have particular numerical problems because the electric field remains finite everywhere. Instead in TM polarization the electric field, that in the real situation without the staircase approximation is finite near the smooth grating profile, becomes infinitely large at the edges and numerical convergence and the computation accuracy problems arise.

One of the major known issue of the FMM is the poor convergence in the TM case. This problem is partially solved when the right factorization rules (4.78) are applied. Even if these improvements are adopted, the problems of convergence can remain. We have already said that, when highly conducting metallic gratings are studied, numerical problems arise. Other numerical issues arise because of the use of Fourier expansions. In fact, it can be shown that the convergence is strictly related to the gradient of permittivity in the grating region. In this way also the so-called Gibbs phenomenon at the discontinuity points plays a role. An effective solution can be the *adaptive spatial resolution* (ASR) proposed by Granet [58]. The key idea is to use a new coordinate system that increases the spatial resolution where the discontinuities of the grating are present by stretching the coordinate around them. However, the cost of this change of coordinates is solving eigenvalue problems also in the homogeneous regions (the boundary conditions are written in the new space) and

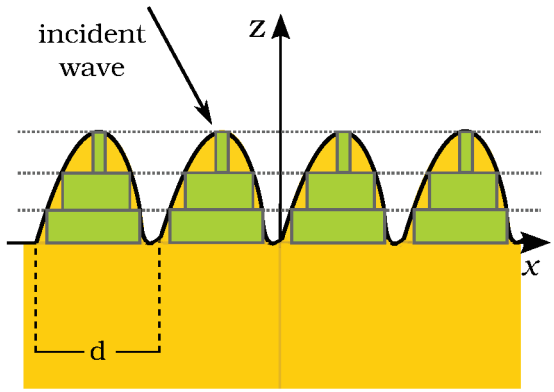

Figure 4.11 – In this figure we show the main idea at the base of the staircase approximation.

thus increasing the computation time.

We briefly discuss now the ASR and let us suppose the transformation $\{x = F(u), y, z\}$ where:

$$F(u) = a_1 + a_2 u + \frac{a_3}{2\pi} \sin\left(2\pi \frac{u - u_{l-1}}{u_l - u_{l-1}}\right) \quad (u_{l-1} \leq u \leq u_l), \tag{4.108}$$

and

$$a_1 = \frac{u_l x_{l-1} - u_{l-1} x_l}{u_l - u_{l-1}}, \quad a_2 = \frac{x_l - x_{l-1}}{u_l - u_{l-1}}, \quad a_3 = G(u_l - u_{l-1}) - (x_l - x_{l-1}). \tag{4.109}$$

The quantity x_l and x_{l-1} are the transition points of the dielectric constant of the grating while G is numerical control parameter. To develop the ASR method we can start from the wave equations (4.62) and (4.63) and considering the coordinates transformation. As a consequence we can write the wave equations in the new coordinate system replacing the partial derivative ∂_x with $(\partial_x u)\partial_u = (1/f)\partial_u$ where $f = \partial_u x$:

$$\frac{1}{f}\frac{\partial}{\partial u}\left(\frac{1}{f}\frac{\partial E_y^{(2)}}{\partial u}\right) + \frac{\partial^2 E_y^{(2)}}{\partial z^2} + k^2 \varepsilon^{(2)}(u)\, E_y^{(2)}(u, z) = 0 \qquad \text{TE}, \tag{4.110}$$

$$\frac{1}{f}\frac{\partial}{\partial u}\left(\frac{1}{\varepsilon^{(2)}(u)}\frac{1}{f}\frac{\partial H_y^{(2)}}{\partial u}\right) + \frac{1}{\varepsilon^{(2)}(u)}\frac{\partial^2 H_y^{(2)}}{\partial z^2} + k^2 \varepsilon^{(2)}(u)\, H_y^{(2)}(u, z) = 0 \qquad \text{TM}. \tag{4.111}$$

In the Fourier space and using the matrix notation already introduced, the equations (4.110) and (4.111) can be cast into the form

$$\frac{d^2 \mathcal{U}}{dz^2} = \left([\![f]\!]^{-1} \alpha [\![f]\!]^{-1} \alpha - k^2 [\![\varepsilon]\!]\right) \mathcal{U}(z) \equiv \mathbb{A}_{\text{TE}} \mathcal{U}(z) \qquad (\text{TE}), \tag{4.112}$$

$$\frac{d^2 \mathcal{U}}{dz^2} = \left[\!\!\left[\frac{1}{\varepsilon}\right]\!\!\right]^{-1} \left([\![f]\!]^{-1} \alpha [\![\varepsilon]\!]^{-1} [\![f]\!]^{-1} \alpha - k^2 \mathbb{1}\right) \mathcal{U}(z) \equiv \mathbb{A}_{\text{TM}} \mathcal{U}(z) \qquad (\text{TM}). \tag{4.113}$$

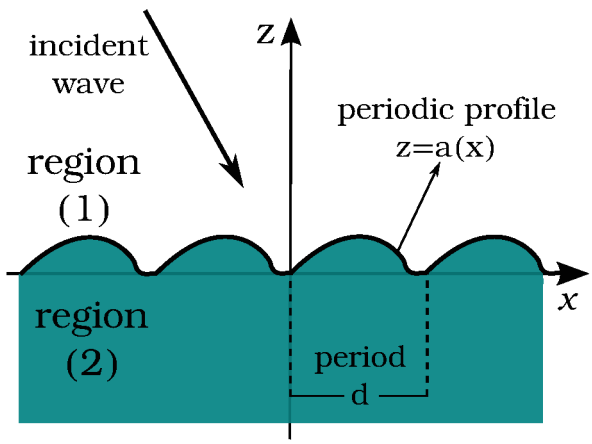

Figure 4.12 – The general situation considered for the C-method.

The solutions of the fields are then like that of the standard FMM in the equation (4.87), where $\mathbb{P}$ and $\mathbb{D}^2$ are respectively the eigenvectors and eigenvalues matrices of the matrix $\mathbb{A}^{1/2}_{(\mathrm{TE})}/\mathbb{A}^{1/2}_{(\mathrm{TM})}$.

We already said before that we solve the problem in the space u also in the region 1 and 3. In the homogeneous regions, solving the eigenproblem, we get

$$\frac{d^2\mathcal{V}}{dz^2} = \left([\![f]\!]^{-1}\alpha[\![f]\!]^{-1}\alpha - k^2\varepsilon_{(\mathrm{i})}\mathbb{1}\right)\mathcal{V}(z) \equiv \mathbb{A}_{(\mathrm{i})}\mathcal{V}(z), \tag{4.114}$$

where $\mathcal{V}(z)$ refers either to the component E_y of the electric field or to the component H_y of the magnetic field and again the solutions are related to the eigenvalues and the eigenvectors of the matrix $\mathbb{A}_{(\mathrm{i})}$. At this stage, as we did for the standard FMM, we can impose the boundary conditions at the interfaces, use the S-matrix approach to find the reflection and transmission matrices in the u space. Finally we can apply an inverse transformation to the matrix $\mathbb{S}$ going back in the x space. Nonetheless, we must say that sometimes this passage to the x space can introduce some problem of convergence because of the ill-conditioned nature of the problem [59].

We now conclude this section on the methods to study the diffraction by gratings discussing the C-method. It was introduced in the 1980 to solve the problem of the diffraction by corrugated gratings. The main problem related to the study of diffraction in these gratings concerns with the boundary conditions. In fact, because of the continuous profile of these gratings, it results nontrivial to impose the boundary conditions between the different interfaces. The simple idea of this method was the introduction of a new coordinate system described by ($u = x$, $v = y$, $w = z - a(x)$), where $a(x)$ is a continuous and differentiable function describing the profile of the surface of the grating. The advantages of this transformation are three. The first is that the corrugated surface is mapped into a planar surface so the boundary conditions are simple to match. The second is that the Maxwell equations in Fourier space are transformed into a matrix eigenvalue problem which numerical solution can be obtained straightforwardly (as for the FMM method). The third is the

possibility to write Maxwell equations in a covariant form. Another powerful characteristic of the C-method is the possibility to apply it to a wide variety of physical systems (many different surface profiles, multi-layer coated gratings). The importance of the C-method is relevant in literature and for example it inspired the ASR, that we previously discussed, and matched coordinates [60].

Let us consider the general configuration in Figure 4.12. The grating has a surface profile described by the function $a(x)$ and it is infinite along the x and y direction. When the electromagnetic field is present, the boundary conditions impose that the tangential components of the electric field vector and the normal component of the displacement field vector are continuous at the surface. This means that the boundary conditions depend on the position on the surface. The coordinate transformation (u, v, z) before mentioned is such that

$$u = x, \quad v = y, \quad w = z - a(x). \tag{4.115}$$

It maps the surface that separates the two region 1 and 2 to the surface $w = 0$ making the boundary conditions in this new coordinate system as that on a planar surface. At this stage we can write the covariant Maxwell equations

$$\xi^{ijk}\partial_j E_k = i\omega\mu_0 \sqrt{g} g^{ij} H_i \tag{4.116}$$

$$\xi^{ijk}\partial_j H_k = -i\omega\varepsilon_0\varepsilon \sqrt{g} g^{ij} E_i \tag{4.117}$$

where g^{ij} is the metric tensor, $g = \det g^{ij}$ and ξ^{ijk} is the Levi-Civita tensor. In the case of the transformation considered we can write the line element

$$\begin{aligned} ds^2 &= dx^2 + dy^2 + dz^2 = du^2 + dv^2 + (dw + \dot{a}du)^2 \\ &= (1 + \dot{a}^2)du^2 + dv^2 + dw^2 + 2\dot{a}du\, dw = g_{ij}dx^i\, dx^j. \end{aligned} \tag{4.118}$$

We deduce

$$g_{ij} = \begin{pmatrix} 1 + \dot{a}^2 & 0 & \dot{a} \\ 0 & 1 & 0 \\ \dot{a} & 0 & 1 \end{pmatrix}, \qquad g^{ij} = \begin{pmatrix} 1 & 0 & -\dot{a} \\ 0 & 1 & 0 \\ -\dot{a} & 0 & 1 + \dot{a}^2 \end{pmatrix}, \qquad g = 1. \tag{4.119}$$

Using these quantities in the Maxwell equations (4.116) and (4.117) we get

$$\begin{cases} \partial_y E_w - \partial_w E_y = i\omega\mu_0 \left(H_x - \dot{a}H_w\right) \\ \partial_x E_y - \partial_y E_x = i\omega\mu_0 \left[(1 + \dot{a}^2)H_w - \dot{a}H_x\right] \\ \partial_w E_x - \partial_x E_w = i\omega\mu_0 H_y \end{cases}, \tag{4.120}$$

$$\begin{cases} \partial_y H_w - \partial_w H_y = -i\omega\varepsilon\varepsilon_0 \left(E_x - \dot{a}E_w\right) \\ \partial_x H_y - \partial_y H_x = -i\omega\varepsilon\varepsilon_0 \left[(1 + \dot{a}^2)E_w - \dot{a}E_x\right] \\ \partial_w H_x - \partial_x H_w = -i\omega\varepsilon\varepsilon_0 E_y \end{cases}. \tag{4.121}$$

From them, using the expansion in Fourier series and the matrix notation, in a similar way as in the FMM, it is possible to see that again the problem to find the field can be reduced to an eigenvalue problem.

4.3 OTE Casimir-Lifshitz force between two dielectric gratings

In this section we study the problem of the OTE Casimir-Lifshitz force between two gratings. This problem has been studied in our original work [39] and represents the most important result of this Chapter. We address the Casimir-Lifshitz force between two dielectric gratings immersed in vacuum ($\varepsilon = 1$) in the geometrical configuration shown in Figure 4.13. We label the two gratings with an index i taking values 1 and 2. The gratings are infinite in x and y directions, with periodicity along the x axis. Their distance d is defined in Figure 4.13 and can only take positive values (i.e. a plane $z = \bar{z}$ must exist separating the two bodies). The gratings share the same period D and have corrugation depth h_i, permittivities $\varepsilon_i(\omega)$ in the homogeneous zone, permittivities $\varepsilon_i(x, \omega)$ along the grating zone having thickness δ_i, and filling factors $f_i = l_i/D$ (l_i is defined as in Figure 4.13).

The physical system, similarly to the system of two slabs studied previously, is out of thermal equilibrium. It means that the gratings have a constant temperature T_i that could be different from each other. The two gratings are supposed to be immersed in a radiation bath having temperature T_e, in general different from the temperatures of the two gratings. The three temperatures involved can be considered constant in time.

As we discussed in Section 4.1, the latter assumption has been used in literature to characterize the properties of the source fields (the fields emitted by the two bodies and coming from the surrounding walls) in terms of field correlation functions. Now we use the same procedure of Section 4.1 to calculate the OTE force of our system. Our starting point is the decomposition of the force as a sum of an equilibrium term and a nonequilibrium term obtained in (4.35) (where the distance dependence is implicit)

$$F_{1z} = F_{1z}^{(\mathrm{eq})}(T_1) + \Delta(T_1, T_2, T_\mathrm{e}), \tag{4.122}$$

where $F_{1z}^{(\mathrm{eq})}(T_1)$ is the force acting on grating 1 at thermal equilibrium at its temperature T_1 given in (4.36) and the non-equilibrium term is given in (4.37).

In order to calculate the force, we now need to compute the reflection and transmission operators associated to a lamellar 1D grating. This will be achieved in the framework of the Fourier Modal Method [61]. In the following, we implement this method, differently than Subsection 4.2.1, in a conical mounting (it means that the incident wave vector stays in a plane different from the xz plane). Moreover we apply it to a grating of finite size along the z axis (see Figure 4.14) in order to take into account finite-size effects on the Casimir-Lifshitz force. We also solve the scattering problem directly in TE and TM components, in order to be coherent with the formalism presented in Section 4.1.

Let us consider a system composed of a grating like that in Figure 4.14. The space is divided in four zones: zone 1 ($z < 0$), zone 2 ($0 < z < h$), zone 3 ($h < z < h + \delta$) and zone 4 ($z > h + \delta$). While zones 1, 3 and 4 are homogeneous with dielectric permittivities $\varepsilon_i(\omega)$ ($i = 1, 3, 4$), zone 2 represents the grating, with a dielectric function $\varepsilon_2(x, \omega)$, periodic in x with period D. In each zone, every physical quantity is independent of y.

We first decompose the electric field in any zone with respect to frequency (only positive

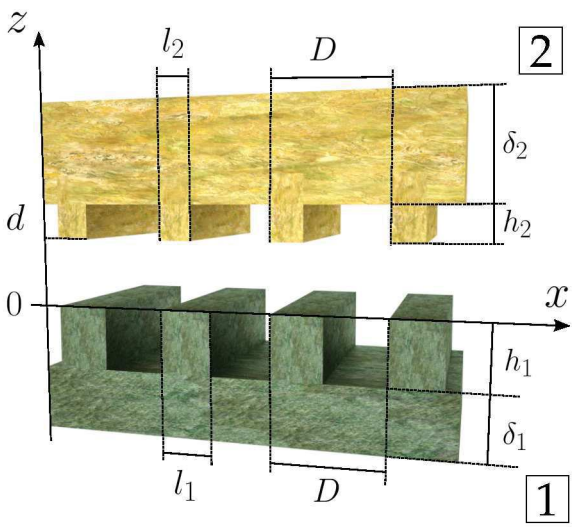

Figure 4.13 – Geometry of the system. Two gratings, labeled with 1 and 2, at a distance d, always assumed to be positive. The gratings, made in general of different materials, are infinite in the xy plane, and periodic in the x direction with the same period D. They have corrugation depths h_i ($i = 1, 2$), thicknesses δ_i and lengths of the upper part of the grating l_i. This defines the filling factors $f_i = l_i/D$.

frequencies will be used):

$$\mathbf{E}^{(i)}(\mathbf{R}, t) = 2\,\mathrm{Re}\left[\int_0^{+\infty} \frac{d\omega}{2\pi} e^{-i\omega t} \mathbf{E}^{(i)}(\mathbf{R}, \omega)\right]. \tag{4.123}$$

In virtue of the translational invariance of our system along the y axis and of the periodicity along the x axis, we will employ a Fourier decomposition of any x-dependent quantity. As a consequence, the wave vector component k_x will be replaced by a new mode variable

$$k_{x,n} = k_x + \frac{2\pi}{D} n, \tag{4.124}$$

with k_x taking values in the first Brillouin zone $[-\pi/D, \pi/D]$ and n assuming all integer values.

Let us consider the homogeneous zones. In these zones, we can use the standard Rayleigh expansion (see Subsection 4.2.1) for the component of the field at frequency ω

$$\mathbf{E}^{(i)}(\mathbf{R}, \omega) = \sum_{p,\phi} \int_{-\frac{\pi}{D}}^{\frac{\pi}{D}} \frac{dk_x}{2\pi} \sum_{n\in\mathbb{Z}} \int_{-\infty}^{+\infty} \frac{dk_y}{2\pi} e^{i\mathbf{K}_n^{(i)\phi}\cdot\mathbf{R}}\, \hat{\boldsymbol{\epsilon}}_p^{(i)\phi}(\mathbf{k}_n, \omega) E_p^{(i)\phi}(\mathbf{k}_n, \omega), \tag{4.125}$$

where the wave vectors are defined as ($n \in \mathbb{Z}$)

$$\mathbf{K}_n^{(i)\phi} = (\mathbf{k}_n, \phi k_{z,n}^{(i)}), \quad \mathbf{k}_n = (k_{x,n}, k_y), \tag{4.126}$$

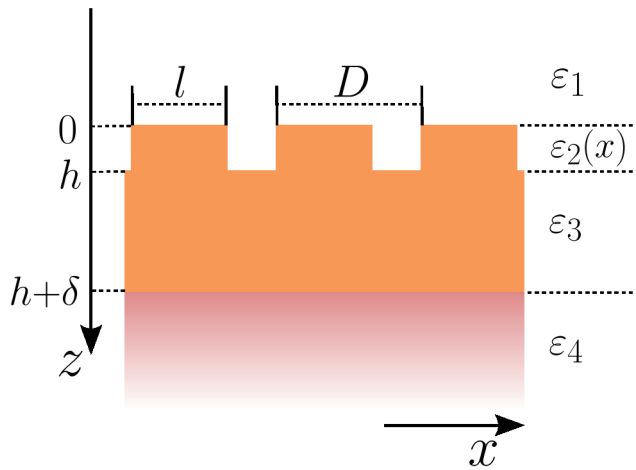

Figure 4.14 – Geometry of the FMM calculation. We consider one grating with interface $z = 0$, corrugation depth h, and underlying thickness δ. This defines four zones (see text) with four (in general different) dielectric permittivities. The period is D and the filling factor is defined as $f = l/D$.

and $k_{z,n}^{(i)}$ is the z component of the wave vector inside each medium

$$k_{z,n}^{(i)} = \sqrt{\varepsilon_i(\omega)\frac{\omega^2}{c^2} - \mathbf{k}_n^2}. \tag{4.127}$$

The unit polarization vectors appearing in (4.125) are defined as

$$\hat{\boldsymbol{\epsilon}}_{\mathrm{TE}}^{(i)\phi}(\mathbf{k}_n, \omega) = \frac{1}{k_n}(-k_y\hat{\mathbf{x}} + k_{x,n}\hat{\mathbf{y}}), \tag{4.128}$$

$$\hat{\boldsymbol{\epsilon}}_{\mathrm{TM}}^{(i)\phi}(\mathbf{k}_n, \omega) = \frac{c}{\omega\sqrt{\epsilon_i(\omega)}}(-k_n\hat{\mathbf{z}} + \phi k_{z,n}^{(i)}\hat{\mathbf{k}}_n). \tag{4.129}$$

For convenience, we assign from now on the following labels to the field amplitudes in the three homogeneous zones (the dependence on p, $\mathbf{k}_n$ and ω is implicit):

$$\begin{aligned} E^{(1)+} &= I, \quad & E^{(1)-} &= R, \\ E^{(3)+} &= C, \quad & E^{(3)-} &= C', \\ E^{(4)+} &= T, \quad & E^{(4)-} &= I', \end{aligned} \tag{4.130}$$

where I, R and T represent the incoming, reflected and transmitted field amplitudes respectively. The amplitude I' is associated to a possible incoming field coming from the other side of the body. Its presence guarantees both the full symmetry of the calculation and the possibility to derive at the same time the reflection and transmission operators $\mathcal{R}^{\pm}$ and $\mathcal{T}^{\pm}$.

The magnetic field in any zone can be easily deduced from Maxwell's equations and it reads

$$\mathbf{B}^{(i)}(\mathbf{R}, \omega) = \frac{\sqrt{\varepsilon_i(\omega)}}{c}\sum_{p,\phi}\int_{-\frac{\pi}{D}}^{\frac{\pi}{D}}\frac{dk_x}{2\pi}\sum_{n\in\mathbb{Z}}\int_{-\infty}^{+\infty}\frac{dk_y}{2\pi}e^{i\mathbf{K}_n^{(i)\phi}\cdot\mathbf{R}}(-1)^p\hat{\boldsymbol{\epsilon}}_{S(p)}^{(i)\phi}(\mathbf{k}_n, \omega)E_p^{(i)\phi}(\mathbf{k}_n, \omega), \tag{4.131}$$

where the function S is defined as $S(1) = 2$ and $S(2) = 1$.

We now move to the periodic region (zone 2) where we write an arbitrary frequency component of the field as

$$\mathbf{E}^{(2)}(\mathbf{R}, \omega) = \int_{-\frac{\pi}{D}}^{\frac{\pi}{D}} \frac{dk_x}{2\pi} \sum_{n\in\mathbb{Z}} \int_{-\infty}^{+\infty} \frac{dk_y}{2\pi} e^{i\mathbf{k}_n\cdot\mathbf{r}} \mathbf{E}^{(2)}(z, \mathbf{k}_n, \omega), \tag{4.132}$$

where $\mathbf{R} = (\mathbf{r}, z)$.

We now write Maxwell's equations

$$\begin{cases} \partial_y E_z - \partial_z E_y = i\omega\mu_0 H_x = ik_0 \widetilde{H}_x \\ \partial_z E_x - \partial_x E_z = i\omega\mu_0 H_y = ik_0 \widetilde{H}_y \\ \partial_x E_y - \partial_y E_x = i\omega\mu_0 H_z = ik_0 \widetilde{H}_z \end{cases}$$

$$\begin{cases} \partial_y H_z - \partial_z H_y = -i\omega\varepsilon\varepsilon_0 E_x \\ \partial_z H_x - \partial_x H_z = -i\omega\varepsilon\varepsilon_0 E_y \\ \partial_x H_y - \partial_y H_x = -i\omega\varepsilon\varepsilon_0 E_z \end{cases} \tag{4.133}$$

where we used $\omega = ck_0$, $\omega\mu_0 = k_0 Z_0$, $\omega\varepsilon_0 = k_0/Z_0$, $Z_0 = \sqrt{\mu_0/\varepsilon_0}$ and defined $\widetilde{H}_i = Z_0 H_i$. From (4.133) we can easily obtain

$$\partial_z \begin{pmatrix} E_x \\ E_y \end{pmatrix} = \begin{pmatrix} -\frac{i}{k_0}\partial_x \frac{1}{\varepsilon(x)}\partial_y & ik_0 + \frac{i}{k_0}\partial_x \frac{1}{\varepsilon(x)}\partial_x \\ -ik_0 - \frac{i}{k_0}\partial_y \frac{1}{\varepsilon(x)}\partial_y & \frac{i}{k_0}\partial_y \frac{1}{\varepsilon(x)}\partial_x \end{pmatrix} \begin{pmatrix} \widetilde{H}_x \\ \widetilde{H}_y \end{pmatrix} \tag{4.134}$$

and

$$\partial_z \begin{pmatrix} \widetilde{H}_x \\ \widetilde{H}_y \end{pmatrix} = \begin{pmatrix} \frac{i}{k_0}\partial_x\partial_y & -ik_0\varepsilon(x) - \frac{i}{k_0}\partial_x\partial_x \\ ik_0\varepsilon(x) + \frac{i}{k_0}\partial_y\partial_y & -\frac{i}{k_0}\partial_y\partial_x \end{pmatrix} \begin{pmatrix} E_x \\ E_y \end{pmatrix}. \tag{4.135}$$

We now employ a Fourier factorization for the fields E and $\widetilde{H}$. Correspondingly, the operator ∂_y is replaced by $i\beta$, β being a scalar, whereas the operator ∂_x is replaced by $i\alpha$, where $\alpha = \mathrm{diag}(k_{x,n})_n$. These replacements allow us to rewrite Maxwell's equations of our system in a more compact form:

$$\partial_z \boldsymbol{\mathcal{E}} = \begin{pmatrix} \frac{i\beta}{k_0}\alpha [\![\varepsilon]\!]^{-1} & ik_0\mathbb{1} - \frac{i\alpha}{k_0}[\![\varepsilon]\!]^{-1}\alpha \\ -ik_0\mathbb{1} + \frac{i\beta^2}{k_0}[\![\varepsilon]\!]^{-1} & -\frac{i\beta}{k_0}[\![\varepsilon]\!]^{-1}\alpha \end{pmatrix} \widetilde{\boldsymbol{\mathcal{H}}} = \mathbb{F}\widetilde{\boldsymbol{\mathcal{H}}}, \tag{4.136}$$

$$\partial_z \widetilde{\boldsymbol{\mathcal{H}}} = \begin{pmatrix} -\frac{i\beta}{k_0}\alpha & -ik_0[\![\varepsilon]\!] + \frac{i\alpha^2}{k_0} \\ ik_0\left[\!\!\left[\frac{1}{\varepsilon}\right]\!\!\right]^{-1} - \frac{i\beta^2}{k_0} & \frac{i\beta}{k_0}\alpha \end{pmatrix} \boldsymbol{\mathcal{E}} = \mathbb{G}\boldsymbol{\mathcal{E}}, \tag{4.137}$$

where for an arbitrary field $\mathbf{U}$ we have introduced the decomposition

$$\boldsymbol{\mathcal{U}} = (\{U_x(z, \mathbf{k}_n, \omega)\}_n, \{U_y(z, \mathbf{k}_n, \omega)\}_n)^T, \tag{4.138}$$

gathering x and y components and denoting with $\{\ldots\}_n$ a set of scattering orders. We have also introduced the Toeplitz matrix $[\![a]\!]$, defined by the relation $[\![a]\!]_{ij} = a_{i-j}$, a_n being the n-th Fourier component of a. We remark that going from (4.134)-(4.135) to (4.136)-(4.137) we have used the modified factorization rule introduced in Subsection 4.2.1.

Of course, in order to exploit numerically the FMM, a truncation has to be made, limiting the number of diffraction orders taken into account. For a given truncation M, this corresponds to keeping $2M + 1$ scattering orders

$$\{A_n\}_n = (A_{-M}, \ldots, A_M), \tag{4.139}$$

and the size of the corresponding column vector $\boldsymbol{\mathcal{U}}$ is thus $2(2M + 1)$. Based on this truncation, we obtain

$$\partial_z^2 \boldsymbol{\mathcal{E}} = \mathbb{F}\mathbb{G}\boldsymbol{\mathcal{E}} = \mathbb{P}\mathbb{D}^2\mathbb{P}^{-1}\boldsymbol{\mathcal{E}}, \tag{4.140}$$

where $\mathbb{P}$ and $\mathbb{D}^2$ are respectively the eigenvectors and eigenvalues $2(2M + 1) \times 2(2M + 1)$ matrices of the matrix $\mathbb{F}\mathbb{G}$

$$\mathbb{P} = \begin{pmatrix} \mathbb{P}^{(11)} & \mathbb{P}^{(12)} \\ \mathbb{P}^{(21)} & \mathbb{P}^{(22)} \end{pmatrix}, \qquad \mathbb{D} = \begin{pmatrix} \mathbb{D}^{(11)} & \mathbb{0} \\ \mathbb{0} & \mathbb{D}^{(22)} \end{pmatrix}. \tag{4.141}$$

Then, from (4.136) and (4.140), we obtain that fields are

$$\begin{cases} \boldsymbol{\mathcal{E}}(z) = \mathbb{P}\left(e^{\mathbb{D}z}\boldsymbol{\mathcal{A}} + e^{-\mathbb{D}z}\boldsymbol{\mathcal{B}}\right) \\ \widetilde{\boldsymbol{\mathcal{H}}}(z) = \mathbb{P}'\left(e^{\mathbb{D}z}\boldsymbol{\mathcal{A}} - e^{-\mathbb{D}z}\boldsymbol{\mathcal{B}}\right) \end{cases} \tag{4.142}$$

$\boldsymbol{\mathcal{A}}$ and $\boldsymbol{\mathcal{B}}$ being arbitrary constant vectors, and where $\mathbb{P}' = \mathbb{F}^{-1}\mathbb{P}\mathbb{D}$.

Based on the knowledge of the electric and magnetic fields in the four regions, we can now impose the continuity of the x and y components of both fields at the three interfaces $z = 0$, $z = h$ and $z = h + \delta$. In the following boundary conditions the values of k_x, k_y and ω are given. Exploiting this fact we use the generic simplified expression $A_{p,n}$ to refer to the amplitude $A_p(\mathbf{k}_n, \omega)$. Before proceeding in the calculation, we introduce an additional phase factor in the expression of the fields in zones 3 and 4. In particular, in zone 3 we replace $\exp[ik_z^{(i)\phi}z]$ with $\exp[ik_z^{(i)\phi}(z - h)]$, while in zone 4 we replace $\exp[ik_z^{(i)\phi}z]$ with $\exp[ik_z^{(i)\phi}(z - h - \delta)]$. These factors make the calculation easier and can be simply recovered at the end. At the first interface $z = 0$ we have for the x and y components of the electric field (repeated indices are implicitly summed over)

$$\begin{pmatrix} -\frac{k_y}{k_n}(I_{1,n} + R_{1,n}) + \frac{c}{\sqrt{\varepsilon_1}\omega}k_{z,n}^{(1)}\frac{k_{x,n}}{k_n}(I_{2,n} - R_{2,n}) \\ \frac{k_{x,n}}{k_n}(I_{1,n} + R_{1,n}) + \frac{c}{\sqrt{\varepsilon_1}\omega}k_{z,n}^{(1)}\frac{k_y}{k_n}(I_{2,n} - R_{2,n}) \end{pmatrix} = \begin{pmatrix} \mathbb{P}_{nm}^{(11)}(A_{x,m} + B_{x,m}) + \mathbb{P}_{nm}^{(12)}(A_{y,m} + B_{y,m}) \\ \mathbb{P}_{nm}^{(21)}(A_{x,m} + B_{x,m}) + \mathbb{P}_{nm}^{(22)}(A_{y,m} + B_{y,m}) \end{pmatrix}, \tag{4.143}$$

while for the magnetic field we get

$$\begin{pmatrix} -\frac{c}{\omega}k_{z,n}^{(1)}\frac{k_{x,n}}{k_n}(I_{1,n}-R_{1,n}) - \sqrt{\varepsilon_1}\frac{k_y}{k_n}(I_{2,n}+R_{2,n}) \\ -\frac{c}{\omega}k_{z,n}^{(1)}\frac{k_y}{k_n}(I_{1,n}-R_{1,n}) + \sqrt{\varepsilon_1}\frac{k_{x,n}}{k_n}(I_{2,n}+R_{2,n}) \end{pmatrix} = \begin{pmatrix} \mathbb{P}'^{(11)}_{nm}(A_{x,m}-B_{x,m}) + \mathbb{P}'^{(12)}_{nm}(A_{y,m}-B_{y,m}) \\ \mathbb{P}'^{(21)}_{nm}(A_{x,m}-B_{x,m}) + \mathbb{P}'^{(22)}_{nm}(A_{y,m}-B_{y,m}) \end{pmatrix}. \tag{4.144}$$

The boundary conditions at $z = h$ give us the following equations for the electric field

$$\begin{aligned} &\begin{pmatrix} -\frac{k_y}{k_n}(C_{1,n}+C'_{1,n}) + \frac{c}{\sqrt{\varepsilon_3}\omega}k_{z,n}^{(3)}\frac{k_{x,n}}{k_n}(C_{2,n}-C'_{2,n}) \\ \frac{k_{x,n}}{k_n}(C_{1,n}+C'_{1,n}) + \frac{c}{\sqrt{\varepsilon_3}\omega}k_{z,n}^{(3)}\frac{k_y}{k_n}(C_{2,n}-C'_{2,n}) \end{pmatrix} \\ &= \begin{pmatrix} \mathbb{P}^{(11)}_{nm}\left(e^{\mathbb{D}^{(11)}_{mm}h}A_{x,m} + e^{-\mathbb{D}^{(11)}_{mm}h}B_{x,m}\right) + \mathbb{P}^{(12)}_{nm}\left(e^{\mathbb{D}^{(22)}_{mm}h}A_{y,m} + e^{-\mathbb{D}^{(22)}_{m}h}B_{y,m}\right) \\ \mathbb{P}^{(21)}_{nm}\left(e^{\mathbb{D}^{(11)}_{mm}h}A_{x,m} + e^{-\mathbb{D}^{(11)}_{mm}h}B_{x,m}\right) + \mathbb{P}^{(22)}_{nm}\left(e^{\mathbb{D}^{(22)}_{mm}h}A_{y,m} + e^{-\mathbb{D}^{(22)}_{mm}h}B_{y,m}\right) \end{pmatrix}, \end{aligned} \tag{4.145}$$

and the following ones for the magnetic field

$$\begin{aligned} &\begin{pmatrix} -\frac{c}{\omega}k_{z,n}^{(3)}\frac{k_{x,n}}{k_n}(C_{1,n}-C'_{1,n}) - \sqrt{\varepsilon_3}\frac{k_y}{k_n}(C_{2,n}+C'_{2,n}) \\ -\frac{c}{\omega}k_{z,n}^{(3)}\frac{k_y}{k_n}(C_{1,n}-C'_{1,n}) + \sqrt{\varepsilon_3}\frac{k_{x,n}}{k_n}(C_{2,n}+C'_{2,n}) \end{pmatrix} \\ &= \begin{pmatrix} \mathbb{P}'^{(11)}_{nm}\left(e^{\mathbb{D}^{(11)}_{mm}h}A_{x,m} - e^{-\mathbb{D}^{(11)}_{mm}h}B_{x,m}\right) + \mathbb{P}'^{(12)}_{nm}\left(e^{\mathbb{D}^{(22)}_{mm}h}A_{y,m} - e^{-\mathbb{D}^{(22)}_{mm}h}B_{y,m}\right) \\ \mathbb{P}'^{(21)}_{nm}\left(e^{\mathbb{D}^{(11)}_{mm}h}A_{x,m} - e^{-\mathbb{D}^{(11)}_{mm}h}B_{x,m}\right) + \mathbb{P}'^{(22)}_{nm}\left(e^{\mathbb{D}^{(22)}_{mm}h}A_{y,m} - e^{-\mathbb{D}^{(22)}_{mm}h}B_{y,m}\right) \end{pmatrix}. \end{aligned} \tag{4.146}$$

Finally, the boundary conditions at $z = h + \delta$ read

$$\begin{aligned} &\begin{pmatrix} -\frac{k_y}{k_n}(e^{ik_{z,n}^{(3)}\delta}C_{1,n} + e^{-ik_{z,n}^{(3)}\delta}C'_{1,n}) + \frac{c}{\sqrt{\varepsilon_3}\omega}k_{z,n}^{(3)}\frac{k_{x,n}}{k_n}(e^{ik_{z,n}^{(3)}\delta}C_{2,n} - e^{-ik_{z,n}^{(3)}\delta}C'_{2,n}) \\ \frac{k_{x,n}}{k_n}(e^{ik_{z,n}^{(3)}\delta}C_{1,n} + e^{-ik_{z,n}^{(3)}\delta}C'_{1,n}) + \frac{c}{\sqrt{\varepsilon_3}\omega}k_{z,n}^{(3)}\frac{k_y}{k_n}(e^{ik_{z,n}^{(3)}\delta}C_{2,n} - e^{-ik_{z,n}^{(3)}\delta}C'_{2,n}) \end{pmatrix} \\ &= \begin{pmatrix} -\frac{k_y}{k_n}(T_{1,n}+I'_{1,n}) + \frac{c}{\sqrt{\varepsilon_4}\omega}k_{z,n}^{(4)}\frac{k_{x,n}}{k_n}(T_{2,n}-I'_{2,n}) \\ \frac{k_{x,n}}{k_n}(T_{1,n}+I'_{1,n}) + \frac{c}{\sqrt{\varepsilon_4}\omega}k_{z,n}^{(4)}\frac{k_y}{k_n}(T_{2,n}-I'_{2,n}) \end{pmatrix}, \end{aligned} \tag{4.147}$$

and the ones for the magnetic field are given by

$$\begin{aligned} &\begin{pmatrix} -\frac{c}{\omega}k_{z,n}^{(3)}\frac{k_{x,n}}{k_n}(e^{ik_{z,n}^{(3)}\delta}C_{1,n} - e^{-ik_{z,n}^{(3)}\delta}C'_{1,n}) - \sqrt{\varepsilon_3}\frac{k_y}{k_n}(e^{ik_{z,n}^{(3)}\delta}C_{2,n} + e^{-ik_{z,n}^{(3)}\delta}C'_{2,n}) \\ -\frac{c}{\omega}k_{z,n}^{(3)}\frac{k_y}{k_n}(e^{ik_{z,n}^{(3)}\delta}C_{1,n} - e^{-ik_{z,n}^{(3)}\delta}C'_{1,n}) + \sqrt{\varepsilon_3}\frac{k_{x,n}}{k_n}(e^{ik_{z,n}^{(3)}\delta}C_{2,n} + e^{-ik_{z,n}^{(3)}\delta}C'_{2,n}) \end{pmatrix} \\ &= \begin{pmatrix} -\frac{c}{\omega}k_{z,n}^{(4)}\frac{k_{x,n}}{k_n}(T_{1,n}-I'_{1,n}) - \sqrt{\varepsilon_4}\frac{k_y}{k_n}(T_{2,n}+I'_{2,n}) \\ -\frac{c}{\omega}k_{z,n}^{(4)}\frac{k_y}{k_n}(T_{1,n}-I'_{1,n}) + \sqrt{\varepsilon_4}\frac{k_{x,n}}{k_n}(T_{2,n}+I'_{2,n}) \end{pmatrix}. \end{aligned} \tag{4.148}$$

In the following, we are going to cast (4.143)-(4.148) under the form

$$\begin{pmatrix} \mathcal{R} \\ \mathcal{A} \end{pmatrix} = \mathbb{S}_1 \begin{pmatrix} \mathcal{I} \\ \mathcal{B} \end{pmatrix}, \quad \begin{pmatrix} \mathcal{B} \\ \mathcal{C} \end{pmatrix} = \mathbb{S}_2 \begin{pmatrix} \mathcal{A} \\ \mathcal{C}' \end{pmatrix}, \quad \begin{pmatrix} \mathcal{C}' \\ \mathcal{T} \end{pmatrix} = \mathbb{S}_3 \begin{pmatrix} \mathcal{C} \\ \mathcal{I}' \end{pmatrix}. \tag{4.149}$$

The column vectors $\mathcal{A}$ and $\mathcal{B}$ appearing in this equation gather two vectors defined as in equation (4.138). On the contrary, all the six other column vectors gather the two polarizations of the field under the form

$$\mathcal{V} = (\{V_1(z, \mathbf{k}_n, \omega)\}_n, \{V_2(z, \mathbf{k}_n, \omega)\}_n)^T. \tag{4.150}$$

The system of equations (4.149) has to be solved for the unknowns $\boldsymbol{\mathcal{R}}$, $\boldsymbol{\mathcal{T}}$, $\boldsymbol{\mathcal{A}}$, $\boldsymbol{\mathcal{B}}$, $\boldsymbol{C}$, and $\boldsymbol{C}'$. The expression of $\boldsymbol{\mathcal{R}}$ and $\boldsymbol{\mathcal{T}}$ as a function of $\boldsymbol{\mathcal{I}}$ and $\boldsymbol{\mathcal{I}}'$ will provide us the desired reflection and transmission operators. The fact that for $\boldsymbol{\mathcal{A}}$ and $\boldsymbol{\mathcal{B}}$ we solve in cartesian components and not in polarization is not an issue since these appear as mute variables not participating to the scattering operators.

The explicit expression of the $\mathbb{S}$ matrices appearing in (4.149) can be obtained by means of algebraic manipulation of (4.143)-(4.148). The final result is

$$\mathbb{S}_1 = \begin{pmatrix} \mathbb{K}_1' & -\mathbb{P} \\ \mathbb{L}_1' & -\mathbb{P}' \end{pmatrix}^{-1} \begin{pmatrix} \mathbb{K}_1 & \mathbb{P} \\ \mathbb{L}_1 & -\mathbb{P}' \end{pmatrix}, \tag{4.151}$$

$$\mathbb{S}_2 = \begin{pmatrix} \sigma_h^{(2)} & \mathbb{0} \\ \mathbb{0} & \mathbb{1} \end{pmatrix} \begin{pmatrix} -\mathbb{P} & -\mathbb{K}_3 \\ \mathbb{P}' & -\mathbb{L}_3 \end{pmatrix}^{-1} \begin{pmatrix} \mathbb{P} & -\mathbb{K}_3' \\ \mathbb{P}' & -\mathbb{L}_3' \end{pmatrix} \begin{pmatrix} \sigma_h^{(2)} & \mathbb{0} \\ \mathbb{0} & \mathbb{1} \end{pmatrix}, \tag{4.152}$$

$$\mathbb{S}_3 = \begin{pmatrix} \sigma_\delta^{(3)} & \mathbb{0} \\ \mathbb{0} & \mathbb{1} \end{pmatrix} \begin{pmatrix} \mathbb{K}_3' & \mathbb{K}_4 \\ \mathbb{L}_3' & \mathbb{L}_4 \end{pmatrix}^{-1} \begin{pmatrix} \mathbb{K}_3 & \mathbb{K}_4' \\ \mathbb{L}_3 & \mathbb{L}_4' \end{pmatrix} \begin{pmatrix} \sigma_\delta^{(3)} & \mathbb{0} \\ \mathbb{0} & \mathbb{1} \end{pmatrix}. \tag{4.153}$$

In these expressions we have defined

$$\begin{aligned} \mathbb{K}_i' &= \begin{pmatrix} -\mathbb{A}_y & -\mathbb{B}_{x,i} \\ \mathbb{A}_x & -\mathbb{B}_{y,i} \end{pmatrix}, & \mathbb{L}_i' &= \sqrt{\varepsilon_i} \begin{pmatrix} \mathbb{B}_{x,i} & -\mathbb{A}_y \\ \mathbb{B}_{y,i} & \mathbb{A}_x \end{pmatrix}, \\ \mathbb{K}_i &= \begin{pmatrix} \mathbb{A}_y & -\mathbb{B}_{x,i} \\ -\mathbb{A}_x & -\mathbb{B}_{y,i} \end{pmatrix}, & \mathbb{L}_i &= \sqrt{\varepsilon_i} \begin{pmatrix} \mathbb{B}_{x,i} & \mathbb{A}_y \\ \mathbb{B}_{y,i} & -\mathbb{A}_x \end{pmatrix}, \end{aligned} \tag{4.154}$$

where

$$\begin{aligned} \mathbb{A}_x &= \operatorname{diag}\left(\frac{k_{x,n}}{k_n}\right)_n, \quad \mathbb{A}_y = \operatorname{diag}\left(\frac{k_y}{k_n}\right)_n, \\ \mathbb{B}_{x,i} &= \frac{c}{\sqrt{\varepsilon_i}\omega} \operatorname{diag}\left(\frac{k_{x,n}}{k_n} k_{z,n}^{(i)}\right)_n, \\ \mathbb{B}_{y,i} &= \frac{c}{\sqrt{\varepsilon_i}\omega} \operatorname{diag}\left(\frac{k_y}{k_n} k_{z,n}^{(i)}\right)_n. \end{aligned} \tag{4.155}$$

The symbol $\operatorname{diag}(a_n)_n$ denotes a $(2M+1)\times(2M+1)$ diagonal matrix having diagonal elements $a_{-M}, a_{-M+1}, \ldots, a_M$. We have also defined the square matrices of dimension $2(2M+1)$

$$\sigma_h^{(2)} \equiv e^{\mathbb{D}h} = \begin{pmatrix} e^{\mathbb{D}^{(11)}h} & \mathbb{0} \\ \mathbb{0} & e^{\mathbb{D}^{(22)}h} \end{pmatrix}, \tag{4.156}$$

$$\sigma_\delta^{(3)} \equiv \begin{pmatrix} \operatorname{diag}(e^{ik_{z,n}^{(3)}\delta})_n & \mathbb{0} \\ \mathbb{0} & \operatorname{diag}(e^{ik_{z,n}^{(3)}\delta})_n \end{pmatrix}. \tag{4.157}$$

Using (4.149) we obtain the final result

$$\begin{pmatrix} \boldsymbol{\mathcal{R}} \\ \boldsymbol{\mathcal{T}} \end{pmatrix} = \mathbb{S} \begin{pmatrix} \boldsymbol{\mathcal{I}} \\ \boldsymbol{\mathcal{I}}' \end{pmatrix}, \tag{4.158}$$

where

$$\mathbb{S} = \mathbb{S}_1 \circledast \mathbb{S}_2 \circledast \mathbb{S}_3, \tag{4.159}$$

having introduced the associative operation $\mathbb{A} = \mathbb{B} \circledast \mathbb{C}$, which for three square matrices $\mathbb{A}$, $\mathbb{B}$ and $\mathbb{C}$ of dimension $4(2M+1)$ is defined in (4.101) - (4.104), where each matrix have been decomposed in four square blocks of dimension $2(2M+1)$.

Equation (4.158) allows to identify the four blocks of $\mathbb{S}$ as the reflection and transmission operators associated to the two sides of the grating. For example, the block $\mathbb{S}_{11}$ is the coefficient linking the reflected amplitudes $\boldsymbol{\mathcal{R}}$ to the incident ones $\boldsymbol{\mathcal{I}}$: it then coincides with the reflection operator $\mathcal{R}^-$ for a wave impinging on the grating of Figure (4.14) from $z < 0$. By analog reasoning, we write the full $\mathbb{S}$ matrix as

$$\mathbb{S} = \begin{pmatrix} \mathcal{R}^- & \mathcal{T}^- \\ \mathcal{T}^+ & \mathcal{R}^+ \end{pmatrix}. \tag{4.160}$$

We now need to calculate the reflection and transmission operators associated to the two gratings represented in Figure 4.13. As far as grating 1 is concerned, the problem we need to solve is exactly the one presented in Section 4.2.1, with the appropriate values of the geometrical parameters. Concerning grating 2, we need to take into account the fact that its interface is the plane $z = d$ and not $z = 0$. The modification of the scattering operators with respect to translations has been discussed in [19] (see also Section 4.1). Based on these results, and using the mode expansion used in this work (see Subsection 4.1.2), the $\mathcal{R}_2^-$ operator of grating 2 can be expressed as a function of the $\widetilde{\mathcal{R}}_2^-$ derived from FMM as

$$\begin{aligned} &\langle p, \mathbf{k}, n, \omega | \mathcal{R}_2^- | p', \mathbf{k}', n', \omega' \rangle \\ &= \exp[i(k_{z,n} + k'_{z,n'})d] \langle p, \mathbf{k}, n, \omega | \widetilde{\mathcal{R}}_2^- | p', \mathbf{k}', n', \omega' \rangle. \end{aligned} \tag{4.161}$$

As we will show later, this operator is the only one associated to grating 2 appearing in the expression of the force for our configuration.

4.3.1 Numerical results

We now present a numerical application concerning the force between two different gratings and we show our results [39],[AN5]. Being both gratings infinite in the xy plane, we actually calculate the pressure acting on any of them, as discussed in the case of two slabs in [19]. In the first configuration we have chosen both gratings to have period $D = 1\,\mu$m, corrugation depth $h = 1\,\mu$m and filling factor $f = 0.5$. As shown in Figure 4.13, the transition points of the two gratings are aligned, i.e. there is no shift along the x axis. Grating 1 is made of Fused Silica (SiO_2) and has thickness $\delta_1 = 10\,\mu$m, while grating 2 is made of Silicon and has infinite thickness. In order to take into account this point we have imposed $\varepsilon_3 = \varepsilon_4$ in the FMM relative to grating 2 (see Subsection 4.2.1) and removed in (4.37) all the terms proportional to the transmission operators of body 2. Physically, this can be explained by observing that because of the infinite thickness all the radiation coming from the upper

side of body 2 is absorbed and does not reach the cavity between the gratings. Both Silicon and Fused Silica have been described by means of optical data taken from [62].

As anticipated in Subsection 4.2.1, the numerical use of FMM demands to choice a truncation order, problem that will be addressed in this Subsection. We noted before that by choosing a truncation order M in the FMM we obtain as a result reflection operators which are square matrices of dimension $2(2M+1)$, that is two polarizations times $2M+1$ diffraction orders. Their typical structure is thus

$$\begin{array}{cc} & \begin{array}{cc} \text{TE} & \text{TM} \end{array} \\ \begin{array}{c} \text{TE} \\ \text{TM} \end{array} & \left(\begin{array}{c|c} A_{1,1}[n,n'] & A_{1,2}[n,n'] \\ \hline A_{2,1}[n,n'] & A_{2,2}[n,n'] \end{array}\right) \end{array}, \tag{4.162}$$

where each block $A_{i,j}[n,n']$ is a $(2M+1)\times(2M+1)$ matrix, the indices n and n' running from $-M$ to M.

It is worth stressing that, for a given M, only the elements closer to the center of each block of the matrix (i.e. close to $n=0$ for each couple of polarizations) are at convergence. Thus, for a given m, we can increase the value of M starting from $M=m$ in order to extract a $2(2m+1)\times 2(2m+1)$ ($m<M$) scattering operator whose elements are at convergence with a given accuracy (in our case of the order of one percent). The operators obtained following this procedure can be used to compute the force using (4.36) and (4.37). Since these equations imply a trace containing also a sum over the diffraction orders n, the series has to be replaced with a finite sum from $-\bar{m}$ to $\bar{m}$. The value of $\bar{m}$ has to be found by imposing the convergence of the series at a chosen accuracy. Also in this case, we required an accuracy smaller than one percent.

The calculation of the pressure at a given distance requires the evaluation of the traces (4.36) and (4.37) at several different values of the wave vector $\mathbf{k}$ and the frequency ω, in order to reach the convergence on the integral on the three variables. We have observed that a single calculation of the trace requires values of $\bar{m}$ of the order of 2 (with peaks going up to 7) and corresponding values of M of the order of 5 (with peaks around 20). Moreover, we have that the values of $\bar{m}$ and M depend on the ratio of the distance to the grating period. This is not unexpected and we have, in fact, that when this ratio increase the values of $\bar{m}$ and M decrease since in this case we have that our systems approximate that of two slabs. A single value of the pressure required a computation time of the order of 16 hours on three 3 GHz CPUs.

In the configuration described above, we have calculated the pressure acting on grating 1. To point out the features of our OTE configuration we present in Figure 4.15 the pressure as a function of distance for different sets of the temperatures (T_1, T_2, T_e).

We clearly see that the modification of the three temperatures strongly affects the value of the force. In particular, three of the four curves show a transition from an attractive to a repulsive behavior, not realizable at thermal equilibrium for this configuration. This qualitative difference is a well-known consequence of the absence of thermal equilibrium and it has already been predicted in the case of two parallel slabs [10, 19]. We stress that the transition point between attraction and repulsion is a function of the temperatures. For

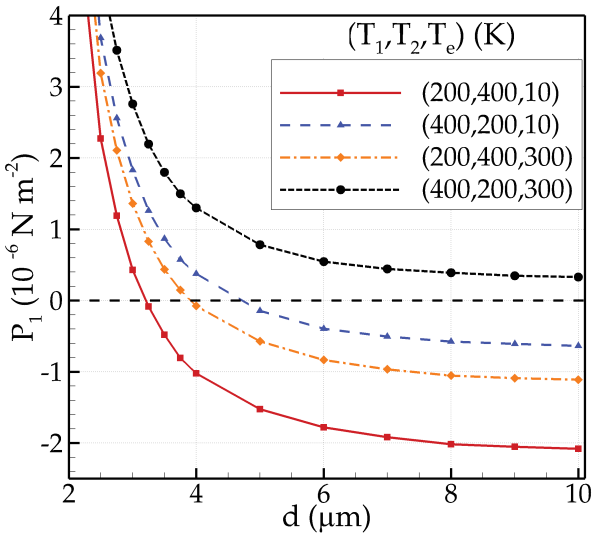

Figure 4.15 – Pressure acting on grating 1 (Fused Silica, having $h_1 = 1\,\mu$m, $\delta_1 = 10\,\mu$m, $D = 1\,\mu$m and $f_1 = 0.5$) in front of grating 2 (Silicon, having $h_2 = 1\,\mu$m, infinite thickness, $D = 1\,\mu$m and $f_2 = 0.5$) as a function of distance d. The four curves correspond to different choices of the three temperatures (T_1, T_2, T_e) as shown in legend.

the values chosen, it roughly varies from 3 to 5 μm.

To underline even more the richness of our OTE configuration, we focus on the temperatures $(T_1, T_2, T_e) = (200, 400, 10)$ K and compare the pressure to its equivalent at thermal equilibrium at the temperature of body 1, i.e. $T_1 = 200$ K. This comparison is presented in Figure 4.16. In the same figure we also plot the pressure, both at and out of thermal equilibrium, for filling factors $f_1 = f_2 = 1$ (corresponding to *filled* gratings, that is a 11 μm-thick SiO_2 slab at distance d from an infinite Si slab) and for $f_1 = f_2 = 0$ (corresponding to *empty* gratings, that is a 10 μm-thick SiO_2 slab at distance $d + 2\,\mu$m from an infinite Si slab).

Besides the transition to a repulsive behavior, Figure 4.16 shows that the pressure in presence of a grating always lies between the two results corresponding to filled and empty ones. As a check of our numerical calculations, we have verified that the asymptotic behavior of the equilibrium pressure correctly reproduces the corresponding analytical result for two slabs. Finally, a comparison between Figs. 4.15 and 4.16 shows that the asymptotic value of the pressure can be tuned by varying the three temperatures of the system to values comparable to the pressure at thermal equilibrium (apart from the sign) at much smaller distances, of the order of 3 μm.

To conclude this Subection, we compare the Casimir-Lifshitz pressure between the two gratings obtained using FMM to the result coming from the PFA (Proximity Force Approximation), typically used to deal with complex geometries such as sphere-plane and nanostructured surfaces. In the case of two aligned gratings with equal filling factors $f_1 = f_2 = f$ the pressure in the PFA reduces to the following weighted sum of the pressures of simple

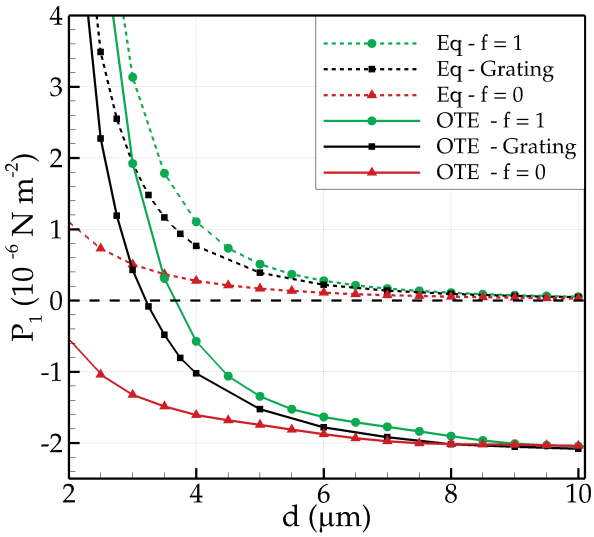

Figure 4.16 – Non-equilibrium (OTE) pressure $[(T_1, T_2, T_e) = (200, 400, 10)\,\mathrm{K}$, solid lines] compared to equilibrium pressure ($T = 200\,\mathrm{K}$, dashed lines) for two gratings (black squares), and two slab-slab configurations corresponding to filled gratings ($f = 1$, green circles) and an empty ones ($f = 0$, red triangles).

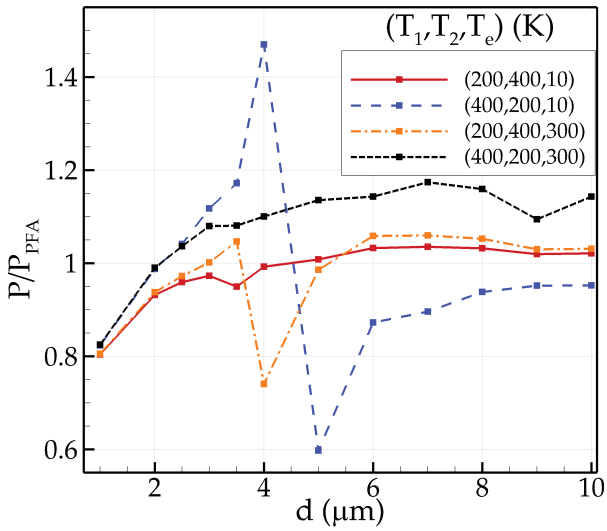

Figure 4.17 – Ratio between the exact pressure and the PFA counterpart (see equation (4.163)), for the same distances and choices of temperatures of Figure (4.15).

slab-slab configurations [48, 45]:

$$P_{1,\mathrm{PFA}}(d) = fP_1^{(\mathrm{ss})}(\delta_1, \delta_2, d) + (1-f)P_1^{(\mathrm{ss})}(\delta_1 - h_1, \delta_2 - h_2, d + h_1 + h_2), \tag{4.163}$$

where $P_1^{(\mathrm{ss})}(\delta_1, \delta_2, d)$ is the pressure acting on a δ_1-thick slab at a distance d from a δ_2-thick slab.

In Figure 4.17 we plot the ratio between the exact pressure and the PFA results for the four temperature configurations used in Figure 4.15. We observe that PFA provides in our range of distances a description of the pressure with a relative error typically well below 20%. The fact the PFA predicts a change of sign not exactly at the position predicted by the exact calculation results in the existence of a vertical asymptote of the ratio P/P_{PFA}, clearly indicated in the blue and orange curves in Figure 4.17.

4.3.2 Dependence on geometrical parameters

It is now interesting to understand how a modification of the geometrical parameters of the gratings is able to tune the value of the pressure. To this end we have chosen as a reference the pressure at a distance $d = 4\,\mu\mathrm{m}$ for $(T_1, T_2, T_\mathrm{e}) = (200, 400, 10)\,\mathrm{K}$, for which the pressure is around $P_0 = -10^{-6}\,\mathrm{N\,m^{-2}}$ (see Figure 4.15). Starting from this result, we have modified one by one the values of the filling factor f, period D, corrugation depth h and calculated the ratio between the modified pressure and the reference P_0.

The results are shown in Figure 4.18, where the pressure ratio is plotted as a function of the ratio between the modified parameter and the reference ones ($f_0 = 0.5$, $D_0 = 1\,\mu\mathrm{m}$ and $h_0 = 1\,\mu\mathrm{m}$). First, we observe that geometrical modifications can tune the pressure by a factor going from 0.5 to 1.6. In particular, this range can be fully explored by varying the filling factor between the two extreme values $f = 0$ and $f = 1$, i.e. between the two limiting slab-slab configurations. Concerning the depth h, its variation also allows a wide variation of the pressure. We remark that for h going to zero we recover the result corresponding to $f = 1$, that is a filled grating. On the contrary, for increasing values of h, we see that we approach to a pressure approximately equal to half the value of the pressure for $f = 1$. This can be interpreted by noticing that roughly speaking at some point the corrugation is so deep that only the upper part (half of the total surface, being $f = 0.5$) contributes to the pressure. Differently, the dependence of the pressure on the period D is less pronounced, and absent within our accuracy in the case of a lateral shift between the gratings, not reported here.

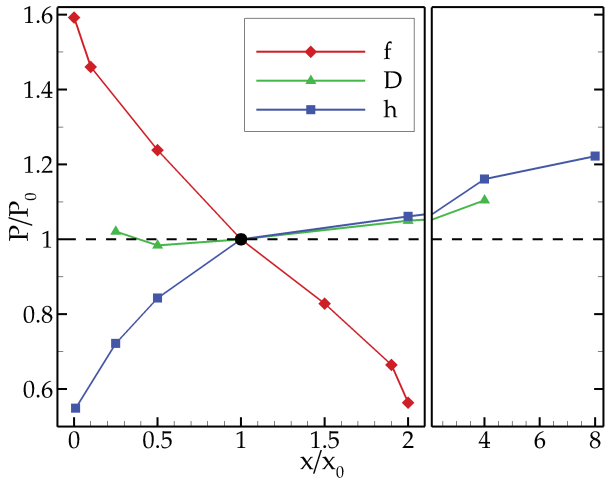

Figure 4.18 – Variation of the pressure between two gratings at $d = 4\,\mu$m [temperatures $(T_1, T_2, T_e) = (200, 400, 10)$ K] as a function of the geometrical parameters. The reference point (black circle) corresponds to the set of parameters $f_1 = f_2 = 0.5$, $h_1 = h_2 = 1\,\mu$m, $\delta_1 = 10\,\mu$m, infinite δ_2, $D = 1\,\mu$m. The three curves show the variation of pressure when changing one parameter at a time (red diamonds for the filling factor, green triangles for the period, blue squares for the corrugation depth). Axis scales are normalized to reference value (P_0, $f_0 = 0.5$, $D_0 = 1\,\mu$m, $h_0 = 1\,\mu$m). Note the scale break on the x axis.

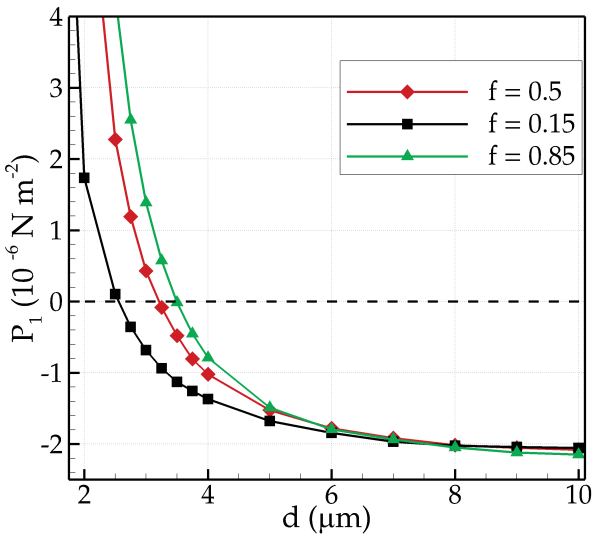

Figure 4.19 – Pressure on grating 1 as a function of distance [temperatures $(T_1, T_2, T_e) = (200, 400, 10)$ K] for three different values of filling factor, all the other geoemtrical parameters being the reference ones.

As we have shown, the filling factor is a promising tool to tailor the behavior of the pressure. This is further pointed out in Figure 4.19, where the distance-dependent pressure is plotted for three different values of f. Whereas the asymptotic value of the pressure is practically the same, we note that for small distances the three curves differ visibly. More interestingly, the attractive-repulsive transition can be tuned approximately from 2.5 to 3.5 μm by changing f from 0.15 to 0.85.

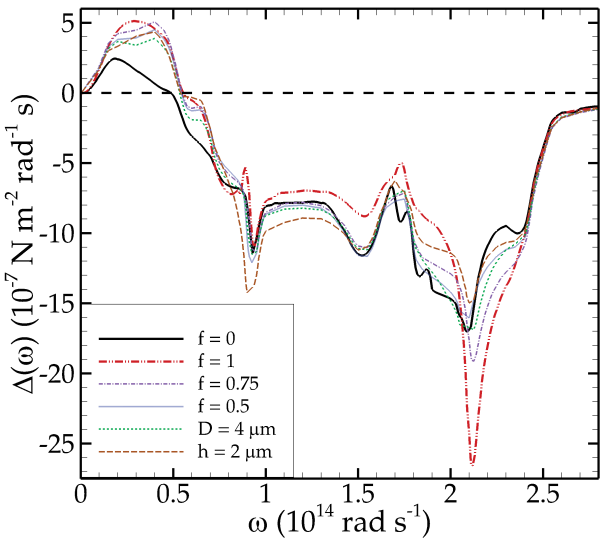

Figure 4.20 – Spectral density of the OTE contribution to the force (defined in (4.164)) at $d = 4\,\mu$m [temperatures $(T_1, T_2, T_e) = (200, 400, 10)$ K]. The solid black line corresponds to filled gratings ($f = 1$), the dot-dot-dashed red line to empty ones ($f = 0$), the dotted blue line to our reference gratings, having $f = 0.5$. In the other curves we vary the geometrical parameters one by one with respect to our reference case: dot-dashed violet line for $f = 0.75$, short-dashed green line for $D = 4\,\mu$m, long-dashed brown line for $h = 2\,\mu$m.

Let us focus now on the spectral properties of the pressure, by analyzing the quantity $\Delta(\omega)$, defined as the spectral component at frequency ω of the non-equilibrium contribution to the force (4.37), that is

$$\Delta(T_1, T_2, T_e) = \int_0^{+\infty} d\omega\, \Delta(\omega). \tag{4.164}$$

Also in this case, we consider our reference point $d = 4\,\mu$m and $(T_1, T_2, T_e) = (200, 400, 10)$ and compare its spectral distribution with the two slab-slab cases ($f = 0$ and $f = 1$) as well as with some variations of one of the three parameters discussed above.

The result is shown in Figure 4.20. We see that no striking spectral difference is present between the configurations compared. Roughly speaking, no new modes (such as the spoof plasmons observed in metal gratings [63, 64]) are observed in the spectral region of interest, that is up to ω of the order of 3×10^{14} rad s^{-1}. The spectral properties for any considered value of the geometrical parameters show small differences with respect to the ones of the two slab-slab configurations.

4.3.3 Modulation of the attractive-repulsive transition

As we have seen in Subection 4.3.2, the filling factor is a promising tool to shift the distance at which the transition between attraction and repulsion takes place. Nevertheless, from an experimental point of view it is more interesting to understand how this transition can be affected by tuning parameters which can be varied during an experiment, such as the three temperatures. This is discussed in this Subsection, where we first consider the case in which the two gratings have a common temperature $T_1 = T_2 = T_b$, in general different from the environmental one T_e. For this configuration, we plot in Figure 4.21 the pressure acting on grating 1 in the reference configuration discussed above as a function of T_b and T_e.

The plot is clearly divided in two regions, corresponding to positive and negative values of the pressure, separated by a solid zero-pressure line. Following this line, we see that repulsion can be obtained only for body temperatures larger than approximately 312 K, and that for larger values of T_b a larger region of T_e realizes repulsion. Moreover, we stress the remarkable feature that for values of T_b close to 312 K the pressure is approximately zero and almost independent on the environmental temperature for T_e up to approximately 150 K.

In the same spirit of our last analysis we now fix only T_1 at three different values (200, 300 and 400 K) and let T_2 and T_e vary. The pressure as a function of the two temperatures is shown in Figure 4.22. We see a behavior similar to that observed in Figure 4.21, that is the existence of a minimum temperature $\bar{T}_2$ below which repulsion is impossible, as well as a region where the pressure is close to zero almost independently of T_e. As manifest from Figure 4.22, the limit temperature $\bar{T}_2$ is a decreasing function of T_1.

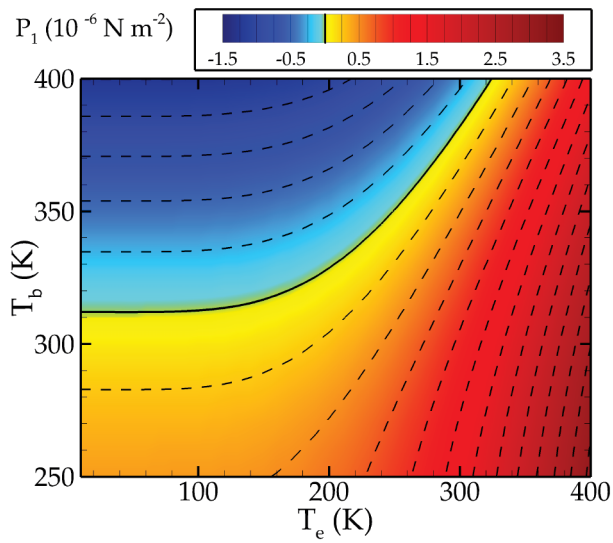

Figure 4.21 – Pressure acting on grating 1 for $d = 4\,\mu$m and $T_1 = T_2 = T_b$ as a function of T_b and T_e. The solid line corresponds to zero pressure, while the dashed lines to the other contour lines shown in legend.

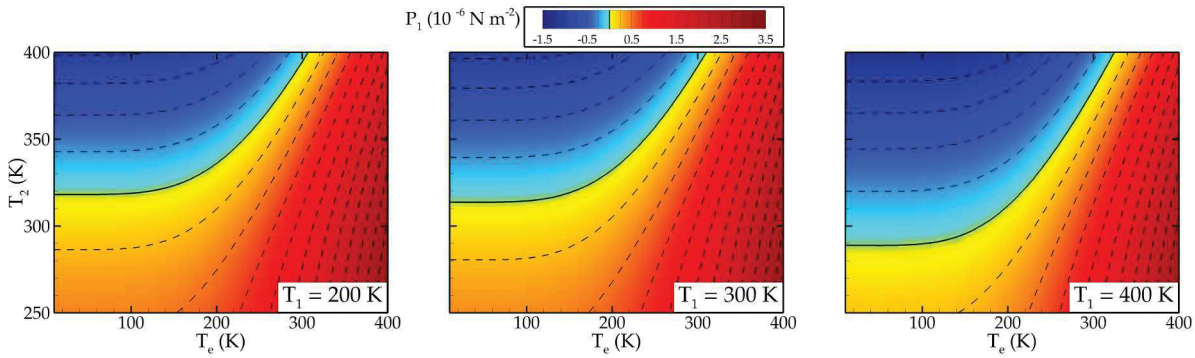

Figure 4.22 – Pressure acting on grating 1 for $d = 4\,\mu$m as a function of T_2 and T_e for three different values of T_1. Same convention of Figure 4.21 for contour lines.

Finally, we discuss how the distance d_0 at which the attractive-repulsive transition takes place can be tuned by changing the three temperatures. This is shown in Figure 4.23, where we fix $T_1 = T_2 = T_b \in \{200, 300, 400\}$ K and plot d_0 as a function of T_e. As a general remark, when T_e is smaller than T_b the distance d_0 tends to a constant value, which decreases from $5.5\,\mu$m to $3\,\mu$m for T_b going from 200 to 400 K. Furthermore, when T_e tends to T_b, i.e. the system approaches thermal equilibrium, d_0 tends to a vertical asymptote, in accordance to the fact that the pressure is always attractive at thermal equilibrium.

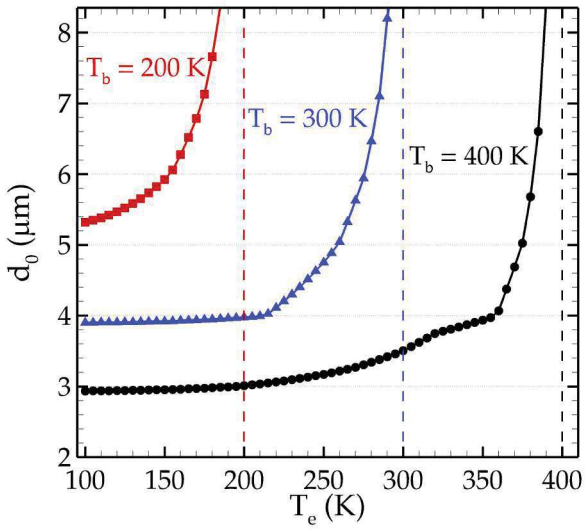

Figure 4.23 – Distance d_0 of the attractive-repulsive transition of the pressure as a function of T_e for three different values of $T_1 = T_2 = T_b$.

4.3.4 Concluding remarks

We calculated the Casimir-Lifsthiz pressure out of thermal equilibrium acting on a 1D dielectric lamellar grating in front of another (in general different) dielectric grating. To

this aim, we implemented the Fourier Modal Method in order to derive the scattering operators associated to each individual grating. Using the general formalism for Casimir-Lifshitz force based on scattering matrices, we calculated the pressure acting on a finite Fused Silica grating in presence of an infinite Silicon grating, and also compared our results to those obtained using the Proximity Force Approximation.

We showed that the combination of geometrical structuring of the surface and absence of thermal equilibrium offers an extremely rich domain of variation both with respect to thermal equilibrium and with respect to planar slabs out of thermal equilibrium [39],[AN5]. In fact, as in the case of two slabs, non-equilibrium is able to produce a repulsive pressure, whose intensity can be tuned by varying the temperatures. In addition, the several geometrical parameters associated to each grating add more tools to tune the pressure. We also pointed out the presence of regimes in which the pressure is close to zero and almost independent of the environmental temperature. Remarkably, the variations of all the parameters strongly affect the distance at which the transition between attractive and repulsive pressure occurs, allowing to obtain transition distances as low as 2.5 μm. This feature is indeed promising for the experimental observation of a repulsive force. Moreover, our results can be relevant in the context of force manipulations on micro-mechanical systems [51]. Finally, an extension of this study to three-body configurations is also promising toward the manipulation of heat transfer [65, 28].

References

[1] H. B. G. Casimir, Proc. K. Ned. Akad. Wet. **51**, 793 (1948).

[2] H. B. G. Casimir and D. Polder, Phys. Rev. **73**, 360 (1948).

[3] I. E. Dzyaloshinskii, E. M. Lifshitz, and L. P. Pitaevskii, Adv. Phys. **10**, 165 (1961).

[4] *Casimir-Lifshitz Physics*, Lecture Notes in Physics Vol. 834, edited by D. Dalvit, P. Milonni, D. Roberts, and F. Da Rosa (Springer-Verlag, Berlin, 2011).

[5] A. Sushkov et al., Nat. Physics **7**, 230 (2011).

[6] M. Antezza, L. P. Pitaevskii, and S. Stringari, Phys. Rev. Lett. **95**, 113202 (2005).

[7] M. Antezza, J. Phys. A: Math. Gen. **39**, 6117 (2006).

[8] J. M. Obrecht, R. J. Wild, M. Antezza, L. P. Pitaevskii, S. Stringari, and E. A. Cornell, Phys. Rev. Lett. **98**, 063201 (2007).

[9] M. Antezza, L. P. Pitaevskii, S. Stringari, and V. B. Svetovoy, Phys. Rev. Lett. **97**, 223203 (2006).

[10] M. Antezza, L. P. Pitaevskii, S. Stringari, and V. B. Svetovoy, Phys. Rev. A **77**, 022901 (2008).

[11] M. Antezza, L. P. Pitaevskii, S. Stringari, Phys. Rev. A **70**, 053619 (2004).

[12] S. Y. Buhmann and S. Scheel, Phys. Rev. Lett. **100**, 253201 (2008).

[13] Y. Sherkunov, Phys. Rev. A **79**, 032101 (2009).

[14] R. O. Behunin and B.-L. Hu, Phys. Rev. A **82**, 022507 (2010).

[15] R. Behunin and B.-L. Hu, J. Phys. A: Math. Theor. **43**, 012001 (2010).

[16] R. O. Behunin and B.-L. Hu, Phys. Rev. A **84**, 012902 (2011).

[17] G. Bimonte, Phys. Rev. A **80**, 042102 (2009).

[18] R. Messina and M. Antezza, Europhys. Lett. **95**, 61002 (2011).

[19] R. Messina and M. Antezza, Phys. Rev. A **84**, 042102 (2011).

[20] M. Krüger, T. Emig, G. Bimonte, and M. Kardar, Europhys. Lett. **95**, 21002 (2011).

[21] M. Krüger, G. Bimonte, T. Emig, and M. Kardar, Phys. Rev. B **86**, 115423 (2012).

[22] A. W. Rodriguez, O. Ilic, P. Bermel, I. Celanovic, J. D. Joannopoulos, M. Soljačić, and S. G. Johnson, Phys. Rev. Lett. **107**, 114302 (2011).

[23] A. P. McCauley, M. T. H. Reid, M. Krüger, and S. G. Johnson, Phys. Rev. B **85**, 165104 (2012).

[24] A. W. Rodriguez, M. T. H. Reid, and S. G. Johnson, Phys. Rev. B **86**, 220302(R) (2012).

[25] M. Krüger, T. Emig, and M. Kardar, Phys. Rev. Lett. **106**, 210404 (2011).

[26] A. W. Rodriguez, M. T. H. Reid, and S. G. Johnson, Phys. Rev. B **88**, 054305 (2013).

[27] L. D. Landau and E. M. Lifshitz, *Electrodynamics of Continuous Media*, (Pergamon Press, Oxford, 1963).

[28] R. Messina and M. Antezza, Phys. Rev. A **89**, 052104 (2014).

[29] B. Bellomo, R. Messina, and M. Antezza, Europhys. Lett. **100**, 20006 (2012).

[30] B. Bellomo, R. Messina, D. Felbacq, and M. Antezza, Phys. Rev. A **87**, 012101 (2013).

[31] B. Bellomo and M. Antezza, Europhys. Lett. **104**, 10006 (2013).

[32] B. Bellomo and M. Antezza, New J. Phys. **15**, 113052 (2013).

[33] R. Buscher and T. Emig, Phys. Rev. A **69**, 062101 (2004).

[34] A. Lambrecht and V. N. Marachevsky, Phys. Rev. Lett. **101**, 160403 (2008).

[35] P. S. Davids, F. Intravaia, F. S. S. Rosa, and D. A. R. Dalvit, Phys. Rev. A **82**, 062111 (2010).

[36] A. M. Contreras-Reyes, R. Guérout, P. A. Maia Neto, D. A. R. Dalvit, A. Lambrecht and S. Reynaud, Phys. Rev. A **82**, 052517 (2010).

[37] A. W. Rodriguez, F. Capasso and S. G. Johnson, Nature Photon. **5**, 211 (2011).

[38] F. Intravaia, P. S. Davids, R. S. Decca, V. A. Aksyuk, D. López, and D. A. R. Dalvit, Phys. Rev. A **86**, 042101 (2012).

[39] A. Noto, R. Messina, B. Guizal, and M. Antezza, Phys. Rev. A **90**, 022120 (2014).

[40] J. Lussange, R. Guérout, and A. Lambrecht, Phys. Rev. A **86**, 062502 (2012).

[41] R. Guérout, J. Lussange, H. B. Chan, A. Lambrecht, and S. Reynaud, Phys. Rev. A **87**, 052514 (2013).

[42] A. A. Banishev, J. Wagner, T. Emig, R. Zandi, and U. Mohideen, Phys. Rev. B **89**, 235436 (2014).

[43] J. Wagner and R. Zandi, Phys. Rev. A **90**, 012516 (2014).

[44] S.-A. Biehs, F. S. S. Rosa and P. Ben-Abdallah, Appl. Phys. Lett. **98**, 243102 (2011).

[45] J. Lussange, R. Guérout, F. S. S. Rosa, J.-J. Greffet, A. Lambrecht, and S. Reynaud, Phys. Rev. B **86**, 085432 (2012).

[46] R. Guérout, J. Lussange, F. S. S. Rosa, J.-P. Hugonin, D. A. R. Dalvit, J.-J. Greffet, A. Lambrecht, and S. Reynaud, Phys. Rev. B **85**, 180301(R) (2012).

[47] H. B. Chan, Y. Bao, J. Zou, R. A. Cirelli, F. Klemens, W. M. Mansfield, and C. S. Pai, Phys. Rev. Lett. **101**, 030401 (2008).

[48] Y. Bao, R. Guérout, J. Lussange, A. Lambrecht, R. A. Cirelli, F. Klemens, W. M. Mansfield, C. S. Pai, and H. B. Chan, Phys. Rev. Lett. **105**, 250402 (2010).

[49] F. Intravaia et al., Nat. Comm. **4**, 2515 (2013).

[50] H. B. Chan, V. A. Aksyuk, R. N. Kleiman, D. J. Bishop, and F. Capasso, Science **291**, 1941 (2001).

[51] J. Zou, A. W. Rodriguez, M. T. H. Reid, A. P. McCauley, I. I. Kravchenko, T. Lu, Y. Bao, S. G. Johnson, and H. B. Chan, Nat. Comm. **4**, 1845 (2013).

[52] P. Ben-Abdallah, K. Joulain, J. Drevillon, and G. Domingues, J. Appl. Phys. **106**, 044036 (2009).

[53] E. M. Lifshitz, Sov. Phys. JETP **2**, 73 (1956).

[54] T. Antonakakis, F. I. Baida, A. Belkhir, K. Cherednichenko, S. Cooper, R. Craster, G. Demesy, J. Desanto,, G. Granet, B. Gralak, et al. *Gratings: Theory and Numeric Applications, Second Revisited Edition* edited by E. Popov, Institut Fresnel, CNRS (2014).

[55] G. Granet, B. Guizal, J. Opt. Soc. Am. A **13**, 1019 (1996).

[56] L. Li, J. Opt. Soc. Am. A **13**, 1870–1876 (1996).

[57] J. D. Jackson, *Classical Electrodynamics*, Wiley (1998).

[58] G. Granet, J. Opt. Soc. Am. A **16**, 2510–2516 (1999).

[59] A. Khavasi and K. Mehrany, IEEE Trans. Antennas Propag. **57**, 1115–1121 (2009).

[60] Th. Weiss, G. Granet, N. Gippius, S. Tikhodeev, and H. Giessen, "Matched coordinates and adaptive spatial resolution in the Fourier modal method," Opt. Express **17**, pp 8051-8061 (2009).

[61] H. Kim, J. Park, and B. Lee, *Fourier Modal Method and Its Applications in Computational Nanophotonics* (CRC Press, Boca Raton, 2012).

[62] *Handbook of Optical Constants of Solids*, edited by E. Palik (Academic Press, New York, 1998).

[63] F. J. García-Vidal, L. Martín-Moreno, and J. B. Pendry, J. Opt. A: Pure Appl. Opt. **7**, S97 (2005).

[64] N. Yu et al., Nat. Mat. **9**, 730 (2010).

[65] R. Messina, M. Antezza, and P. Ben-Abdallah, Phys. Rev. Lett. **109**, 244302 (2012).

Conclusions

Casimir forces are one of the most startling consequences of the existence of vacuum fluctuations and of the quantum nature of the electromagnetic field. They are quantum interactions of electromagnetic origin between neutral microscopic or macroscopic objects in the vacuum and are the main topic of this thesis. These interactions, although they are weak, are measurable and have been observed in many different configurations. It is well known that they are strongly related to the geometry of the system, to the boundary conditions and magnetodielectric properties of the objects involved, and to the temperature of the system. We have been inspired by these remarkable features of Casimir forces for the research project summarized in this thesis. In particular, the theoretical effects occurring when out of equilibrium conditions are considered, and the possibility to tune and control the force in specific systems, have led our research to study the following new configurations: atoms uniformly accelerated, atoms in front of an oscillating mirror, dielectric gratings out of thermal equilibrium. These are the main original problems studied during the PhD. We now summarize the original results obtained.

The first part of our research concerned with the Casimir-Polder interaction between atoms uniformly accelerating. This system is in an out of dynamical equilibrium, due to the uniform accelerated motion of the atoms. In a first work we studied the problem with the help of an heuristic semiclassical model, based on the spatial correlations of vacuum fluctuations, already used in the literature to describe the Casimir-Polder forces in the static case. We showed significant qualitative modifications of these interactions due to the acceleration, and in particular we stressed that their distance dependence is modified both in the near and in the far zone (respectively, new terms as R^{-5} and R^{-6} appear). For this physical system it is also important to consider the connection with the Unruh effect. In fact, the qualitative change of the Casimir-Polder interaction suggests a new possibility to detect the Unruh effect indirectly, measuring the modifications of the Casimir-Polder force induced by the accelerated motion of the atoms. Moreover, we have found a temporal dependence of the force for the system considered. This adds a further possibility to detect the Unruh effect through the Casimir-Polder interaction, without the extremely large accelerations necessary for other radiative processes such as the Lamb shift (it allows to decrease the acceleration by increasing the observation time). We have also investigated the same problem with a more rigorous approach, extending a known general statistical procedure to separate the contributions from vacuum fluctuations and radiation reaction. Using this approach we again found a significant change of the scalar Casimir-Polder force induced by acceleration.

In addition to the previous case, we showed a novel transition in the distance-dependence of the force. We noticed that this new transition occurs at a characteristic length scale, where there is a breakdown of the local inertial frame approximation. For distances larger than this characteristic length scale, the non-inertial character of relativistic acceleration must be taken into account. We have then considered the Casimir-Polder resonant force between accelerated atoms, when the two atoms, one in the ground state and the other in an excited state, are prepared in a correlated state. We have considered both cases of interaction with a scalar and an electromagnetic field. Also in this case, we found a qualitative modification of the distance-dependence of the interaction compared to the case of inertial atoms, and we have discussed the close connection of our results with the Unruh effect. Possible developments on this topic could aim to envisage realistic experimental setups to detect the Unruh effect through Casimir-Polder interactions.

In the second part of our work, we considered the Casimir-Polder interaction between a Rydberg atom and an oscillating effective mirror (dynamical mirror). We showed that this optomechanical coupling may produce a new near-field resonant atomic excitation. We have found that the excitation probability, consistently with our approximation, can be of the order of 20 per cent using physical parameters currently achievable in the laboratory. To detect this new effect, we also proposed an experimental configuration composed of a cold Rydberg atoms gas trapped at a distance of about $2 \times 10\,\mu$m from a dynamical mirror. The latter is made of a semiconductor layer whose dielectric constant is periodically driven by an external laser pulse train. Since the system we studied is related to the dynamical Casimir effect, we also compared the atom-excitation probability due to our near-field effect to that related to the dynamical Casimir effect. We found that our near-field excitation process is much more effective than the atomic excitation due to the absorption of the photons emitted by dynamical Casimir effect. We finally stressed how our dynamical effect can be used to realize an effective optomechanical coupling between a macroscopic body and an elementary quantum system and how the quantum fluctuations may change the internal state of this kind of system. Future perspectives of our work involve refinements of the model used in view of possible experiments, for example: effect of dielectric properties of the oscillating wall and of the patch potentials, temperature effects and possible dissipative effects.

Finally, in the third part of our research, we studied and analyzed in detail a system in an out of thermal equilibrium condition. The system is composed of two 1D lamellar dielectric gratings. In order to study such a system, we used a general formalism for the Casimir-Lifshitz force based on scattering matrices. The necessary scattering operators of the lamellar gratings were deduced with the implementation of the Fourier Modal Method (FMM). We then numerically evaluated the Casimir-Lifshitz pressure acting on a finite Fused Silica grating in the presence of an infinite Silicon grating when the temperature of the bodies and of the environment were in general different. We stressed the possibility to observe a repulsive force and we showed that, for the system we studied, the combination of geometrical structuring of the gratings surface and the temperatures involved in the system give the possibility to tune and control the force. For example, we showed that the distance between the gratings at which the transition between attractive and repulsive

pressure occurs can be easily controlled. In our system the minimum transition distance is around 2.5 μm, a value smaller than the transition distances of the analogous case of two slabs. This feature makes the system we studied promising for the detection of the repulsive Casimir-Lifshitz force. Future planned work on this subject is relative to the extension to metallic gratings, as well as the Casimir-Lifshitz lateral force between gratings and the study of different grating profiles.

PhD Publications

[AN1] A. Noto and R. Passante, Phys. Rev. D **88**, 025041 (2013).

[AN2] J. Marino, A. Noto, R. Passante, L. Rizzuto and S. Spagnolo, Phys. Scr. **T160**, 014031 (2014).

[AN3] J. Marino, A. Noto, R. Passante, Phys. Rev. Lett. **113**, 020403 (2014).

[AN4] M. Antezza, C. Braggio, G. Carugno, A. Noto, R. Passante, L. Rizzuto, G. Ruoso, and S. Spagnolo, Phys. Rev. Lett. **113**, 023601 (2014).

[AN5] A. Noto, R. Messina, B. Guizal, and M. Antezza, Phys. Rev. A **90**, 022120 (2014).

[AN6] A. Noto, J. Marino and R. Passante, in preparation (2015).

[AN7] L. Rizzuto, M. Lattuca, J. Marino, A. Noto, S. Spagnolo and R. Passante, in preparation (2015).

Appendix A

Linear susceptibility

In this Appendix we give the expression of the linear susceptibility of the electromagnetic field in the proper reference frame . It can be obtained from the correlation function (2.162). We have

$$\chi^F_{\ell m}(x_A(\tau), x_B(\tau')) = \frac{i}{\hbar}\langle 0|[E_\ell(x_A(\tau)), E_m(x_B(\tau'))]|0\rangle \tag{A.0.1}$$

$$= \frac{ia^4}{2\pi c^7}\Bigg\{[\delta_{\ell m} - \frac{za}{4c^2}n_\ell k_m]\sinh^2\frac{a(\tau-\tau')}{2c} + (\frac{za}{2c^2})^2[\delta_{\ell m} - 2n_\ell n_m] \times\Bigg[1 + 2(\delta_{\ell m} - k_\ell k_m)\sinh^2\frac{a(\tau-\tau')}{2c}\Bigg]\Bigg\}$$

$$\times\Bigg[\frac{1}{[\sinh^2\frac{a(\tau-\tau'-i\epsilon)}{2c} - (\frac{za}{2c^2})^2]^3} - \frac{1}{[\sinh^2\frac{a(\tau-\tau'+i\epsilon)}{2c} - (\frac{za}{2c^2})^2]^3}\Bigg] \tag{A.0.2}$$

For our purposes, it is more convenient to express Equation (A.0.2) as integrals over frequencies. Using the same procedure as in the reference [39] of Chapter 2, after some calculation, we obtain

$$\chi_{\ell m}(x_A(\tau), x_B(\tau)) = \frac{ia^4}{\pi c^7}\frac{1}{\sqrt{N(z,a)}}F(T,u)\Bigg\{M_{\ell m}\Bigg[c_1(z,a)]\frac{d^2}{dT^2} + c_2(z,a)\frac{d}{dT} + c_3(z,a)\Bigg] + Q_{\ell m}\Bigg[c_4(z,a)\frac{d}{dT} + c_5(z,a)\Bigg]\Bigg\} \tag{A.0.3}$$

where we introduced the tensors

$$M_{\ell m} = 2(\delta_{\ell m} - n_\ell n_m) - \frac{za}{2c^2}n_\ell k_m + \frac{z^2a^2}{2c^4}(\delta_{\ell m} - n_\ell n_m)(\delta_{\ell m} - k_\ell k_m) \tag{A.0.4}$$

$$Q_{\ell m} = -2(\delta_{\ell m} - 3n_\ell n_m) - \frac{za}{2c^2}n_\ell k_m + \frac{z^2a^2}{2c^4}(\delta_{\ell m} - n_\ell n_m)(\delta_{\ell m} - k_\ell k_m) \tag{A.0.5}$$

taking into account the dependence of the anti-symmetric correlation function on the spatial directions, and

$$F(T,u) = \int_0^\infty d\omega\,\sin(\omega T)(e^{i\omega u} - e^{-i\omega u}), \quad u = \tau - \tau', \quad T = \frac{2c}{a}\sinh^{-1}\left(\frac{za}{2c^2}\right) \tag{A.0.6}$$

Also, we defined the coefficients $c_i(z,a)$ $(i = 1, ...5)$

$$
\begin{aligned}
c_1(z,a) &= \frac{c^5}{Nza^4} \\
c_2(z,a) &= -\frac{3c^2}{4N^{3/2}a^2} \\
c_3(z,a) &= -\frac{c^3}{4N^2za^2}\left(1 - \frac{a^2z^2}{2c^4}\right) \\
c_4(z,a) &= \frac{c^6}{N^{1/2}z^2a^4} \\
c_5(z,a) &= -\left(\frac{c^2}{za}\right)^2\left(\frac{c^3}{za^2} + \frac{z}{4Nc}\right)
\end{aligned}
$$

(for simplicity, we have omitted in N the explicit dependence on z and a). Equation (A.0.3) shows that the symmetric correlation function of the electromagnetic field depends on the atomic acceleration, through the presence of the coefficients c_i and the factor N. In particular, these quantities depend on the interatomic distance and are responsible of the qualitative change of the resonant interaction energy, due to the atomic acceleration, as we have discussed in Section 2.6.2.

We now evaluate the resonance interaction between the two accelerated atoms. Putting Eqs. (A.0.3) and (2.165) into Equation (2.161), we get

$$
\delta E = \mp\frac{1}{4}\mu_\ell^A\mu_m^B\int_{\tau_0}^{\tau} d\tau'\chi_{\ell m}(x_A(\tau), x_B(\tau'))\left(e^{i\omega_{12}(\tau-\tau')} + e^{-i\omega_{12}(\tau-\tau')}\right) \tag{A.0.7}
$$

We now perform integration over time taking the limits $\tau_0 \to -\infty$, $\tau \to \infty$; after some algebra, we obtain

$$
\begin{aligned}
\delta E = \pm\frac{1}{2}\mu_\ell^A\mu_m^B\frac{a^4}{\pi c^7N^{1/2}}\Bigg\{&M_{\ell m}\left[c_1(z,a)]\frac{d^2}{dT^2} + c_2(z,a)\frac{d}{dT} + c_3(z,a)\right] \\
&+ Q_{\ell m}\left[c_4(z,a)\frac{d}{dT} + c_5(z,a)\right]\Bigg\} \\
\times\int_0^\infty d\omega\,\sin(\omega T)&\left(\frac{1}{\omega+\omega_0} + \frac{1}{\omega-\omega_0}\right)
\end{aligned} \tag{A.0.8}
$$

The integral above can be easily evaluated and after some algebraic manipulations the resonance interaction assumes the form given in Equation (2.166)

$$
\delta E = \pm(\mu_{21}^A)_\ell(\mu_{12}^B)_m\left(V_{\ell m}(\omega_0,z,a) + \left(\frac{za}{N(z,a)\,2c^2}\right)^2 U_{\ell m}(\omega_0,z,a)\right) \tag{A.0.9}
$$

where we introduced the tensor potentials

$$V_{\ell m} = \frac{1}{N^{1/2}} \frac{1}{z^3} \left\{ (\delta_{\ell m} - 3n_\ell n_m) \left[\cos(\omega_0 T) + \frac{1}{N^{1/2}} \frac{z\omega_0}{c} \sin(\omega_0 T) \right] \right.$$
$$\left. - (\delta_{\ell m} - n_\ell n_m) \frac{1}{N} \frac{z^2 \omega_0^2}{c^2} \cos(\omega_0 T) \right\} \tag{A.0.10}$$

$$U_{\ell m} = \frac{1}{N^{1/2}} \frac{1}{z^3} \left\{ (\delta_{\ell m} - 3n_\ell n_m) \left[1 - \frac{1}{N} \left(1 - \frac{z^2 a^2}{2c^4} \right) \right] \cos(\omega_0 T) - \frac{3}{N} (\delta_{\ell m} - n_\ell n_m) \frac{\omega_0 z}{c} \sin(\omega_0 T) \right\} \tag{A.0.11}$$

Acknowledgements

To conclude this thesis, please, let me thank the people that kept me company during the journey of my PhD. They induced and represented, in this period, a very important evolution in my professional and human life.

At first, I want to thank my supervisors, they showed me the direction to take for my PhD research. I thank Roberto Passante for his scientific and human support and for the confidence he always gave me. I thank Mauro Antezza for the opportunity he offered me to work in Montpellier and learn more about research. I thank Brahim Guizal for his advices on numerical simulations and for his funny explanations about the etymology of French, English and Arabic words.

I wish to thank Riccardo Messina for the many stimulating scientific discussions made working shoulder to shoulder and for his very important contribution in my professional growth.

I thank Lucia Rizzuto, Jamir Marino, Salvo Spagnolo and Margherita Lattuca for their willingness to help me and for their encouragement. I wish to thank Antonio Emanuele, Stefan Buhmann and Marco Pettini for their perusal of this thesis and for their important and useful comments.

Now, pardon me, I want to say something in Italian.

Il mio periodo del dottorato ha visto davvero tante persone che hanno arricchito le mie giornate. Non vi nominerò tutte una ad una ma credo che ognuno potrà riconoscersi nelle seguenti criptiche definizioni e sentire il mio davvero sentito ringraziamento.

Beh, voglio cominciare con un profondo grazie a chi mi ha permesso di fare questo percorso, a coloro che sono stati sempre presenti, coloro che mi hanno sempre sostenuto in maniera incondizionata e che stanno alla base di tutto: grazie a mia madre, mio padre, mio fratello, mia cognata, mia zia ed i miei cugini.

Parlando di dottorato inevitabile per me è e sarà pensare a Montpellier. Voglio ringraziare tutti gli amici incontrati in questa città che mi ha segnato. Fra questi, un ringraziamento particolare va all'ami-maître-pianiste-chef-macaronier e al randomico saggio-burlone mate KB (amici del fantomatico ma onnipresente Fabio), al mio omonimo virtuale ma non reale il cui nome è andato LOST, al sostenitore di Antonellina (non la Clerici) e della sua pasta. Un grazie particolare a voi per i vostri consigli, la vostra guida e per aver portato allegria nelle mie giornate d'oltralpe.

Ma chi mi conosce sa che sono testardamente siciliano e riservo quindi per ultimi i ringraziamenti a voi appartenenti a questa terra piena di contraddizioni. Grazie a tutti gli amici di Palermo, agli storici coinquilini, agli ancor più storici amici fraterni di "Quelli del... Che si fa stasera?", (mi sopportate e supportate ormai da N anni), agli amici più nuovi di "E poi arrivò l'arcobaleno". Grazie cioè a tutti voi che siete la famiglia allargata che mi fa sentire importante. Infine un particolare grazie agli amici del "Coffee break" e alla "Pazienza africana", agli amici del "Cioccolato" e a quelli di "Solo noi", grazie di esserci stati in qualche modo sempre, grazie per avermi sostenuto nel quotidiano e per l'enorme affetto che mi avete dato.

Ehm... Sì, dimenticavo: "Un amico vero lo riconosci subito... trasforma la tua vita in una vita speciale!"

Grazie a tutti. Thank you all.